

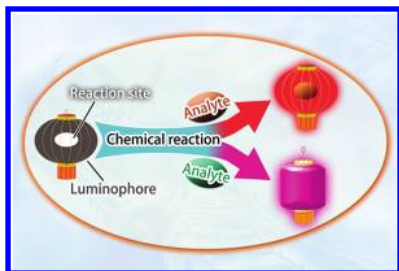
Luminescent Chemodosimeters for Bioimaging^{II}

Yuming Yang,^{†,§} Qiang Zhao,^{‡,§} Wei Feng,[†] and Fuyou Li*,[†]

[†]Department of Chemistry and State Key Laboratory of Molecular Engineering of Polymers and Institutes of Biomedical Sciences, Fudan University, Shanghai 200433, P. R. China

[‡]Key Laboratory for Organic Electronics and Information Displays (KLOEID) and Institute of Advanced Materials (IAM), Nanjing University of Posts and Telecommunications, Nanjing 210046, P. R. China.

Supporting Information



CONTENTS

1. Introduction	194
2. Advantages of Luminescent Chemodosimeters As Bioimaging Probes	195
3. Design Principles of Luminescent Chemodosimeters for Bioimaging	195
3.1. Extent of π -Electron System	195
3.2. Effect of Substituents with Electron-Donating or Electron-Withdrawing Groups	195
3.3. Photoinduced Intramolecular Charge Transfer	195
3.4. Photoinduced Electron Transfer	195
3.5. Excited-State Intramolecular Proton Transfer	195
3.6. Special Charge Transfer in Phosphorescent Heavy-Metal Complexes	195
3.7. Energy Transfer from Ligand to Lanthanide Ions in Luminescent Lanthanide Complexes	196
3.8. Förster Resonance Energy Transfer	196
4. General Requirements of Luminescent Chemodosimeters for Bioimaging	196
5. Luminescent Chemodosimeters for Metal Cations	196
5.1. Luminescent Chemodosimeters for Hg^{2+}	196
5.1.1. Desulfation or Deselenization Process	197
5.1.2. Desulfation and Cyclization Processes	197
5.1.3. Thiol Elimination Process	199
5.1.4. Rhodamine Spirolactam Ring-Opening Process	199
5.1.5. Sulfur-Containing Rhodamine Spirolactam Ring-Opening Process	201
5.1.6. Spirolactam Ring-Opening and Cyclization Processes	201
5.1.7. Spirolactam Ring-Opening and Hydrolysis Processes	202
5.1.8. Alkyne or Vinyl Ether Oxymercuration Process	202

5.1.9. Hg^{2+} -Promoted Hydrolysis of Vinyl Ether and Cyclization Reaction	203
5.1.10. $Hg^{(II)}$ -Mediated Propargyl Amide to Oxazole Transformation	203
5.1.11. Selective Mercuration Reaction	203
5.1.12. Phosphorescent Chemodosimeters for Hg^{2+}	203
5.1.13. FRET-Based Chemodosimeters for Hg^{2+}	205
5.1.14. Upconversion Luminescence-Based Energy Transfer Chemodosimeters for Hg^{2+}	205
5.1.15. Luminescent Chemodosimeters for Bioimaging Methylmercury	206
5.2. Luminescent Chemodosimeters for Cu^{2+}	206
5.2.1. Cu^{2+} -Coordination-Induced Spirolactam Ring-Opening Process	206
5.2.2. Cu^{2+} -Induced Hydrolysis Process	207
5.2.3. Cu^{2+} -Induced Spirolactam Ring-Opening and Hydrolysis Processes	207
5.2.4. Cu^{2+} -Induced Oxidation Process	208
5.2.5. Cu^{2+} -Induced Oxidative Cyclization Process	209
5.2.6. Cu^{2+} -Induced Retro-Reaction	209
5.2.7. Cu^{2+} -Induced Thiol Elimination Process	209
5.3. Luminescent Chemodosimeters for Fe^{3+}	209
5.3.1. Fe^{3+} -Induced Spirolactam Ring-Opening Process	210
5.3.2. Fe^{3+} -Induced Spirolactam Ring-Opening and Hydrolysis Processes	211
5.3.3. Fe^{3+} -Induced Oxidation and Hydrolysis Reaction Processes	211
5.4. Luminescent Chemodosimeters for Cr^{3+}	211
5.4.1. Fluorescence Turn-On Chemodosimeters for Cr^{3+}	211
5.4.2. FRET-Based Chemodosimeters for Cr^{3+}	212
5.5. Luminescent Chemodosimeters for Zn^{2+}	212
5.5.1. Zn^{2+} -Complexation-Induced Spirolactam Ring-Opening Process	212
5.5.2. Zn^{2+} -Complexation-Induced Hydrolysis Process	212
5.6. Luminescent Chemodosimeters for Cd^{2+}	213
5.7. Luminescent Chemodosimeters for Pb^{2+}	213

Received: October 27, 2011

Published: June 18, 2012

5.8. Luminescent Chemodosimeters for Au^+ / Au^{3+}	213	7.2.3. HOCl-Induced Spirolactam Ring-Opening and Oxidation Reactions	228
5.8.1. Au^{3+} -Induced Spirolactam Ring-Opening Process	213	7.2.4. HOCl-Induced Spirolactam Ring-Opening and Hydrolyzation Processes	228
5.8.2. Au^{3+} -Induced Spirolactam Ring-Opening and Intramolecular Cyclization Processes	213	7.2.5. OCl^- -Induced Cleavage of the Ether Moiety	229
5.8.3. Au^{3+} -Induced Spirolactam Ring-Opening and Hydrolysis of Acylsemicarbazide	214	7.3. Luminescent Chemodosimeters for ${}^1\text{O}_2$	229
5.8.4. Au^{3+} -Induced Conversion of Propargyl to Acetonyl Process	214	7.3.1. ${}^1\text{O}_2$ -Induced Formation of Endoperoxide	229
5.9. Luminescent Chemodosimeters for Ag^+	214	7.3.2. ${}^1\text{O}_2$ -Induced 1,4-Cycloaddition of Imidazole	230
5.10. Luminescent Chemodosimeters for Pd(II)/ Pd(0)/Pt(0)	214	7.4. Luminescent Chemodosimeters for O_2^-	230
5.10.1. Pd/Pt-Catalyzed Deallylation Process	214	7.4.1. O_2^- -Induced Oxidation Reaction	230
5.10.2. Pd-Coordination-Induced Spirolactam Ring-Opening Process	215	7.4.2. Reaction of O_2^- with Nitroxide	231
5.11. Fluorescent Chemodosimeters for VO^{2+}	215	7.4.3. O_2^- -Induced Protection-Deprotection Reaction	231
6. Luminescent Chemodosimeters for Anions	215	7.5. Luminescent Chemodosimeters for $\cdot\text{OH}$	231
6.1. Luminescent Chemodosimeters for F^-	215	7.5.1. Reaction of $\cdot\text{OH}$ with Nitroxide	231
6.1.1. F^- -Triggered Cleavage of Si—O Bonds	215	7.5.2. $\cdot\text{OH}$ -Induced Cleavage of a DNA Strand	232
6.1.2. F^- -Triggered Cleavage Reaction of Si—C Bond	216	7.5.3. $\cdot\text{OH}$ -Induced Aromatic Hydroxylation	232
6.1.3. Nucleophilic Addition Reaction of F^-	217	7.6. Luminescent Chemodosimeters for O_3	233
6.1.4. F^- -Induced Intramolecular Cyclization Reaction	217	7.7. Luminescent Chemodosimeters for Oxidative Stress	233
6.1.5. F^- -Triggered Si—O Bond-Cleavage and Cyclization Reactions	217	7.8. Luminescent Chemodosimeters for Hypoxia	233
6.1.6. Fluorescent F^- Chemodosimeters Based on Organoboron Compounds	217	7.8.1. Reduction Metabolism of Nitroaromatic Compound	234
6.2. Luminescent Chemodosimeters for CN^-	218	7.8.2. Reduction of Azobenzene Derivative	234
6.2.1. Michael Addition Reaction	218	8. Luminescent Chemodosimeters for Reactive Nitrogen Species	234
6.2.2. Nucleophilic Addition Reaction	219	8.1. Luminescent Chemodosimeters for NO	235
6.2.3. Coordination Reaction of CN^-	220	8.1.1. NO-Induced Diamine Cyclization Process	235
6.2.4. Fluorescent CN^- Chemodosimeters Based on Organoboron Compounds	220	8.1.2. NO-Induced Diazo-Ring-Generation Process	236
6.2.5. CN^- -Induced Decomplexation Reaction	222	8.1.3. NO-Induced Spirolactam-Ring-Opening Process	236
6.3. Luminescent Chemodosimeters for BO_3^-	222	8.1.4. NO-Triggered Selective Ligand Dissociation of Metal Complex	237
7. Luminescent Chemodosimeters for Reactive Oxygen Species	222	8.1.5. NO-Triggered Reduction of Cu^{2+} and Release of Fluorescent Ligand	237
7.1. Luminescent Chemodosimeters for H_2O_2	222	8.1.6. NO-Induced Spirolactam Ring-Opening, Reduction of Cu^{2+} , and Nitrosylation of Fluorescent Ligand	238
7.1.1. H_2O_2 -Trigger Transformation of Diboronate to Phenols	223	8.2. Luminescent Chemodosimeters for HNO	238
7.1.2. H_2O_2 -Trigger Transformation of Monoboronate to Phenols	224	8.3. Luminescent Chemodosimeters for ONOO^-	238
7.1.3. H_2O_2 -Trigger Deprotection Reaction of Amine	224	8.3.1. Specific Reaction between Ketone and ONOO^-	238
7.1.4. H_2O_2 -Trigger Oxidation of Phenylboronic Acid	225	8.3.2. ONOO^- -Induced Se(II) Oxidation	239
7.1.5. H_2O_2 -Mediated Hydrolysis of Sulfonic Esters	225	8.3.3. ONOO^- -Induced Aromatic Nitration	239
7.1.6. H_2O_2 -Trigger Transformation of Benzyl to Benzoic Acid	226	8.4. Luminescent Chemodosimeters for NO_2^+	240
7.1.7. H_2O_2 -Trigger Oxidation of Triphenylphosphine	226	8.5. Luminescent Chemodosimeters for NO_2^-	240
7.1.8. H_2O_2 -Trigger Cleavage of Diaminophenyl Ether	226	9. Luminescent Chemodosimeters for Reactive Sulfur Species	240
7.1.9. H_2O_2 -Trigger Oxidation of Fe Complexes	226	9.1. Luminescent Chemodosimeters for Thiol	240
7.2. Luminescent Chemodosimeters for HOCl/ OCl^-	226	9.1.1. Nucleophilic Addition of Squaraine	240
7.2.1. HOCl-Induced Oxidation Process	227	9.1.2. Michael Addition of Thiols to α,β -Unsaturated Carbonyl Moiety	241
7.2.2. OCl^- -Induced Destruction of the C=N Bond	227	9.1.3. Nucleophilic Addition and Spirolactam-Ring-Opening Processes	242
		9.1.4. Reaction between Iodoacetamide and Thiol	242
		9.1.5. Sulfonethers or Sulfonamides Cleavage Process	242

9.1.6. Multi-Nitrobenzyl Ester-Cleavage Process	243
9.1.7. Cleavage of Disulfide-Based Carbamate Protecting Group	243
9.1.8. Cleavage of Se–N bond	244
9.1.9. Native Chemical Ligation Reaction	244
9.1.10. Cleavage Reaction of Disulfide Bond	245
9.1.11. Demetalization and Hydrolysis Processes	245
9.1.12. Denitration and Glutathionylation	245
9.2. Luminescent Chemodosimeters for Cys/Hcy	245
9.2.1. Cyclization Process of Arylic Aldehyde	247
9.2.2. Nucleophilic Addition Process	247
9.2.3. Michael Addition Process	248
9.2.4. Michael Addition and Intramolecular Cyclization Reactions	248
9.3. Luminescent Chemodosimeters for $\text{H}_2\text{S}/\text{S}^{2-}$	248
9.3.1. H_2S -Mediated Reduction of Azide to Amine	248
9.3.2. H_2S -Induced Nucleophilic Reaction	249
9.3.3. High Affinity of S^{2-} to Cu(II)	249
9.3.4. Nucleophilic Reaction of S^{2-}	249
9.3.5. Addition Reaction of S^{2-} and Michael Addition	250
9.4. Fluorescent Chemodosimeters for $\text{HSO}_3^-/\text{SO}_3^{2-}$	250
9.5. Luminescent Chemodosimeters for Oxone	250
10. Luminescent Chemodosimeters for Nerve Gas DCP	250
10.1. DCP-Induced Intramolecular Cyclization Process	250
10.2. DCP-Induced Spirolactam Ring-Opening Process	251
10.3. DCP-Induced Spirolactam Ring-Opening and Intramolecular Cyclization Processes	251
10.4. DCP-Induced Formation of Phosphoramido	251
11. Luminescent Chemodosimeters for Amino Acids	251
11.1. Luminescent Chemodosimeters for Alanine	251
11.2. Luminescent Chemodosimeters for Histidine and Histidine-Rich Protein	251
12. Summary and Prospects	253
13. Appendix I: Summary of Physiochemical Properties of Luminescent Chemodosimeters for Bioimaging	253
Associated Content	260
Supporting Information	260
Author Information	260
Corresponding Author	260
Author Contributions	260
Notes	260
Biographies	260
Acknowledgments	260
Dedication	260
Abbreviations	261
References	261
Note Added after ASAP Publication	270

1. INTRODUCTION

Luminescence bioimaging offers a unique approach for visualizing morphological details of tissues with subcellular resolution and has become a powerful tool for the manipulation

and investigation of microspecies from living cells and animals.^{1–5} In luminescence bioimaging, luminescent probes are used to label a molecule of interest and to render luminescent signals. Many new luminescent probes, including fluorescent proteins,^{6,7} organic dyes,^{3,8–12} metal complexes,^{13–20} semiconductor nanocrystals,²¹ upconversion nanophosphors,^{22,23} and other nanoparticles,^{24–26} have been synthesized for bioimaging application. Most can be utilized as probes to monitor biomacromolecules (such as proteins and DNA) in living biological samples through high-affinity antibody–antigen interactions and ligand–acceptor interactions.²⁷ However, the selective and sensitive monitoring of cations, anions, amino acids, and small neutral molecules in living cells is less readily achieved by this method, due to variability in the concentration, charges, and binding sites of these analytes. When designing luminescent systems (the host) for the recognition of cations, anions, amino acids, or small neutral molecules (the guest), it is crucial to utilize specific host–guest interactions or chemical reactions that invoke a change in the luminescent emission properties of the system. If the specific interaction between the host and the guest is noncovalent and reversible, and the interaction can be disrupted under certain conditions, the indicator is referred

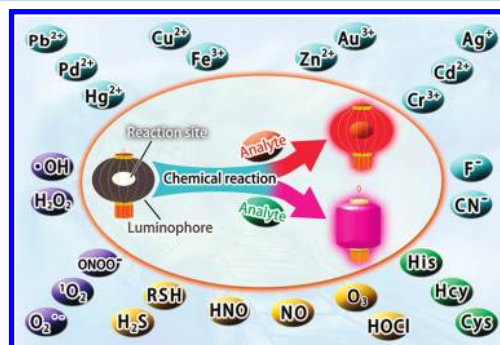


Figure 1. Schematic principle of chemodosimeters based on two different detection approaches: the analyte reacts with the chemodosimeter and remains covalently attached (red arrow), and the analyte catalyzes a chemical reaction (purple arrow). Some analytes summarized in this review are also shown.

to as a chemosensor.^{28–30} If the binding interaction between the host and the guest is based on an irreversible chemical reaction, the indicator is described as a chemodosimeter.^{31–33}

Chemodosimeters require at least two functional units (Figure 1). The first is the reaction site, where the host binds to the analyte, whereas the second provides a spectroscopic signal that is dependent on the interaction with the analyte. Both the interaction between the chemodosimeter and the analyte and the change in detectable signal are, in principle, irreversible. Two main approaches used in the design of luminescent chemodosimeters are shown in Figure 1. In the first approach, the analyte acts as a reactant and is covalently bound to the chemodosimeter to form a new product after reaction. In the second approach, the analyte catalyzes a chemical reaction, which results in the modification of the chemodosimeter with a concomitant change in its optical characteristics.³¹

Because of their rapid response, high sensitivity, and excellent selectivity, the design, synthesis, and application of chemodosimeters in luminescence bioimaging have attracted increasing attention and become a very active research field. Because

of the rapid development of luminescent chemodosimeters for bioimaging, a systematic survey of the progress in this research field is required, although six reviews have previously dealt with the study of colorimetric and fluorogenic chemodosimeters for solution detection.^{32–37}

In this review, we focus on the recent progress in luminescent chemodosimeters for photoluminescent bioimaging of various metal cations, anions, amino acids, and neutral molecules in living biological samples. To date, approximately 200 luminescent chemodosimeters have successfully been applied in bioimaging of living biological samples. Data indicating the change in photophysical properties and experimental conditions of these reported chemodosimeters for bioimaging and solution detection are shown in Appendix I and Table S1 in Supporting Information, respectively. To better understand the rational design approaches and discuss how the luminescent chemodosimeters react with the analytes, all of the reported luminescent chemodosimeters for solution detection have also been summarized in this review, although some of them have not been applied to bioimaging. This review is not intended to be comprehensive but rather to highlight novel receptors, interaction modes, sensing mechanisms, and other timely or interesting aspects of the works discussed.

2. ADVANTAGES OF LUMINESCENT CHEMOSIMETERS AS BIOIMAGING PROBES

Chemodosimeters are used to detect a target analyte through a usually irreversible chemical reaction between the dosimeter molecule and the analyte. Hence, the selectivity of chemodosimeters for the target analyte is often very high. Using photoluminescent emission as detection signal, chemodosimeters exhibit high sensitivity. In addition, chemodosimeters usually show rapid response to the target analyte. Importantly, most reported luminescent chemodosimeters are based on luminescence “turn-on” or (and) emission wavelength shifts. In addition, most of the reported chemodosimeters based on lanthanide complexes show prolonged luminescent lifetime, which is suitable for time-resolved luminescence bioimaging. Luminescent chemodosimeters therefore provide a useful alternative to chemosensors for detecting analytes in biological systems, especially for detecting heavy-metal cations, which often cause luminescence quenching in chemosensor systems. In addition, few cases of luminescent chemosensors have been reported for highly selective detection of small neutral molecules, due to relatively weak host–guest interaction of neutral small molecules. Meanwhile, neutral small molecules show high chemical reaction activity. Therefore, luminescent chemodosimeters are suitable as probes for selective detection of neutral small molecules. For these reasons, the application of luminescent chemodosimeters to bioimaging is attracting increasing research interest.

3. DESIGN PRINCIPLES OF LUMINESCENT CHEMOSIMETERS FOR BIOIMAGING

One basic requirement of a luminescent chemodosimeter is that the luminescent properties (including luminescent intensity, wavelength, and lifetime) of the product can be distinguished from that of the reagent after reaction with the analyte. Therefore, all factors affecting luminescence properties can be utilized to design luminescent chemodosimeters.

3.1. Extent of π -Electron System

Almost all organic fluorescent compounds are aromatic. Varying the degree of conjugation of the π -electron system will generally change the fluorescent emission wavelength and (or) the fluorescence quantum yield, and even the fluorescent lifetime.^{38,39} If an analyte interacts specifically with the organic fluorescent compound and changes the degree of the π -conjugation system, the fluorescent compound can be used as a luminescent chemodosimeter for the analyte.

3.2. Effect of Substituents with Electron-Donating or Electron-Withdrawing Groups

The effect of substituents on the fluorescence characteristics of aromatic systems is often complex. In general, the introduction of electron-donating or electron-withdrawing substituents can induce an increase in the molar absorption coefficient and a shift in the fluorescence spectrum. In reported luminescent chemodosimeters, the main electron-donating substituents used to date have been aromatic amines and phenols, whereas the main electron-withdrawing substituents have been aldehyde, ketone, nitrile, amide, and nitro groups.

3.3. Photoinduced Intramolecular Charge Transfer

When both electron-donating and electron-withdrawing groups are conjugated into one π -electron system, an electron donor– π -conjugation bridge–electron acceptor (D– π –A) molecule is generated.^{38–40} Intramolecular charge transfer (ICT), which changes the overall charge distribution of the molecule, dominates the excited state of such D– π –A molecules. The formation of ICT results in a fluorophore with large polarity that shows intense fluorescence in the visible region and even in the near-infrared region. To date, most of the reported luminescent chemodosimeters summarized in this review adopt this ICT-based strategy by changing either the electron-donating or electron-withdrawing ability or π -conjugation degree of the fluorophores upon interaction with the analyte.

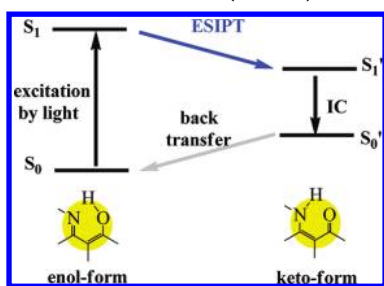
3.4. Photoinduced Electron Transfer

Photoinduced electron transfer (PET)^{38,39,41} is often used to generate luminescent chemodosimeters that feature fluorescence quenching or enhancement. If another part of the fluorophore provides an orbital that has energy between those of the highest occupied molecular orbital (HOMO) and lowest unoccupied molecular orbital (LUMO) of the fluorophore, an intramolecular PET can take place. PET can occur from a filled orbital to the HOMO of the fluorophore or from the excited LUMO of the fluorophore to an empty orbital, depending on the nature of the “nearby” orbital incorporated.⁴² Deactivation processes without radiation can therefore occur, and fluorescence quenching is observed. For luminescent chemodosimeters based on PET process, a reaction between the fluorophore and the analyte induces either the appearance or the removal of the “nearby” orbital between HOMO and LUMO of the fluorophore, resulting in fluorescence quenching or enhancement, respectively.

3.5. Excited-State Intramolecular Proton Transfer

Excited-state intramolecular proton transfer (ESIPT)⁴³ has also been used for designing luminescent chemodosimeters because of its unique and outstanding spectral sensitivity to the environmental medium. The general mechanism is that the ESIPT process incorporates a fast excited-state proton transfer from a proton donor (usually hydroxyl or amino group) to an acceptor group (often either oxygen or nitrogen) mediated by

Scheme 1. Schematic Representation of the Excited-State Intramolecular Proton Transfer (ESIPT) Process



an intramolecular hydrogen bond (H-bond). A typical representation of an ESIPT process is shown in Scheme 1. The ESIPT process radically decreases the probability of photochemical reactions of excited molecules and significantly enhances the photostability of the molecules. In addition, a large apparent Stokes shift can also be observed. Thus, the ESIPT process is very suitable for designing luminescent chemodosimeters with spectral shift for selective detection.

3.6. Special Charge Transfer in Phosphorescent Heavy-Metal Complexes

Chemodosimeters can also be designed based on phosphorescent heavy-metal complexes with a unique d^6 , d^8 , and d^{10} -electron configuration, with the resultant chemodosimeters demonstrating phosphorescence emission. In general, the excited-state properties of phosphorescent heavy-metal complexes, such as Re(I), Ru(II), Ir(III), Pt(II), Os(II), Cu(I), and Au(I) complexes, are very complicated.^{44–54} Many kinds of excited states can be formed, depending on the metal centers, ligand structures, intramolecular/intermolecular interactions, and the local environment.^{44,48–54} The excited states of heavy-metal complexes can include metal-to-ligand charge-transfer (MLCT), intraligand charge-transfer (ILCT), ligand-to-ligand charge-transfer (LLCT), metal–metal-to-ligand charge-transfer (MMLCT),⁵⁴ and metal-to-ligand–ligand charge-transfer (MLLCT) states, as well as metal-centered (MC) excited states.^{55–57} Different excited states can result in different photophysical properties for the heavy-metal complexes. One popular design strategy for heavy-metal complexes as phosphorescent chemodosimeters involves inducing a change in the degree of π -conjugation of the ligand upon interaction with the analyte. Another strategy is based on the displacement of a ligand upon interaction with the analyte.

3.7. Energy Transfer from Ligand to Lanthanide Ions in Luminescent Lanthanide Complexes

Luminescent lanthanide complexes exhibit some advantages for application in sensing and bioimaging, such as long emission lifetime, large Stokes shift, and sharp emission profile.⁵⁸ Especially the long emission lifetimes of lanthanide ions allow the use of time-resolved luminescence detection to eliminate scattering excitation lights and short-lived autofluorescence from both biological samples and optical components. Because lanthanide ions exhibit low molar extinction coefficients, they often require sensitization with organic ligand as sensitizers capable of energy transfer to lanthanide excited states. Thus, the luminescence of lanthanide complexes depends on the energy-transfer efficiencies from ligand sensitizers to lanthanide ions, which are determined by the chemical structures and triplet energy levels of ligands.⁵⁹ If the reaction of ligand with the analyte changes its chemical structure and triplet energy

level, the energy-transfer efficiency from ligand to lanthanide ions will be changed, which results in the variation in luminescence properties of lanthanide ions. Thus, luminescent chemodosimeters based on lanthanide complexes can be realized.

3.8. Förster Resonance Energy Transfer

Förster resonance energy transfer (FRET) is a distance-dependent interaction between the electronic excited states of two chromophores in which excitation is transferred from a donor chromophore to an acceptor chromophore through nonradiative dipole–dipole coupling.⁶⁰ When both chromophores are fluorescent, the term “fluorescence resonance energy transfer” is often used instead. The efficiency of FRET is dependent on the inverse sixth power of the intermolecular separation, such that it can only occur over very short distances, typically within 10 nm. Beyond the spatial proximity requirement, the emission spectrum of the donor must overlap effectively the absorption spectrum of the acceptor. By exciting the donor and then monitoring the relative ratio of donor and acceptor emissions, either sequentially or simultaneously, the presence and efficiency of the FRET interaction can be monitored, realizing the detection.

4. GENERAL REQUIREMENTS OF LUMINESCENT CHEMODOSIMETERS FOR BIOIMAGING

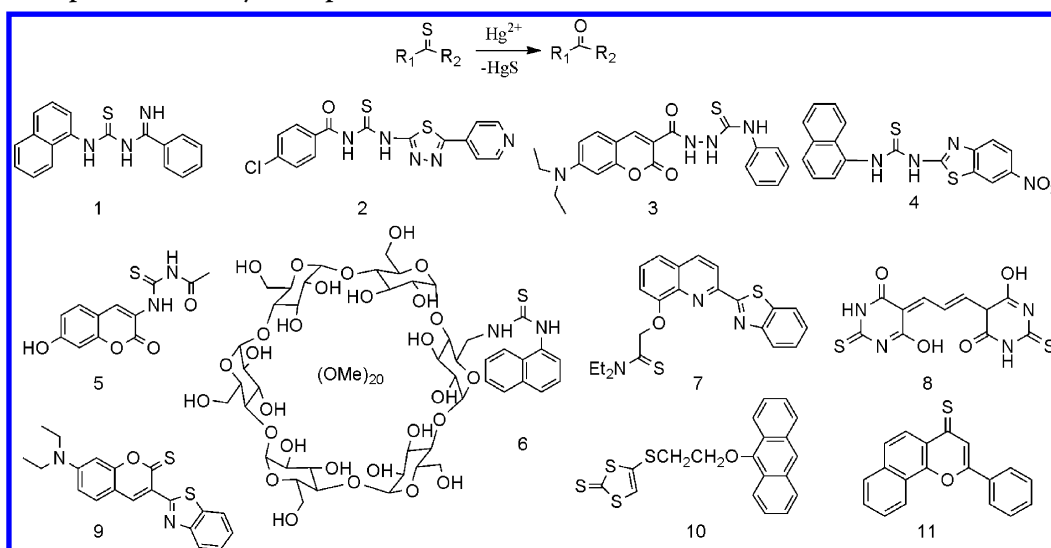
Several characteristics must be tuned to generate a luminescent chemodosimeter that can be successfully used for bioimaging, including excitation and emission wavelength, luminescent brightness, cellular penetration, and cytotoxicity. To be applied in bioimaging, chemodosimeters must exhibit a high luminescent quantum yield upon interaction with the analyte under excitation at visible, even near-infrared (NIR), wavelengths. The brighter the agent, the less excitation light is needed and therefore the deeper is the possible depth penetration above a certain signal-to-noise ratio. The chemodosimeters must also demonstrate suitable water solubility, demonstrate low cytotoxicity, and have good cellular uptake property, crossing the outer lipid membrane rapidly. Beyond these general requirements, an excellent luminescent chemodosimeter for imaging should exhibit luminescence “turn-on” or (and) a clear shift in emission wavelength upon reacting with the analyte. Finally, luminescent chemodosimeters should show high selectivity, excellent sensitivity, and rapid response in detecting the analyte in biological samples. In addition, for application in bioimaging *in vivo*, luminescent chemodosimeters are required that can be excited in the NIR region, as near-infrared light of around 650–900 nm is less readily absorbed by biological substances and can therefore penetrate more deeply into tissues.^{8,61,62}

5. LUMINESCENT CHEMODOSIMETERS FOR METAL CATIONS

5.1. Luminescent Chemodosimeters for Hg^{2+}

Mercury is one of the most hazardous and ubiquitous pollutants.^{63–65} Mercury bioaccumulation can involve inorganic mercury and methylmercury species (CH_3HgX), which enter the food chain and are subsequently ingested by humans. Neurological problems associated with methylmercury intoxication include prenatal brain damage, cognitive and motion disorders, vision and hearing loss, and death.^{66–68} Therefore, the monitoring of mercury and methylmercury species in living

Scheme 2. Proposed Mechanism of Fluorescent Hg^{2+} Chemodosimeters 1–11 Based on the Desulfation Reaction of a Thiocarbonyl Group into a Carbonyl Group



biosamples is an important area of research. Although a large number of Hg^{2+} -sensitive luminescent chemosensors based on reversible sensing processes have been reported,^{59,70} luminescent dosimetric detection based on irreversible chemical reaction has become an important strategy for Hg^{2+} detection because of its high sensitivity and rapid response time. To date, various chemical reaction mechanisms have been developed to allow luminescent dosimetric detection of Hg^{2+} , as discussed in further sections.

5.1.1. Desulfation or Deselenization Process. (1). Hg^{2+} -Induced Desulfation Process. The Hg^{2+} ion is highly thiophilic,⁷¹ and desulfurization reactions have been used to design fluorescent chemodosimeters for Hg^{2+} ion. A major desulfurization reaction is based on the Hg^{2+} -triggered transformation of the thiocarbonyl group to the carbonyl one (Scheme 2), which can change the emission properties of fluorescent chemodosimeters and allow selective detection. To date, 11 organic dye-based fluorescent chemodosimeters for Hg^{2+} ion (including thioureas 1,⁷² 2,⁷³ 3,⁷⁴ 4,⁷⁵ 5,⁷⁶ and 6,⁷⁷ thioamides⁷⁸ and thiones 8,⁷⁹ 9,⁸⁰ 10,⁸¹ and 11;⁸² Scheme 2) have been reported with sensing mechanisms based on the desulfation of thiocarbonyl groups.

This Hg^{2+} -triggered transformation of the thiocarbonyl group to carbonyl usually results in the enhancement of fluorescence emission and can be carried out in semiaqueous environments, thereby providing a benefit for bioimaging. For example, 9⁸⁰ exhibits relatively weak fluorescence centered at 511 nm. Upon interaction with Hg^{2+} ions, its fluorescence intensity at 511 nm increases 25.8-fold. Such signaling of Hg^{2+} is highly selective and very rapid, and the detection can be carried out in semiaqueous environments. In particular, Liu and co-workers have developed a water-soluble naphthylthiourea derivative 6 by introduction of cyclodextrin, and 6 was used to detect Hg^{2+} with high selectivity and sensitivity in water, by desulfation reaction of the thiocarbonyl group.⁷⁷ Furthermore, 6 has been successfully applied to the fluorescent imaging of Hg^{2+} in living cells (Figure 2).

(2). Hg^{2+} -Induced Deselenization Reaction. Similar to desulfation reactions, Hg^{2+} can also induce irreversible deselenization reactions, and this has been used as the basis of detection systems.⁸³ Phosphane selenide compound 12

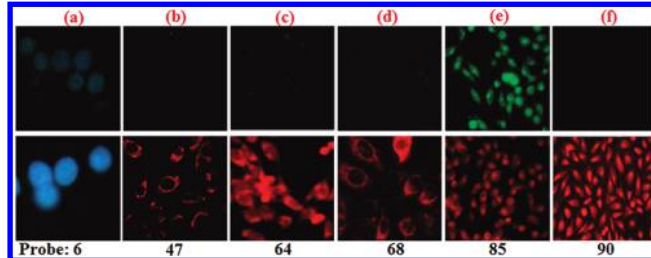
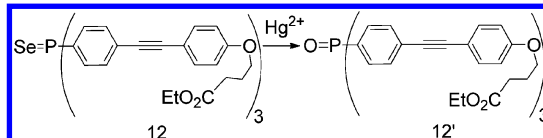


Figure 2. Selected examples of fluorescence imaging of living cells in the absence (upper) or presence (lower) of Hg^{2+} (or CH_3Hg^+) using chemodosimeters 6 (a), 47 (b), 64 (c), 68 (d), 85 (e), and 90 (f) as fluorescent probes. (a) Reprinted with permission from ref 77. Copyright 2011 The Royal Society of Chemistry. (b) Reprinted with permission from ref 115. Copyright 2007 American Chemical Society. (c) Reprinted with permission from ref 130. Copyright 2006 American Chemical Society. (d) Reprinted with permission from ref 135. Copyright 2010 American Chemical Society. (e) Ratiometric images. $\lambda_{em} = 515 \pm 15$ nm (green channel) and 590 ± 25 nm (red channel). $\lambda_{ex} = 488$ nm. Reprinted with permission from ref 158. Copyright 2011 Wiley-VCH Verlag GmbH & Co. KGaA, Weinheim. (f) Reprinted with permission from ref 178. Copyright 2010 Elsevier Ltd.

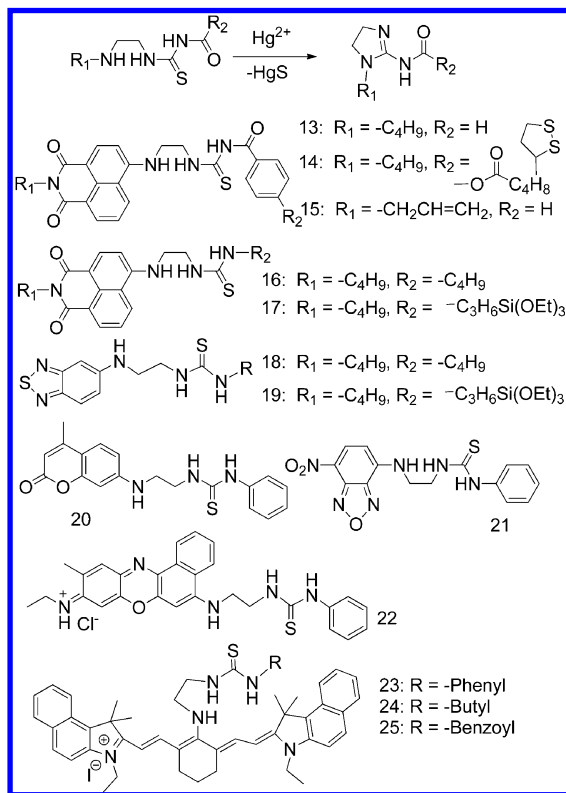
Scheme 3. Chemodosimeter 12 Based on Hg^{2+} -Induced Deselenization Reaction



(Scheme 3), which has a push–pull electronic structure, shows very weak fluorescence.⁸⁴ Upon addition of mercury salt, an irreversible deselenization reaction occurs, resulting in the formation of phosphane oxide 12' and fluorescence enhancement (100-fold). Thus, a highly selective and sensitive detection for Hg^{2+} was realized.

5.1.2. Desulfation and Cyclization Processes. A combination of both the desulfation and cyclization processes (Scheme 4) has been utilized for designing fluorescent chemodosimeters for Hg^{2+} . Such combined reactions often result in significant changes to the fluorescent properties,

Scheme 4. Proposed Mechanism of Hg²⁺-Induced Desulfation and Cyclization Reactions for Chemodosimeters 13–25

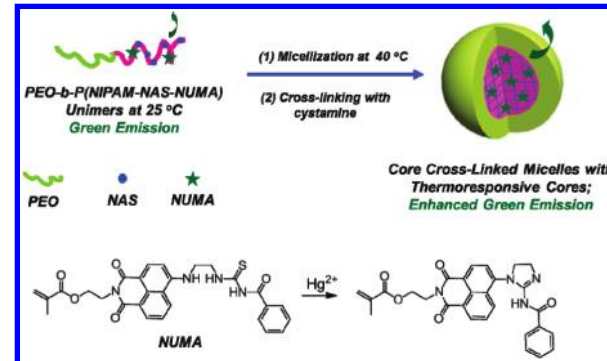


including spectral shift or fluorescent enhancement or both. These characteristics make such chemodosimeters very suitable for bioimaging.

(1). *Formation of Imidazoline*. The most widely used desulfation and cyclization reaction is based on the Hg²⁺-triggered transformation of the thiourea unit of the chemodosimeter into an imidazoline moiety. On the basis of this transformation, some excellent fluorescent chemodosimeters (13,⁸⁵ 14,⁸⁶ 15,⁸⁷ 16–17,⁸⁸ 18–19,⁸⁹ 20,⁹⁰ 21,⁹¹ 22,⁹² and 23–25,⁹³ Scheme 4) for Hg²⁺ have been developed. The addition of Hg²⁺ to the solutions of compounds 13–18 causes Hg²⁺-promoted desulfation and intramolecular cyclic guanylation of thiourea, resulting in a decrease in the electron-donating ability of the amine group in these fluorophors, corresponding to significant blue-shift in the fluorescent emission and a change in the color of emission. For example, Tian and co-workers reported the first case of dual fluorescent and colorimetric chemodosimeter based on the naphthalimide derivative 13.⁸⁵ The reaction conditions can be optimized to yield high selectivity for Hg²⁺. The chemodosimeter 13 exhibits yellowish-green fluorescence with emission maximum at 530 nm in a solution of acetonitrile and H₂O (4:1, v:v). Upon addition of Hg²⁺, the emission maximum is blue-shifted to 475 nm and a new naphthalimide derivative with intense blue fluorescence is formed, which is attributed to the Hg²⁺-promoted intramolecular cyclic reaction. Accordingly, the absorption maximum is also blue-shifted from 435 to 350 nm. Furthermore, 13 was modified by introducing a disulfide moiety, and a new chemodosimeter 14⁸⁶ was synthesized and self-assembled on the surface of gold nanoparticles to fabricate organic–inorganic hybrid chemodosimeters for Hg²⁺. In the case of 15,⁸⁷ the

addition of Hg²⁺ changes fluorescent emission from 548 to 496 nm. Furthermore, 15 was developed for monitoring intracellular Hg²⁺ levels in EG 277 cells by confocal fluorescence microscopy and two-photon fluorescence microscopy. By replacing the benzoyl thiourea moiety of 13 with a butyl group, Tian and co-workers have devised another fluorescent chemodosimeter 16⁸⁸ for ratiometric detection of Hg²⁺. Further modified by triethoxysilane group for the purpose of covalently attaching to the silica network, 17⁸⁸ and 19⁸⁹ could be grafted on the mesoporous silica, and hybrid chemodosimeters were successfully fabricated for selective determination of Hg²⁺ in aqueous solution. Interestingly, using a red emission at 652 nm as an output signal, Nile blue derivative 20⁹⁰ can be used to detect Hg²⁺ in biological media, such as blood plasma and albumin. The detection limit is <1 ppb, which corresponds to

Scheme 5. Schematic Illustration of Core Cross-linked (CCL) Micelles with Thermoresponsive Cores from Diblock Copolymer PEO-*b*-P(NIPAM-*co*-NAS-*co*-NUMA) in Aqueous Solution and the Hg²⁺-Reactive Mechanism of NUMA Moieties



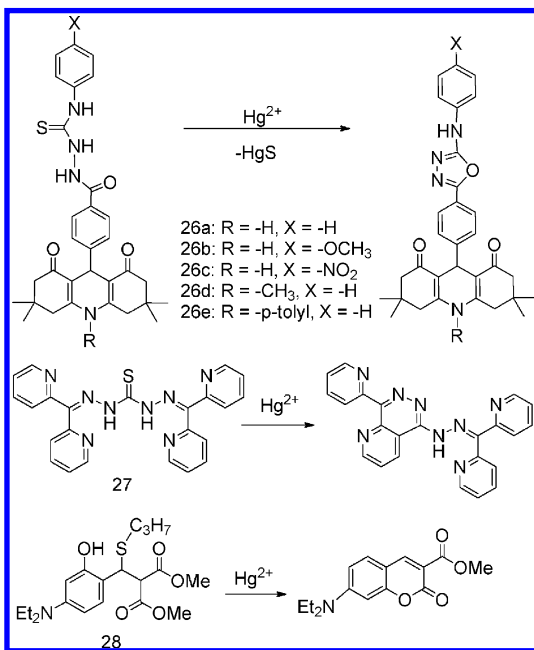
the U. S. Environmental Protection Agency's limit for drinking water.

Utilizing the similar Hg²⁺-triggered desulfation and cyclization process of 13, Liu and co-workers have demonstrated that core cross-linked (CCL) micelles possessing thermoresponsive cores and fluorescent unit nuclear mitotic apparatus (NUMA) (Scheme 5) could be used as sensitive and selective ratiometric Hg²⁺ chemodosimeters with thermo-tunable detection efficiency. Upon Hg²⁺ addition, the aqueous dispersion of the CCL micelles exhibit a fluorometric transition from green to bright blue. Compared with the unimers at 25 °C, the Hg²⁺ detection limit of CCL micelles was significantly enhanced to 3.0 from 10.1 nM. When elevating the temperature of CCL micelles to 40 °C, the detection limit was further improved to be 1.8 nM, corresponding to a thermo-tunable detection efficiency. Moreover, the CCL micelles can be taken up into living cells and sensitively respond to the intracellular Hg²⁺ ions by fluorescence microscopy.⁹⁴

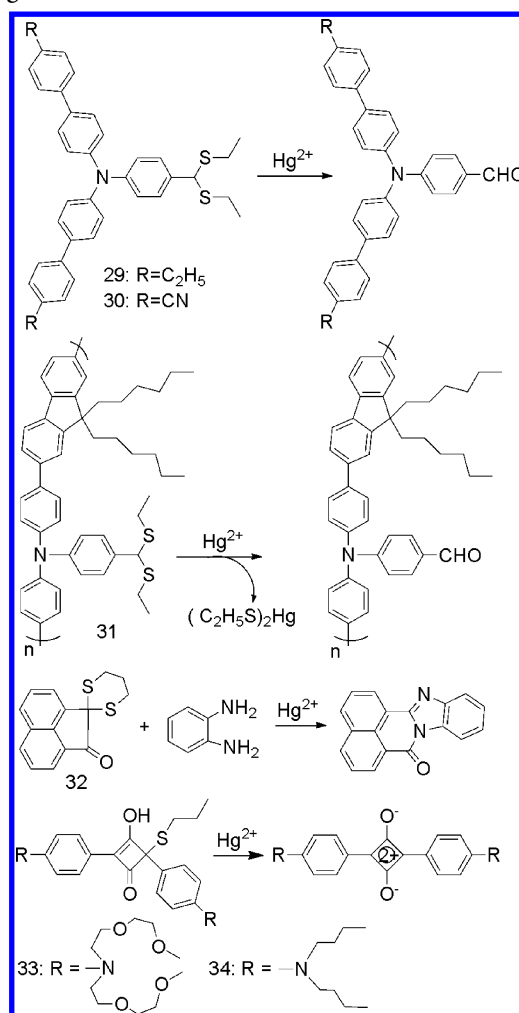
Recently, Tian and co-workers have demonstrated that, unlike the fluorescent blue-shift of 13–22, tricarbocyanine dyes 23–25⁹³ with near-infrared (NIR) fluorescence show significant red-shifts in their fluorescence emission upon exposure to Hg²⁺ ions, allowing ratiometric detection. For chemodosimeters 23–25, mercury-promoted desulfation and intramolecular cyclic guanylation of thiourea cause a decrease of the electron-donating ability of the NH group, corresponding to the amine group in the benzoindole moiety becoming the main

donor and resulting in an increase of the degree of π -conjugation. As a result, 23–25 display a characteristic fluorescence turn-off mode at 780 nm and a turn-on mode at 830 nm upon exposure to Hg^{2+} ions. These dyes also have excellent membrane permeability and low toxicity. In particular, 23 and 24 can be successfully used to monitor Hg^{2+} in living cells.⁹³

Scheme 6. Fluorescent Hg^{2+} Chemodosimeters 26–28 Based on Hg^{2+} -Induced Desulfuration and Cyclization Reactions



Scheme 7. Fluorescent Hg^{2+} Chemodosimeters 29–34 Based on Hg^{2+} -Induced Thiol Elimination Process



(2). *Formation of Other Heterocyclic Compounds.* There are also other cyclization reactions that can be utilized for designing Hg^{2+} chemodosimeters, accompanied by a formation of 1,3,4-oxadiazole, triazanaphthalene, or coumarin. On the basis of the Hg^{2+} -induced desulfurization of thiourea and formation of the 1,3,4-oxadiazole moiety, Ramamurthy and co-workers reported a series of fluorescence turn-off chemodosimeters (26,⁹⁵ Scheme 6), accompanying an efficient intramolecular photoinduced electron transfer (PET) process. Furthermore, 26e has successfully been used for two-photon fluorescence imaging of Hg^{2+} in living cells. Chemodosimeter 27 is based on the Hg^{2+} -promoted desulfurization of thiourea to form a triazanaphthalene ring, resulting in a turn-on fluorescence response for Hg^{2+} in aqueous media.⁹⁶ In addition, 28 utilizes Hg^{2+} -catalyzed facile desulfurization–lactonization cascade transformation,⁹⁷ which generates a highly emissive coumarin derivative from a nonfluorescent stannum precursor and produces a highly selective and sensitive turn-on fluorescent chemodosimeter for Hg^{2+} in pure aqueous media.

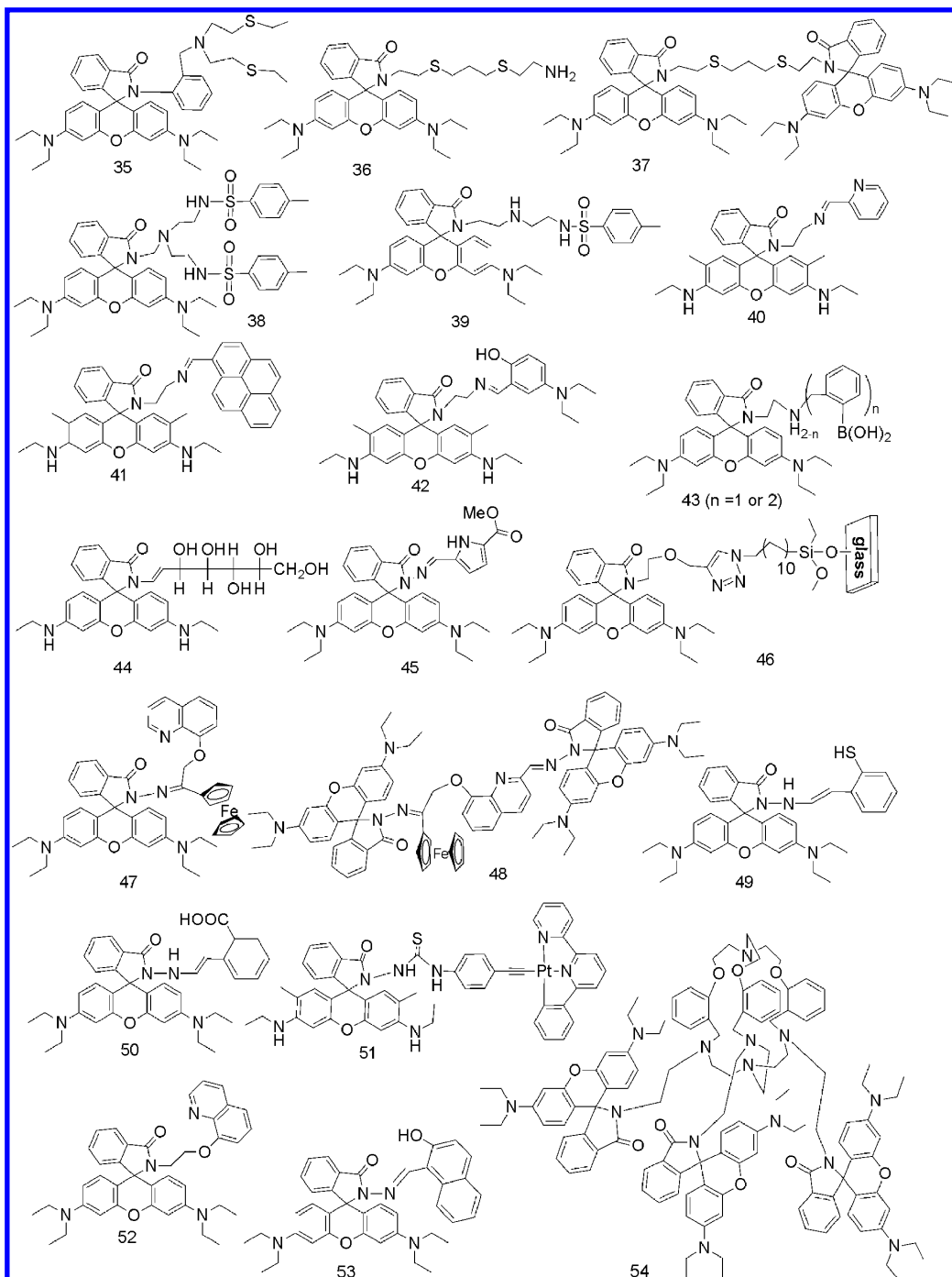
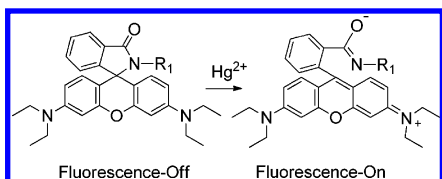
5.1.3. Thiol Elimination Process. Another design strategy for luminescent chemodosimeters for Hg^{2+} is based on the Hg^{2+} -induced thiol elimination reaction. It is well-known that the aldehyde group protected by mercaptan can be converted to the previous aldehyde only in the presence of Hg^{2+} . Utilizing this reaction mechanism, Hg^{2+} -selective chemodosimeters 29–30⁹⁸ and 31⁹⁹ (Scheme 7) with fluorescence turn-on response or spectral shift or both can be realized. Furthermore, 32 utilizes a Hg^{2+} -induced thiol elimination and intermolecular

cyclization reaction (Scheme 7).¹⁰⁰ Likewise, for chemodosimeters 33 and 34 (Scheme 7), the addition of Hg^{2+} induces the thiol elimination reaction and leads to the recovery of the intramolecular charge transfer (ICT) process and the release of squaraine dye, corresponding to a chromo- and fluorogenic “switching-on” response for Hg^{2+} .¹⁰¹

5.1.4. Rhodamine Spirolactam Ring-Opening Process.

Rhodamine dyes are widely used as fluorescent probes owing to their high absorption coefficient, fluorescence emission in visible region, and high fluorescence quantum yield.^{102–104} Spirolactam-type rhodamine derivatives are nonfluorescent and colorless, whereas spirolactam ring-opening gives rise to strong fluorescence emission and a pink color. Some metal cations can induce spirolactam ring-opening process, and great progress has achieved in the development of new luminescent chemodosimeters based on this process in the past several years.^{102–104} To date, approximately 35 rhodamine derivatives (35–68) have been reported as Hg^{2+} -selective chemodosimeters based on this spirolactam ring-opening process (Chart 1). Most of these chemodosimeters show fluorescent turn-on responses.

To promote mercury-induced spirolactam ring-opening, N-, O-, and S-based chelating groups have been introduced at the R_1 position of the rhodamine system (Scheme 8). For example, chemodosimeters 35,¹⁰⁵ 36,¹⁰⁶ and 37¹⁰⁶ contain sulfur atoms

Chart 1. Hg^{2+} -Selective Chemodosimeters Based on Mercury-Induced Spirolactam Ring-Opening ProcessesScheme 8. Proposed Mechanism Based on Hg^{2+} -Induced Spirolactam Ring-Opening Process

as the binding sites. Probe 38¹⁰⁷ is a novel tris(2-aminoethyl)-amine (tren)-based tripodal chemodosimeter that bears a rhodamine and two tosyl groups. Compared with 39,¹⁰⁷ which contains one tosyl group, 38 exhibits a more sensitive and

selective binding ability toward Hg^{2+} ions, with an association constant of $1.59 \times 10^6 M^{-1}$. This implies that the tripodal structure (tren) is superior to the dipodal group (diethylenetriamine) for Hg^{2+} binding. In addition, several other rhodamine derivatives (40,¹⁰⁸ 41,¹⁰⁹ 42,¹¹⁰ 43,¹¹¹ 44,¹¹² 45,¹¹³ and 46¹¹⁴) containing multichelate groups have also been developed as Hg^{2+} -selective chemodosimeters giving a fluorescence turn-on response. In particular, a fluorescent self-assembled monolayer on a glass substrate has been prepared based on 46, giving facile Hg^{2+} detection in water.¹¹⁴

To improve the complexation of Hg^{2+} , 8-hydroxyquinoline was introduced as a coordination site, and a new multisignaling chemodosimeter 47¹¹⁵ having a ferrocene substituent has been

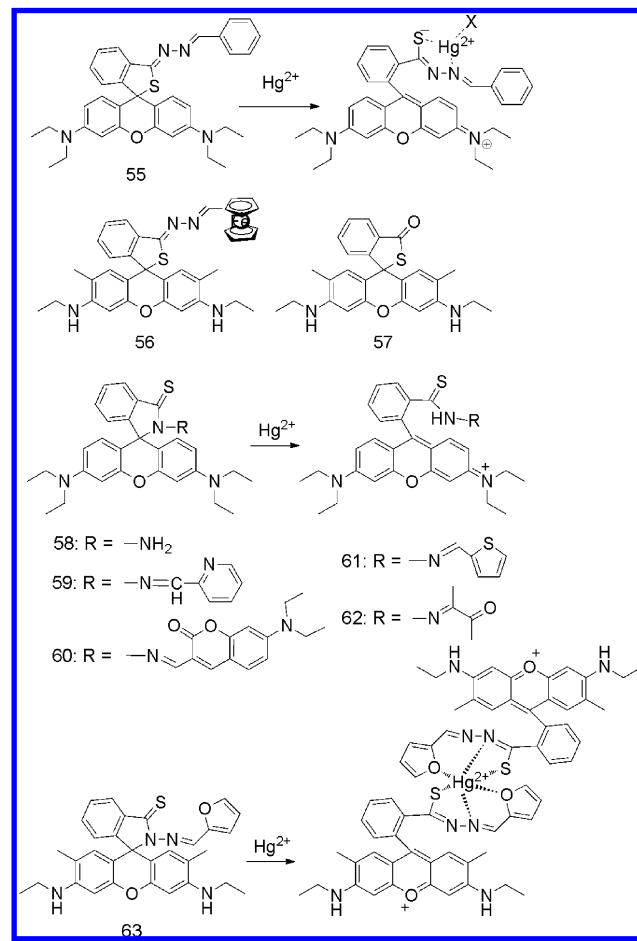
developed by our group. By means of confocal fluorescence microscopy experiments, **47** can be used as an off-on fluorescent probe to monitor Hg^{2+} in living cells and to map its subcellular distribution (Figure 2). Similar results were also obtained for chemodosimeter **48**.¹¹⁶ In addition, two hydrazone derivatives (**49** and **50**)¹¹⁷ bearing thiol and carboxylic acid groups, respectively, were also designed as selective fluorescence turn-on chemodosimeters for visualizing Hg^{2+} accumulated in the nematode *Caenorhabditis elegans*, demonstrating that they could be employed for in vivo imaging of nanomolar concentrations of Hg^{2+} . For chemodosimeter **51**,¹¹⁸ which contains a cyclometalated platinum(II) complex, the presence of the Pt(II)-alkynyl moiety improves the nonlinear absorption property, and **51** has been applied successfully to the two-photon fluorescence imaging of Hg^{2+} in living cells. In addition, **52**¹¹⁹ and **53**¹²⁰ can also be used to monitor Hg^{2+} in living cells with turn-on fluorescence response.

Another successful rhodamine-based Hg^{2+} probe, which displays high selectivity and sensitivity, is chemodosimeter **54**¹²¹ conjugated with a cryptand ligand. Hg^{2+} ions bind from outside the cryptand cavity, which accelerates the spirolactam bond cleavage and allows a more selective response. As a result, **54** can selectively detect Hg^{2+} ion in aqueous media at ppb level in the presence of other biologically relevant metal ions. Moreover, **54** also shows good biocompatibility in the HEK 293 cell line.

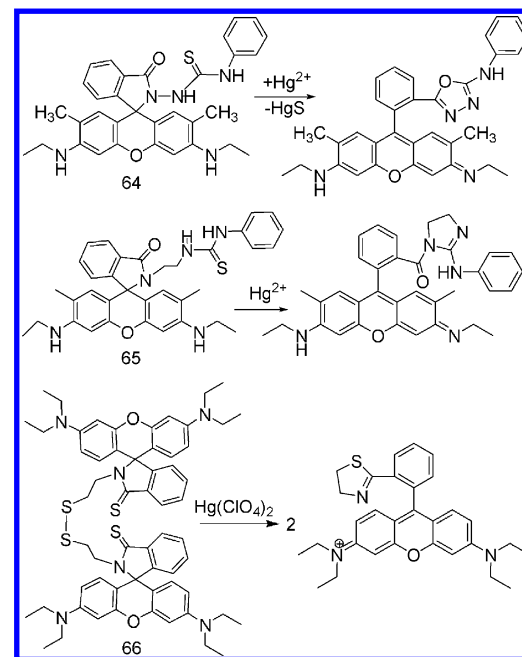
5.1.5. Sulfur-Containing Rhodamine Spirolactam Ring-Opening Process. Taking advantage of the high thiophilicity of the Hg^{2+} ion, the introduction of a S atom into the amide of rhodamine, to form a thioamide or thioether, is another useful strategy of designing rhodamine-based chemodosimeters for Hg^{2+} . To date, three rhodamine thioethers (**55**,¹²² and **56** and **57**¹²³) and six rhodamine thioamides (**58**,¹²⁴ **59**,¹²² **60**,¹²⁵ **61**,¹²⁶ **62**,¹²⁷ and **63**¹²⁸) have been reported (Scheme 9), and they allow the highly selective detection of Hg^{2+} with a fluorescence turn-on response. Among these chemodosimeters, **57**, **61**, and **63** have been successfully applied in fluorescent bioimaging. Yoon and co-workers reported that the rhodamine thioether **57** showed 200-fold fluorescence enhancement in CH_3CN -HEPES buffer (0.01 M, pH 7.4) (1:99, v/v), only upon addition of Hg^{2+} among the various metal ions examined.¹²³ Furthermore, **57** can detect Hg^{2+} at concentrations as low as the nanomolar range, making it viable for fluorescent bioimaging. Chemodosimeter **61** was designed to combine a thiospirolactam chromophore and a thiophene ring.¹²⁶ It exhibits high selectivity and excellent sensitivity toward Hg^{2+} in aqueous solution. Moreover, **61** has been successfully applied in the fluorescent imaging of Hg^{2+} in MCF-7 cells.

5.1.6. Spirolactam Ring-Opening and Cyclization Processes. The one-step mercury-induced spirolactam ring-opening process discussed above is usually reversible, leading to relatively low sensitivity. Recently, two-step reactions involving spirolactam ring-opening and subsequent cyclization processes based on rhodamine derivatives have been developed in the design of Hg^{2+} -selective chemodosimeters (Scheme 10). Such an approach was first reported by the Tae group. Through a Hg^{2+} -promoted desulfurization reaction of thiourea, a spiro-lactam ring-opening process, and a cyclization reaction to form a 1,3,4-oxadiazole, they designed rhodamine-based chemodosimeter **64**.¹²⁹ Addition of Hg^{2+} ions to a water-methanol (4:1, v/v) solution of **64** caused an instantaneous 26-fold increase in fluorescence intensity. The selectivity of **64** for Hg^{2+}

Scheme 9. Fluorescent Sulfur Atom-Containing Chemodosimeters 55–63 Based on Hg^{2+} -Induced Spirolactam Ring-Opening Processes



Scheme 10. Fluorescent Chemodosimeters 64–66 Based on Hg^{2+} -Induced Spirolactam Ring-Opening and Cyclization Processes



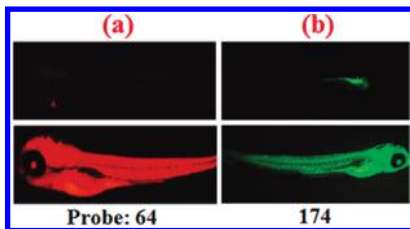
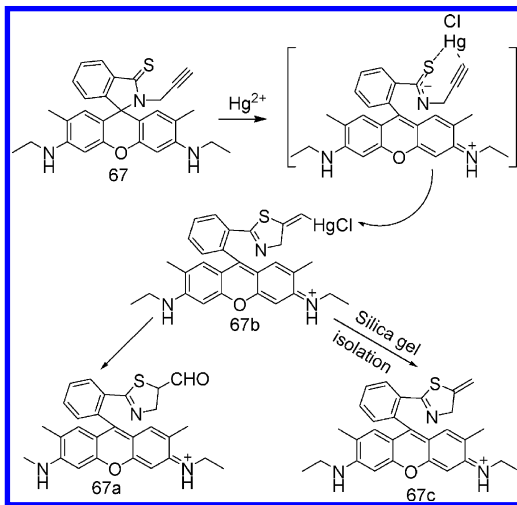


Figure 3. In vivo fluorescence imaging of zebrafish pretreated without (upper) and with (lower) Hg^{2+} (or Pd^{2+}) using the chemodosimeter **64** (or **174**) as fluorescent probe, respectively. Reprinted with permission from refs 130 and 280. Copyright 2006 American Chemical Society and Copyright 2010 Royal Society of Chemistry, respectively.

over other metal ions is remarkably high, and its sensitivity is <2 ppb in aqueous solution. Furthermore, Tae and co-workers demonstrated that **64** could be applied in monitoring the real-time uptake of Hg^{2+} ions in living cells (Figure 2) and the accumulation of Hg^{2+} ions in organisms (Figure 3).^{130,131} Similarly, through a Hg^{2+} -induced intramolecular guanylation, **65**¹³² can be used to determine Hg^{2+} within a wide pH range (5–10) with turn-on fluorescence. Thiorhodamine **66**,¹³³ which is a disulfide-linked dimer, exhibits real-time responses toward Hg^{2+} ions in a wide pH range from 4 to 9. The mechanism is ascribed to the transformation of the thiorhodamine spirolactam to a ring-opened thiazoline-derivative

Scheme 11. Sensing Mechanism of Chemodosimeter 67 by Hg^{2+} -Induced Spirolactam Ring-Opening and Cyclization Processes



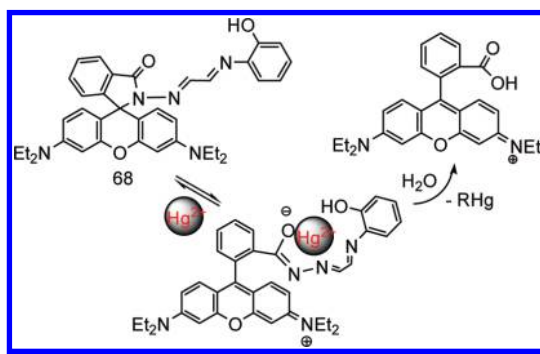
through Hg^{2+} -induced desulfurization. Because of its extremely high sensitivity and unique selectivity for Hg^{2+} , **66** has been developed for monitoring mercury levels in living HK-2 cells. Moreover, low concentration of Hg^{2+} could be detected, including concentration at the human safety limit.¹³³

Interestingly, in another chemodosimeter **67**,¹³⁴ both the S atom and the alkyne moiety were found to play a cooperative role in the sensing mechanism (Scheme 11). Compounds **67a** and **67b** were formed in the absence or presence of H_2O , respectively, which is dependent on protonolysis. In contrast to the sensing mechanisms of **64–66** introduced previously, the S atom of **67** is not removed during this process but instead takes part in the cyclization process. The chemodosimeter **67** is

further applicable to Hg^{2+} mapping in living cells with a turn-on fluorescent response.¹³⁴

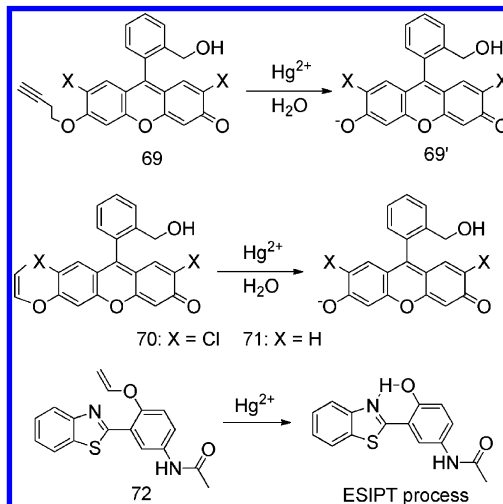
5.1.7. Spirolactam Ring-Opening and Hydrolysis Processes. Because of the thiophilicity of Hg^{2+} ions, Hg^{2+}

Scheme 12. Sensing Mechanism of Chemodosimeter 68 by Hg^{2+} -Induced Spirolactam Ring-Opening and Hydrolysis Processes



monitoring in living biosamples is usually hampered by the presence of cysteine (Cys) and glutathione (GSH). Recently, on the basis of the Hg^{2+} -induced spirolactam ring-opening and hydrolysis processes, Peng and co-workers have developed an interesting fluorescent chemodosimeter **68**¹³⁵ for detection of Hg^{2+} without interference from Cys and GSH. In the presence of Hg^{2+} , the complex **68**– Hg^{2+} has been shown to induce ring-opening and was further hydrolyzed to form fluorescent rhodamine B in the presence of water (Scheme 12). As a result, after addition of Hg^{2+} , the intensity of fluorescence emission at 579 nm was enhanced by >370 -fold. In particular,

Scheme 13. Sensing Mechanism of Chemodosimeters 69–72 by Hg^{2+} -Induced Alkyne or Vinyl Ether Oxymercuration Process



68 can distinguish between safe and toxic levels of Hg^{2+} in more complex natural water systems and can also detect Hg^{2+} in sulfur-rich environments, such as in living cells (Figure 2).¹³⁵

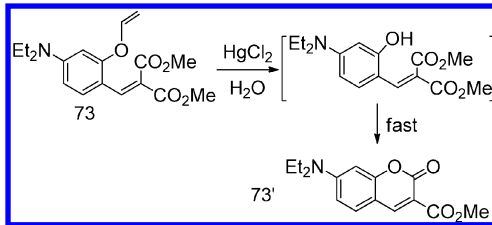
5.1.8. Alkyne or Vinyl Ether Oxymercuration Process.

(1). *Oxymercuration–Elimination of Alkyne Ether.* Because of the affinity of Hg^{2+} toward alkynes, Hg^{2+} can catalyze the hydration of alkynes to their corresponding ketone.¹³⁶ This mechanism has been used to generate excellent Hg^{2+}

chemodosimeters (Scheme 13). Koide and co-workers reported the nonemissive fluorescein derivative containing an alkyne group **69**¹³⁷ that detects Hg^{2+} based on an oxymercuration–elimination reaction. Addition of Hg^{2+} results in the formation of a new compound **69'**, with a 219-fold enhancement in fluorescence intensity.¹³⁷ This chemodosimeter **69** is very sensitive and specific, and has been used to monitor mercury concentrations in fish.

(2). *Oxymercuration–Elimination of Vinyl Ether*. Koide and co-workers have also developed two Hg^{2+} -sensitive chemodosimeters (**70**¹³⁸ and **71**,¹³⁸ Scheme 13), taking advantage of a vinyl ether oxymercuration mechanism for detection. Hg^{2+} -promoted hydrolysis of the nonfluorescent vinyl ethers **70** and **71** leads to the formation of highly fluorescent products **70'** and **71'**. This method allows the detection of Hg^{2+} in river water and dental samples. Chemodosimeter **71** was found to be 242 times more reactive than the probe **70** toward Hg^{2+} at ambient temperature.¹³⁸ In addition, utilizing the Hg^{2+} -promoted hydrolysis of vinyl ether and the formation of an excited-state intramolecular proton transfer (ESIPT) process in the product, a ratiometric

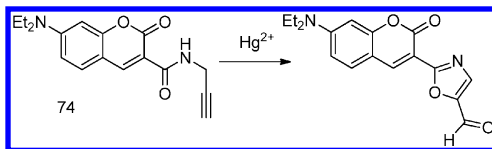
Scheme 14. Sensing Mechanism of 73 by Hg^{2+} -Promoted Hydrolysis of Vinyl Ether and Cyclization Reaction



luminescent chemodosimeter **72**¹³⁹ for Hg^{2+} was realized. This shows a marked fluorescence change from blue to cyan (a bathochromic shift of ~ 80 nm) by virtue of the ESIPT process.

5.1.9. Hg^{2+} -Promoted Hydrolysis of Vinyl Ether and Cyclization Reaction. Chemodosimeter for Hg^{2+} can also be realized based on both the above Hg^{2+} -promoted hydrolysis of the vinyl ether group and a subsequent cyclization reaction (Scheme 14). Using this strategy, the nonemissive chemo-

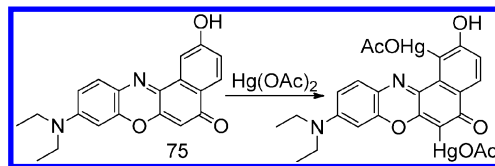
Scheme 15. Sensing Mechanism of 74 by Hg^{2+} -Mediated Propargyl Amide to Oxazole Transformation



dosimeter **73**¹⁴⁰ can be converted into a highly fluorescent coumarin derivative **73'** upon addition of Hg^{2+} , in other words, a turn-on fluorescence response.

5.1.10. $Hg^{(II)}$ -Mediated Propargyl Amide to Oxazole Transformation. Recently, a new Hg^{2+} chemodosimeter **74**¹⁴¹ was reported based on the alkynophilicity of Hg^{2+} . For **74**, Hg^{2+} can activate the alkyne and induce a cyclization reaction to afford an oxazole ring (Scheme 15). Thus, a noticeable red-shift with increasing fluorescence intensity was observed for **74** upon addition of Hg^{2+} , giving a ratiometric fluorescent response. **74** also exhibits high selectivity for Hg^{2+} over other metal ions in aqueous ethanol media.

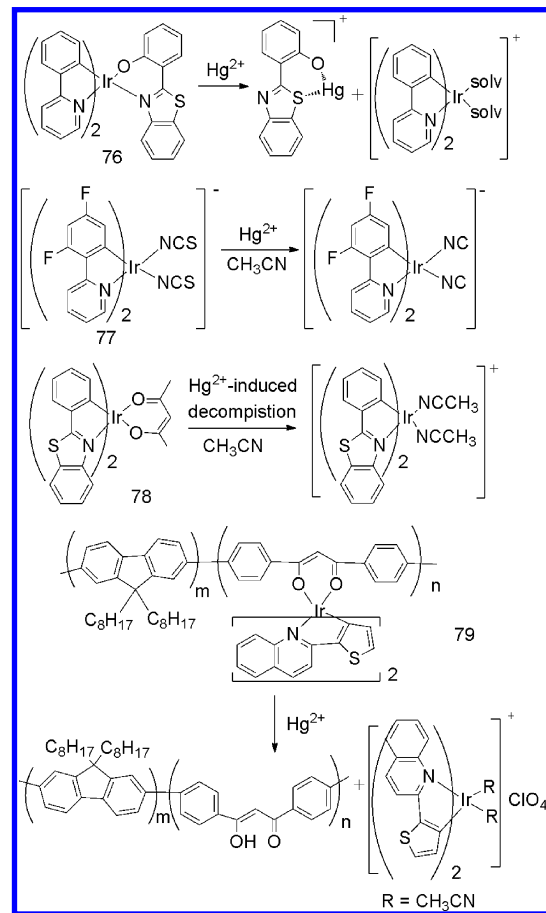
Scheme 16. Sensing Mechanism of 75 by Mercuration Reaction



5.1.11. Selective Mercuration Reaction. Mercuration of a fluorescence dye can be used for designing a Hg^{2+} -selective chemodosimeter (Scheme 16). The 2-hydroxy derivative of Nile Red **75**¹⁴² exhibits a significant fluorescent change with Hg^{2+} ions in aqueous environments by selective dimercuration at the 1,6-positions. This has been confirmed by ¹H NMR measurements.

5.1.12. Phosphorescent Chemodosimeters for Hg^{2+} . All chemodosimeters for Hg^{2+} discussed above are based on fluorescent organic molecules. Because of the advantages of phosphorescence signals, such as relatively long emission

Scheme 17. Phosphorescent Hg^{2+} Chemodosimeters 76–79 Based on Iridium(III) Complexes



lifetimes and significant Stokes shifts for easy separation of excitation and emission,^{19,143,144} we have recently reported several iridium(III) complexes containing a sulfur atom in the ligand as phosphorescent chemodosimeters for Hg^{2+} . The general sensing principle is based on the specific coordination between Hg^{2+} and sulfur to tune the excited-state properties (Scheme 17). Complex **76**,¹⁴⁵ containing a sulfur atom in the $N^{\wedge}O$ ligand, could serve as a highly selective chemodosimeter

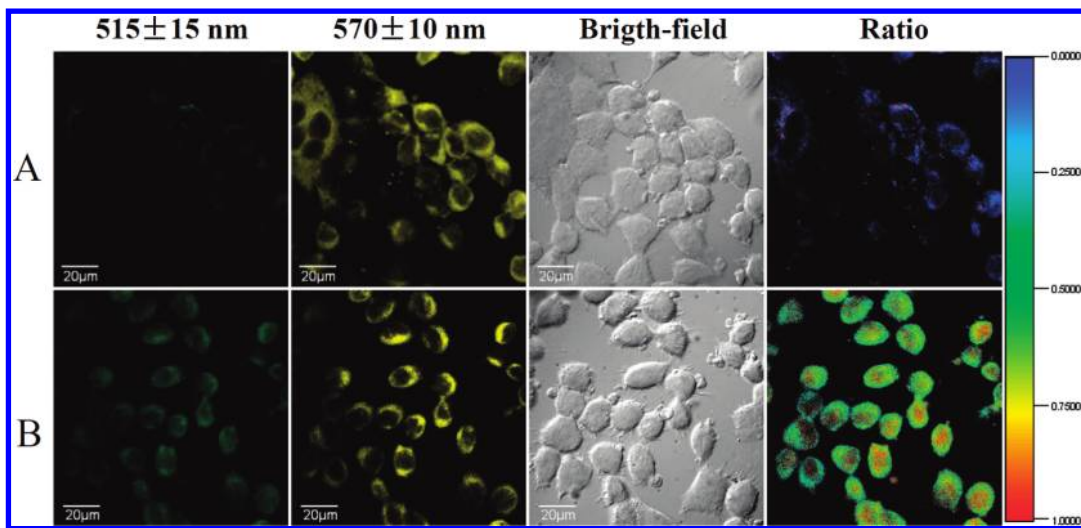
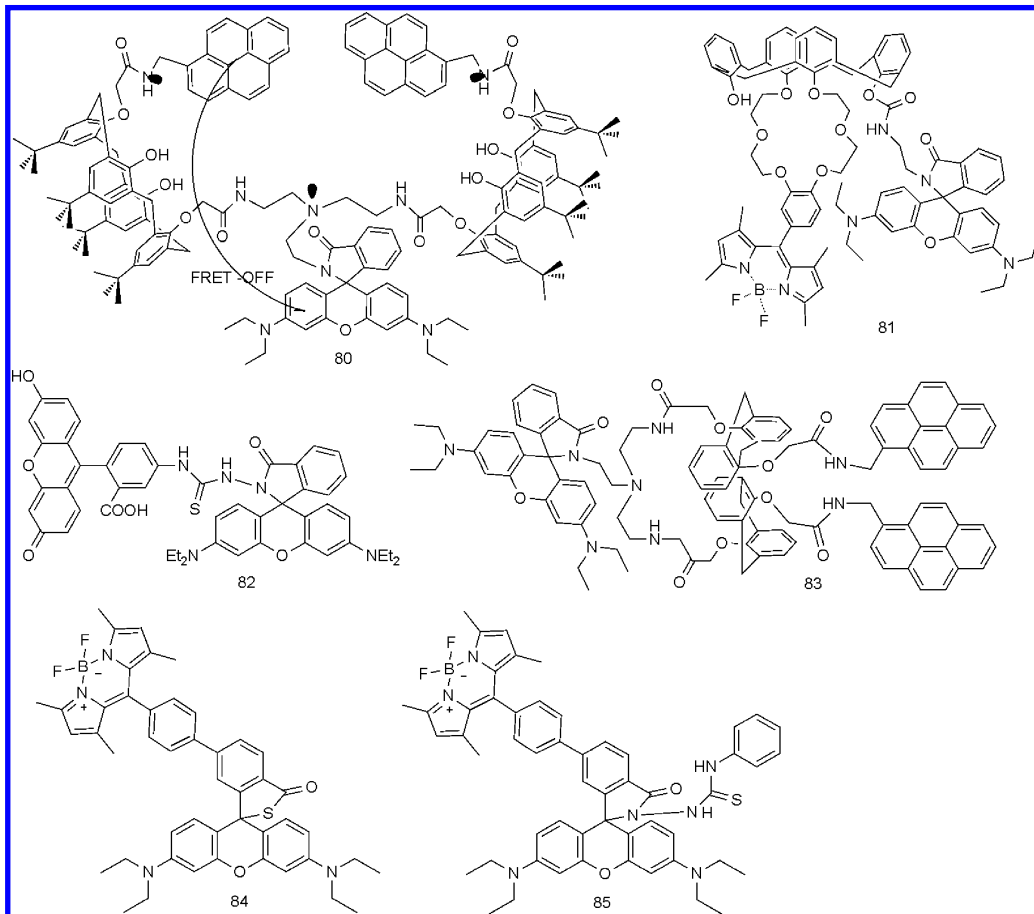


Figure 4. Ratiometric phosphorescence images of KB cells incubated with **78** for 15 min (A) and then further treated with 100 μM Hg^{2+} for 1 h (B). Emission was collected by the green channel ($515 \pm 15 \text{ nm}$) and yellow channel ($570 \pm 10 \text{ nm}$) ($\lambda_{\text{ex}} = 405 \text{ nm}$). Ratio of emission intensity at $515 \pm 15 \text{ nm}$ to $570 \pm 10 \text{ nm}$ is also shown. Reprinted with permission of ref 147. Copyright 2011 American Chemical Society.

Chart 2. FRET-Based Hg^{2+} Chemodosimeters (80–85) with Rhodamine Unit As an Energy Acceptor



for Hg^{2+} using ratiometric phosphorescence detection. The sensing mechanism has been assigned to the Hg^{2+} -induced dissociation of the $\text{N}^{\text{+}}\text{O}$ ligand of **76**. Another turn-off type phosphorescent chemodosimeter, **77**,¹⁴⁶ for Hg^{2+} was based on the special chemical reaction between Hg^{2+} and the sulfur atom of the thiocyanate group. For complex **78**,¹⁴⁷ containing sulfur atoms in $\text{C}^{\text{+}}\text{N}$ ligands, addition of Hg^{2+} to its acetonitrile

solution induced significant blue-shifts in both absorption and phosphorescent emission bands, which can be assigned to the Hg^{2+} -induced decomposition of **78** to form a new solvent complex. Moreover, using a ratiometric phosphorescence mode, **78** can readily monitor the changes in intracellular Hg^{2+} concentration (Figure 4).¹⁴⁷

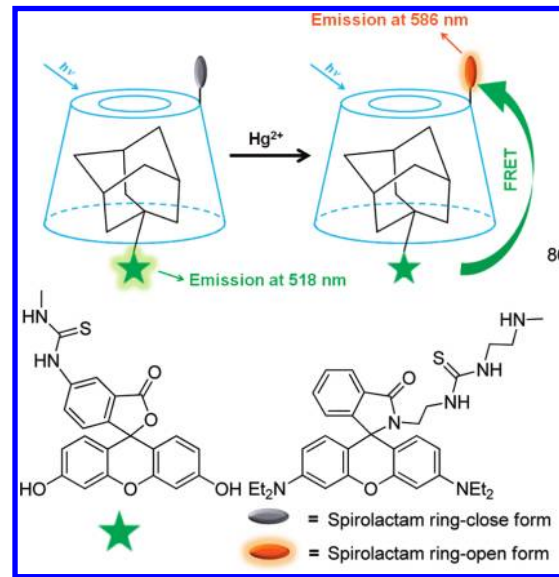
Considering the amplified signal outputs of conjugated polymers,¹⁴⁸ Huang and Zhao et al. have recently developed a series of polyfluorenes containing phosphorescent Ir(III) complexes (**79**¹⁴⁹) as ratiometric chemodosimeters for Hg²⁺. In the absence of Hg²⁺, efficient energy transfer occurs between polyfluorenes and Ir(III) complexes, resulting in red phosphorescent emission. The addition of Hg²⁺ can induce the decomposition of Ir(III) complex moieties and an intrachain charge-transfer state can occur in the polymers, leading to yellow-green fluorescence emission. Thus, the addition of Hg²⁺ induced a switch between phosphorescence and fluorescence signals, realizing ratiometric detection. Such a conversion of phosphorescence into fluorescence emission is significantly different from the small-molecular iridium complexes for Hg²⁺ detection.^{150,151} Furthermore, solid films of these polymer chemodosimeters also exhibited high sensitivity and rapid response to Hg²⁺, which is very helpful for their practical application as portable sensing devices.

5.1.13. FRET-Based Chemodosimeters for Hg²⁺. The above chemodosimeters are mainly based on a change in fluorescent intensity. Compared with intensity-based chemodosimeters, ratiometric detection based on two distinct measurable signals in the presence or absence of the analyte exhibits some advantages, such as minimization of potential external interference from variations in chemodosimeter concentration and environment.^{152,153} FRET imaging, which affords simultaneous recording of two fluorescent intensities at different wavelengths in the presence and absence of analyte, provides a facile method for visualizing complex biological processes at the molecular level. Hence, significant efforts have been made to design FRET-based chemodosimeters.

Recently, several FRET-based chemodosimeters (**80**,¹⁵⁴ **81**,¹⁵⁵ **82**,¹⁵⁶ **83**,¹⁵⁷ **84**,¹⁵⁸ **85**,¹⁵⁸ and **86**¹⁵⁹) have been successfully used to monitor Hg²⁺ in living samples (Chart 2). The design principle for these chemodosimeters has been based on a Hg²⁺-induced ring-opening reaction of spirolactam, with the rhodamine unit as an energy acceptor. The energy donors used differed between chemodosimeters **80**, **81**, **82**, and **86** with pyrene, boron dipyrromethene (BODIPY), and fluorescein isothiocyanate (FITC), respectively.

Recently, Qian and co-workers reported that two ratiometric fluorescence chemodosimeters (**84** and **85**) exhibited excellent sensitivity and selectivity for Hg²⁺, as well as pH insensitivity.¹⁵⁸ In the absence of Hg²⁺, the emission spectrum of **85** displayed the features of the BODIPY unit only. Upon addition of Hg²⁺, however, spirolactam ring-opening and cyclization processes were induced, and a highly efficient FRET from BODIPY to rhodamine then occurred, resulting in decreased BODIPY emission at 510 nm and increased rhodamine emission at 584 nm. After rapid incubation with Hg²⁺ for 6 min, **85**-treated HeLa cells showed fluorescence color changes from green to yellow-orange when studied using confocal fluorescence microscopy (Figure 2). Similar results were also obtained for **84**. Interestingly, **85** exhibited higher sensitivity and faster response than **84**, which may be due to the use of a Hg²⁺-promoted desulfurization reaction of thiourea, a spirolactam ring-opening process, and a cyclization reaction to form 1,3,4-oxadiazole for **85**.¹⁵⁸ In addition, Zeng and co-workers reported a supramolecular FRET-based chemodosimeter **86** that uses the host-guest interaction of β -cyclodextrin and adamantine (Scheme 18).¹⁵⁹ Upon interaction with Hg²⁺ ion, the rhodamine unit undergoes a ring-opening process and serves as the energy acceptor, which constitutes the FRET system

Scheme 18. Supramolecular FRET-Based Hg²⁺ Chemodosimeter **86 with Rhodamine Unit As an Energy Acceptor**



with the FITC donor. The cyclodextrin not only conjugates with the FITC and rhodamine unit but also makes **86** water-soluble and cell-membrane permeable.

5.1.14. Upconversion Luminescence-Based Energy Transfer Chemodosimeters for Hg²⁺. If rare-earth ions-based luminescent centers act as donors in the similar energy-transfer process, it is usually called a luminescence resonance energy-transfer (LRET) process. Because of some special luminescent properties, such as long lifetime and narrow emission band, originated from the characteristic f-f transitions of rare earth ions, this LRET process can have longer effective distance between donors and acceptors. Under continuous-wave excitation at 980 nm, rare-earth nanoparticles (NPs) codoped with Yb³⁺ (sensitizer) and Er³⁺ or Tm³⁺ (emitter) show unique upconversion luminescence (UCL) with sharp emission lines, long luminescence lifetime, a large anti-Stokes shift of several hundred nanometers, and superior photostability,^{160,161} and they have been applied in high-contrast bioimaging with no autofluorescence from the biosamples.¹⁶²⁻¹⁷¹ Recently, Liu and co-workers have reported that the UCL-based LRET effect can be achieved between different rare-earth ions, and the process can be observed even among different nanoparticles.¹⁷² This result suggests that the UCL-based LRET process has a longer effective distance than the commonly used system, profiting the possible application of such a kind of FRET chemodosimeter.

Recently, we have demonstrated a water-soluble NaYF₄:20% Yb, 1.6% Er, 0.4% Tm upconversion nanophosphors (UCNPs) coated with a chromophoric ruthenium complex **87**, as a Hg²⁺-selective chemodosimeter for UCL bioimaging (Figure 5).¹⁷³ The strategy is based on modulating upconversion luminescence-based energy transfer (UCLET) in this dye-assembled nanosystem **87**-UCNPs comprised of a upconversion luminescence donor (UCNPs) and a Hg²⁺-respective acceptor (**87**). Upon addition of Hg²⁺, the absorption peak of **87** was blue-shifted (~55 nm). This led to a reduced overlap between UCL emission of Er³⁺ and absorption of **87**, resulting in the enhancement of UCL emission of Er³⁺ at 541 nm. Using UCL at 800 nm of Tm³⁺ as the internal standard, this dye-assembled

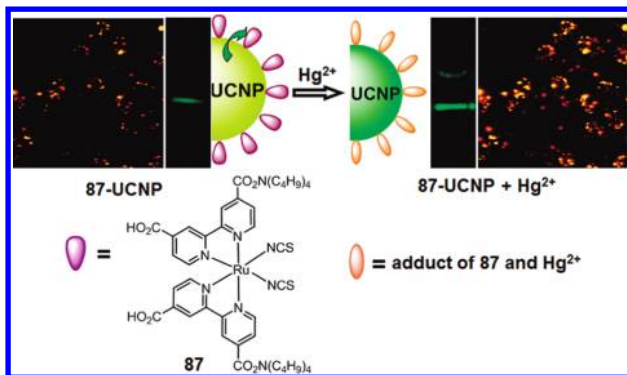
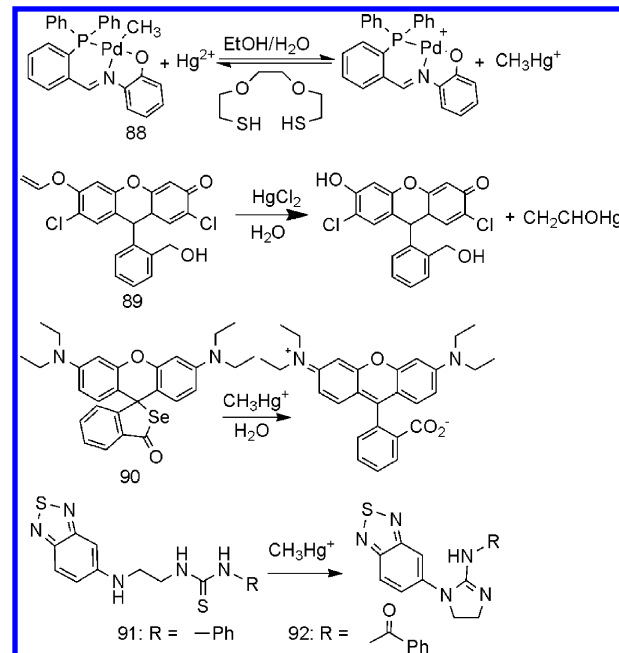


Figure 5. Schematic illustration of 87–UCNPs and its upconversion luminescence (UCL) response to Hg^{2+} in aqueous solution and in living cells. UCL images of HeLa cells incubated with 200 $\mu\text{g}/\text{mL}$ 87–UCNPs for 3 h (left) and then further incubated with Hg^{2+} for 15 min (right). $\lambda_{\text{ex}} = 980 \text{ nm}$; $\lambda_{\text{em}} = 540 \pm 20 \text{ nm}$. Reprinted with permission from ref 173. Copyright 2011 American Chemical Society.

nanosystem 87–UCNPs can be used for ratiometric UCL imaging to detect Hg^{2+} in aqueous solution with high selectivity, a rapid response time (<10 s), and excellent sensitivity (detection limit of 1.95 ppb). Such a detection limit of Hg^{2+} is only one-tenth that of pure complex 87 in chromophoric sensing Hg^{2+} . Importantly, the nanoprobe 87–UCNPs has been shown to be capable of monitoring changes in the distribution of Hg^{2+} in living cells by UCL bioimaging (Figure 5).¹⁷³

5.1.15. Luminescent Chemodosimeters for Bioimaging Methylmercury. Although a variety of luminescent chemodosimeters for imaging mercury ions have been developed in recent years, those that allow the evaluation of methylmercury (CH_3Hg^+) accumulation in the living environment remain not well developed. Because of the particularly high toxicity of methylmercury toward humans,^{174,175} its monitoring is very important. Torroba and co-workers reported

Scheme 19. Sensing Mechanism of Hg^{2+} Chemodosimeters 88–92



the first chemodosimeter, 88¹⁷⁶ (Scheme 19), that allows selective naked-eye detection of CH_3Hg^+ and Hg^{2+} . Unfortunately, this organopalladium regenerative chemodosimeter 88 is not fluorescence-active. Recently, Shin and co-workers have reported an exciting chemodosimeter 89¹⁷⁷ for inorganic and methylmercury species based on the mercury-promoted hydrolysis reaction of vinyl ethers as discussed in section 5.1.7. Upon addition of methylmercury species or HgCl_2 , 89 became strongly emissive. Comparing the fluorescence recovery time, CH_3HgCl was found to act more slowly than HgCl_2 . Most importantly, 89 was effective for the fluorescent imaging of mammalian cells and organisms incubated with organomercury species. In addition, Yoon and co-workers demonstrated that the selenolactone-based chemodosimeter 90¹⁷⁸ could detect inorganic mercury/methylmercury species in cells (Figure 2) with fluorescence enhancement. Interestingly, 90 can also image the zebrafish organs treated with mercury species HgCl_2 or CH_3HgCl (Figure 6) by fluorescence microscopy. The detection mechanism can be assigned to the removal of selenium. In addition, on the basis of the CH_3Hg^+ -induced transformation of the thiourea unit of the chemodosimeter into an imidazoline moiety by the removal of CH_3HgSH , Tian's group has designed and synthesized two organic compounds 91 and 92 as fluorescent chemodosimeters for detecting CH_3Hg^+ with high selectivity and sensitivity in aqueous solution.¹⁷⁹

5.2. Luminescent Chemodosimeters for Cu^{2+}

Copper is the third most abundant essential trace element in the human body after zinc and iron; it plays a vital role in many cellular processes including gene expression and the functioning and structural enhancement of proteins, and is also required by the human nervous system.^{180,181} Copper deficiency may lead to various diseases. In contrast, high levels of copper ions may also lead to Wilson disease, gastrointestinal disorders, and kidney damage.¹⁸² As a result, the sensing and recognition of copper ions has attracted considerable attention in recent years, and numerous fluorescent sensors for copper ions have been developed.^{70,183,184} Most of these involve a turn-off process, however, as copper ions often act as a quencher via energy- or electron-transfer processes, and this limits their application in bioimaging. Herein, we focus on the luminescent chemodosimeters that have been developed for copper ion bioimaging, based on different reaction mechanisms.

5.2.1. Cu^{2+} -Coordination-Induced Spirolactam Ring-Opening Process. In addition to Hg^{2+} , Cu^{2+} can also induce the spirolactam ring-opening process of rhodamine derivatives, which has become the major strategy for designing Cu^{2+} -selective luminescent chemodosimeters with a luminescence turn-on response (Chart 3). In the reported chemodosimeters 93 ($n = 1–5$),^{185,186} 94,¹⁸⁷ 95,¹⁸⁸ and 96¹⁸⁹ 97,¹⁸⁹ 98¹⁹⁰ and 99,¹⁹¹ 100,¹⁹² 101,¹⁹³ 102,¹⁹⁴ 103,¹⁹⁵ 104,¹⁹⁶ 105,¹⁹⁷ 106,¹⁹⁸ 107,¹⁹⁹ 108,²⁰⁰ 109,²⁰¹ and 110,²⁰² some nitrogen-, oxygen-, and sulfur-containing chelate groups are used as the coordination sites of Cu^{2+} . Interestingly, 104¹⁹⁶ can act as a dual-mode Cu^{2+} -selective chemodosimeter via a fluorescence off-on response arising from the rhodamine ring-opening mechanism and a ratiometric fluorescent signal when Cu^{2+} displaces the bound Zn^{2+} in the 104– Zn^{2+} complex. In addition, dual-rhodamine derivative 111²⁰³ and tripodal receptor 112²⁰⁴ have also been reported for the selective and sensitive determination of Cu^{2+} based on the same process.

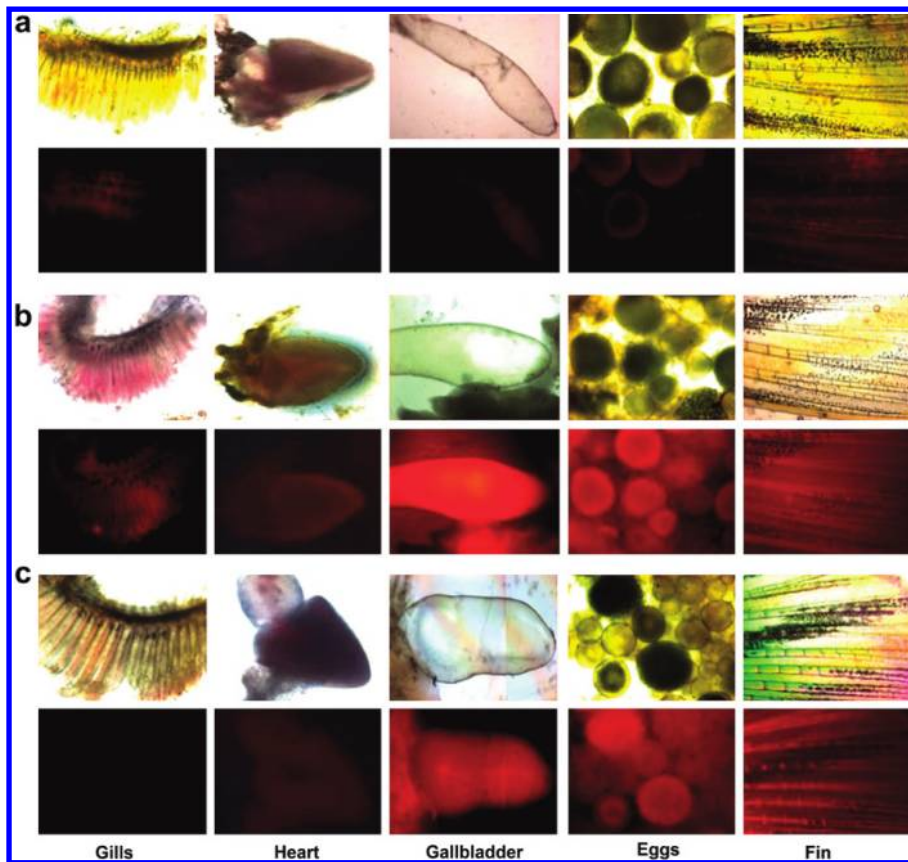


Figure 6. Images of zebrafish organs treated with $20\ \mu\text{M}$ chemodosimeter 90 (0.2% dimethylsulfoxide (DMSO)) and $500\ \text{nM}$ HgCl_2 or $500\ \text{nM}$ CH_3HgCl . (a) Images of zebrafish organs treated with 90 in the absence of HgCl_2 or CH_3HgCl , (b) the presence of $500\ \text{nM}$ HgCl_2 , or (c) the presence of $500\ \text{nM}$ CH_3HgCl (upper, microscopic images; lower, fluorescence images). Reprinted with permission from ref 178. Copyright 2010 Elsevier Ltd.

All of these chemodosimeters (93–112) can detect Cu^{2+} in solution with fluorescence turn-on response, and 98, 105, 106, 107, 108, 109, and 110 have successfully been used for fluorescent bioimaging of Cu^{2+} in living cells. For example, boronic acid-linked rhodamine 98 exhibits an 80-fold fluorescence intensity enhancement upon addition of 10 equiv of Cu^{2+} and was used to monitor Cu^{2+} ions in mammalian cells and organisms.¹⁹⁰ Chemodosimeter 109 also exhibits high sensitivity and selectivity to Cu^{2+} , with a 40-fold fluorescence enhancement.²⁰¹ Moreover, incubation of HeLa cells with 10 mM 109 gave almost no intracellular fluorescence, and further incubation with growth medium containing 50 mM of Cu^{2+} leads to a remarkable enhancement of the intracellular fluorescence (Figure 7).

5.2.2. Cu^{2+} -Induced Hydrolysis Process. It has been known for almost 50 years that Cu(II) ions can promote the hydrolysis of α -amino acid esters at rates much greater than those of other metal ions. In addition, Cu^{2+} can also induce the hydrolysis of activated esters, shift-bases, and hydrazone. This is a stoichiometric process because the products of the reaction bind the metal ion substantially more strongly than the starting materials. As a result, Cu^{2+} -induced catalytic hydrolysis has become an important design strategy for Cu^{2+} -selective chemodosimeters (Scheme 20). Compounds 113,²⁰⁵ 114,²⁰⁶ and 115²⁰⁷ are examples of fluorescence off-on chemodosimeters that detect Cu^{2+} via selective hydrolysis of an acetyl group by blocking a photoinduced electron transfer (PET) process. Similarly, on the basis of Cu^{2+} -promoted hydrolysis of

lactone and a hydrazone group in coumarin, 116²⁰⁸ and 117²⁰⁹ have been developed as efficient Cu^{2+} -selective chemodosimeters with fluorescence turn-on response.

5.2.3. Cu^{2+} -Induced Spirolactam Ring-Opening and Hydrolysis Processes. The combination of Cu^{2+} -promoted hydrolysis and spirolactam ring-opening of rhodamine into one system is a useful strategy to generate fluorescent turn-on chemodosimeters for the selective detection of Cu^{2+} ions (Chart 4). As early as 1997, an example (118²¹⁰) of this type of chemodosimeter was reported by the Czarnik group. As a result of Cu^{2+} -promoted ring-opening, oxidation, and hydrolysis reactions, the fluorescence characteristics of rhodamine B appear instantly upon addition of $\text{Cu}(\text{OAc})_2$ to the colorless solution of hydrazide 118 in acetonitrile, in an irreversible process. Other rhodamine derivatives of hydrazide 119,²¹¹ hydroxylamine 120,²¹² amide 121,²¹³ hydrazines 122,²¹⁴ 123,²¹⁵ and 124,²¹⁶ and thioureas 125,²¹⁷ 126,²¹⁸ and 127²¹⁹ have also been reported as fluorescent turn-on Cu^{2+} -selective chemodosimeters.

We have devised one interesting example (125²¹⁷) of Cu^{2+} chemodosimeters, whose detection mechanism involves Cu^{2+} -promoted ring-opening, oxidation, and hydrolysis reactions. The rhodamine derivative 125, which contains a highly electron-rich S atom, can selectively recognize Cu^{2+} in aqueous media with a rapid response time ($\leq 1\ \text{min}$) and high sensitivity (detection limit $\leq 10\ \text{ppb}$). Confocal fluorescence microscopy and two-photon fluorescence microscopy experiments established the utility of 125 in monitoring Cu^{2+} within living HeLa

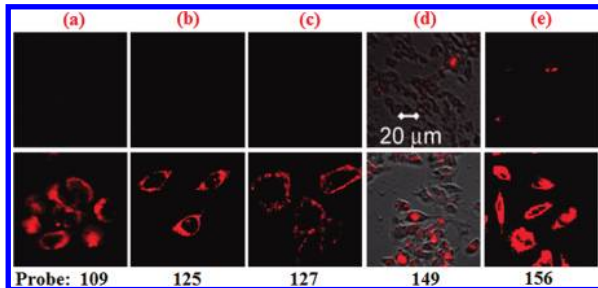
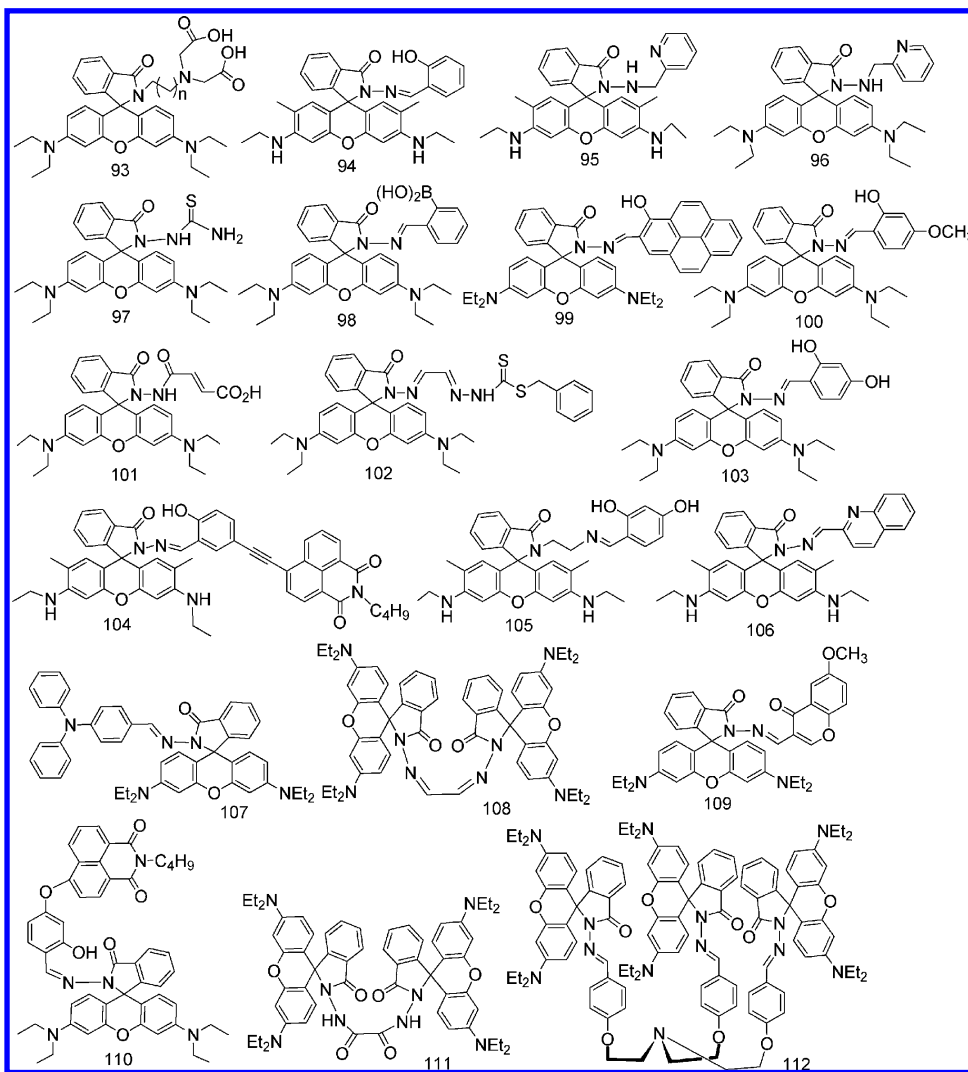
Chart 3. Fluorescent Chemodosimeters 93–112 Based on Cu²⁺-Induced Spirocyclic Ring-Opening

Figure 7. Selected examples of fluorescence imaging of living cells in the absence (upper) or presence (lower) of Cu²⁺ (for 109, 125, and 127), Fe³⁺ (for 149), and Cr³⁺ (for 156) using chemodosimeters as fluorescent probes. (a) Reprinted with permission from ref 201. Copyright 2011 Royal Society of Chemistry. (b) Reprinted with permission from ref 217. Copyright 2008 Wiley-VCH Verlag GmbH & Co. KGaA, Weinheim. (c) Reprinted with permission from ref 219. Copyright 2011 Royal Society of Chemistry. (d) Reprinted with permission from ref 242. Copyright 2010 Royal Society of Chemistry. (e) Reprinted with permission from ref 249. Copyright 2008 American Chemical Society.

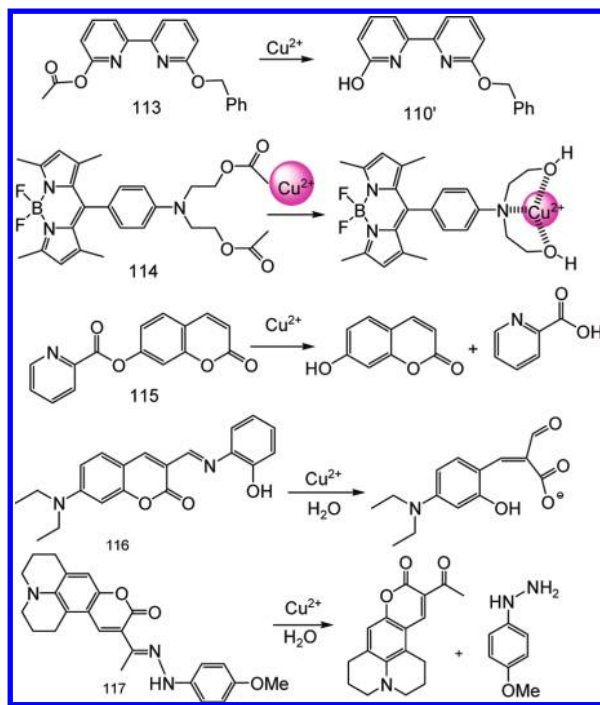
cells and mapping its subcellular distribution (Figure 7).²¹⁷ Recently, Zeng and co-workers also demonstrated that 126²¹⁸ can also detect Cu²⁺ in living cells, based on Cu²⁺-induced

spirolactam ring-opening and hydrolysis processes. In addition, we have recently reported mesoporous silica nanoparticles with a thiourea rhodamine derivative 127 for the selective detection of Cu²⁺ in solution and in living cells (Figure 7).²¹⁹

Combining the advantages of the analyte-responsive fluorescent probes and photocaging technology can lead to a novel type of photocontrollable probe. The nitrobenzyl-caged fluorescein dye 128²²⁰ is nonfluorescent, and its sensing activity to Cu²⁺ in the dark is modest (Scheme 21). Upon exposure to light, however, the photolabile nitrobenzyl groups were removed to release the active Cu²⁺-responsive fluorescent unit, which could detect Cu²⁺ in solutions with a 350-fold fluorescence enhancement through a Cu²⁺-induced hydrolysis process. Such a photocontrollable sensing process can also be realized in living cells with high spatial resolution. Compared to traditional analyte-responsive fluorescent probes, photocontrollable chemodosimeters have the intrinsic advantage of spatiotemporal control.

5.2.4. Cu²⁺-Induced Oxidation Process. Taking advantage of the ability of Cu²⁺ ions to oxidize aromatic sulfur and amines, 129,²²¹ 130,²²² 131,²²³ and 132²²⁴ (Scheme 22) were developed as Cu²⁺-selective luminescent turn-on chemodosimeters. For these chemodosimeters, the detection mechanism is based on a change in electron donation as a result of a

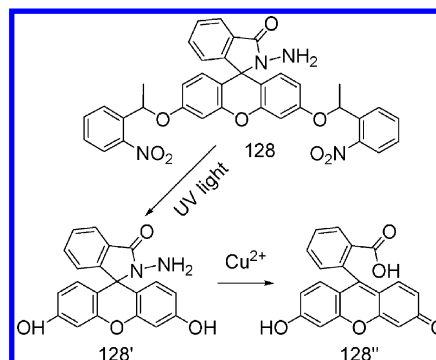
Scheme 20. Sensing Mechanism of 113–117 Based on Cu²⁺-Induced Hydrolysis Process



Cu²⁺-induced oxidation process and inhibition of photoinduced electron transfer (PET). These generate highly emissive products. In particular, 132 showed high selectivity and sensitivity toward Cu²⁺, with a detection limit of 2.61×10^{-7} M, which is much lower than the typical concentration of blood copper in normal individuals.²²⁴ Chemodosimeter 132 is cell-membrane permeable and displays a fluorescence turn-on response to Cu²⁺ in living cells. It is the first fluorescence turn-on probe based on metal-mediated oxidation that can detect Cu²⁺ under biological conditions.

5.2.5. Cu²⁺-Induced Oxidative Cyclization Process. In addition, some Cu²⁺-selective chemodosimeters have been developed on the basis of a Cu²⁺-induced oxidative cyclization reaction (Scheme 23). For example, the Cu²⁺-promoted intramolecular cyclization of thiourea and N-acylhydrazone

Scheme 21. Sensing Mechanism of Phototrigger Cu²⁺ Chemodosimeters 128



moieties results in a dramatic fluorescence enhancement in 133,²²⁵ 134,²²⁶ 135,²²⁷ 136,²²⁸ and 137.²²⁸

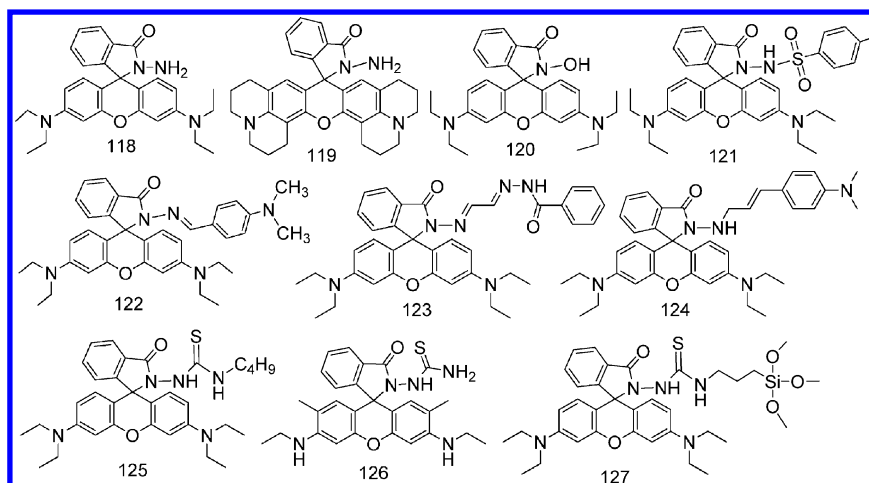
5.2.6. Cu²⁺-Induced Retro-Reaction. The acridane ketobenzimidazole adduct 138²²⁹ also functions as a fluorescent chemodosimeter, as a result of a Cu²⁺-induced retro-reaction (Scheme 24). The coordination of Cu²⁺ with the N and O binding sites of 138 polarizes the C–C bond connecting acridane with ketobenzimidazole, while the acridane–N lone pair provides the ultimate push to trigger the retro-reaction, thereby releasing the Cu²⁺-coordinated chelate and the acridinium ion. 138 is weakly fluorescent, whereas the newly formed acridinium ion is highly fluorescent, thus achieving a turn-on fluorescence response to Cu²⁺.²²⁹

5.2.7. Cu²⁺-Induced Thiol Elimination Process. Another design strategy for a luminescent chemodosimeter for Cu²⁺ is based on the Cu²⁺-induced thiol elimination reaction, for example, Cu²⁺-induced conversion of the protected aldehyde group to aldehyde by mercaptan in chemodosimeter 139²³⁰ (Scheme 25). As a result, 139 showed a ratiometric fluorescent response to Cu²⁺ with a large emission-wavelength shift (>100 nm) and displayed high selectivity for Cu²⁺ over other metal ions.²³⁰

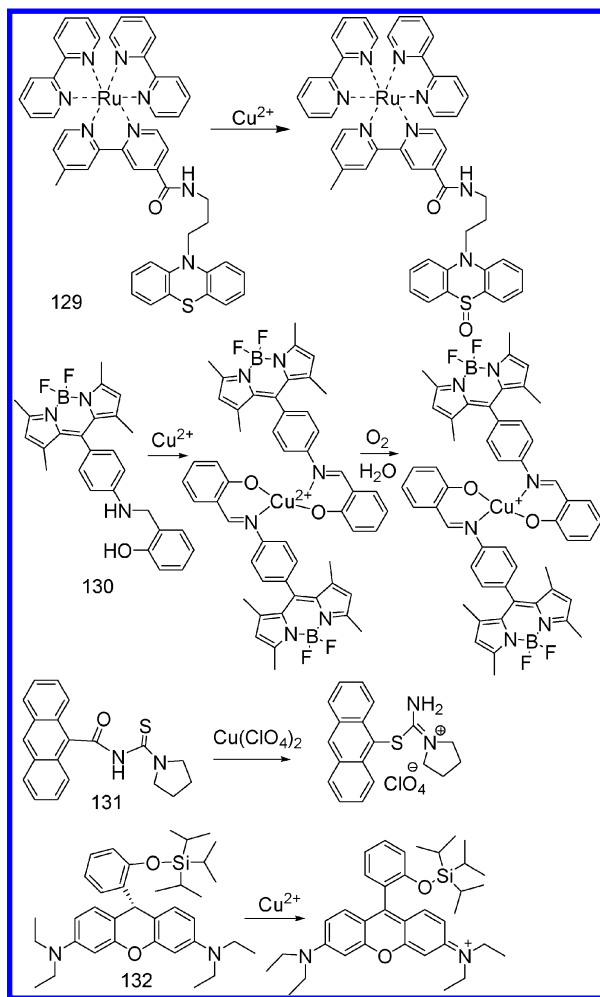
5.3. Luminescent Chemodosimeters for Fe³⁺

Iron plays an important role in human and animal health. However, high levels of iron ions within the body are associated with an increased incidence of certain cancers and organ

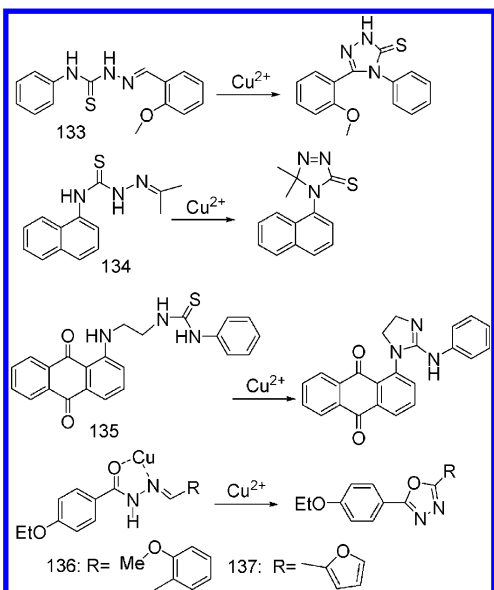
Chart 4. Fluorescent Cu²⁺ Chemodosimeters 118–127 Based on Cu²⁺-Induced Hydrolysis and Spirolactam Ring-Opening Processes



Scheme 22. Sensing Mechanism of 129–132 Based on Cu²⁺-Induced Oxidation Process

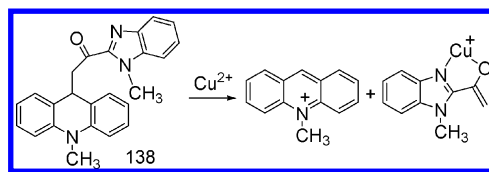


Scheme 23. Sensing Mechanism of 133–137 Based on Cu²⁺-Induced Oxidative Cyclization Process

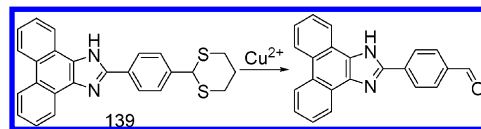


dysfunction.^{231,232} The detection of iron content in the physiological environment is therefore very important. In

Scheme 24. Sensing Mechanism of 138 Based on Cu²⁺-Induced Retro-reaction

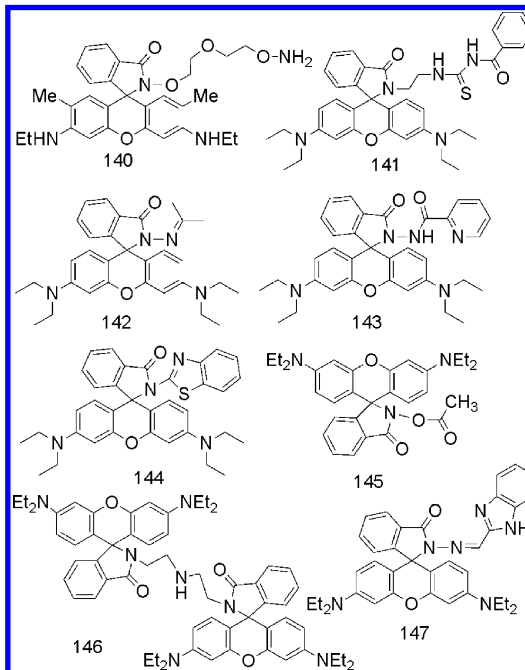


Scheme 25. Sensing Mechanism of 139 Based on Cu²⁺-Induced Thiol Elimination



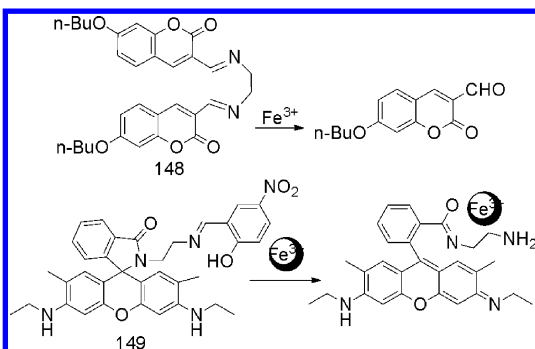
most practical applications of bioimaging, fluorescence enhancement is more desirable than fluorescence quenching. Fe³⁺-selective chemodosimeters provide a useful system with turn-on fluorescence.

Chart 5. Chemodosimeters 140–147 Based on Fe³⁺-Induced Spirolactam Ring-Opening Process



5.3.1. Fe³⁺-Induced Spirolactam Ring-Opening Process. Rhodamines are also applicable to Fe³⁺ detection, based on Fe³⁺-induced spiro lactam ring-opening. Compounds 140,²³³ 141,²³⁴ 142,²³⁵ 143,²³⁶ 144,²³⁷ 145,²³⁸ 146,²³⁹ and 147²⁴⁰ are typical Fe³⁺-selective chemodosimeters and exhibit high selectivity and sensitivity toward Fe³⁺ in aqueous media (Chart 5). Interestingly, by introducing a more electron-withdrawing carbonyl group to the thiourea moiety of 141, the electron density on the sulfur atom of the thiourea group decreased, lowering the mercury affinity of 141 and leading to a higher binding affinity toward Fe³⁺ than other metal ions.²³⁴ Moreover, 142²³⁵ and 145²³⁸ were successfully applied to bioimaging and could be used for monitoring Fe³⁺ in living cells. In particular, we have demonstrated that 142 was a two-

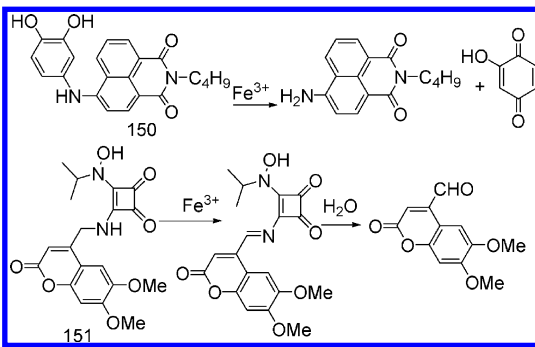
Scheme 26. Sensing Mechanism of 148 and 149 Based on Fe³⁺-Induced Hydrolysis Process



photon active probe for Fe³⁺ with a turn-on fluorescent response.²³⁵

5.3.2. Fe³⁺-Induced Spirolactam Ring-Opening and Hydrolysis Processes. It is well-known that Fe³⁺ facilitates Schiff-base hydrolysis by coordinating acidic water molecules, and this process was used for the design of the fluorescent turn-on chemodosimeter 148²⁴¹ (Scheme 26). A combination of Fe³⁺-induced Schiff-base hydrolysis and rhodamine spirolactam ring-opening in one system was shown to be an efficient strategy to achieve the specific detection of Fe³⁺. Chemodosimeter 149,²⁴² containing a rhodamine core and 2-hydroxy-5-nitrobenzaldehyde via a hydrolyzable imine linkage, is nonemissive but shows significant fluorescence enhancement upon addition of Fe³⁺ (Scheme 26). A quantum yield of 0.6 was achieved due to the spirolactam ring-opening and hydrolysis reaction. Moreover, the chemodosimetric reaction of 149 with

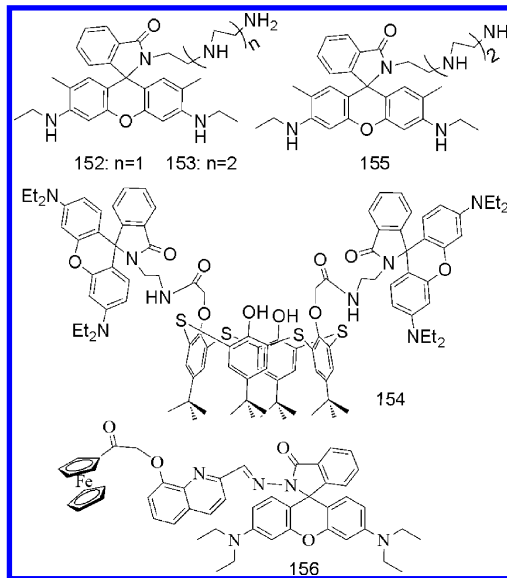
Scheme 27. Sensing Mechanism of 150 and 151 Based on Fe³⁺-Induced Oxidation and Hydrolysis Reactions



free Fe³⁺ in liver cells (Figure 7) can be used as a bioimaging probe for free Fe³⁺ without any detrimental effect on Fe³⁺-based enzymes.²⁴²

5.3.3. Fe³⁺-Induced Oxidation and Hydrolysis Reaction Processes. Fe³⁺ is a redox-active metal ion. Luminescent chemodosimeters for Fe³⁺ have been designed based on this redox behavior (Scheme 27). 150,²⁴³ which contains naphthalimide as the fluorophore and catechol as the Fe³⁺ receptor, has a weak emission in the absence of Fe³⁺. Upon exposure to Fe³⁺, the catechol is oxidized to the corresponding quinine and is subsequently hydrolyzed to liberate a fluorescent aminonaphthalimide derivative. Thus, 150 is a turn-on chemodosimeter for Fe³⁺. In addition, the (aminomethyl)-coumarin portion of 151²⁴⁴ is oxidized to an iminocoumarin that can be further hydrolyzed to produce a highly fluorescent coumarin aldehyde, giving a turn-on fluorescence response.

Chart 6. Fluorescent Cr³⁺ Chemodosimeters 152–156 Based on Cr³⁺-Induced Spirolactam Ring-Opening Process



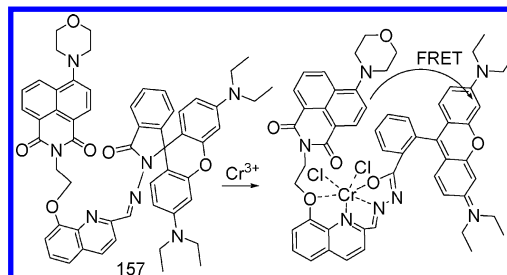
5.4. Luminescent Chemodosimeters for Cr³⁺

A deficiency of chromium in the human body leads to a variety of diseases, including diabetes and cardiovascular disease.²⁴⁵ Recently, Cr³⁺ has been reported to show toxicity in vivo. Therefore, it is useful to detect Cr³⁺ ions. To date, six turn-on luminescent chemodosimeters have been reported to detect Cr³⁺, all of which were based on the spirolactam ring-opening process of rhodamine unit (Chart 6).

5.4.1. Fluorescence Turn-On Chemodosimeters for Cr³⁺. Rhodamine-based derivatives containing an oligoethoxy-amine group (152²⁴⁶ and 153²⁴⁶) and thiocalix[4]arene (154²⁴⁷) can detect both Cr³⁺ and Fe³⁺ with fluorescence enhancement but cannot distinguish the two ions. Interestingly, 155,²⁴⁸ which has a similar structure to 153, can only be used to detect Cr³⁺.

On the basis of the spirolactam ring-opening process, we have designed and developed two rhodamine derivatives 156²⁴⁹ and 157²⁵⁰ containing an 8-hydroxyquinoline group for selective detection of Cr³⁺ over other metal ions. 156 displays a 15-fold enhancement in fluorescence at 587 nm within 1 min of binding with Cr³⁺ and has been used as a fluorescent chemodosimeter to monitor Cr³⁺ in living cells and to map its subcellular distribution (Figure 7).²⁴⁹

Scheme 28. Sensing Mechanism of FRET-Based Cr³⁺ Chemodosimeters 157



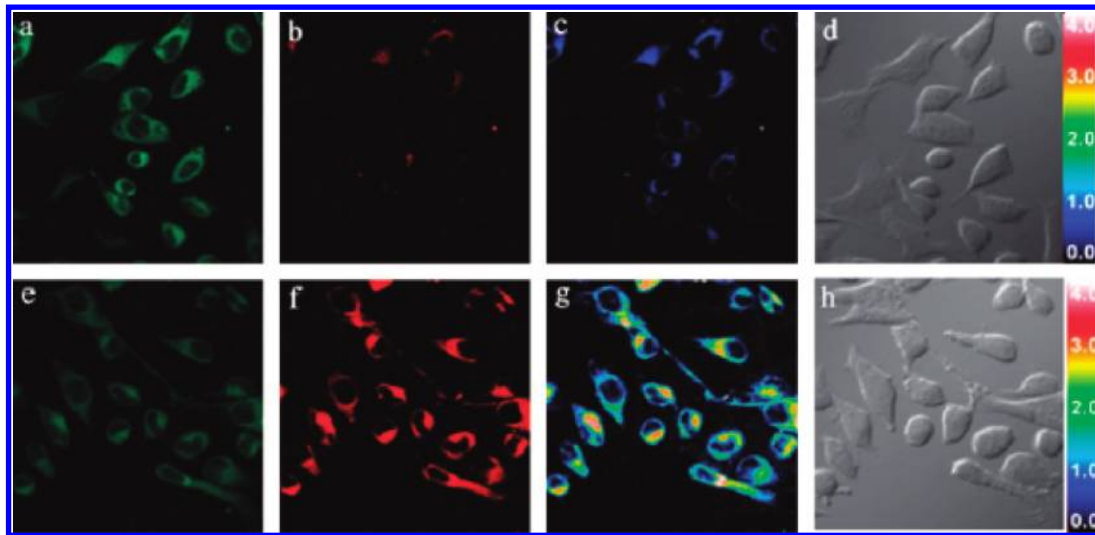


Figure 8. FRET images of **157** for Cr^{3+} in HeLa cells. (Top, a–d) Cells incubated with $5 \mu\text{M}$ **157** for 30 min. (Bottom, e–f) Cells incubated with both 50 mM Cr^{3+} and $5 \mu\text{M}$ **157** for 30 min. Emission was collected by the green channel at $530 \pm 20 \text{ nm}$ (a and e) and the red channel at $610 \pm 40 \text{ nm}$ (b and f). (c and g) FRET images with ratio function with red and green channel ($\lambda_{\text{ex}} = 405 \text{ nm}$). Reprinted with permission from ref 250. Copyright 2008 The Royal Society of Chemistry.

5.4.2. FRET-Based Chemodosimeters for Cr^{3+} . Furthermore, we have demonstrated that **157²⁵⁰** (Scheme 28) could be used as a FRET-based chemodosimeter for Cr^{3+} . In this system, 1,8-naphthalimide and the ring-open rhodamine were used as energy donor and acceptor, respectively. Binding to Cr^{3+} induces the ring-opening of the rhodamine moiety, and excitation of the 1,8-naphthalimide chromophore results in an intense red emission of rhodamine as a result of a FRET process. **157** could also be used to monitor intracellular Cr^{3+} with FRET methods (Figure 8), corresponding to the ratiometric fluorescence response.²⁵⁰

5.5. Luminescent Chemodosimeters for Zn^{2+}

Zn^{2+} is the second most abundant transition metal in the human body and plays vital roles in numerous biological processes, including neural signal transmission, regulation of

serves as both a reporter and a receptor due to enhanced fluorescence occurring upon Zn^{2+} chelation. Upon addition of Zn^{2+} , there was an obvious color change in the fluorescence from dark cyan to greenish yellow, allowing ratiometric measurement.²⁵⁶ The rhodamine derivative **159²⁵⁷** containing bis(2-pyridylmethyl)amine can be used for detecting Zn^{2+} with high selectivity. Zn^{2+} can promote the transformation of **159** from the lactam form to the ring-opened one, realizing a turn-

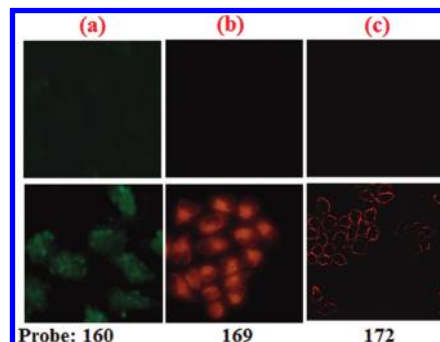


Figure 9. Selected examples of fluorescence imaging of living cells in the absence (upper) or presence (lower) of Zn^{2+} (for **160**), Au^{3+} (for **169**), or Ag^+ (for **172**) using the chemodosimeters as fluorescent probes. Imaging at bottom for (a) Reprinted with permission from ref 258. Copyright 2011 Elsevier B.V. (b) Reprinted with permission from ref 272. Copyright 2011 Royal Society of Chemistry. (c) Reprinted with permission from ref 276. Copyright 2010 American Chemical Society.

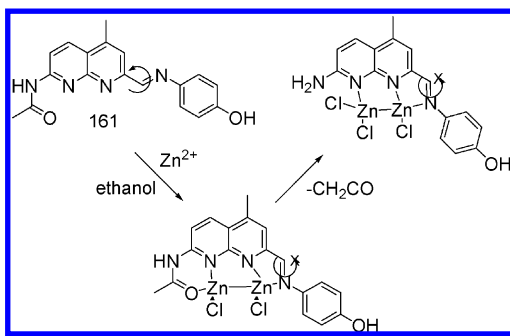
metalloenzymes, and gene transcription.^{251–253} Hence, the exploitation of fluorescent chemodosimeters for Zn^{2+} detection is very important.^{254,255}

5.5.1. Zn^{2+} -Complexation-Induced Spirolactam Ring-Opening Process. The mechanisms of Zn^{2+} -complexation-induced spirolactam ring-opening or hydrolysis are the main methods that have been used for designing fluorescent chemodosimeters for Zn^{2+} (Chart 7). Recently, Tong and co-workers reported a rhodamine-based fluorescent chemodosimeter **158²⁵⁶** for Zn^{2+} . In **158**, a salicylaldimine moiety

on fluorescence response. Furthermore, **159** is cell-permeable and can monitor the change in intracellular Zn^{2+} with significant fluorescence enhancement by confocal fluorescence microscopy.²⁵⁷ Another hydrophilic chemodosimeter, **160**, containing a sulfonated β -naphthol as receptor, can also be used for detecting Zn^{2+} in water with a turn-on fluorescence response and for further monitoring Zn^{2+} in living cells with high sensitivity and selectivity (Figure 9).²⁵⁸

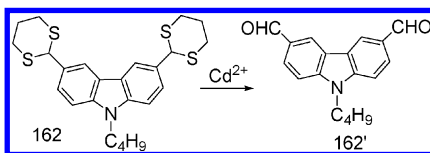
5.5.2. Zn^{2+} -Complexation-Induced Hydrolysis Process. Zn^{2+} -complexation-induced hydrolysis has also been adopted

Scheme 29. Sensing Mechanism of Fluorescent Zn²⁺ Chemodosimeter 161



for designing Zn²⁺ chemodosimeters. Zhang and co-workers reported another Zn²⁺ chemodosimeter **161** based on 1,8-naphthyridine (Scheme 29).²⁵⁹ This chemodosimeter exhibits a turn-on fluorescent response to Zn²⁺ with high selectivity. The detection mechanism can be assigned to the formation of a complex between Zn²⁺ and **161**, accompanied by the hydrolysis of the acetamide group to an amino group and restriction of rotation of an acyclic C=N. Furthermore, the sensitivity of **161** to Zn²⁺ was demonstrated in living cells by using confocal fluorescence microscopy, which indicated its potential application for the intracellular imaging of Zn²⁺.²⁵⁹

Scheme 30. Sensing Mechanism of Fluorescent Cd²⁺ Chemodosimeter 162



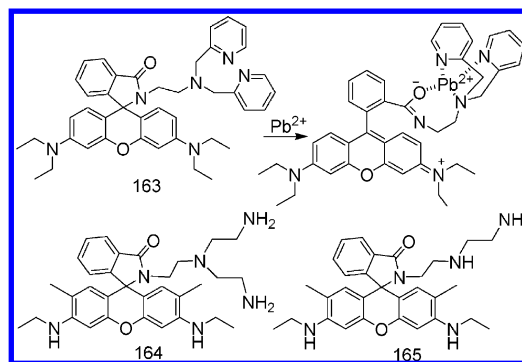
5.6. Luminescent Chemodosimeters for Cd²⁺

Cd²⁺ is widely used in industry and agriculture, for the production of batteries and fertilizers. It is toxic, and its bioaccumulation can result in many serious diseases and even some types of cancer.^{260,261} Hence, it is important to develop a fluorescence dosimetric method for the detection of Cd²⁺. To date, only one fluorescent chemodosimeter **162** for Cd²⁺ has been reported, based on the protection/deprotection of the aldehyde group (Scheme 30). Because of the thiophilic affinity of Cd²⁺, the electron-rich 1,3-dithiane protective group in **162**²⁶² can be removed by Cd²⁺ ions to form the new compound **162'** with two electron-deficient dialdehyde groups. Thus, an ICT process from the electron-donating N-butylcarbazole moiety to the electron-withdrawing aldehyde group can form in **162'**, leading to a significant bathochromic shift (>50 nm) in the emission spectrum and achieving a ratiometric fluorescent response to Cd²⁺.²⁶²

5.7. Luminescent Chemodosimeters for Pb²⁺

Pb²⁺ is a highly neurotoxic environmental pollutant. Exposure to Pb²⁺ is associated with behavioral abnormalities, learning impairment, hearing difficulties, and impaired cognitive functions in humans.²⁶³ To date, only three examples of fluorescent chemodosimeters for Pb²⁺ have been reported (Scheme 31). All are based on Pb²⁺ coordination inducing the

Scheme 31. Sensing Mechanism of Fluorescent Pb²⁺ Chemodosimeters 163–165



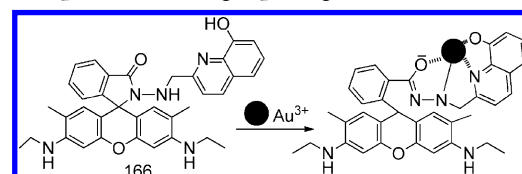
rhodamine spirolactum ring-opening process of the rhodamine unit.

Yoon and co-workers developed a rhodamine derivative **163**²⁶⁴ containing bis(2-pyridylmethyl)amine moiety as fluorescent chemodosimeter for selective detection of Pb²⁺ in acetonitrile. A significant fluorescence red-shift of ~30 nm and 100-fold emission enhancement were observed for **163** upon addition of Pb²⁺, with an association constant of $1.95 \times 10^5 \text{ M}^{-1}$.²⁶⁴ Kim and co-workers reported that self-assembled monolayers of two rhodamine derivatives having multinitrogen atoms, **164** and **165**,²⁶⁵ on glass surfaces exhibited selective turn-on fluorescence response with Pb²⁺ over various metal ions in CH₃CN.

5.8. Luminescent Chemodosimeters for Au⁺/Au³⁺

Metallic gold is stable and biocompatible, but its ionic forms are very reactive and potentially toxic to humans. In particular, Au³⁺ ions can bind strongly to DNA and nervous

Scheme 32. Sensing Mechanism of 166 Based on Au³⁺-Induced Spirolactam Ring-Opening Process

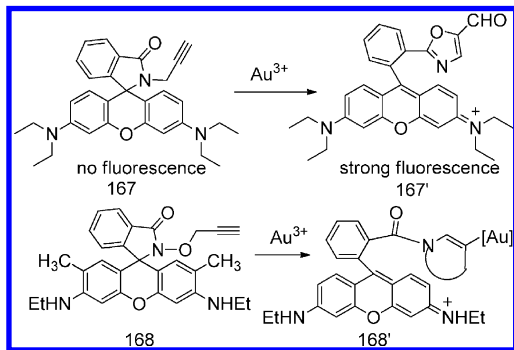


systems.^{266,267} Thus, the detection of gold ions in biological systems is desirable. Up to now, most Au³⁺ chemodosimeters have been based on the spirolactam ring-opening process.

5.8.1. Au³⁺-Induced Spirolactam Ring-Opening Process. One interesting example of fluorescent Au³⁺ chemodosimeters is the rhodamine derivative **166**.²⁶⁸ On the basis of the Au³⁺-triggered spirolactam ring-opening process through its complexation with the two oxygen atoms and the two nitrogen atoms (Scheme 32), **166** was used for sensing Au³⁺ ions with high selectivity. Moreover, **166** was also applied for imaging Au³⁺ ions in living HeLa cells.²⁶⁸

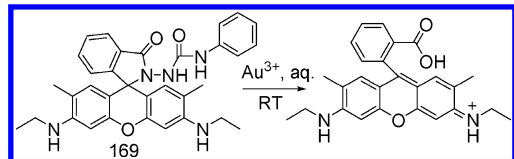
5.8.2. Au³⁺-Induced Spirolactam Ring-Opening and Intramolecular Cyclization Processes. The Yoon group reported the first fluorescent Au³⁺ chemodosimeter, **167**,²⁶⁹ that displayed high selectivity toward Au³⁺ among the other metal ions examined (Scheme 33). With Au³⁺, **167** showed a 250-fold fluorescence enhancement, which was attributed to an Au³⁺-induced spirolactam ring-opening, followed by intramolecular cyclization to form oxazolecarbaldehyde **167'**.

Scheme 33. Sensing Mechanism of 167 and 168 Based on Au³⁺-Induced Spirolactam Ring-Opening and Intramolecular Cyclization Processes



Furthermore, **167** was explored for the detection of other gold ion species (AuCl and AuCl_3), as well as air-stable cationic $\text{Ph}_3\text{PAuCl}-\text{AgNTf}_2$ species in aqueous media.²⁷⁰ Importantly, **167** has been successfully applied to cell imaging of Au^{3+} . In addition, on the basis of the Au^{3+} -induced conversion of

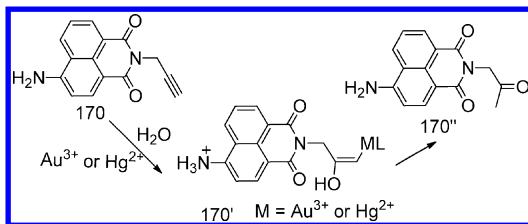
Scheme 34. Sensing Mechanism of 169 Based on Au³⁺-Induced Spirolactam Ring-Opening and Hydrolysis of Acylsemicarbazide



propargylamide to oxazolecarbaldehyde through an irreversible chemical reaction between an alkyne and Au^{3+} ions (Scheme 33), **168** was developed as a highly selective fluorogenic chemodosimeter that can be used to monitor Au^{3+} ions in biological systems.²⁷¹

5.8.3. Au³⁺-Induced Spirolactam Ring-Opening and Hydrolysis of Acylsemicarbazide. Rhodamine derivative **169** can also be realized as a Au^{3+} chemodosimeter based on Au^{3+} -mediated spirolactam ring-opening and hydrolysis of acylsemicarbazide to carboxylic acid (Scheme 34).²⁷² **169**

Scheme 35. Sensing Mechanism of Fluorescent Au³⁺ Chemodosimeters 170

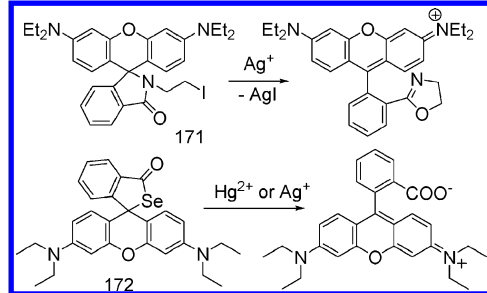


exhibited very weak fluorescence in solution. However, upon treatment with Au^{3+} , an intense new fluorescence emission band at 549 nm was observed rapidly, corresponding to a 233-fold enhancement. Furthermore, cells loaded with **169** alone are nonfluorescent, whereas cells preloaded with **169** and then incubated with Au^{3+} displayed intense fluorescence, allowing the detection of Au^{3+} in living cells by application of **169**.²⁷²

5.8.4. Au³⁺-Induced Conversion of Propargyl to Acetonyl Process. Utilizing the strong alkynophilicity of

gold ions, **170**²⁷³ (Scheme 35) can be used for the ratiometric detection of Au^{3+} as a result of the change of the maximum fluorescence emission band from 509 to 473 nm in $\text{MeOH}-\text{H}_2\text{O}$ (95:5, v/v, pH = 9.0) solution (Figure 9). Interestingly, in neutral or acidic pH, there appears a solution-selective ratiometric recognition of Hg^{2+} with an emission shift from 543 to 486 nm. Thus, selective recognition of Au^{3+} and Hg^{2+} can be achieved by adjusting the test conditions. The detection mechanisms are similar and proceed through the vinyl gold or vinyl mercury intermediate (**170'**), which is then converted to the final ketone **170''**.²⁷³

Scheme 36. Sensing Mechanism of Fluorescent Ag⁺ Chemodosimeters 171 and 172



5.9. Luminescent Chemodosimeters for Ag⁺

Silver(I) ion is associated with organ failure and reduction in mitochondrial function through the promotion of oxidative stress.²⁷⁴ Because of the increasingly common use of silver in industry, the potential risks to human health associated with the toxicity of silver(I) ions has become a major concern. Hence, the development of fluorescent Ag^+ chemodosimeters is of significant value.

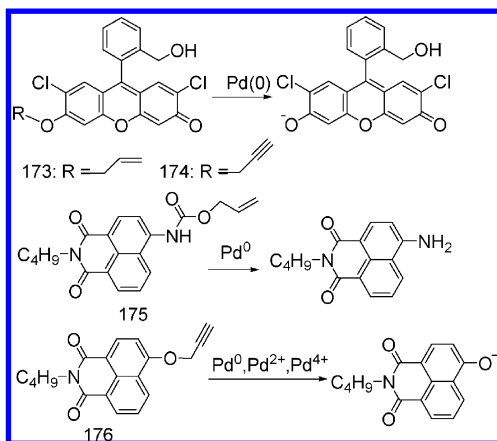
Ahn and co-workers devised a rhodamine B derivative **171** as a luminescent chemodosimeter for Ag^+ in aqueous media (Scheme 36).²⁷⁵ The detection mechanism is based on oxazoline formation upon binding of Ag^+ to the iodide, which induces spirolactam ring-opening. **171** showed little cytotoxicity to HeLa cells up to 100 μM level for 24 h. In light of the strong affinity of selenium to mercury and silver, rhodamine B selenolactone **172**, which incorporates a Se atom into the spirocyclic structure of rhodamine, was designed to detect Hg^{2+} and Ag^+ (Scheme 36).²⁷⁶ Chemodosimeter **172** is membrane-permeable and has great potential as a fluorescent probe for imaging Ag^+ in living cells, even in the presence of Cl^- (Figure 9). However, the reaction of **172** with Ag^+ inside cells occurs much more slowly than that with Hg^{2+} .

5.10. Luminescent Chemodosimeters for Pd(II)/Pd(0)/Pt(0)

Palladium and platinum are widely used precious metals that are found in various materials including dental crowns, catalytic converters, fuel cells, and jewelry.²⁷⁷ Despite the beneficial aspects of platinum and palladium compounds, certain forms of these metals are considered to be potential health hazards. To date, seven chemodosimeters for platinum and palladium have been reported, based on Pd/Pt-catalyzed deallylation reactions or spirolactam ring-opening.

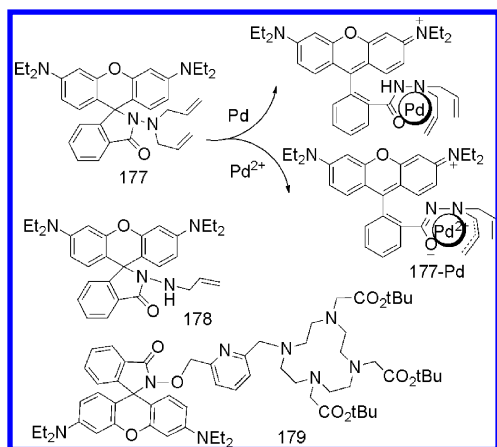
5.10.1. Pd/Pt-Catalyzed Deallylation Process. Recently, as a consequence of the Pd/Pt-catalyzed deallylation reaction, four luminescent chemodosimeters for Pd based on fluo-

Scheme 37. Sensing Mechanism of 173–176 Based on Pd/Pt-Catalyzed Deallylation Process



resceine and naphthalimide derivatives have been reported (Scheme 37). Garner and Koide demonstrated a fluorescence chemodosimeter **173** for the detection of Pd/Pt in various oxidation states, based on a Pd⁰/Pt⁰ catalyzed Tsuji–Trost-type reaction.^{278,279} In this system, the starting stable metal species of M^{II/IV} (M = Pd^{II}/Pt^{II/IV}) is first reduced by phosphine and the resultant M⁰L_{4-n} (L = PR₃ or solvent) then inserts into the C–O bond of the nonfluorescent allylic ether **173** to form a π-complex. This π-complex then reacts with a nucleophile to form the fluorescent product **173'**. This method also allows for the detection of platinum in heterogeneous samples such as human serum or sheep serum samples. As the Pd-catalyzed deallylation of **173** is 158 times faster than that of the Pt-catalyzed reaction at pH 4, palladium can be selectively detected in the presence of platinum by altering the pH of the reaction medium.^{278,279} Similarly, a fluorescein-based chemodosimeter **174** containing a propargyl ether can selectively detect palladium species in all its typical oxidation states (0, +2, and +4) based on a palladium-catalyzed depropargylation reaction.²⁸⁰ More importantly, **174**

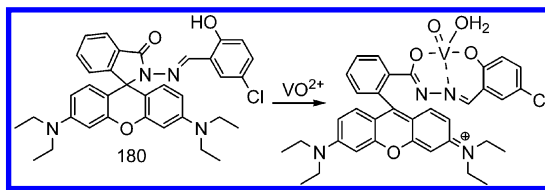
Scheme 38. Sensing Mechanism of Fluorescent Cu²⁺ Chemodosimeters 177–179



has been used for the fluorescent imaging of palladium chloride in living zebrafish (Figure 3). In addition, the naphthalimide derivatives **175**²⁸¹ and **176**²⁸² can realize ratiometric fluorescence detection for typical palladium species (0, +2, and +4). In particular, **176** can also monitor PdCl₂ in live RAW 264.7 macrophage cells by ratiometric fluorescence imaging.

5.10.2. Pd-Coordination-Induced Spirolactam Ring-Opening Process. On the basis of rhodamine spirolactam ring-opening induced by the π-affinity of Pd to allyl groups, **177**²⁸³ can selectively detect palladium in both Pd²⁺ and Pd⁰ states with no interference by Pt (Scheme 38). Also, a fluorescence turn-on was observed. Interestingly, the **177**–Pd⁰ system displays a much stronger fluorescence than **177**–Pd²⁺ does. In particular, **177** has been used successfully for the fluorescent imaging of palladium ions in 5-day-old zebrafish.²⁸³ Similarly, rhodamine derivative **178** can also be used for detecting Pd²⁺ (Scheme 38).²⁸⁴ In addition, another rhodamine derivative **179** with a cyclen-*tert*-butyl ester and a pyridine moiety as binding units was also reported for sensing Pd²⁺, which could discriminate Pd²⁺ over Pt²⁺ ions (Scheme 38).²⁸⁵

Scheme 39. Sensing Mechanism of Fluorescent VO²⁺ Chemodosimeter 180



5.11. Fluorescent Chemodosimeters for VO²⁺

Vanadium (VO²⁺) is an essential trace element and has significant roles in the environment and industry as well as for physiological systems.²⁸⁶ The development of fluorescent probes for VO²⁺ is important. Recently, the rhodamine derivative **180**²⁸⁷ has been developed as a fluorescence turn-on chemodosimeter for highly selective detection of VO²⁺. Upon treatment with VO²⁺, the emission peak of **180** at 583 nm increased dramatically, which was attributed to the VO²⁺-induced spirolactam ring-opening process of the rhodamine unit (Scheme 39).²⁸⁷

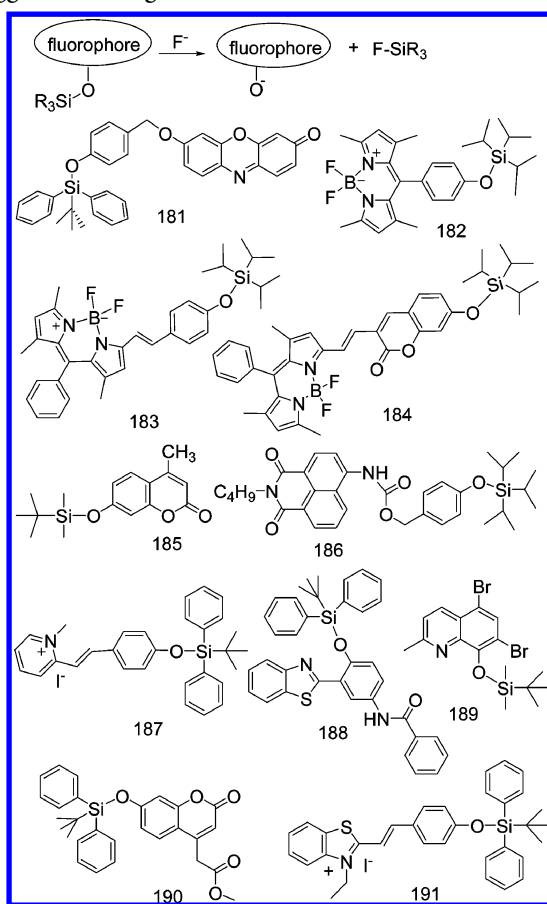
6. LUMINESCENT CHEMODOSIMETERS FOR ANIONS

6.1. Luminescent Chemodosimeters for F⁻

Fluoride anions play an essential role in a broad range of biological, medical, and chemical processes, such as dental care, osteoporosis treatment, and water supply treatment, and even in chemical warfare agents.^{288–291} Therefore, the detection of F⁻ is growing interest. To date, a large number of synthetic fluorophores have been designed as chemosensors for F⁻. Thioureas, ureas, amides, pyrrole, imidazole, and imidazolium are particularly effective in sensing F⁻, either through an intramolecular hydrogen-transfer process or based on the formation of a hydrogen bond between an active N–H group and F⁻.^{292–299} However, most reported F⁻-selective sensors based on an intramolecular hydrogen-transfer process work only in organic solvents, and F⁻ detection is inhibited by the presence of water. Thus, these chemosensors cannot be applied in fluorescence bioimaging to monitor F⁻ ions in biological samples. The design of luminescent chemodosimeters is therefore important for selective detection of F⁻ in living systems.

6.1.1. F⁻-Triggered Cleavage of Si–O Bonds. It is well-known that silicon has a high affinity for fluoride ions. On the basis of F⁻-triggered Si–O bond cleavage and the concomitant release of fluorophores (Scheme 40), a series of F⁻ chemo-

Scheme 40. Proposed Mechanism of 181–191 Based on F⁻-Triggered Cleavage of Si–O Bonds



dosimeters **181–191** have been designed. Suitable chemodosimeters can exhibit high selectivity for F⁻ with turn-on or ratiometric fluorescence response or both. More importantly, the detection process can also be realized in aqueous solution. All of these advantages make them suitable as bioimaging probes for F⁻.

The first example based on F⁻-triggered cleavage of a Si–O bond was **181**.³¹⁰ The presence of F⁻ induces the release of resorufin through a F⁻-triggered Si–O bond cleavage. On the basis of this mechanism, **181** can detect F⁻ in the presence of H₂O. Upon addition of F⁻, a drastic change in fluorescence emission was observed in CH₃CN/H₂O (50:50, v/v). On the basis of the similar mechanism of F⁻-triggered Si–O cleavage and the release of the fluorophore unit, some BODIPY derivatives **182–183**³¹¹ and **184**,³¹² a coumarin derivative **185**,³¹³ a naphthalimide derivative **186**,³¹⁴ and a phenylpyridylvinylene derivative **187**³¹⁵ have been developed as fluorescent F⁻ chemodosimeters. In particular, **188**³¹⁶ and **189**³¹⁷ have utilized both the desilylation reaction and excited-state intramolecular proton transfer (ESIPT) from their desilylation products with F⁻ and can detect F⁻ in aqueous solutions. For example, upon addition of F⁻ in water, bright yellow emission is observed for **188**.

To image F⁻ in living cells, the fluorescent probe should be water-soluble, be nontoxic, be cell-membrane permeable, and display intense fluorescence upon the detection of F⁻ in cellular systems. However, very few probes can satisfy the above requirements. Recently, Park and Hong et al. designed a coumarin derivative **190** as a noncytotoxic fluorescence

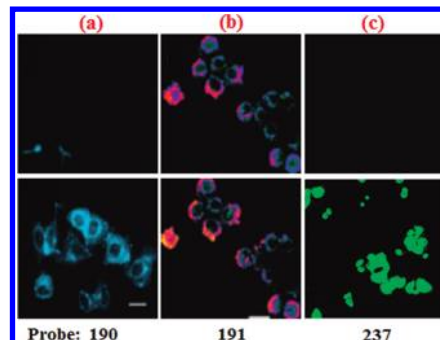
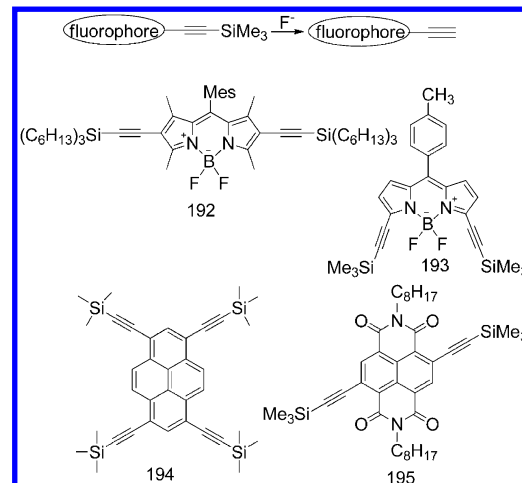


Figure 10. Selected examples of fluorescence imaging of living cells in the absence (upper) or presence (lower) of F⁻ (for **190** and **191**) and CN⁻ (for **237**) using the chemodosimeters as fluorescent probes, respectively. (a) Reprinted with permission from ref 318. Copyright 2009 Royal Society of Chemistry. (b) Ratiometric images. $\lambda_{\text{em}} = 490 \pm 20 \text{ nm}$ (blue channel) and $560 \pm 20 \text{ nm}$ (orange channel). $\lambda_{\text{ex}} = 405 \text{ nm}$. Reprinted with permission from ref 319. Copyright 2011 Royal Society of Chemistry. (c) Reprinted with permission from ref 368. Copyright 2011 American Chemical Society.

chemodosimeter for F⁻.³¹⁸ The presence of the methyl ester group can increase water solubility and enhance cell permeability. More than 4-fold enhancement of fluorescence intensity of **190** is observed upon treatment with 1 mM NaF for 3 h in phosphate-buffered solution (PBS). After incubating with NaF, the **190**-loaded A549 cells exhibited a significant increase in the fluorescence intensity (Figure 10), showing that **190** can detect F⁻ in living system.³¹⁸ However, one potential

Scheme 41. Proposed Mechanism of 192–195 Based on F⁻-Triggered Cleavage of Si–C Bond

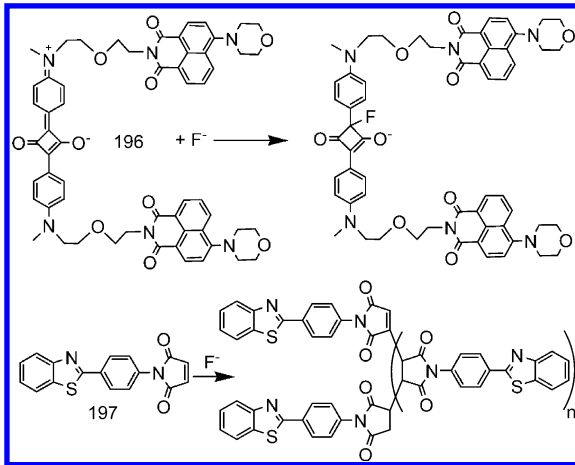


drawback of **190** for fluorescent bioimaging is that its excitation wavelength is in the UV region. Another fluorescent chemodosimeter **191** based on the benzothiazoliumhemicyanine dye³¹⁹ exhibited ratiometric fluorescence response to F⁻ with a significant emission red-shift (58 nm) from 500 to 558 nm. Furthermore, the ratiometric fluorescence imaging of F⁻ in living cells has been demonstrated with visible light excitation (Figure 10).

6.1.2. F⁻-Triggered Cleavage Reaction of Si–C Bond. Another alternative method for detecting F⁻ is based on the fluoride-triggered cleavage reaction of the Si–C bond in —C≡C—SiMe₃ (Scheme 41), due to the easier cleavage of Si–C compared with Si–O. To date, a new class of luminescent

chemodosimeters, such as the BODIPY derivatives **192**³²⁰ and **193**,³²¹ the pyrene derivative **194**,³²² and the naphthalene diimide derivative **195**,³²³ have been developed to detect F⁻

Scheme 42. Sensing Mechanism of **196** and **197** Based on Nucleophilic Addition Reaction of F⁻

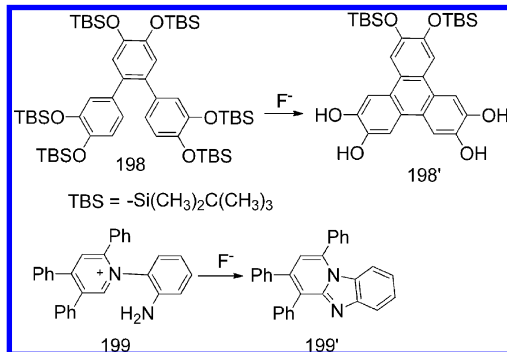


based on this cleavage reaction. For these, the cleavage of the Si—C bond often leads to a blue-shift of the fluorescence emission. For example, the addition of F⁻ to an acetone solution of **192** results in a decrease of the fluorescence intensity at 571 nm and an increase of the peak intensity at 554 nm.³²⁰

6.1.3. Nucleophilic Addition Reaction of F⁻. Chemodosimeters for F⁻ have been designed based on the nucleophilic addition of F⁻ to electron-deficient fluorophores. Because of its significant electron-deficiency, squaraine is readily attacked by nucleophiles, such as F⁻, to generate colorless and non-fluorescent products (Scheme 42). Xiao and co-workers reported a FRET-based ratiometric F⁻ chemodosimeter **196**, which contains two naphthalimide donors and a squaraine acceptor.³²⁴ Energy transfer from the naphthalimide donor to the squaraine acceptor can occur. The addition of F⁻ leads to attack on the electron-deficient squaraine center of **196**, resulting in the loss of the FRET process due to the removal of the spectral overlap. Thus, the donor emission was recovered and ratiometric detection for F⁻ was realized.

Another F⁻ chemodosimeter based on nucleophilic addition reaction of F⁻ is nonfluorescent benzothiazole-substituted maleimide **197**. The addition reaction of F⁻ to the C=C

Scheme 43. Sensing Mechanism of **198** and **199** Based on F⁻-Induced Intramolecular Cyclization Reaction

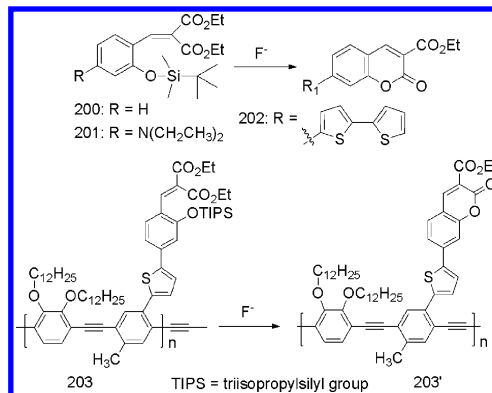


double bond of the maleimide moiety can initiate its polymerization, causing a dramatic, ca. 10-fold increase in fluorescence intensity. This sensing system can tolerate up to 5% water in the solvent of DMSO.³²⁵

6.1.4. F⁻-Induced Intramolecular Cyclization Reaction.

In addition to the above mechanisms for the design of F⁻ chemodosimeters, some new mechanisms have been reported recently, including F⁻-induced intramolecular cyclization (Scheme 43). The OTBS groups of terphenyl derivative **198** can be deprotected by the addition of F⁻, and the unprotected product can then undergo an irreversible cyclization to form triphenylene **198'**.³²⁶ This induces a red-shift and enhancement of the fluorescence emission of the solution, and **198** can be used as a luminescent chemodosimeter for F⁻. In addition, a

Scheme 44. Sensing Mechanism of **200–203** Based on F⁻-Triggered Si—O Bond-Cleavage and Cyclization Reactions



fluoride-induced intramolecular cyclization of pyridinium **199** to pyrido[1,2-a]benzimidazole **199'** has also been reported as a turn-on fluorescence chemodosimeter for F⁻.³²⁷

6.1.5. F⁻-Triggered Si—O Bond-Cleavage and Cyclization Reactions.

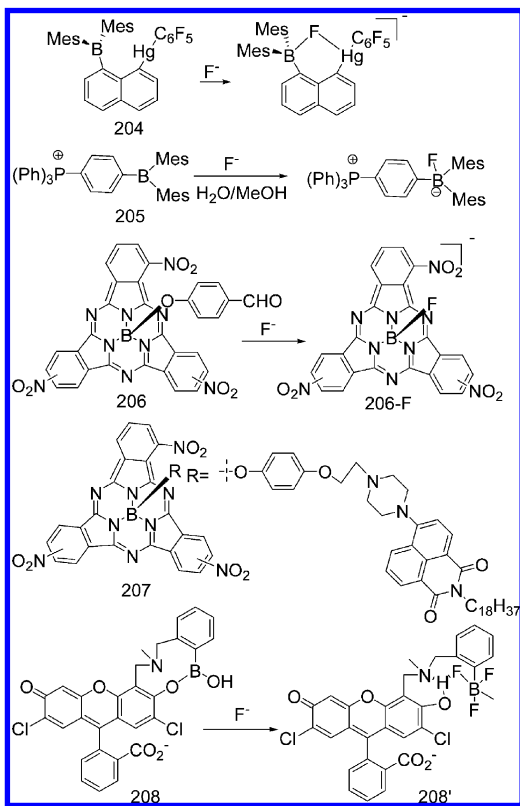
On the basis of the formation of a highly fluorescent coumarin through fluoride-triggered Si—O bond-cleavage and cyclization reactions, Kim and Swager constructed a series of coumarin derivatives **200–202** with varying electron-donating groups at the coumarin 7-position as ratiometric fluoride chemodosimeters (Scheme 44).³²⁸ Furthermore, the sensitive F⁻ detection has been successfully amplified by the conjugated polymer chemodosimeter **203** (Scheme 44).³²⁸

6.1.6. Fluorescent F⁻ Chemodosimeters Based on Organoboron Compounds.

Advantage has also been taken of the strong Lewis acid–base affinity of boron toward F⁻ to develop an efficient approach to F⁻ detection.³²⁹ Since the pioneering work of Yamaguchi, Akiyama, and Tamao on fluoride probes based on boron-containing π-electron systems,³³⁰ organoboron compounds containing B—O bonds or dimesitylboryl (BMes₂) groups have been reported to be selective chemodosimeters for F⁻.^{290,331–335} In the presence of F⁻, a strong interaction between the boron atom and F⁻ can break B—O bonds or interrupt the extended π-conjugation of the organoboron derivative, thereby causing a dramatic change in their fluorescent properties. Several reviews have been published summarizing the F⁻ probes based on organoboron compounds.^{335,336} Here, we focused on the development of selective chemodosimeters for F⁻ in aqueous condition and living cells.

(1). *B–F Interaction of Triarylboron Compounds.* Fluoride displays a high hydration enthalpy ($\Delta H^\circ = -504 \text{ kJ/mol}$); thus,

Scheme 45. Sensing Mechanism of Fluorescent F⁻ Chemodosimeters 204–208 Based on Organoboron Compounds



its detection in aqueous environments is particularly difficult.³³⁷ To achieve detection of F⁻ in water, the fluoride affinity of triarylboranes must be enhanced. Gabbai and co-workers have developed several strategies to enhance the F⁻ affinity of triarylborane compounds. In early studies, they reported several bidentate boranes³³⁸ that have F⁻ binding constants exceeding those of simple triarylboranes by at least 3 orders of magnitude. One typical example is the heteronuclear bidentate Lewis acid compound 204 (Scheme 45).³³⁹ The proximity of two Lewis acidic sites enforced by the 1,8-naphthalenediyl backbone promote F⁻ chelation and are responsible for the high binding constant ($\sim 2.3 \times 10^4 \text{ M}^{-1}$). The interplay of conjugative and spin-orbit coupling effects mediated by the boron and mercury atoms, respectively, resulted in phosphorescent signaling upon fluoride binding.

Gabbai and co-workers then developed a strategy using cationic boranes for the complexation of F⁻ in water, taking advantage of the increased anion affinity caused by Coulombic effects. Cationic substituents were used to exert a strong negative inductive effect, to achieve an increase in Lewis acidity of the boron atom. For example, phosphonium borane 205 is sufficiently fluorophilic to bind F⁻ below the EPA contaminant level in pure water (Scheme 45).³⁴⁰

(2). F⁻-Induced B–O Disruption. Tian and co-workers have reported subphthalocyanine (SubPc) derivative 206³⁴¹ and 207³⁴² as fluorescent F⁻ chemodosimeters, based on an axial-substitution along with a B–O disruption process (Scheme 45). The SubPc unit acts not only as a fluorophore but also as a selective receptor for the F⁻. F⁻ complexation leads to a large perturbation in the delocalized 14 π-electron system of 206, resulting in a substantial decrease in emission intensity at 578

nm.³⁴¹ In particular, 206 is an irreversible probe and possesses a high selectivity toward F⁻. For 207, a ratiometric detection of F⁻ was realized.³⁴²

Fluorescein derivative 208 is another chemodosimeter based on a F⁻-binding-induced B–O disruption mechanism (Scheme 45).³⁴³ It displays a selective fluorescence change in the presence of F⁻ and is not affected by other halide ions. This high F⁻ selectivity is quite unique and is due to the fluorescein core structure and the boron–fluoride interaction. In the fluoride adduct of 208', the phenolic hydrogen forms a strong hydrogen bond with F⁻ as well as the benzylic amine, which blocks the PET process and results in fluorescence enhancement.

6.2. Luminescent Chemodosimeters for CN⁻

The cyanide ion is extremely toxic to mammals, leading to vomiting, convulsions, loss of consciousness, and eventual death.³⁴⁴ Despite its toxic nature, CN⁻ is commonly used in various processes, such as in the production of raw material for synthetic fibers and resins and in the gold-extraction process. According to the World Health Organization (WHO), cyanide concentrations lower than 1.9 μM are acceptable in drinking water.³⁵ Thus, there exists a need to develop efficient chemodosimeters for CN⁻ in environmental and biological samples.

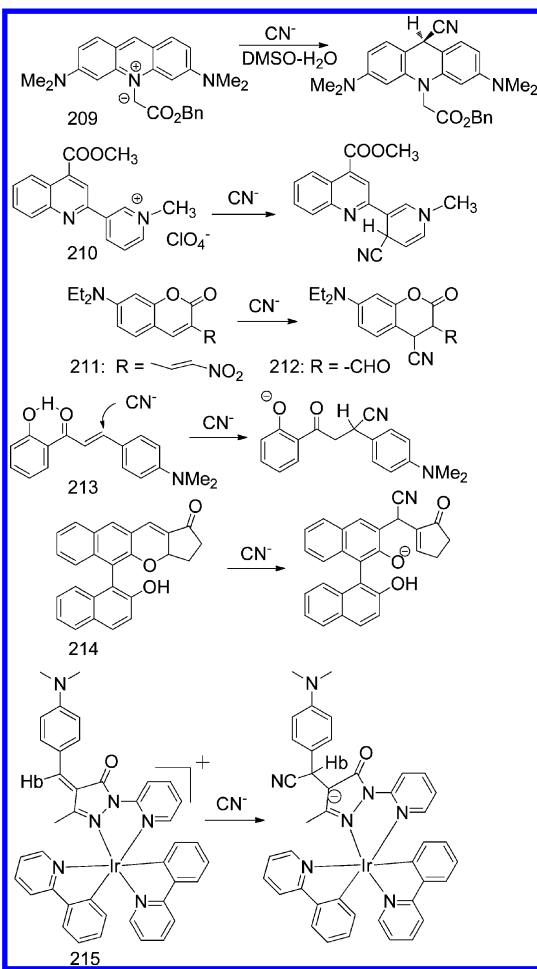
In recent years, different molecular reactions have been used as sensing mechanisms for CN⁻, including hydrogen bonding and coordinative bonding. The detection mechanism of the majority of CN⁻ chemodosimeters is based on addition processes, due to the strongly nucleophilic nature of CN⁻.

6.2.1. Michael Addition Reaction. On the basis of Michael addition by cyanide anions, a series of fluorescent compounds 209–215, which contain carbon–carbon double bonds conjugated with an electron-withdrawing group, were successfully developed as CN⁻-selective chemodosimeters.

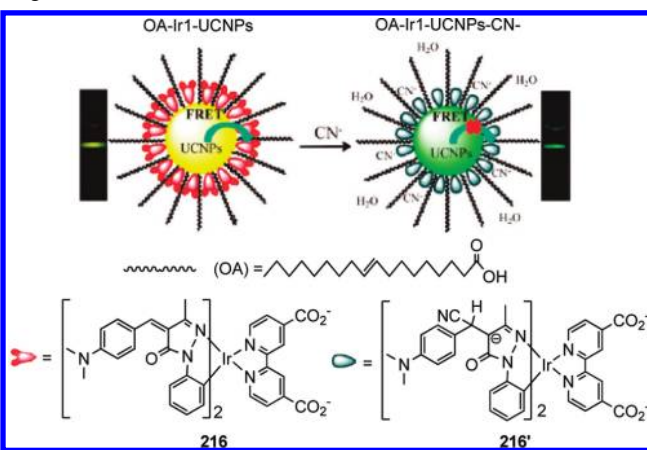
(1). CN⁻ Addition to the Pyridinium Ring. Chemodosimeters 209³⁴⁵ and 210³⁴⁶ are based on the addition reaction of CN⁻ to acridinium and pyridinium units, respectively (Scheme 46). 209 can selectively detect CN⁻ in DMSO–water (95:5 v/v) with a 14-fold decrease in fluorescence intensity. This detection is based on the irreversible nucleophilic addition of CN⁻ to the 9-position of the acridinium ion.³⁴⁵ The fluorescent detection limit is <1.9 μM. Different from 209, the CN⁻ chemodosimeter 210 is based on an enhanced ICT process and cancellation of the PET process from an excited quinoline fluorophore to the redox-active pyridinium ion (Scheme 46). This is induced by CN⁻ addition to the pyridinium ring and results in fluorescence off-on response.³⁴⁶

(2). CN⁻ Addition to α,β-Unsaturated Carbonyl Moiety. Probes 211,³⁴⁷ 212,³⁴⁸ 213,³⁴⁹ and 214³⁵⁰ are fluorescent CN⁻ chemodosimeters that use electron-withdrawing nitro, aldehyde, or ketone groups as the Michael acceptor (Scheme 46). CN⁻ adds to the β/δ-position of the Michael acceptor, which is activated by the nitro, aldehyde, or ketone group, and results in significant fluorescence changes in the chemodosimeters. In particular, Bian, Huang, and co-workers have recently reported a phosphorescent iridium(III) complex 215 to be an excellent multisignaling CN⁻ chemodosimeter that features remarkable luminescence enhancement.³⁵¹ Interestingly, 215 exhibits a much faster reaction rate than its corresponding organic ligand does, which is attributed to the strong electron-withdrawing effect of the iridium(III) center.

Scheme 46. Sensing Mechanism of Fluorescent CN⁻ Chemodosimeters 209–215



Scheme 47. Proposed Recognition Mechanism and the Upconversion Luminescence-Based LRET Process Toward CN⁻ of Upconversion NaYF₄:Yb,Er,Tm Nanophosphors Coated with the Iridium(III) Complex 216 and Oleic Acid Ligands^a



^aChange in green UCL emission is also shown in their corresponding photos. Reprinted with permission from ref 352. Copyright 2011 American Chemical Society.

(3). Upconversion Luminescence-Based Energy-Transfer Chemodosimeters for CN⁻. Recently, we have devised an

upconversion luminescence-based energy-transfer (UCLET) chemodosimeter for highly sensitive and selective determination of CN⁻.³⁵² By introducing two carboxylic acids into 215, another iridium(III) complex 216 (Scheme 47) was synthesized and assembled on the surface of upconversion NaYF₄:Yb,Er,Tm nanophosphors, and nanoprobe 215-UCNP was achieved for UCLET-based detection of CN⁻. Upon addition of CN⁻, the green upconversion luminescence (UCL) emission at 514–560 nm was enhanced, which is attributed to the inhibition of energy transfer from green UCL emission to the absorption of 216. Interestingly, when the UCL emission at 800 nm was used as an internal standard, and the ratio of UCL emission at 540 nm to 800 nm (I_{540}/I_{800}) was chosen as the detection signal, the detection limit of this nanoprobe 215-UCNP was estimated to be 0.18 μM. Such a low detection limit can be attributed to the ratiometric detection and a low fluorescence background for UCL detection. Furthermore, by means of laser scanning upconversion luminescence microscopy (LSUCLM) experiments, this nanoprobe 215-UCNP can be used for monitoring CN⁻ in living cells using a ratiometric UCL signal (Figure 11).³⁵²

Furthermore, we have developed a general method to transfer a hydrophobic chemodosimeter to work in the pure water surroundings. After coating an amphiphilic block polymer, poly(maleic anhydride-*alt*-1-octadecene)-poly(ethylene glycol), onto the surface of rare-earth upconversion nanophosphors (NaYF₄: 20%Yb, 2%Ho), hydrophobic chemodosimeter 215 can be easily loaded into the polymer layer to form a hybrid nanosystem. These upconversion emissive nanoparticles have been successfully used to detect CN⁻ in pure water, by monitoring the intensity of green UCL emission.³⁵³

6.2.2. Nucleophilic Addition Reaction. Cyanide is capable of nucleophilic attack on carbonyl functional groups that are activated by linking an electron-withdrawing moiety (usually $-CF_3$) or by local phenol protons through intramolecular hydrogen bonding (Scheme 48). In addition, CN⁻ can interact with the positively charged indolium group or cleave the C–O bond of oxazine through nucleophilic addition reaction.

(1). *Nucleophilic Addition Reaction of CN⁻ with Trifluoromethyl-Activated Carbonyl Group.* BODIPY-based 217,³⁵⁴ a CN⁻ selective chemodosimeter, was developed using an approach of CN⁻ attack on a trifluoromethyl-activated carbonyl group. However, 217 is a fluorescent on–off-type probe with a 14-fold decrease in emission intensity at 571 nm. Interestingly, addition of CN⁻ to the solution of 218 can induce the spirolactam ring-opening of rhodamine,³⁵⁵ realizing a turn-on fluorescent response. In addition, another chemodosimeter 219 containing the trifluoroacetyl (TFA) group can detect micro-molar concentrations of CN⁻ in water with rapid turn-on fluorescence response and high selectivity.³⁵⁶

(2). *Intramolecular H-Bonding-Assisted Nucleophilic Addition Reaction of CN⁻ with Carbonyl Group.* In 2006, Ahn and co-workers first discovered that the anion-binding affinity of the carbonyl group can be significantly enhanced by introducing an H-bond donor (orthocarboxamido group).³⁵⁷ Several CN⁻ chemodosimeters 220–222 were designed based on intramolecular H-bonding-assisted nucleophilic addition processes.

Chemodosimeter 220 consists of a TFA moiety as the binding site and a dansyl moiety as the signaling unit.³⁵⁷ The dansyl sulfonamide proton of 220 can bestow H-bonding assistance to the TFA group for CN⁻ binding and also

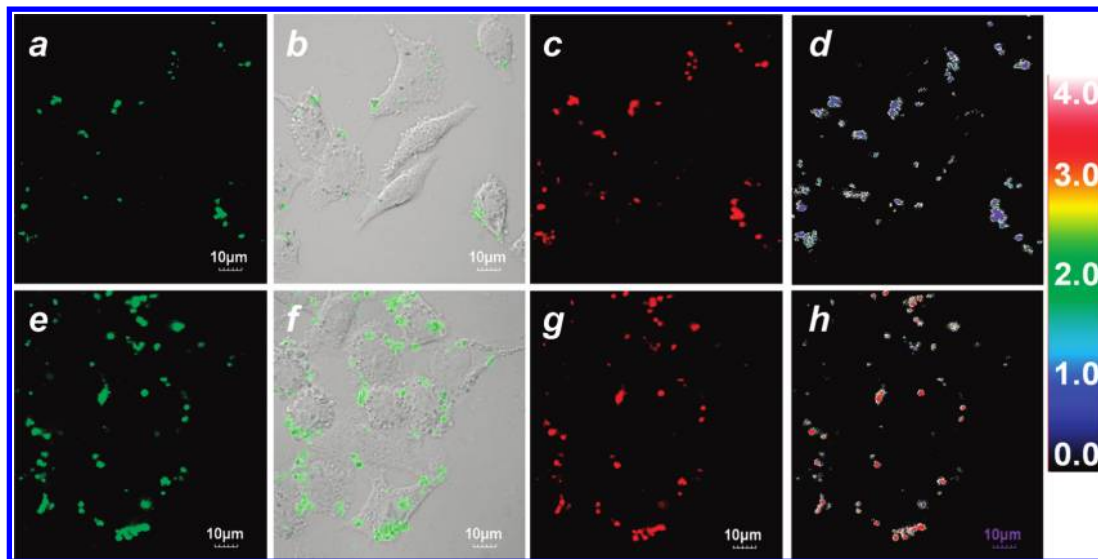


Figure 11. Ratiometric UCL images in HeLa cells (top, a–d) and 50 μM CN^- pretreated HeLa Cells (bottom, e–h) incubated with 5 μM 216-coating $\text{NaYF}_4:\text{Yb},\text{Er},\text{Tm}$ nanophosphors for 2 h at 37 $^\circ\text{C}$. Emission was collected by green UCL channel from 515 to 560 nm (a and e) and red channel from 635 to 680 nm (c and g). (d and h) Ratiometric UCL images with ratio function with green channel and red channel; (b and f) overlay of brightfield images and green UCL images ($\lambda_{\text{ex}} = 980 \text{ nm}$). Reprinted with permission from ref 352. Copyright 2011 American Chemical Society.

modulate the fluorescence signaling by stabilizing its anionic adduct. Upon addition of CN^- , a 5-fold fluorescence enhancement occurred, accompanied by a hypsochromic shift of 36 nm. 220 exhibited a high selectivity and sensitivity toward CN^- anions, but its water solubility was poor.

Cyanide is also capable of nucleophilic attack on the aldehyde group that is activated by local phenol protons through intramolecular hydrogen bonding. On the basis of this mechanism, Yoon and co-workers reported that the luminescent chemodosimeter 221 showed more than 200-fold fluorescent enhancement, only with CN^- , in $\text{CH}_3\text{CN}-\text{H}_2\text{O}$ (9:1, v/v) solution.³⁵⁸ The aldehyde group in salicylaldehyde is activated toward nucleophilic attack of CN^- by intramolecular hydrogen bonding with the phenol proton. The practical applicability of 221 was demonstrated by fluorescent imaging of cyanide in living cells. Similar to 221, coumarin 222 was also designed as a luminescent chemodosimeter for CN^- , and it showed a remarkably high selectivity.³⁵⁹ Moreover, 222 could also be applied to the detection of cyanide in living P19 cells.

(3). *Nucleophilic Addition of CN^- with Indolium Group.* Recently, an indolium-conjugated coumarin 223 was used as a CN^- chemodosimeter.³⁶⁰ In 223, an ICT process takes place from the amine group of coumarin to the positively charged indolium group through a π -conjugated spacer. This ICT is, however, disrupted by the nucleophilic addition of CN^- onto the $-\text{C}=\text{N}^+$ moiety of 223, inducing a break in the indolium conjugation, corresponding to a distinct fluorescence change from weak blue to intense green.

(4). *Opening of the [1,3]Oxazine Ring Induced by Nucleophilic Addition of CN^- .* Tian and co-workers have reported two highly sensitive and selective CN^- chemodosimeters 224 and 225 based on fused indoline and benzooxazine fragments.³⁶¹ In a $\text{CH}_3\text{CN}/\text{H}_2\text{O}$ solution of 224 and 225, the nucleophilic CN^- can specifically attack at the spiro carbon, resulting in the opening of the [1,3]oxazine ring to form the opened forms of 224' and 225', respectively, corresponding to the evident change in optical properties. As a result, the detection of CN^- was realized.

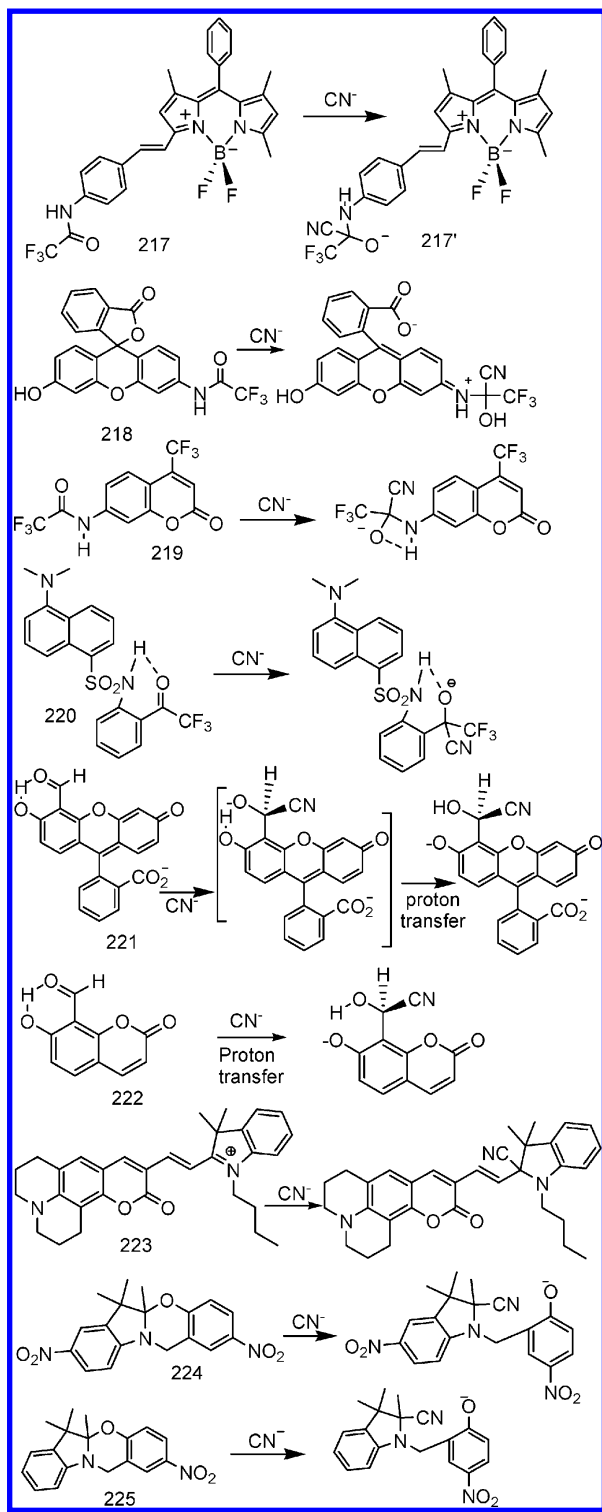
6.2.3. Coordination Reaction of CN^- . A $\text{Co}(\text{II})$ –salen complex 226, which contains coumarin derivatives at the 1,2-positions of the ethylenediamine of the salen ligand and a cobalt(II) ion as a fluorescence quencher, was developed to selectively recognize CN^- (Scheme 49).³⁶² 226 exhibited weak fluorescence emission due to the existence of an intramolecular PET from the coumarin moiety to the cobalt cation. CN^- can coordinate with Co^{2+} in a 1:2 binding stoichiometry, causing a change in the HOMO and LUMO energy levels and leading to a significant enhancement in the fluorescence intensity of 226 by blocking the PET pathway.

6.2.4. Fluorescent CN^- Chemodosimeters Based on Organoboron Compounds. Organoboron compounds can be used for the design of CN^- chemodosimeters, by taking advantage of the strong affinity of boron toward CN^- .

(1). *Nucleophilic Displacement of CN^- with $B-O$ Bond.* Geddes and co-workers reported a series of luminescent chemodosimeters 227–232 that detect CN^- in aqueous solution based on a nucleophilic displacement process.³⁶³ These chemodosimeters take advantage of the ability of boronic acids to interact with CN^- , changing from the neutral $\text{R}-\text{B}(\text{OH})_2$ form to the anionic $\text{R}-\text{B}(\text{CN}^-)_3$ one and thereby perturbing the charge-transfer nature of the excited state (Scheme 50). 227–230 are typical chemodosimeters based on the PET mechanism for detection of CN^- . For example, the addition of 10 mM CN^- almost completely quenched the fluorescence of 230 with a linear change in fluorescence intensity at 425 nm.³⁶³ In contrast with PET-based chemodosimeters 227–230, 231 and 232 are ICT-based chemodosimeters that show a hypsochromic shift of ~40 nm with an increase in fluorescence intensity observed at higher CN^- concentrations.³⁶⁴

(2). *Formation of $B-\text{CN}^-$ Bond.* A subphthalocyanine (SubPc) dye 233 has been developed as an on–off luminescent chemodosimeter for CN^- determination (Scheme 51), with an excellent detection limit of <0.1 ppm in acetonitrile/water (9:1 v/v).³⁶⁵ The detection mechanism is based on the constrained conical structure and the boron-deficient central atom that make SubPcs reactive. In the presence of nucleophiles, either

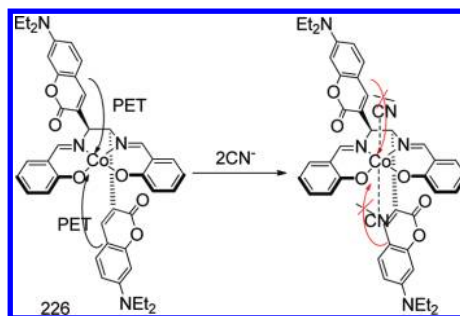
Scheme 48. Sensing Mechanism of 217–225 Based on Nucleophilic Addition Reaction of CN^-



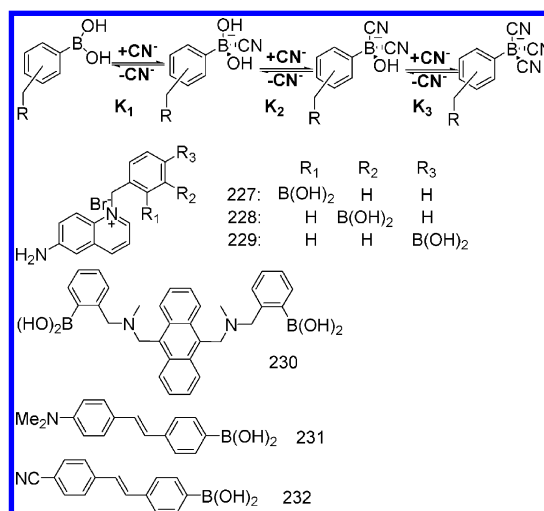
axial substitution or attack on the imine-type core takes place, resulting in ring-opening. However, 233 cannot distinguish CN^- from fluoride anions. In addition, mesoporous TiO_2 films functionalized with another subphthalocyanine derivative 234 containing a carboxylic acid moiety can also detect CN^- in water (Scheme 51).³⁶⁵

In addition to the detection of F^- , cationic boranes can also be designed to sense CN^- in water (Scheme 51). The

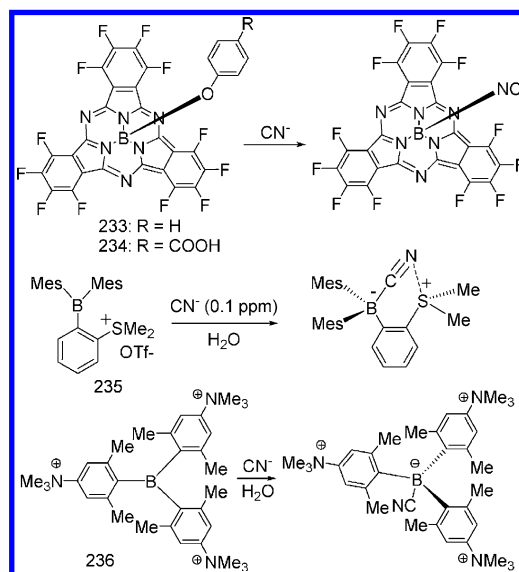
Scheme 49. Sensing Mechanism of 226 Based on Coordination Reaction of CN^-



Scheme 50. Proposed Mechanism of 227–232 Based on Nucleophilic Displacement Reaction of CN^- with B–O Bond

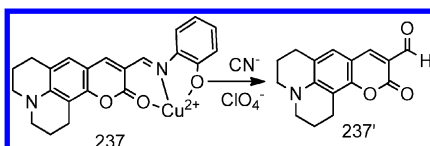


Scheme 51. Sensing Mechanism of Fluorescent CN^- Chemodosimeters 233–236 Based on Formation of B–CN $^-$ Bond



sulfonium borane 235 can be used for the fluorescent detection of CN^- in pure water.³⁶⁶ Its high affinity for CN^- is attributed to the favorable Coulombic effects that serve to stabilize the

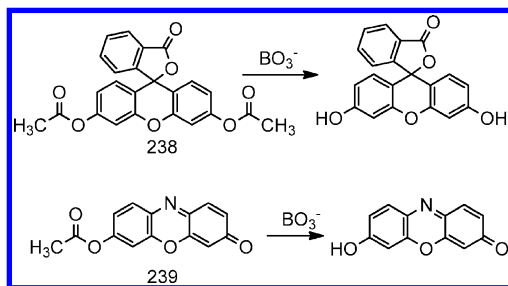
Scheme 52. Sensing Mechanism of 237 Based on CN⁻-Induced Decomplexation Reaction



cyanoborane complex against dissociation. In the case of 236, which contains three cationic moieties,³⁶⁷ both the anion affinity and the water solubility of the borane are improved, allowing it to determine CN⁻ in pure water.

6.2.5. CN⁻-Induced Decomplexation Reaction. The detection of CN⁻ can also be realized using the copper(II) complex 237 through a decomplexation reaction (Scheme 52).³⁶⁸ CN⁻ ion has strong binding ability to Cu²⁺, forming a stable [Cu(CN)_x]ⁿ⁻ complex. Thus, addition of CN⁻ to a solution of 237 induces the decomplexation reaction and subsequent hydrolysis of its Schiff base with aid of water to form highly fluorescent coumarinaldehyde 237', giving a turn-on fluorescence response. Such CN⁻-selective detection with 237 in a biological application has also been performed in

Scheme 53. Sensing Mechanism of Fluorescent BO₃⁻ Chemodosimeters 238 and 239



HepG2 cells to show the off-on fluorescence cellular image (Figure 10).³⁶⁸

6.3. Luminescent Chemodosimeters for BO₃⁻

Perborate (BO₃⁻) is a class of reagent widely used in daily life. It is an effective oxidant and can oxidize various groups, such as thiols and amines. In addition, sodium perborate was found to be a direct-acting *in vitro* mutagen.³⁶⁹ Thus, it is very important to monitor its usage. To date, only two acetate derivatives of functional dyes 238 and 239 have been developed as luminescent chemodosimeters for selective detection of BO₃⁻ (Scheme 53).³⁷⁰

Recently, Chang and co-workers found that fluorescein diacetate 238³⁷⁰ can be used as an off-on fluorescent chemodosimeter for BO₃⁻ detection. Upon treatment with BO₃⁻, a clear fluorescence enhancement was observed at 517 nm, which can be completed within 5 min. In addition, 238 also exhibited excellent selectivity for BO₃⁻ over other anions and oxidants. Such an excellent sensing performance has been attributed to the selective BO₃⁻-induced deprotection of fluorescein diacetate. On the basis of a similar mechanism, resorufin acetate 239³⁷⁰ exhibited a selective fluorescence turn-on behavior toward BO₃⁻.

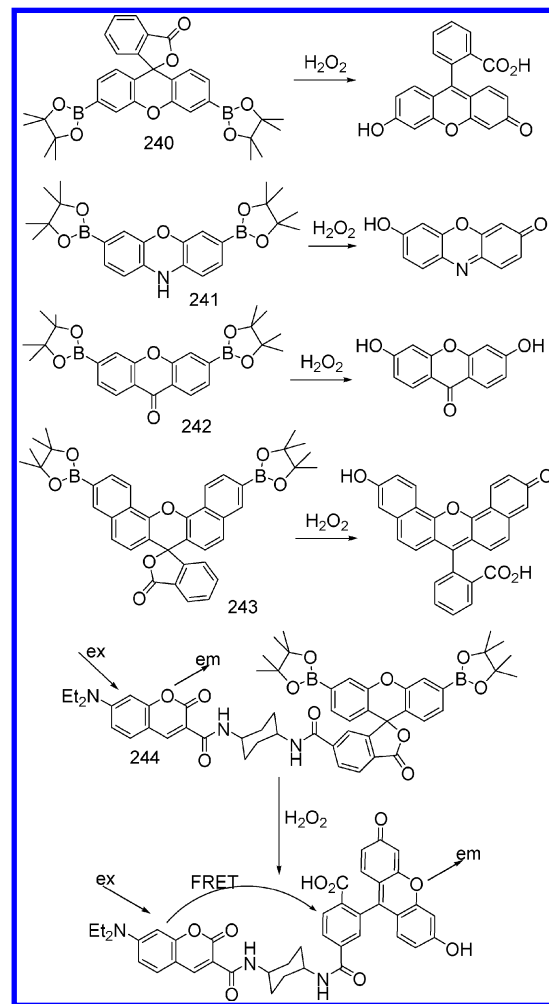
7. LUMINESCENT CHEMODOSIMETERS FOR REACTIVE OXYGEN SPECIES

Reactive oxygen species (ROS) are another class of chemically reactive species and include hydrogen peroxide (H₂O₂), hypochlorous acid (HOCl) and hypochlorite (OCl⁻), singlet oxygen (¹O₂), superoxide (O₂⁻), hydroxyl radicals (OH), and ozone (O₃).³⁷¹ ROS are involved in a wide range of physiological and pathological processes, such as signal transduction, inflammation, carcinogenesis, and neurodegenerative injury. Hence, it is very important to develop and exploit high-quality luminescent chemodosimeters for ROS.

7.1. Luminescent Chemodosimeters for H₂O₂

Generally, hydrogen peroxide (H₂O₂) is toxic to cells. The mismanagement and accumulation of ROS in mammals leads to a condition broadly referred to as oxidative stress, and this has been linked to aging and a host of diseases, including cancer

Scheme 54. Sensing Mechanism of 240–244 Based on H₂O₂-Trigger Transformation of Diboronate to Phenols



and neurodegenerative Alzheimer's and Parkinson's diseases.^{372–374} H₂O₂ is produced transiently in response to the activation of various cell-surface receptors and can be used as a secondary messenger in cellular signaling.^{375–378} Hence, there has been increasing demand for the detection and quantitation of H₂O₂.

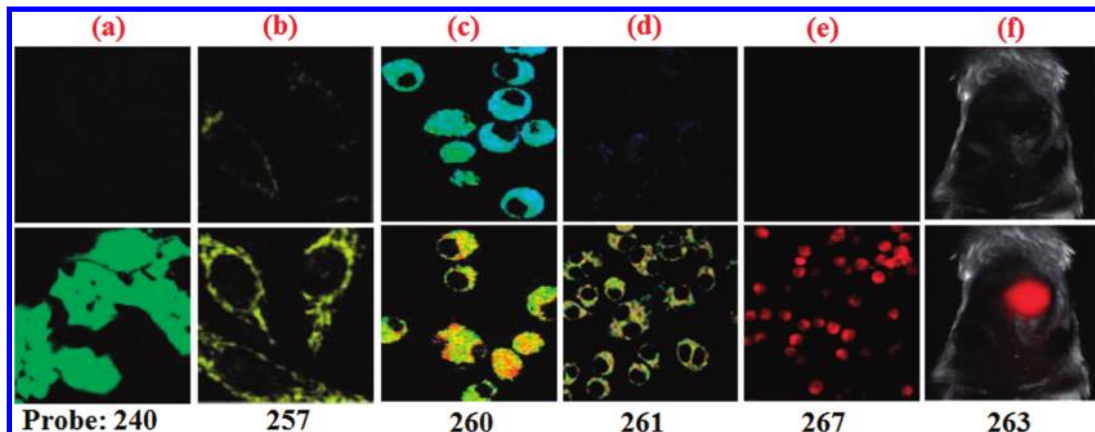
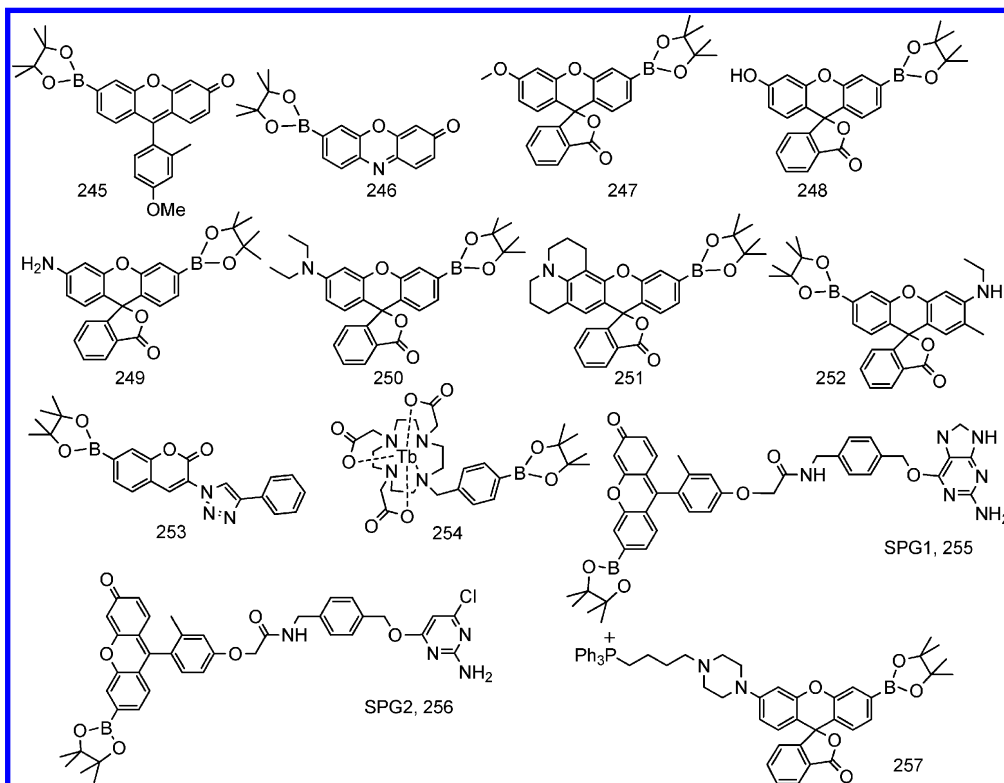


Figure 12. Selected examples of fluorescence imaging of living cells in the absence (upper) or presence (lower) of H_2O_2 using chemodosimeters (240, 257, 260, 261, 267, and 263) as fluorescent probes. Imaging for (a) Reprinted with permission from ref 379. Copyright 2004 American Chemical Society. (b) Reprinted with permission from ref 390. Copyright 2008 American Chemical Society. (c) $\lambda_{\text{ex}} = 820$ nm, ratio of emission intensities collected in optical windows between 535 and 600 (green) and 430–495 nm (blue). Reprinted with permission from ref 393. Copyright 2008 American Chemical Society. (d) Ratiometric images ($F_{\text{green}}/F_{\text{blue}}$). $\lambda_{\text{em}} = 390$ –465 nm (blue channel) and 500–550 nm (green channel). $\lambda_{\text{ex}} = 750$ nm. Reprinted with permission from ref 394. Copyright 2011 Royal Society of Chemistry. (e) Reprinted with permission from ref 397. Copyright 2005 The Royal Society of Chemistry. (f) Reprinted with permission from ref 395. Copyright 2011 American Chemical Society.

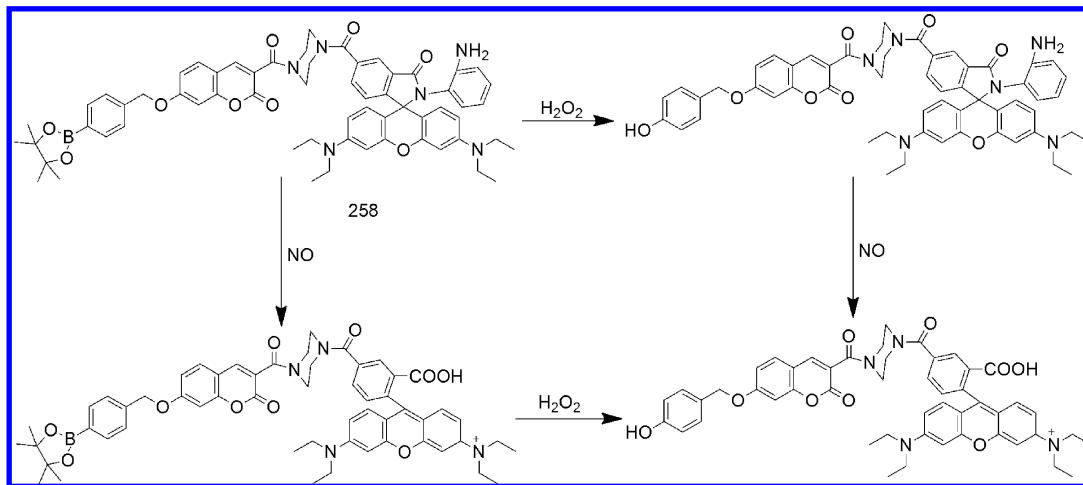
Chart 8. Fluorescence Chemodosimeters 245–257 Based on H_2O_2 -Trigger Single Boronate Deprotection



7.1.1. H_2O_2 -Trigger Transformation of Diboronate to Phenols. (1). *Fluorescence Off-On Chemodosimeter.* Chang's group designed a family of xanthene-based diboronate reagents 240,³⁷⁹ 241,³⁸⁰ 242,³⁸⁰ and 243³⁸⁰ that behave as H_2O_2 chemodosimeters via H_2O_2 -promoted chemoselective boronate deprotection (Scheme 54). All of the chemodosimeters are nonfluorescent, and the addition of H_2O_2 triggers a prompt fluorescence increase. The fluorescence responses of 240–243 to H_2O_2 over other ROS are highly selective. 240–243 are membrane-permeable and can respond to micromolar changes in H_2O_2 concentration within living

cells (Scheme 54). Moreover, two-photon active 242 is capable of imaging changes in intracellular H_2O_2 concentrations using two-photon fluorescence microscopy.³⁸⁰ In addition, 240 is also capable of detecting peroxide-triggered oxidative stress in living hippocampal neurons (Figure 12).³⁷⁹ Flow cytometry experiments in RAW264.7 macrophages established that 243 can also report changes in H_2O_2 levels in living cells.³⁸¹ In addition, by attaching 240 to the dendrimer PAMAM-G5 via amide linkages, a low-toxicity nanoprobe could be prepared for monitoring H_2O_2 in live RAW 264.7 macrophage cells.³⁸²

Scheme 55. Sensing Mechanism of Fluorescence Chemodosimeter 258



(2). *FRET-Based Chemodosimeters.* To quantitatively measure the changes of H_2O_2 concentrations in heterogeneous biological samples, Chang and co-workers synthesized **244** as a ratiometric luminescent chemodosimeter of H_2O_2 .³⁸³ In the absence of H_2O_2 , the boronate protecting groups force the fluorescein acceptor to adopt a closed and nonfluorescent lactone form. Spectral overlap between coumarin emission and fluorescein absorption is minimized and FRET is suppressed, corresponding to only blue donor emission upon excitation of the coumarin chromophore. Upon selective reaction with H_2O_2 , the open and fluorescent fluorescein moiety is generated. Spectral overlap is enhanced, and excitation of the coumarin (donor) results in increased green fluorescein (acceptor) emission by FRET. Changes in H_2O_2 concentration can be detected by measuring the ratio of blue and green fluorescence intensities. Experiments with viable mitochondria show that **244** can detect and quantify endogenous H_2O_2 production in living systems.³⁸³

7.1.2. H_2O_2 -Trigger Transformation of Monoboronate to Phenols. In addition to the above diboronate reagents, to date 13 monoboronate reagents (**245–257**) have also been developed as fluorescence chemodosimeters of H_2O_2 based on H_2O_2 -promoted single boronate deprotection (Chart 8). These chemodosimeters used fluorescein and rhodol, resorufin, coumarin, and 1,8-naphthalimide units as fluorophores. Compounds **245–246**,³⁸⁴ **247–251**,³⁸⁵ **252**,³⁸⁶ **253**,³⁸⁷ and **254**³⁸⁸ act as off-on luminescent chemodosimeters for H_2O_2 -selective detection over a range of rationally tunable visible excitation and emission wavelengths.

The typical examples based on this principle are **245** and **246**,³⁸⁴ which exhibit highly specific responses to H_2O_2 in aqueous solution and living cells, including endogenous intracellular H_2O_2 generated by EGF/Nox activation. In addition, **246** provides strong evidence for H_2O_2 signaling in brain systems through growth factor signaling in live hippocampal neurons. Similarly, **247–251**³⁸⁵ and **252**³⁸⁶ are capable of visualizing changes in H_2O_2 levels in living cells in situations of oxidative stress. In particular, **248**, **250**, and **251** can be used to image low levels of H_2O_2 produced in live samples. Moreover, dual-color imaging experiments using **251**, along with the green-fluorescent highly reactive oxygen species (hROS) probe, allow for selective discrimination between changes in H_2O_2 and hypochlorous acid levels in macrophages,

as well as identification of phagosomes that produce H_2O_2 and/or hROS during an endogenous immune response.³⁸⁵

Taking advantage of the SNAP-tag technology for site-specific protein labeling with small molecules on the surface or interior of living cells, the Chang group went on to develop a new method for monitoring local and subcellular changes in H_2O_2 levels by fluorescence imaging.³⁸⁹ SNAP-PG1 (**255**) and SNAP-PG2 (**256**) having appropriately derivatized boronates bioconjugated to SNAP-tag fusion proteins could specifically detect H_2O_2 over other biologically relevant ROS. Moreover, these hybrid small-molecule/protein reporters can be used in live mammalian cells expressing SNAP-tag fusion proteins directed to the plasma membrane, nucleus, mitochondria, or endoplasmic reticulum. Confocal imaging experiments establish organelle-specific localization of the SNAP-tag probes and their fluorescence turn-on response to changes in local H_2O_2 levels.³⁸⁹

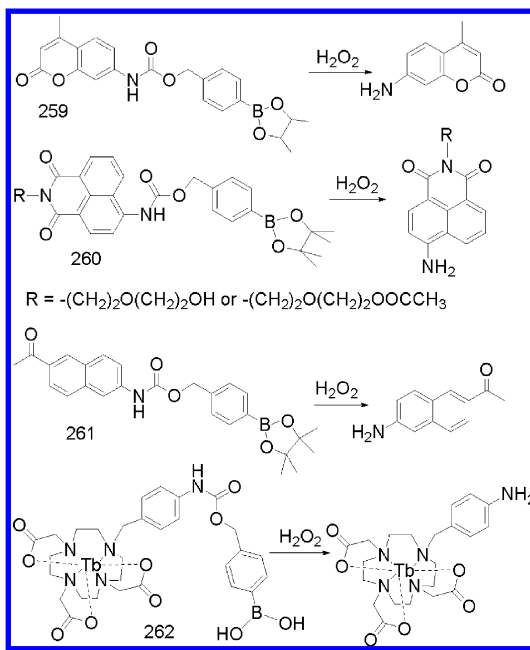
Furthermore, Chang and co-workers reported the first mitochondrial-targeted chemodosimeter **257**, which can selectively image mitochondrial H_2O_2 in living cells (Figure 12).³⁹⁰ The overall strategy is to create bifunctional dyes that contain both a mitochondrial-targeting moiety and a H_2O_2 -responsive element. **257** is capable of imaging changes in the levels of H_2O_2 within the mitochondria of a variety of mammalian cell lines (Figure 12), as well as H_2O_2 elevations caused by an oxidative stress model of Parkinson's disease.

Recently, Lin and co-workers reported an exciting luminescent chemodosimeter **258** for the two-color imaging of H_2O_2 and NO (Scheme 55).³⁹¹ In **258**, the boronate moiety works as a H_2O_2 reaction site, and a phenylenediamine-based reaction site is introduced to respond to NO. 7-Hydroxycoumarin and rhodamine, which have well-separated absorption wavelengths and no cross-talk in the emission spectra, were chosen as the donor and acceptor for FRET system, respectively. Interestingly, **258** can respond to H_2O_2 , NO, and $\text{H}_2\text{O}_2/\text{NO}$ with three different sets of fluorescence signals. Furthermore, **258** is capable of simultaneously monitoring endogenously produced NO and H_2O_2 in living macrophages cells in multicolor imaging.³⁹¹

7.1.3. H_2O_2 -Trigger Deprotection Reaction of Amine.

The amine protecting group in a 2,3-butanediol ester of a *p*-dihydroxyborylbenzoyloxycarbonyl (Dobz) derivative can be selectively removed by H_2O_2 . By combining the transformation of monoboronates to phenols and amine deprotection of the

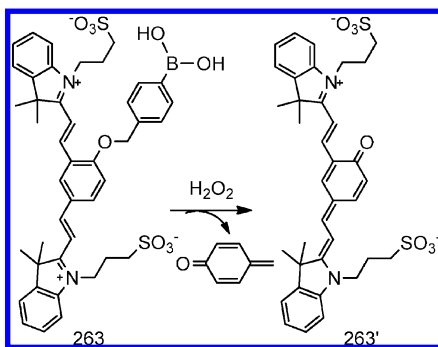
Scheme 56. Sensing Mechanism of 259–262 Based on H₂O₂-Trigger Deprotection Reaction of Amine



Dobz group, a new strategy is generated for the design of H₂O₂-selective luminescent chemodosimeters. To date, four chemodosimeters **259**,³⁹² **260**,³⁹³ **261**,³⁹⁴ and **262**³⁸⁸ have been reported to selectively detect H₂O₂, by using coumarin, 1,8-naphthalimide, and lanthanide complexes as luminophores, respectively (Scheme 56).

259 and **260** are monoboronate ratiometric fluorescent reporters useful for imaging H₂O₂ produced in living systems. The approach to ratiometric fluorescence detection of intracellular H₂O₂ relies on enhanced electron donation of the amine group on a 1,8-naphthalimide of **259** or naphthalyl unit of **260** upon reaction with H₂O₂, accompanied with an ICT-induced red-shift in emission maxima. **260** is capable of imaging H₂O₂ at natural immune response levels in living cells (Figure

Scheme 57. Sensing Mechanism of 263 Based on H₂O₂-Trigger Oxidation of Phenylboronic Acid



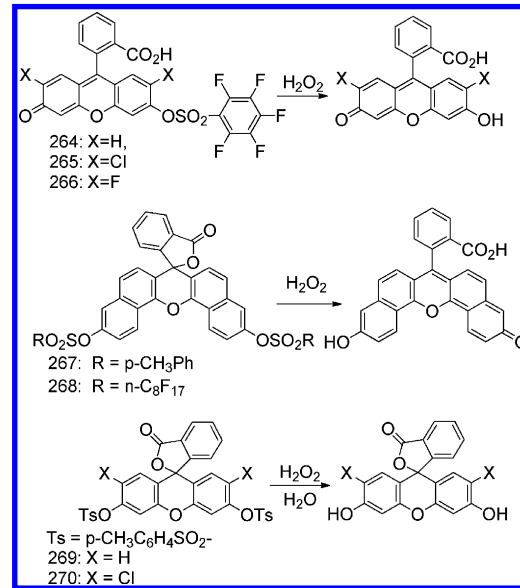
12).³⁹³ Moreover, its ratiometric readout allows for detection of highly localized changes in H₂O₂ concentrations at phagocytic sites while visualizing variations in H₂O₂ concentration throughout the rest of the cytoplasm. Importantly, **261** is two-photon fluorescent-active and can be used for two-photon ratiometric imaging of the changes of H₂O₂ levels deep within live tissue (Figure 12).³⁹⁴ In addition to purely organic probes

for H₂O₂ detection, the Chang group also reported a lanthanide-based luminescent probe **262**, which can detect changes in H₂O₂ levels in living cells by sensitized lanthanide luminescence.³⁸⁸

7.1.4. H₂O₂-Trigger Oxidation of Phenylboronic Acid.

Another important chemodosimeter for H₂O₂ is the sulfonated derivative of cyanine dye **263**,³⁹⁵ containing phenylboronic acid attached through an ether linkage (Scheme 57). Incubation of

Scheme 58. Sensing Mechanism of 264–270 Based on H₂O₂-Mediated Hydrolysis of Sulfonic Esters



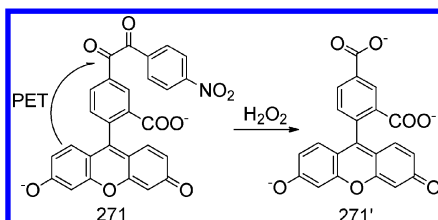
H₂O₂ with **263** under physiological conditions results in oxidation of the phenylboronic acid, followed by hydrolysis and 1,6-elimination of *p*-quinone methide to release the emissive fluorophore **263'**. Because of the formation of ICT process in **263'**, a turn-on fluorescence response was observed. In particular, **263** was successfully demonstrated to efficiently image endogenous H₂O₂ produced in an acute inflammation model in mice (Figure 12).³⁹⁵

7.1.5. H₂O₂-Mediated Hydrolysis of Sulfonic Esters.

Most conventional chemodosimeters for H₂O₂ detection are based on oxidation mechanisms, but they are limited by low selectivity toward H₂O₂. H₂O₂-mediated hydrolysis of sulfonates is an alternative and effective strategy used to generate fluorescent H₂O₂-selective chemodosimeters (Scheme 58). Maeda and co-workers reported three fluorescein monosulfonates **264**–**266** as novel chemodosimeters that show high selectivity toward H₂O₂. Their detection method is based on simple deprotection, rather than oxidation.³⁹⁶ These new chemodosimeters, and their analogues, facilitate the measurement of cell-derived H₂O₂ and have been used to elucidate the dynamic functions of oxidative stress, not only in algal cells but also in phagocytes and vascular endothelium cells.

Chemodosimeters **267**,³⁹⁷ **268**,³⁹⁷ **269**,³⁹⁸ and **270**³⁹⁸ are based on H₂O₂-mediated hydrolysis of disulfonates. They exhibit high selectivity for H₂O₂ over other reactive oxygen species, with strong fluorescence turn-on responses. Upon treatment with H₂O₂, hydrolytic deprotection promotes the conversion of closed, colorless, and nonfluorescent lactones into open, colored, and fluorescent products. Compared with fluorescein-based chemodosimeters **269**–**270**, naphthofluor-

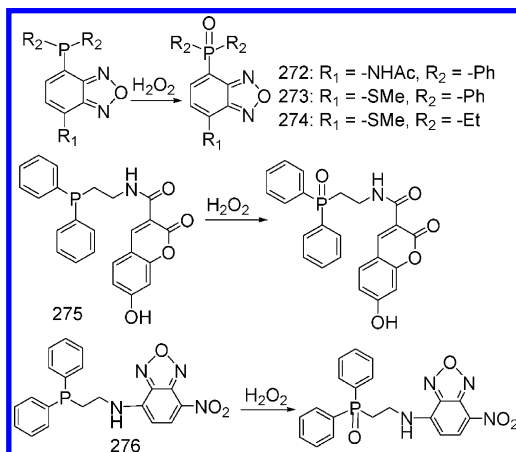
Scheme 59. Sensing Mechanism of 271 Based on H₂O₂-Trigger Transformation of Benzyl to Benzoic Acid



escein-based probes **267** and **268** show longer-wavelength excitation and emission, avoiding background fluorescence interference. Moreover, they are cell-permeable and can detect micromolar changes in H₂O₂ concentration in living cells. **267** can respond to nanomolar changes in H₂O₂ concentration within living cells (Figure 12), whereas native cellular species such as GSH and ascorbic acid do not contribute to the fluorescence imaging.³⁹⁷

7.1.6. H₂O₂-Trigger Transformation of Benzyl to Benzoic Acid. Through a Baeyer–Villiger-type reaction, the benzyl group can react with H₂O₂ to form benzoic anhydride, which is subsequently hydrolyzed to give benzoic acid (Scheme 59).³⁹⁹ On the basis of this reaction mechanism, the 5-benzoylcarbonylfluorescein derivative **271**⁴⁰⁰ was designed as a fluorescence chemodosimeter for H₂O₂. Because of efficient quenching via the PET process, **271** showed extremely weak fluorescence. Upon reaction with H₂O₂, **271** was transformed to **271'**, accompanied by a very large increase of the fluorescence intensity. Furthermore, **271** has been successfully

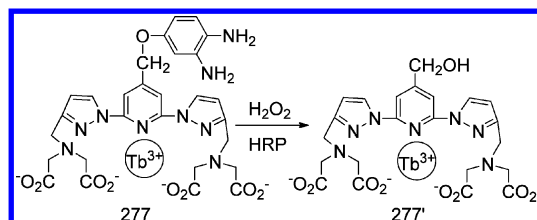
Scheme 60. Sensing Mechanism of 272–276 Based on H₂O₂-Trigger Oxidation of Triphenylphosphine



applied to the imaging of H₂O₂ generation in live RAW 264.7 macrophages and A431 cells.

7.1.7. H₂O₂-Trigger Oxidation of Triphenylphosphine. The use of the derivatization reagent diphenyl-1-pyrenylphosphine (DPPP) as a probe for the detection of H₂O₂ has proven to be a very useful method. Triarylphosphines can be chosen as the reactive moieties, because they are stable and can react with H₂O₂ to give the corresponding phosphine oxides under mild conditions. On the basis of this reaction, linking a fluorophore unit with triarylphosphine is another useful strategy in the design of H₂O₂-selective chemodosimeters. Compounds **272**–**274**,⁴⁰¹ **275**,⁴⁰² and **276**⁴⁰³ are based on this strategy, using

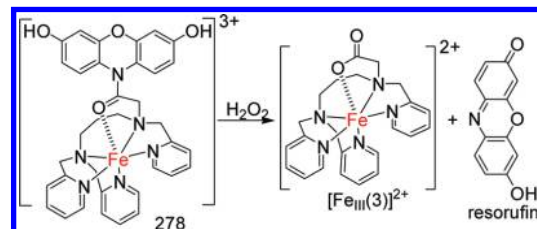
Scheme 61. Sensing Mechanism of 277 Based on H₂O₂-Trigger Cleavage of Diaminophenyl Ether



2,1,3-benzoxadiazole, 7-nitro-2,1,3-benzoxadiazole, and 7-hydroxycoumarin moieties, respectively, as fluorophores (Scheme 60). They show fluorescent turn-on response, because PET from the triarylphosphine to the fluorophore is inhibited upon reaction with H₂O₂. Unfortunately, these chemodosimeters have not been applied to fluorescent bioimaging of H₂O₂ in living cells.

7.1.8. H₂O₂-Trigger Cleavage of Diaminophenyl Ether. H₂O₂ can also induce the cleavage reaction of diaminophenyl ether. Utilizing this reaction, the Tb³⁺ complex **277** was reported to act as a luminescent turn-on chemodosimeter for H₂O₂ (Scheme 61).⁴⁰⁴ The luminescence from **277** is effectively quenched by the electron-rich diaminophenyl moiety

Scheme 62. Sensing Mechanism of 278 Based on H₂O₂-Trigger Oxidation of Fe Complexes



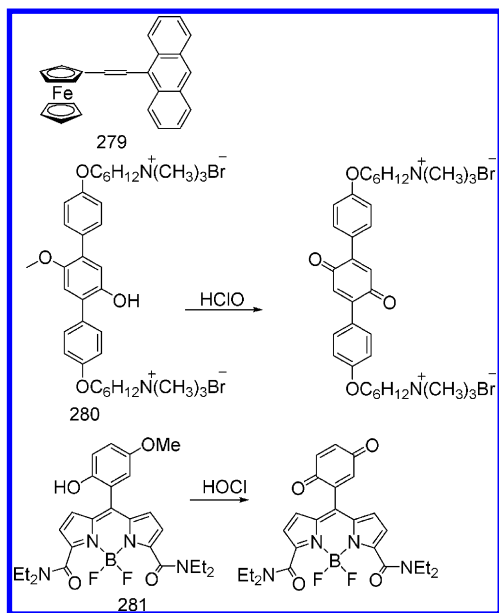
through the PET process. However, the diaminophenyl ether can be cleaved when **277** reacts with H₂O₂ in the presence of peroxidase, resulting in the formation of highly emissive **277'** accompanied by an increase in luminescence intensity (39-fold) and emission lifetime from 1.95 to 2.76 ms. However, the sole addition of H₂O₂ or peroxidase does not induce such a change of luminescent signal. Furthermore, considering the long emission lifetime of the Tb³⁺ complex, **277** has been used for the time-resolved luminescence imaging of the oligosaccharide-induced generation of H₂O₂ in tobacco leaf epidermal tissues, which eliminates the short-lived background fluorescence.⁴⁰⁴

7.1.9. H₂O₂-Trigger Oxidation of Fe Complexes. Recently, Hitomi and co-workers designed and synthesized a metal-based fluorescent chemodosimeter **278** for H₂O₂ (Scheme 62).⁴⁰⁵ In **278**, the iron complex acts as a reaction site for H₂O₂ and a 3,7-dihydroxyphenoxazine derivative acts as the fluorescent reporter. Upon addition of H₂O₂, the iron complex can react with H₂O₂ to form the oxidized product quickly, leading to the conversion of nonfluorescent 3,7-dihydroxyphenoxazine moiety to strongly luminescent resorufin, corresponding to a turn-on fluorescence response. The detection of enzymatically generated H₂O₂ can also be realized by **278**, even in the presence of phenol derivatives.⁴⁰⁵

7.2. Luminescent Chemodosimeters for HOCl/OCl[–]

Hypochlorous acid (HOCl) and hypochlorite (OCl[–]) are also reactive oxygen species. HOCl is weakly acidic and partially

Scheme 63. Sensing Mechanism of 279–281 Based on HOCl-Induced Oxidation



dissociates into the OCl^- under physiological pH conditions.⁴⁰⁶ HOCl/ OCl^- reacts with various biomolecules including DNA, RNA, fatty acids, cholesterol, and proteins and has strong antibacterial properties. However, abnormal amounts of HOCl/ OCl^- are involved in several human diseases, including neuron degeneration, cardiovascular diseases, and osteoarthritis.⁴⁰⁷ Therefore, a lot of effort has been made to the development of luminescent chemodosimeters for HOCl/ OCl^- detection based on oxidation, spirolactam ring-opening processes, and cleavage of the ether moiety.

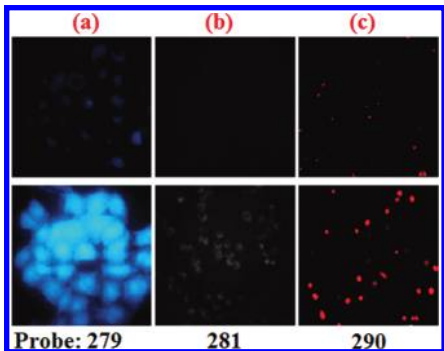


Figure 13. Selected examples of fluorescence imaging of living cells in the absence (upper) or presence (lower) of HOCl/ OCl^- using chemodosimeters (**279**, **281**, and **290**) as fluorescent probes. (a) Reprinted with permission from ref 408. Copyright 2010 Royal Society of Chemistry. (b) Reprinted with permission from ref 410. Copyright 2008 American Chemical Society. (c) Reprinted with permission from ref 419. Copyright 2010 Elsevier B.V.

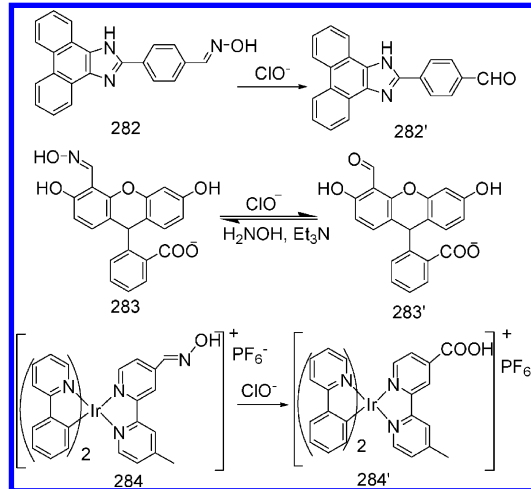
7.2.1. HOCl-Induced Oxidation Process. Three compounds (**279**–**281**, Scheme 63) were designed as HOCl luminescent chemodosimeters, based on the strong oxidation characteristics of the analyte.

(1). *Oxidation of Double Bond.* Anthracene fluorescence is strongly quenched by the electron-donor ferrocene in **279**, via an intramolecular charge-transfer process (Scheme 63).⁴⁰⁸ However, the double bond of **279** can be readily oxidized by

HOCl, causing the destruction of the quenching process and thus the recovery of anthracene fluorescence. Chemodosimeter **279** exhibits a high selectivity toward HOCl among reactive oxygen species and other ions. In addition, the application of **279** to imaging of HOCl in HeLa cells was demonstrated (Figure 13).

(2). *Oxidation of p-Methoxyphenol into Quinone.* Similarly, on the basis of the HOCl-induced oxidation of *p*-methoxyphenol into benzoquinone, **280**⁴⁰⁹ and **281**⁴¹⁰ were developed as the luminescent chemodosimeters for HOCl detection (Scheme 63). For **280**, the oxidation of *p*-methoxyphenol by HOCl results in the quenching of the fluorescence. **281**, however, exhibits fluorescence enhancement after oxidation of *p*-methoxyphenol by HOCl. As the HOMO energy level of the *p*-methoxyphenol moiety is higher than that of the BODIPY unit, the fluorescence of the BODIPY unit is

Scheme 64. Sensing Mechanism of 282–284 Based on OCl^- -Induced Deoximation Reaction

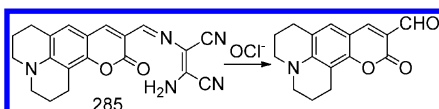


quenched through a PET process. The HOMO energy level of the benzoquinone moiety is lowered by oxidation with HOCl, inhibiting the quenching process and thus generating a fluorescent product. Interestingly, **281** selectively detects HOCl over OCl^- and could be successfully employed in selective imaging of the production of HOCl in living macrophage cells.⁴¹⁰

7.2.2. OCl^- -Induced Destruction of the C=N Bond.

(1). *OCl^- -Induced Deoximation Reaction.* It is known that OCl^- can selectively react with oxime to form aldehyde or carboxylic acid under mild conditions.⁴¹¹ Utilizing this OCl^- -induced deoximation reaction, three excellent chemodosimeters **282**,⁴¹² **283**,⁴¹³ and **284**⁴¹⁴ have been reported for selective detection of OCl^- (Scheme 64). For **282**, the oxime protective group can be removed by OCl^- to give the aldehyde group (**282'**), which results in an obvious change of the emission color of the solution from blue to green, allowing ratiometric detection.⁴¹² In a similar mechanism, **283** was also designed as a luminescent chemodosimeter for OCl^- . Most recently, a cationic iridium(III) complex **284** was reported as a phosphorescent chemodosimeter for OCl^- . Because of the rapid isomerization of C=N–OH, which leads to an effective nonradiative decay process, **284** exhibits very weak emission in solution. Upon addition of OCl^- , the oxime is readily oxidized to carboxylic acid and a new highly emissive complex **284'** is formed, along with a remarkable phosphorescence enhance-

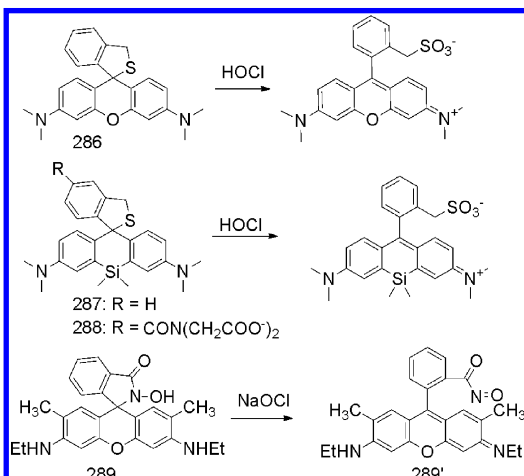
Scheme 65. Sensing Mechanism of 285 Based on OCl^- -Induced Dediaminomaleonitrile Reaction



ment. Importantly, **284** exhibits high selectivity and sensitivity for OCl^- compared with other reactive oxygen species and metal ions.⁴¹⁴

(2). OCl^- -Induced Dediaminomaleonitrile Reaction. Utilizing the OCl^- -induced dediaminomaleonitrile reaction, com-

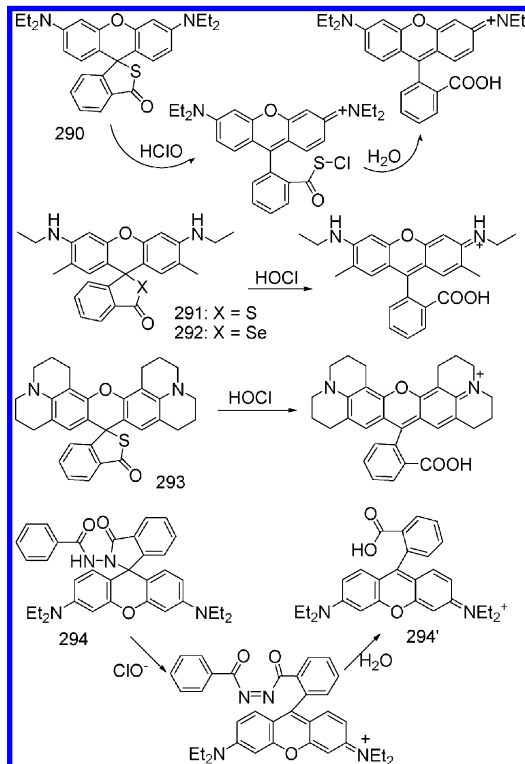
Scheme 66. Sensing Mechanism of 286–289 Based on HOCl-Induced Spirolactam Ring-Opening and Oxidation Reactions



pound **285** was designed as a ratiometric luminescent chemodosimeter for OCl^- (Scheme 65).⁴¹⁵ **285** displays an emission peak with a maximum at ~ 585 nm. Upon addition of OCl^- , the emission intensity at 585 nm decreased gradually with the simultaneous appearance of a new blue-shifted emission band centered at 505 nm, realizing the ratiometric detection. Furthermore, **285** was used for ratiometric imaging of OCl^- in live MCF-7 cells.

7.2.3. HOCl-Induced Spirolactam Ring-Opening and Oxidation Reactions. Several rhodamine-based HOCl chemodosimeters **286–289** were designed that relied on HOCl-induced spirolactam ring-opening and oxidation reaction (Scheme 66). These chemodosimeters exhibited high selectivity toward HOCl with strong fluorescence enhancement. Nagano and co-workers found that rhodamine derivative **286**⁴¹⁶ detects HOCl selectively over the OCl^- anion via ring-opening induced by oxidation of the S atom. **286** was successfully applied to the visualization of phagocytosis by porcine neutrophils, with opsonized zymosan derived from *Saccharomyces cerevisiae* as a target. On the basis of a similar mechanism, two NIR-emitting fluorescence HOCl chemodosimeters based on Si-rhodamine **287** and **288** have been reported.⁴¹⁷ The relative fluorescence detected in the abdomen of mice after intraperitoneal administration was 1 order of magnitude greater with **287** than with the visible light-emitting **286**, demonstrating that **287** is superior to **286** for in vivo bioimaging applications. Furthermore, **287** has been successfully applied in the detection of HOCl generation during phagocytosis. The noninvasive in vivo imaging of HOCl generation in a mouse peritonitis model

Scheme 67. Sensing Mechanism of 290–294 Based on HOCl-Induced Spirolactam Ring-Opening and Hydrolyzation Processes

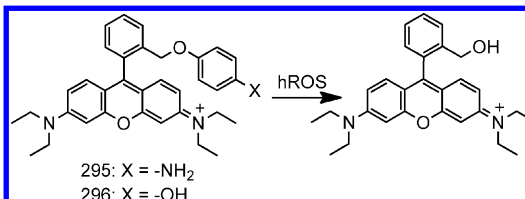


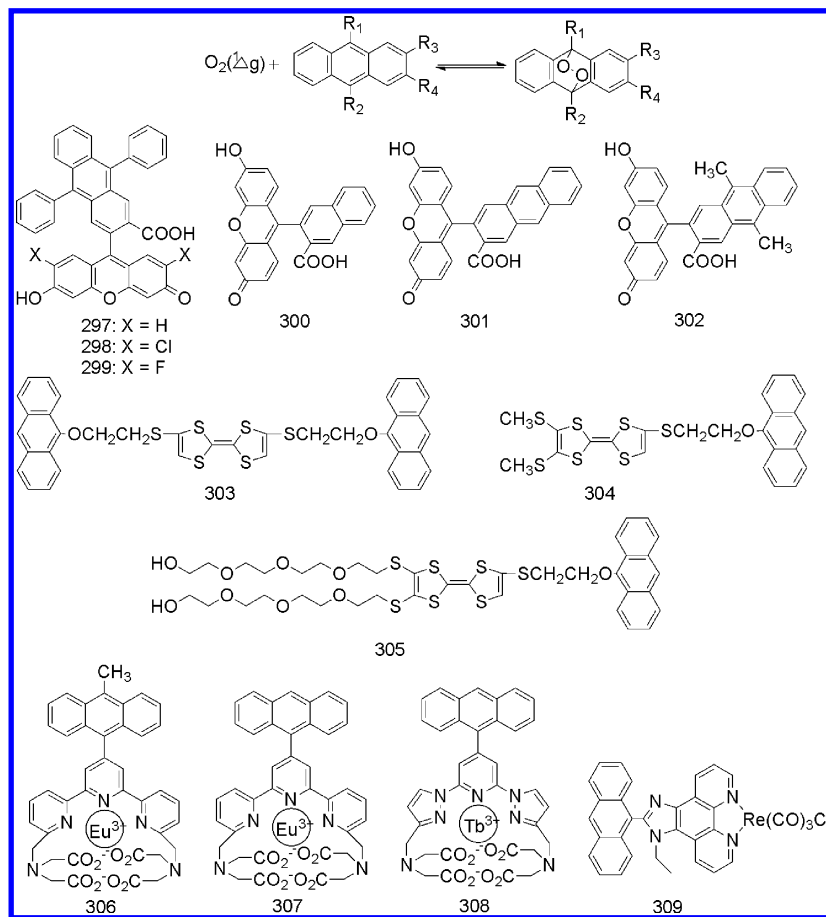
was also achieved based on the more hydrophilic **288**.⁴¹⁷ In addition, **289** has also been applied to bioimaging in A549 cells and 5-day-old zebrafish.⁴¹⁸

7.2.4. HOCl-Induced Spirolactam Ring-Opening and Hydrolyzation Processes. On the basis of the HOCl-induced spirolactam ring-opening and hydrolyzation processes, four rhodamine thiospirolactone-based chemodosimeters, **290**⁴¹⁹ and **291–293**,⁴²⁰ have been reported, exhibiting turn-on fluorescence detection of HOCl with high selectivity among various ROS (Scheme 67). In the sensing process, a HOCl-promoted chlorination reaction occurs, opening the spiro-ring to form a fluorogenic intermediate that was further hydrolyzed to release a rhodamine unit. Importantly, **290** and **291** can selectively visualize HOCl generated in living cells by fluorescence microscopy (Figure 13). In particular, because of the high selectivity and sensitivity for the detection of HOCl, **291** has been applied for the imaging of microbe-induced HOCl production in animal tissues.⁴²⁰

Recently, Ma and co-workers have reported another rhodamine derivative **294** as a fluorescent turn-on chemodosimeter for selective detection of OCl^- . For nonluminescent

Scheme 68. Sensing Mechanism of 295 and 296 Based on HOCl-Induced Cleavage of the Ether Moiety



Scheme 69. Proposed Mechanism of Anthracene-Based Chemodosimeters 297–309 for $^1\text{O}_2$ 

294, the hydrazone group was selectively oxidized upon addition of the OCl^- anion, to form an analogue of dibenzoyldiimide, which in turn hydrolyzes and releases the rhodamine fluorophore (Scheme 67).⁴²¹ As a result, its fluorescence is switched on.

7.2.5. OCl^- -Induced Cleavage of the Ether Moiety. For rhodamine derivatives **295** and **296**, their fluorescences were quenched via the PET process from 4-amino- or 4-hydroxylphenyl ether moieties to xanthene moiety (Scheme 68).⁴²² The addition of OCl^- can cause the cleavage of the ether moiety, affording the highly fluorescent units and realizing turn-on fluorescence response. In addition to OCl^- , other highly reactive oxygen species (hROS), such as $\cdot\text{OH}$ and ONOO^- , can also induce the fluorescence response. Importantly, **295** and **296** can sensitively and selectively detect mitochondrial hROS generation in living cells.

7.3. Luminescent Chemodosimeters for $^1\text{O}_2$

Singlet oxygen ($^1\text{O}_2$) is an excited state of molecular oxygen and is a highly reactive molecule that is potentially damaging to biological systems. It can oxidize various kinds of biological molecules such as DNA, proteins, and lipids.^{423,424} To date, the main mechanisms for sensing $^1\text{O}_2$ are based on the formation of endoperoxide and the $^1\text{O}_2$ -induced 1,4-cycloaddition of the anthracene ring (Scheme 69).

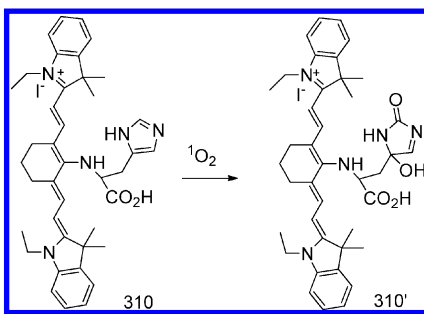
7.3.1. $^1\text{O}_2$ -Induced Formation of Endoperoxide. The most widely used $^1\text{O}_2$ trap is anthracene or 9,10-diphenylanthracene (DPA) derivatives, which react rapidly with $^1\text{O}_2$ specifically to form the thermostable endoperoxide.⁴²⁵

(1). On the Basis of Fluorescent Organic Chromophores.

To date, a series of fluorescein derivatives **297–302** containing anthracene or the DPA moiety have been reported as chemodosimeters for $^1\text{O}_2$. They are almost nonfluorescent due to the PET process. Upon reaction with $^1\text{O}_2$, the newly formed endoperoxide derivatives are highly fluorescent. Thus, **297–299**⁴²⁶ and **300–302**⁴²⁷ work as good turn-on fluorescence chemodosimeters for $^1\text{O}_2$. For the tetrathiafulvalene (TTF)-based chemodosimeters **303**,⁴²⁸ **304**,⁴²⁹ and **305**,⁴³⁰ which are nonemissive due to the PET between TTF and anthracene units, reaction with $^1\text{O}_2$ causes inhibition of the PET process, so **303** and **305** exhibit a significant luminescent enhancement response to $^1\text{O}_2$.

(2). On the Basis of Luminescent Metal Complexes. Some lanthanide complexes **306–308** and the Re(I) complex **309** have been developed as luminescent turn-on chemodosimeters for $^1\text{O}_2$. The design principle is based on the inhibition of the triplet–triplet quenching effect through the reaction of anthracene with $^1\text{O}_2$ to form endoperoxide. For the lanthanide complexes **306**,⁴³¹ **307**,⁴³² and **308**,⁴³³ the strong triplet (terpyridine)–triplet (anthracene) quenching blocks the effective energy transfer from ligand to Eu³⁺ or Tb³⁺ ion, leading to weak luminescence. After the reaction with $^1\text{O}_2$, this triplet–triplet quenching disappears and the lanthanide complexes become strongly luminescent. Moreover, as a result of the long emission lifetime, time-gated luminescence imaging using **306** as a probe to monitor time-dependent $^1\text{O}_2$ generation in living cells has been demonstrated.⁴³¹ A similar result has been obtained using the Tb(III) complex **308**. In

Scheme 70. Sensing Mechanism of 310 Based on $^1\text{O}_2$ -Induced 1,4-Cycloaddition Reaction of Imidazole



addition, the Re(I) complex **309**⁴³⁴ has also been shown to be a visible light excited phosphorescent chemodosimeter for selective detection of $^1\text{O}_2$.

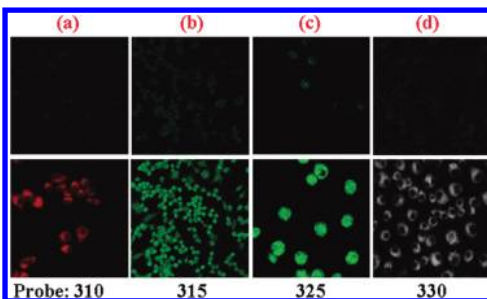


Figure 14. Selected examples of fluorescence imaging of living cells in the absence (upper) or presence (lower) of $^1\text{O}_2$ (for **310**), O_2^- (for **315** and **325**), or $^\bullet\text{OH}$ (for **330**) using the chemodosimeters as fluorescent probes. Imaging at lower for (a) Reprinted with permission from ref 435. Copyright 2011 Royal Society of Chemistry. (b) Reprinted with permission from ref 443. Copyright 2007 The Authors Journal Compilation. (c) Reprinted with permission from ref 448. Copyright 2007 Wiley-VCH Verlag GmbH & Co. KgaA, Weinheim. (d) Reprinted with permission from ref 453. Copyright 2010 Wiley-VCH Verlag GmbH & Co. KgaA, Weinheim.

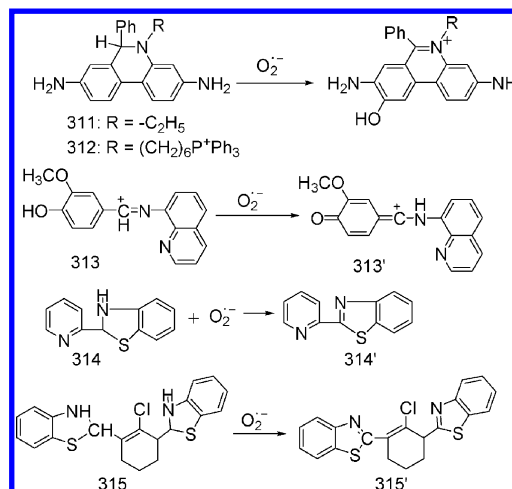
7.3.2. $^1\text{O}_2$ -Induced 1,4-Cycloaddition of Imidazole. Recently, $^1\text{O}_2$ -induced 1,4-cycloaddition reaction of the imidazole ring has also been used for detecting $^1\text{O}_2$. Tang and co-workers reported the cyanine dye **310**⁴³⁵ containing histidine as a NIR fluorescent chemodosimeter of $^1\text{O}_2$ (Scheme 70). Because of the photoinduced electron transfer from histidine to the excited fluorophore, **310** shows weak fluorescence. Upon reaction of **310** with $^1\text{O}_2$, the imidazole group is oxidized through 1,4-cycloaddition of the imidazole ring, and the PET is inhibited, leading to the recovery of fluorescence from the cyanine fluorophore. Furthermore, **310** can respond to changes of $^1\text{O}_2$ concentrations in living cells (Figure 14).

7.4. Luminescent Chemodosimeters for O_2^-

Superoxide (O_2^-) is a product of a one-electron reduction of molecular oxygen. It has a short half-life and is involved in a variety of physiological processes in living organisms, such as aging, muscle fatigue, ischemia-reperfusion, and inflammation.^{436,437} Therefore, real-time monitoring of O_2^- under physiological conditions is of increasing importance.

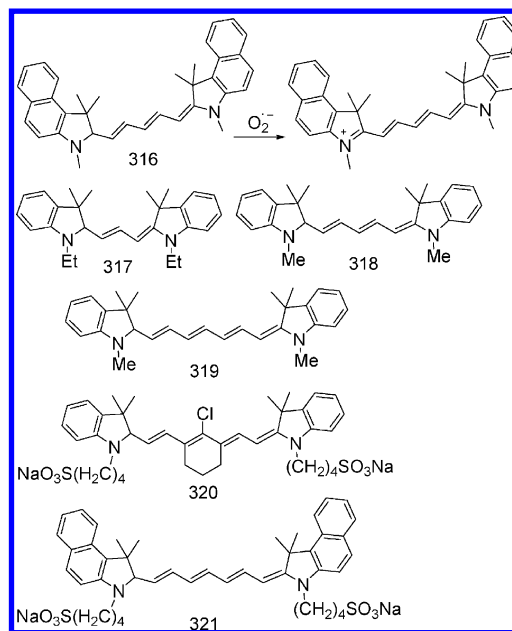
7.4.1. O_2^- -Induced Oxidation Reaction. One of the most widely used assays for the detection of intracellular O_2^- involves the reaction between O_2^- and hydroethidine **311** (Scheme 71).^{438,439} The oxidation of **311** results in the

Scheme 71. Sensing Mechanism of 311–315 Based on O_2^- -Induced Oxidation Reaction



formation of a fluorescent product 2-hydroxyethidium **311'**. The primary radical is derived from the loss of an aromatic amino hydrogen atom that, upon rearrangement, further reacts with another O_2^- to form **311'**. Other reactive oxygen and nitrogen species cannot oxidize **311** to the same product. Furthermore, **311'** can be used for detecting intracellular O_2^- .

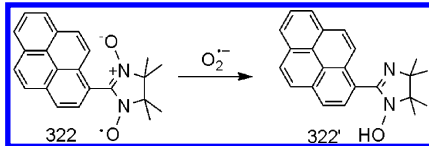
Scheme 72. Sensing Mechanism of 316–321 Based on O_2^- -Induced Oxidation Reaction



When bovine aortic endothelial cells (BAECs) were pretreated with different concentrations of menadione intracellular O_2^- generator and were further treated with **311**, a dose-dependent increase in red fluorescence was observed.⁴³⁹ However, the autoxidation or nonsuperoxide-dependent cellular processes can oxidize **311** to ethidium. Furthermore, another excellent luminescent O_2^- chemodosimeter **312** containing the triphenylphosphonium cation as the target moiety for mitochondria has been developed, with minimal interference from other nonspecific oxidation products (Scheme 71).⁴⁴⁰ **312** can be used for the detection of mitochondrial superoxide.

There have been some other fluorophores 313–321 used for detecting O_2^- based on oxidation reactions (Scheme 72). Except for the Schiff's base derivative 313,⁴⁴¹ the other chemodosimeters 314,⁴⁴² 315,⁴⁴³ and 316–321⁴⁴⁴ exhibit a fluorescence turn-on response to O_2^- through O_2^- -induced oxidation reactions. An interesting example is the cell-permeable chemodosimeter 315.⁴⁴³ It reacts with O_2^- with high selectivity, yielding a strong fluorescence product 315' with an emission maximum at 559 nm and is able to respond to

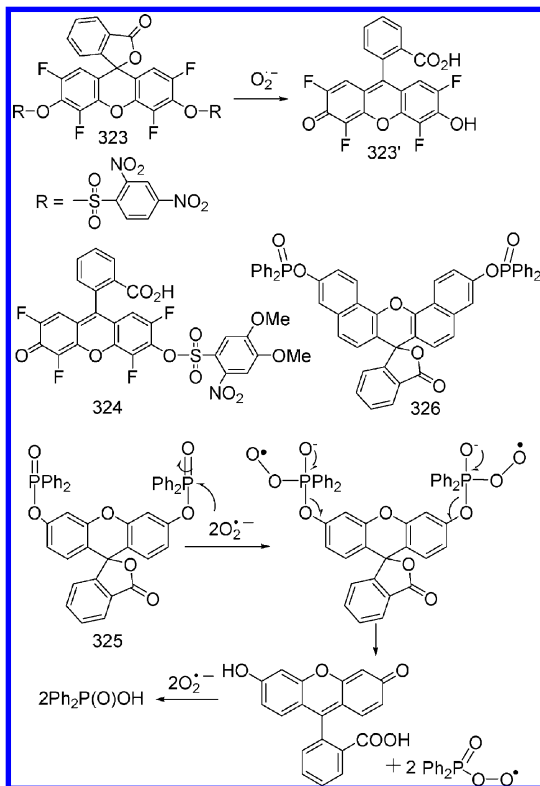
Scheme 73. Sensing Mechanism of 322 Based on Reaction of O_2^- with Nitroxide



micromolar changes in O_2^- concentration within live RAW264.7 macrophages (Figure 14). The more interesting case of O_2^- selective chemodosimeters is the series of hydrocyanines 316–321.⁴⁴⁴ These hydrocyanines are weakly fluorescent because of their disrupted π -conjugation. Oxidation with O_2^- forms cyanine dyes by regenerating their extended π -conjugation, accompanied by significant enhancement of the fluorescence intensity. Furthermore, the hydrocyanines can image O_2^- in cell culture, in tissue explants, and, for the first time, *in vivo*.⁴⁴⁴

7.4.2. Reaction of O_2^- with Nitroxide. Luminescent chemodosimeters for O_2^- can also be realized by utilizing the reaction between O_2^- and nitroxide (Scheme 73). 322 contains the nitroxide fragment, which is a strong intramolecular

Scheme 74. Sensing Mechanism of 323–326 Based on O_2^- -Induced Deprotection Reaction



quencher of the fluorescence from the pyrene fragment.⁴⁴⁵ The addition of O_2^- induces the reduction of 322 to the hydroxylamine derivative 322', resulting in a turn-on fluorescence response to O_2^- .

7.4.3. O_2^- -Induced Protection–Deprotection Reaction. Utilizing the O_2^- -induced deprotection of sulfonylated and diphenyl phosphinated fluoresceins, a series of excellent fluorescent chemodosimeters 323–326 for O_2^- have been realized.

(1). *Deprotection of 2,4-Dinitrobenzenesulfonyl Group.* The bis(2,4-dinitrobenzenesulfonyl) fluorescein 323⁴⁴⁶ is transformed to 323' by a deprotection reaction with O_2^- , corresponding to a turn-on fluorescence response (Scheme 74). This fluorescent response can also be realized in neutrophils by fluorescence microscopy. However, 323 also exhibits undesirable reactivity toward thiols and reductases, which precludes its use in the specific measurement of O_2^- in real biological systems. In these circumstances, the more practical O_2^- -chemodosimeter 324 has been developed, which exhibits greater specificity toward O_2^- over GSH and ROS (Scheme 74).⁴⁴⁷ Furthermore, using flow cytometry and fluorescence microscopy, the intracellular generation of O_2^- in human Jurkat T cells stimulated by butyric acid has been measured, utilizing 324 as the fluorescent probe.

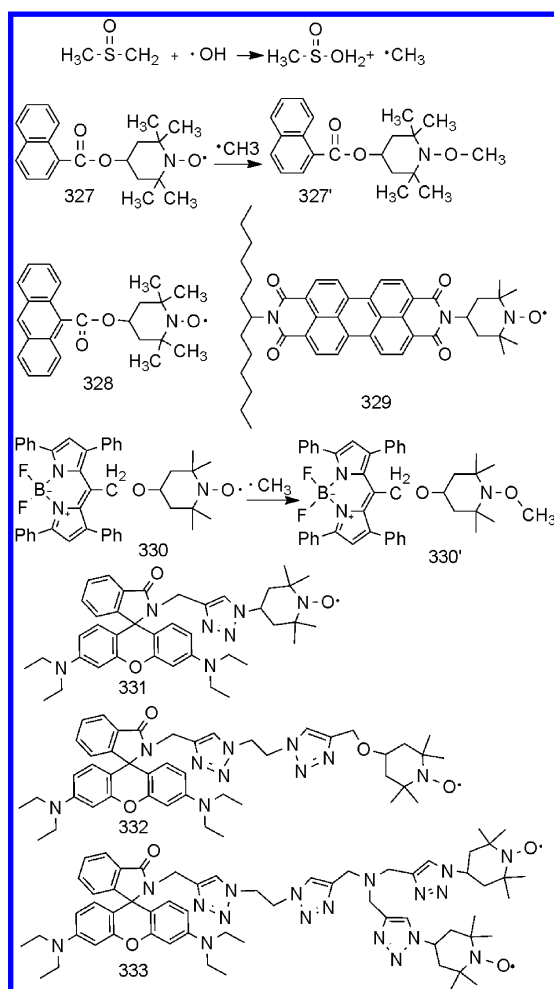
(2). *Deprotection of Diphenylphosphinyl Group.* On the basis of the O_2^- -induced deprotection of the diphenylphosphinyl unit, two phosphinate-based dyes 325⁴⁴⁸ and 326⁴⁴⁹ have been developed as luminescent chemodosimeters for O_2^- (Scheme 74). The nucleophilic reaction of O_2^- mediates the deprotection of nonfluorescent 325 to give emissive fluorescein, showing a turn-on fluorescence response. Importantly, 325 exhibits high selectivity for O_2^- over other ROS and some biological compounds and has successfully been used for imaging O_2^- in live mouse peritoneal macrophages (Figure 14). The specificity of 325 for O_2^- was further confirmed by the observation that the intracellular fluorescence was markedly suppressed for cells pretreated with a nonenzymatic superoxide scavenger T-iron (1,2-dihydroxy-3,5-benzenedisulfonic acid disodium salt).⁴⁴⁸ Following a similar mechanism, another phosphinate-based chemodosimeter 326 has been developed for detecting nanomolar changes in O_2^- concentrations in living RAW 264.7 macrophages, with a red fluorescent turn-on response.⁴⁴⁹

7.5. Luminescent Chemodosimeters for $\cdot\text{OH}$

The hydroxyl radical ($\cdot\text{OH}$) is formed nonenzymatically from H_2O_2 in a metal-dependent reaction. It is highly reactive and primarily responsible for cellular disorders and cytotoxic effects that contribute to oxidative damage to DNA, proteins, and lipids. To date, nine luminescent chemodosimeters 327–335 for $\cdot\text{OH}$ have been reported.

7.5.1. Reaction of $\cdot\text{OH}$ with Nitroxide. For a fluorophore covalently linked to a nitroxide moiety, both radical trapping and fluorescence quenching can be observed through an electron-exchange mechanism. However, when such a fluorophore reacts with a carbon-centered radical such as $\cdot\text{CH}_3$, the nitroxide moiety can be reduced to its corresponding hydroxylamine, forming a diamagnetic product and eliminating the intramolecular quenching pathway, corresponding to a significant fluorescence enhancement. Because the methyl radical ($\cdot\text{CH}_3$) can be formed quantitatively by reaction of $\cdot\text{OH}$ with DMSO, the fluorescence detection of $\cdot\text{OH}$ can be realized by utilizing the above mechanism. On this basis, four

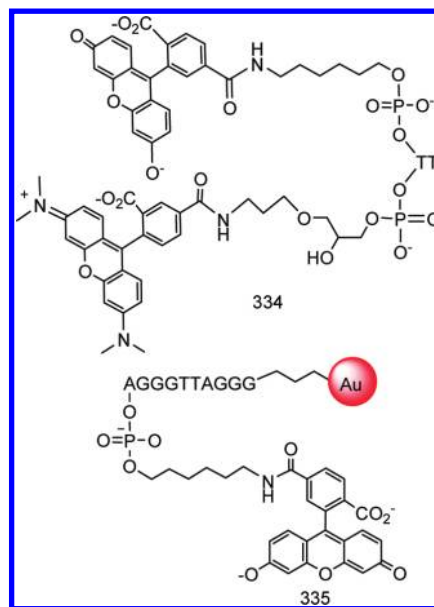
Scheme 75. Sensing Mechanism of 327–333 Based on Reaction of ·OH with Nitroxide



nitroxide-based chemodosimeters with naphthalene **327**,⁴⁵⁰ anthracene **328**,⁴⁵¹ perylene disimide **329**,⁴⁵² and BODIPY **330**⁴⁵³ as the fluorophore units have been reported for ·OH detection with a turn-on fluorescence response (Scheme 75). Their relative photophysical properties are summarized in Appendix 1 and Table S1 in the Supporting Information. In particular, **330** can respond rapidly to ·OH with a detection limit of 18 pM with high photostability, pH insensitivity, and high selectivity. Moreover, **330** has been used for selectively detecting intracellular ·OH in living mice macrophages, normal human liver cells, and human hepatoma cells, without causing cellular damage (Figure 14).⁴⁵³ Recently, three rhodamine nitroxides as fluorescent chemodosimeters **331**–**333** have been reported for sensing ·OH with high selectivity and turn-on fluorescence response both in aqueous solution and in living HepG2 cells (Scheme 75).⁴⁵⁴ The interference from other ROS can be avoided.

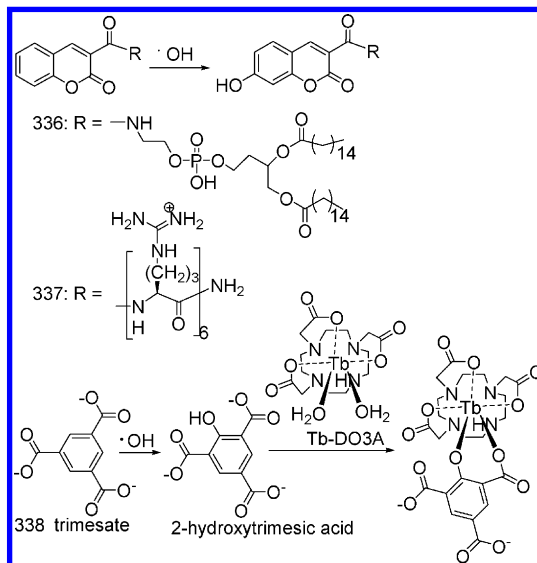
7.5.2. ·OH-Induced Cleavage of a DNA Strand. The cleavage of a DNA strand is an important reaction of ·OH. Utilizing this reaction, two FRET-based chemodosimeters **334** and **335** with 5-carboxytetramethyl rhodamine (5-TAMRA) and gold nanoparticles (Au NP) as energy acceptors, respectively, have been developed for ·OH detection (Scheme 76).⁴⁵⁵ For both **334** and **335**, 6-carboxyfluorescein (6-FAM) acts as an energy donor. Upon reaction of **334** with ·OH, the phosphate linker is cleaved, and the FRET from 6-FAM to 5-TAMRA was

Scheme 76. FRET-Based O₂^{·-} Chemodosimeters **334 and **335****



inhibited, corresponding to an increase in the fluorescence signal from FAM at 518 nm and a decrease in the fluorescence emission from TAMRA at 576 nm. Thus, a ratiometric detection of ·OH was achieved. For the fluorophore–gold nanocomposite **333**, ·OH induced strand breakage in the single-stranded DNAs, which switches off the FRET process from 6-FAM to the Au NPs, leading to fluorescence turn-on detection for ·OH. Furthermore, **335** has been used for imaging

Scheme 77. Sensing Mechanism of 336–338 Based on ·OH-Induced Aromatic Hydroxylation



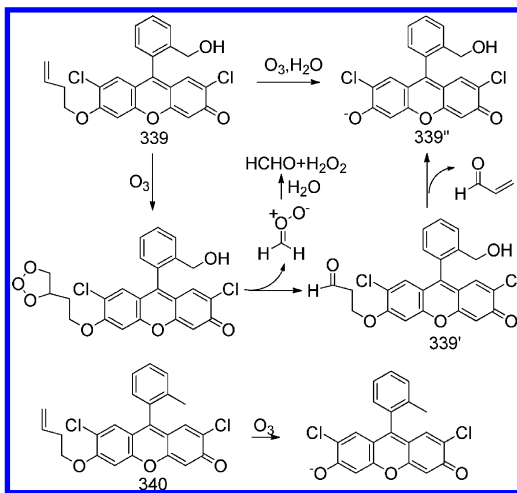
of intracellular ·OH in mouse peritoneal macrophages and HepG2 cells.⁴⁵⁶

7.5.3. ·OH-Induced Aromatic Hydroxylation. Another commonly used method for designing luminescent chemodosimeters for ·OH is based on ·OH-induced aromatic hydroxylation in which the hydroxylated products are generated from the attack of ·OH on aromatic compounds.

(1). *Coumarin As Aromatic Unit*. On the basis of ·OH-induced aromatic hydroxylation mechanism, two coumarin derivatives **336**⁴⁵⁷ and **337**⁴⁵⁸ have been developed as luminescent chemodosimeters for selective detection of ·OH with fluorescent enhancement, depending on the concentration of ·OH (Scheme 77).

(2). *Sensitizer Ligand of Terbium Complex As Aromatic Unit*. On the basis of a similar mechanism, an interesting luminescent chemodosimeter (**338**) for ·OH has been reported, based on a Tb³⁺ complex system (Scheme 77).⁴⁵⁹ For Tb³⁺ complexes, the luminescence is often determined by the triplet energy level (³T) of the sensitizer ligand and the number of water molecules coordinated. In **338**, trimesate is a weak lanthanide chelator and a poor sensitizer for Tb³⁺ luminescence. Upon reaction with ·OH, the newly formed 2-hydroxytrimesic acid becomes a more efficient sensitizer of Tb³⁺ luminescence and coordinates the Tb³⁺ ion in a bidentate

Scheme 78. Sensing Mechanism of Fluorescence O₃ Chemodosimeters **339 and **340****



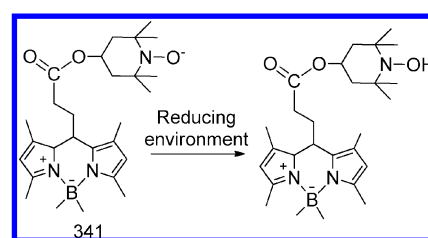
manner, by replacing two inner-sphere water molecules. Thus, a turn-on luminescence response to ·OH is observed. Considering the long lifetime of Tb³⁺ luminescence, the time-gated luminescence response to ·OH has been demonstrated to show 11-fold enhancement of the luminescence intensity.

7.6. Luminescent Chemodosimeters for O₃

Tropospheric or ground-level ozone (O₃) is toxic and damages the respiratory tract, although ozone (O₃) in the stratosphere protects the earth from harmful ultraviolet light. In addition, O₃ can be produced endogenously in inflammation and antibacterial responses of the immune system.⁴⁶⁰ To date, two luminescent chemodosimeters **339** and **340** for O₃ have been reported (Scheme 78).⁴⁶¹

Koide and co-workers reported an excellent luminescent chemodosimeter **339** for O₃.⁴⁶¹ The sensing mechanism is that the nonemissive chemodosimeter **339** can react with O₃ to give the aldehyde **339'**, which subsequently undergoes β-elimination to form the fluorescent product **339''**. This results in a turn-on fluorescence response to O₃. **339** can be used to detect O₃ even in the presence of other ROS and physiologically relevant antioxidants. Furthermore, another chemodosimeter **340** has been used to sense O₃ in living cells. Compound **340** remains weakly fluorescent when incubated with human bronchial epithelial cells. After treatment with ozone gas, fluorescence

Scheme 79. Sensing Mechanism of Fluorescence Chemodosimeter **341 for Oxidative Stress**



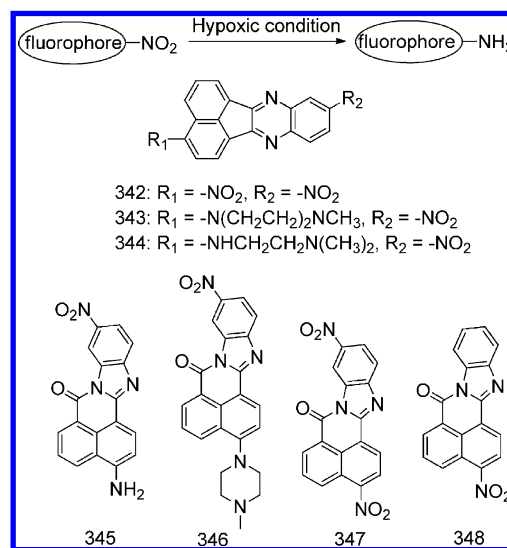
signals in living cells are observed. In addition, **340** can detect O₃ in atmospheric samples.⁴⁶¹

7.7. Luminescent Chemodosimeters for Oxidative Stress

In living cells, there exist many antioxidants, which can interact with ROS in a balanced way.⁴⁶² If too many ROS are generated in relation to the available antioxidants, oxidative stress will occur, which is involved in the development and progression of some serious diseases.

Recently, Tian and co-workers reported a fluorescence turn-on chemodosimeter **341**⁴⁶³ for quantifying cellular oxidative stress (Scheme 79). The fluorescence of **341** is effectively quenched by the nitroxide moiety. Interestingly, the reduction of the nitroxide moiety to hydroxylamine can improve the fluorescence of the BODIPY fluorophore. Thus, **341** can be used to reveal the redox status or monitor the oxidative stress of living cells by fluorometric methods.

Scheme 80. Proposed Mechanism Based on Reduction Metabolism of Nitroaromatic Compounds **342–**348** in Hypoxic Conditions**



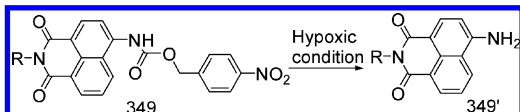
7.8. Luminescent Chemodosimeters for Hypoxia

Hypoxia is caused by an inadequate oxygen supply and is usually observed in solid tumors, which can affect the therapy of tumor cells by preventing the proper metabolism of various anticancer drugs. These hypoxic cells provide a tumor-specific targeting strategy for therapy.^{464,465} Therefore, it is of considerable clinical significance to develop luminescent chemodosimeters for hypoxia detection.

7.8.1. Reduction Metabolism of Nitroaromatic Compound.

An effective design principle is based on the quenching

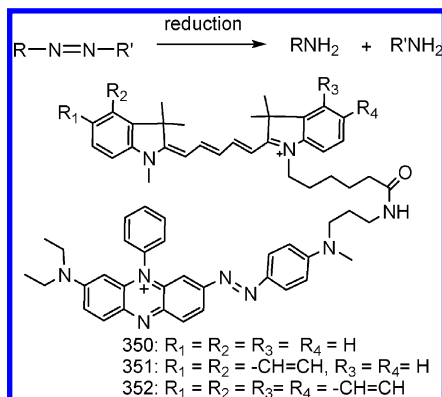
Scheme 81. Sensing Mechanism of Fluorescence Hypoxic Chemodosimeter 349



of fluorescence by the nitro group in oxic cells and the bioreduction of the nitro group in hypoxic cells to give an enhanced fluorescence (Scheme 80). Thus, nitroaromatic compounds become ideal candidate as luminescent chemodosimeters for hypoxia.

Utilizing this mechanism, Qian and co-workers reported that a series of nitroaromatic compounds 342–348 acted as luminescent chemodosimeters for hypoxic cells (Scheme 80).^{466,467} The evaluation of 342–348 for the detection of tumor hypoxia was carried out using V79 cells *in vitro* using a fluorescence microplate reader. This showed very significant differential fluorescence between hypoxic and oxic cells.

Scheme 82. Proposed Mechanism Based on Reduction Reaction of Azobenzene Derivatives 350–352 in Hypoxia Conditions



Furthermore, the Qian group reported another ratiometric luminescent chemodosimeter 349⁴⁶⁸ with the hypoxia pro-drug moiety of *p*-nitrobenzyl for the detection of microenvironmental hypoxia (Scheme 81). Upon reduction of the nitro group in hypoxia conditions, the amino group of 349 was released to form 349' and the fluorescence color changed from blue to green. Importantly, 349 was successfully applied to the ratiometric fluorescence imaging of hypoxia in an A549 cell line, displaying a notable increase in green fluorescence emission under hypoxic conditions.⁴⁶⁸

7.8.2. Reduction of Azobenzene Derivative. Azobenzene derivatives can be reduced by various reductases to form aniline derivatives (Scheme 82), and such reduction of azobenzene can be strongly influenced by the oxygen concentration. Thus, azobenzene derivatives become good candidates for hypoxia-sensitive moieties.

On the basis of this mechanism, Nagano and co-workers synthesized three hypoxia-sensitive near-infrared chemodosimeters 350–352⁴⁶⁹ by choosing dicarbocyanines as NIR fluorophores and Black Hole Quencher (BHQ-3) as the hypoxia-sensitive moiety. BHQ-3 has a very wide absorption, from visible to NIR, and can quench the NIR emissions of dicarbocyanines through the FRET process. Thus, under normal oxic conditions, 350–352 are nonfluorescent. Under hypoxic conditions, however, BHQ-3 is readily reduced and loses its NIR absorption. Hence, FRET is inhibited and the NIR fluorescence of dicarbocyanine unit was recovered. 350–352 can detect intracellular hypoxia with a turn-on fluorescence response. In addition, the fluorescence of 350 was dependent on the oxygen concentration and could distinguish oxygen concentrations inside cells. Furthermore, 350–352 were demonstrated to be the first fluorescent probes suitable for real-time *in vivo* imaging of acute ischemia in live mice. Very interestingly, the *in vivo* fluorescence signal was enhanced rapidly, occurring within 1 min of vessel ligation, using 350 as the fluorescence probe (Figure 15).⁴⁶⁹

8. LUMINESCENT CHEMODOSIMETERS FOR REACTIVE NITROGEN SPECIES

Reactive nitrogen species (RNS) are one class of chemically reactive species that are involved in cell signaling during a variety of physiological and pathological processes.⁴⁷⁰ RNS include nitric oxide (NO), nitroxyl (HNO), and peroxynitrite ($ONOO^-$). Owing to their significance in human health and disease, it is very important to develop effective luminescent chemodosimeters for selective detection of RNS.

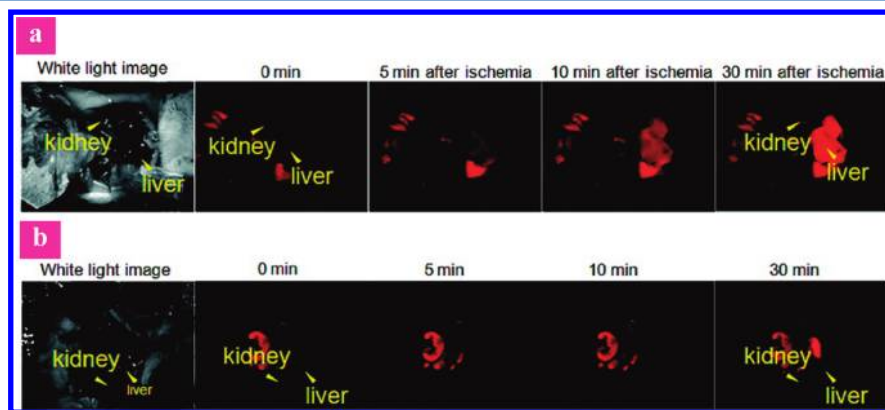
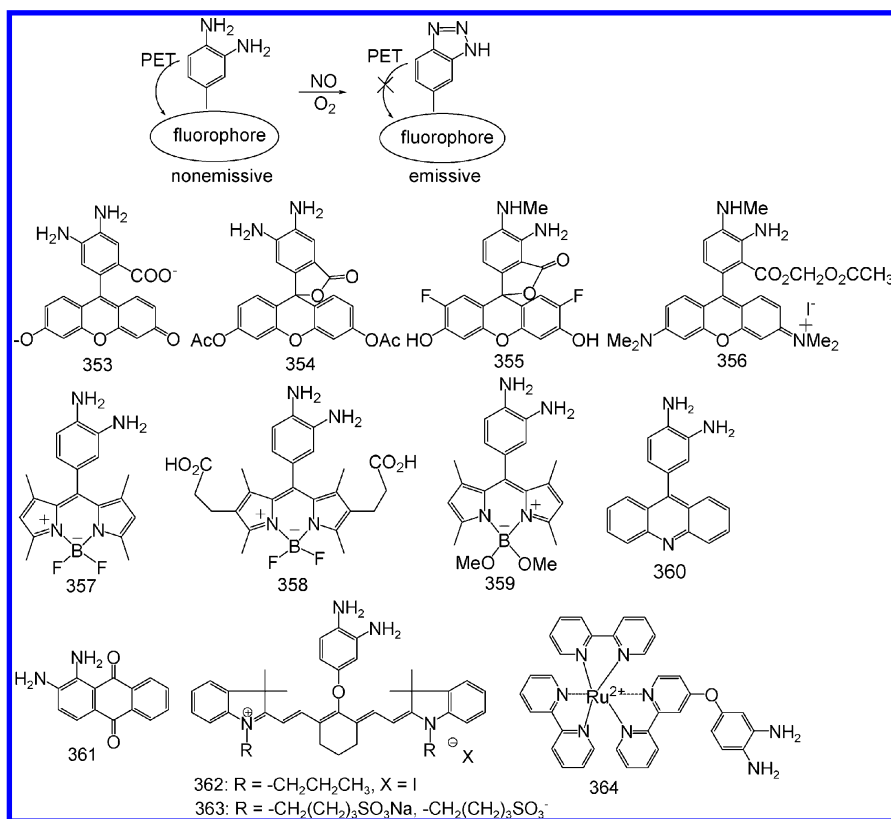


Figure 15. (a) Fluorescence images of living mouse after injection of 350 followed by vessel ligation as described in the text. Fluorescence images were obtained for 30 min, with excitation at 620 nm and emission at 680 nm. (b) Fluorescence images of living mouse after injection of 350 without vessel ligation. Reprinted with permission from ref 469. Copyright 2010 American Chemical Society.

Scheme 83. Sensing Mechanism of Luminescent NO Chemodosimeters 353–364 Based on the Diamine Cyclization Process



8.1. Luminescent Chemodosimeters for NO

As a diatomic free radical, NO functions as the endothelium-derived relaxation factor that promotes vascular smooth muscle relaxation when it binds and activates soluble guanylyl cyclase, regulates vasodilation in the circulatory system, and causes long-term potentiation in the brain.^{471–473} However, micro-molar concentrations of NO can trigger the formation of reactive nitrogen species, leading to carcinogenesis and neurodegenerative disorders.^{474,475} Therefore, developing selective and sensitive chemodosimeters for direct and real-time NO detection are highly desirable.^{476–478}

8.1.1. NO-Induced Diamine Cyclization Process. Generally, fluorophores attached with a phenyldiamine are nonemissive due to the PET process from *o*-phenylenediamine to the excited fluorophore. When phenyldiamine reacts with NO, cyclization occurs and the electron-donating group of phenyldiamine is transformed into a less strongly electron-donating group triazole. This allows fluorescence emission to be recovered. On the basis of this strategy, a series of luminescent chemodosimeters 353–364 (Scheme 83) have been developed for NO detection. These chemodosimeters are composed of two moieties: a fluorophore and a NO-sensitive modulator (such as *o*-phenylenediamine).

(1). Fluoresceine as Fluorophore. Nagano and co-workers reported a series of diaminofluoresceines (DAFs) 353–356 as luminescent chemodosimeters for NO detection, based on the reactivity of aromatic vicinal diamines with NO in the presence of dioxygen.^{479–481} Interestingly, the reaction of 353 and NO is completely independent of Ca²⁺ and Mg²⁺ at physiological concentrations.⁴⁷⁹ The membrane-permeable chemodosimeter 354 can be used for real-time bioimaging of NO with fine temporal and spatial resolution.⁴⁸⁰ 355 is an improved DAF

analogue that forms triazole 355' after reaction with NO. 355' shows stable and intense fluorescence over a wide pH range, whereas the fluorescence intensities of the triazole products formed from other DAF analogues dramatically decrease in acidic solutions. Furthermore, 355 was successfully applied to detect intracellular NO release in biological specimens.⁴⁸¹

To obtain higher photostability and longer excitation wavelengths, Nagano and co-workers further designed diaminorhodamine 356 as a fluorescence NO chemodosimeter, using rhodamine as the fluorophore.⁴⁸² Reaction with NO induces 840-fold fluorescence enhancement, with a detection limit of 7 nM, and the fluorescence showed no pH dependency above pH 4. Moreover, 356 was successfully applied to practical bioimaging of NO production in bovine aortic endothelial cells.

(2). BODIPY as Fluorophore. Nagano, Kikuchi, and co-workers reported a series of luminescent chemodosimeters 357–359 for NO based on the BODIPY fluorophore.^{483,484} Chemodosimeter 357 showed high selectivity for NO over various reactive oxygen species. Conversion of the diamino form to the triazole form by reaction with NO caused a large fluorescence enhancement, a characteristic feature of intramolecular PET probe. However, the fluorescence of product 357' decreased strikingly when the pH was above 7. This is an undesirable property for the bioimaging application. To circumvent this problem, they synthesized another BODIPY fluorophore 358 as a pH-independent NO chemodosimeter. In 358, the carboxyl functional groups effectively prevent stacking due to their higher hydrophilicity, whereas the ethylene chains block the PET process by changing the reduction potential.⁴⁸³ Subsequently, 359 was designed and found to be suitable for NO detection in aqueous solutions. Compared with 357, 359 exhibits higher solubility and greater pH-independency of the fluorescence intensity of its triazole form.⁴⁸⁴

(3). *Acridine and Anthraquinone As Fluorophores.* On the basis of a similar NO-induced diamine cyclization-blocked PET mechanism, diaminobenzoacridine **360**⁴⁸⁵ and 1,2-diaminoanthraquinone **361**^{486,487} were also developed as fluorescent NO chemodosimeters. Moreover, Galindo and co-workers reported that **361** could be used to monitor intracellular NO in living RAW 264.7 cells by confocal fluorescence microscopy.⁴⁸⁷

(4). *Tricarbocyanine Dye As Fluorophore.* Although much progress has been made in the development of visible emission fluorophores as NO chemodosimeters, fluorescent imaging deep into human tissues becomes difficult using visible fluorescence chemodosimeters as probes. To conquer this limitation, the Nagano group designed two NIR luminescent

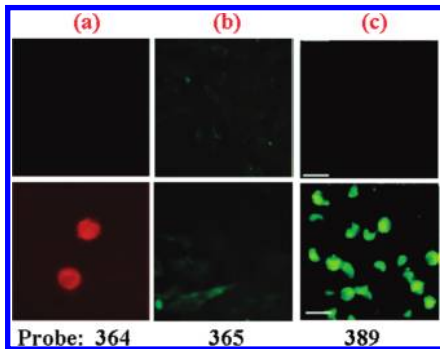
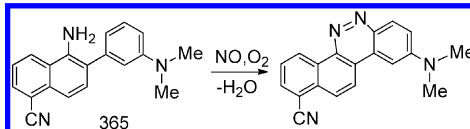


Figure 16. Selected examples of luminescence of living cells in the absence (upper) or presence (lower) of NO using chemodosimeters (**364**, **365**, and **389**) as luminescent probes. (a) Reprinted with permission from ref 489. Copyright 2010 Wiley-VCH Verlag GmbH & Co. KgaA, Weinheim. (b) Reprinted with permission from ref 490. Copyright 2010 American Chemical Society. (c) Reprinted with permission from ref 503. Copyright 2011 American Chemical Society.

chemodosimeters (**362** and **363**) for NO detection.⁴⁸⁸ Probe **362**, which has two propyl groups, was designed to penetrate cellular membranes, whereas **363**-containing sulfonate groups are highly soluble in water. **362** functions in biological systems

Scheme 84. Sensing Mechanism of Fluorescent NO Chemodosimeter **365**

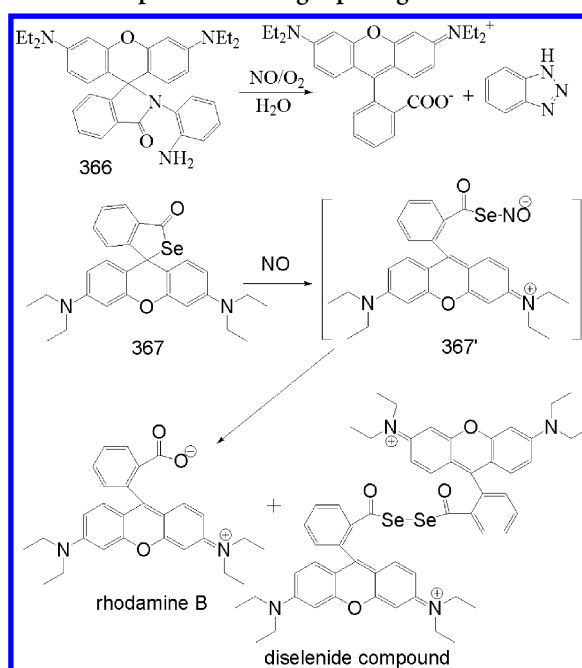


ex vivo, and its fluorescence could be detected from outside the kidney.

(5). *Phosphorescent Heavy-Metal Complex As Lumino-phore.* In addition to the previously mentioned organic compounds, the ruthenium(II) complex **364** acts as a highly sensitive and selective phosphorescent chemodosimeter for the detection of NO, based on diamine cyclization and blocking of PET.⁴⁸⁹ **364** can react selectively with NO in aqueous buffers under aerobic conditions to yield a triazole derivative, accompanied by a substantial increase in luminescent intensity. Moreover, **364** was successfully used for luminescence imaging of exogenous NO in mouse macrophage cells and endogenous NO in gardenia cells (Figure 16).

8.1.2. NO-Induced Diazo-Ring-Generation Process. Recently, the D- π -A dye **365** containing dimethylamino and cyano groups was designed as a NO-selective luminescent

Scheme 85. Sensing Mechanism of **366** and **367** Based on NO-Induced Spirolactam-Ring-Opening Process

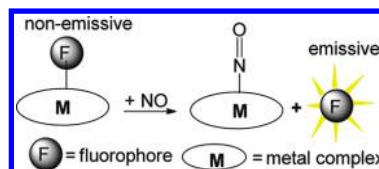


chemodosimeter (Scheme 84).⁴⁹⁰ Upon reaction of **365** with NO, a diazo ring was rapidly generated to form a rigid and plate π -conjugation system, accompanied by a red-shifted 1500-fold fluorescence enhancement. Excellent selectivity was observed against other reactive oxygen/nitrogen species. **365** crosses cell membranes but not nuclear membranes and is suitable for both intra- and extracellular NO quantification. Good cytocompatibility was found during in vitro studies with neonatal spinal astrocytes and the pheochromocytoma-derived PC12 cell line (Figure 16).⁴⁹⁰

8.1.3. NO-Induced Spirolactam-Ring-Opening Process. The NO chemodosimeter **366** was designed based on a rhodamine unit following a NO-induced spirolactam-ring-opening reaction (Scheme 85).⁴⁹¹ The *o*-phenylenediamine acts as an NO-reactive group in lactam form. **366** exhibits turn-on fluorogenic behavior toward NO in aqueous solutions with great sensitivity and selectivity.

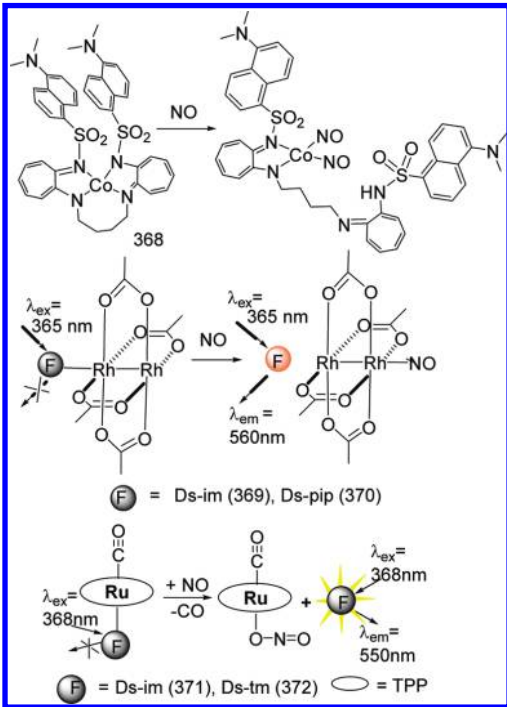
Recently, Ma and co-workers reported a new strategy for the fluorescence detection of NO utilizing the interaction between NO and a selenide (Scheme 85). The rhodamine B selenolactone derivative **367**⁴⁹² emits very weak fluorescence. Upon addition of NO to a solution of **367**, a significant fluorescence enhancement is immediately produced. The reaction of NO with the Se atom of **367** leads to the formation of an unstable intermediate compound **367'**, which is then hydrolyzed into rhodamine B or undergoes a complicated

Scheme 86. Sensing Mechanism Based on NO-Triggered Selective Ligand Dissociation of Transition Metal Complexes



coupling reaction to form a diselenide compound. Other reactive oxygen/nitrogen species do not show such behavior, indicating that 367 has a high selectivity for NO. Furthermore,

Scheme 87. Sensing Mechanism of 368–372 Based on NO-Triggered Selective Ligand Dissociation of Transition Metal Complexes



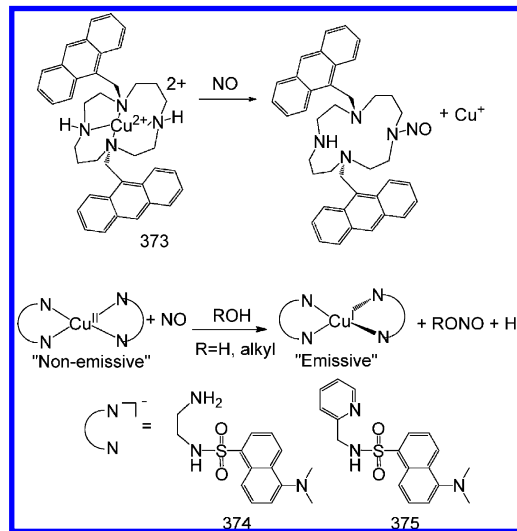
367 could well image the concentration change of NO in HeLa cells.⁴⁹²

8.1.4. NO-Triggered Selective Ligand Dissociation of Metal Complex. When a fluorophore as ligand is coordinated to transition metal ions with partly filled d-shell, the fluorescence emission is quenched due to energy or electron transfer between the excited states of the fluorophore and the partially filled d orbitals of the metal ion. In the presence of NO, the formation of a metal–NO adduct selectively displaces a fluorescent ligand, thereby removing it from the quenching environment and turning on fluorescence emission of fluorophore (Scheme 86). To date, the metal ions successfully used have included Co(II), Fe(II), Rh(II), Ru(II), and Cu(II).

On the basis of this mechanism, Lippard and co-workers prepared a family of paramagnetic metal complexes based on dansyl aminotroponimine (H^R DATI) ligands for NO detection (Scheme 87).^{493,494} For example, the fluorescence of the DATI ligands is quenched in the Co(II) complex $[Co(^R$ DATI)₂] 368.⁴⁹³ Under an NO atmosphere, however, a solution of 368 rapidly displays a 4-fold increase in fluorescence at 505 nm.

Similarly, dirhodium complexes $[Rh_2(i-O_2CCH_3)_4(L)_2]$, with L = dansylimidazole (Ds-im) (369) or dansylpiperazine (Ds-pip) (370),⁴⁹⁵ and ruthenium complexes $[Ru(TPP)(CO)(Ds-im)]$ (TPP = tetraphenylporphinato dianion, 371) and $[Ru(TPP)(CO)(Ds-tm)]$ (Ds-tm = dansyl thiomorpholine, 372)⁴⁹⁶ have been reported as luminescent chemodosimeters for NO detection. In these complexes, the dansyl fluorophores are coordinated at the axial sites of the metal core through imidazole or piperazine moieties, respectively. When NO is

Scheme 88. Sensing Mechanism of 373–375 Based on NO-Triggered Reduction of Cu²⁺ and Release of Fluorescent Ligand



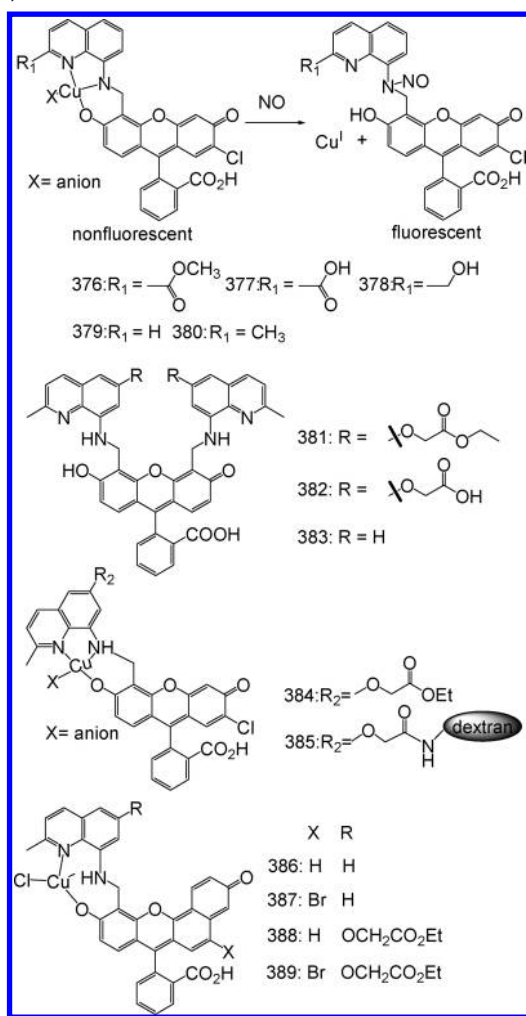
present, the displacement of Ds-im or Ds-tm from their axial positions occurs, liberating the fluorophore moieties from the quenching environment of the metal center and restoring fluorescence. Thus, a significant fluorescent enhancement was observed. Interestingly, 371 and 372 display turn-on fluorescent detection of NO that is 1–2 orders of magnitude more rapid than Co(II)-based chemodosimeter 368.⁴⁹⁶

8.1.5. NO-Triggered Reduction of Cu²⁺ and Release of Fluorescent Ligand. Although all of the previously mentioned complexes can directly interact with NO, they are either not soluble or unstable in aqueous solutions. Most will slowly hydrolyze if their solutions are exposed to air for several days, as water can outcompete the fluorophore for coordination to the metal center. To circumvent these shortcomings, a series of Cu(II) complex-based chemodosimeters 373⁴⁹⁷ and 374 and 375⁴⁹⁸ (Scheme 88) were synthesized for NO detection. The strategy involves the formation of a Cu(I) species via NO-triggered reduction of paramagnetic Cu(II) that was associated with NO coordination to a copper center and the release of the fluorescent nitrosylated ligand, corresponding to fluorescence enhancement.

For example, Cu(DAC)²⁺ (DAC = 1,8-bis(9-anthracylmethyl)) derivative of the macrocyclic tetraamine cyclam, 373,⁴⁹⁷ could selectively detect NO in aqueous methanol by reduction of the Cu²⁺ ion, accompanied by intramolecular nitrosylation of an amine coordination site and release of the modified DAC ligand (Scheme 88). The key step is the attack of NO on a deprotonated amine site with concerted electron transfer to the coordinated Cu²⁺ ion. In addition, water-soluble chemodosimeters 374 and 375 are also Cu(II)-reduction-based NO chemodosimeters⁴⁹⁸ and show better sensitivity than 373 does (Scheme 88).

On the basis of a similar mechanism, Lippard and co-workers reported a series of nonemissive Cu(II) fluorescein complexes 376–389 (Scheme 89) as promising fluorescence turn-on chemodosimeters for NO detection.^{499–503} Complex 380 is the first example capable of detecting NO under physiological conditions with fluorescence turn-on in the absence of oxygen.⁵⁰⁰ 379 has been successfully used to monitor NO production in bacterial cell cultures, but it diffuses out of the

Scheme 89. Mechanism of Fluorescence Response for Cu(II)-Based NO Chemodosimeter 376–389



cells under profusion conditions, making analysis of results difficult.⁵⁰⁰ Using 381, 382, and 383^{501,502} as probes, fluorescence caused by NO production from mammalian olfactory bulb tissue slices was visualized. Recently, two cell-trappable Cu(II) fluorescein-based chemodosimeters (384 and

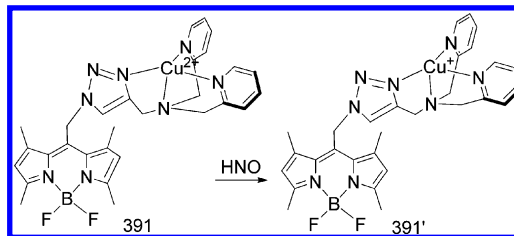
Scheme 90. Mechanism of Fluorescence Response for NO Chemodosimeter 390



385) have been developed for NO detection, either by the incorporation of hydrolyzable esters or by conjugation to aminodextran polymers to impart cell trappability.⁵⁰⁴ Both 384 and 385 are highly selective for NO over other reactive oxygen and nitrogen species (RONS) and allow monitoring of NO produced endogenously in live RAW 264.7 cells. Recently, Lippard and co-workers have reported a series of fluorescent seminaphtho fluorescein-based chemodosimeters (386–389⁵⁰³) for NO, which exhibited longer emission wavelengths than 376–385. The application of these turn-on fluorescence

chemodosimeters for detecting NO in RAW 264.7 macrophages has been demonstrated (Figure 16).

Scheme 91. Mechanism of Fluorescence Response for HNO Chemodosimeter 391



8.1.6. NO-Induced Spirolactam Ring-Opening, Reduction of Cu²⁺, and Nitrosylation of Fluorescent Ligand.

Recently, Duan and co-workers have developed an interesting example of fluorescent NO-selective chemosensor 390 (Scheme 90).⁵⁰⁵ For 390, the NO-induced reduction of Cu²⁺ and nitrosylation process lead to the spiro-ring-opening of rhodamine moiety, resulting in 700-fold fluorescent enhancement. Importantly, 390 could be applied for monitoring intracellular NO by confocal fluorescence microscopy.

8.2. Luminescent Chemodosimeters for HNO

Nitroxyl (HNO), the protonated form of NO under physiological conditions, has important roles in pharmacological processes distinct from those of nitric oxide.⁵⁰⁶ To date, rather little effort has been focused on the synthesis of probes for HNO detection. Recently, Lippard and co-workers reported a BODIPY-based fluorescent HNO chemodosimeter 391 (Scheme 91).⁵⁰⁷ 391 displays very weak fluorescence, which is attributed to PET process from the BODIPY excited state to the bound Cu²⁺ ion. However, upon treatment with excess HNO, a significant fluorescence increase was observed concomitant with reduction of the paramagnetic Cu²⁺ complex to give 391' and production of NO(g). In addition, 391 exhibits excellent selectivity for HNO over other biologically relevant reactive nitrogen species, including nitric oxide. 391 was also successfully applied for HNO detection in HeLa cells, indicating its utility as the fluorescent probe with visible excitation and emission.⁵⁰⁷

8.3. Luminescent Chemodosimeters for ONOO⁻

Peroxynitrite (ONOO⁻), which can be formed in vivo between nitric oxide (NO) and superoxide (O₂⁻), is a highly reactive species implicated in the pathogenesis of numerous diseases, including acute and chronic inflammatory processes, ischemic-reperfusion injury, multiple sclerosis, sepsis, and neurodegenerative disorders.⁵⁰⁸ To date, several mechanisms have been proposed for designing chemodosimeters for peroxynitrite.

8.3.1. Specific Reaction between Ketone and ONOO⁻.

Peroxynitrite (ONOO⁻) can react with activated ketone 392⁵⁰⁹ to form dioxirane, which would selectively oxidize the phenyl ring to afford the dienone product 392' and release the fluorescent molecule (Scheme 92). On the basis of this mechanism, a series of luminescent chemodosimeters for ONOO⁻ have been reported by Yang and co-workers.^{510–512} For probe 393,⁵¹⁰ possessing a ketone unit linked to a dichlorofluorescein moiety through an aryl ether linkage, it can yield the strongly fluorescent product 393' upon reaction with

Scheme 92. Proposed Mechanism of 392–395 Based on ONOO⁻-Induced Oxidation of Phenyl Ring to Afford the Dienone

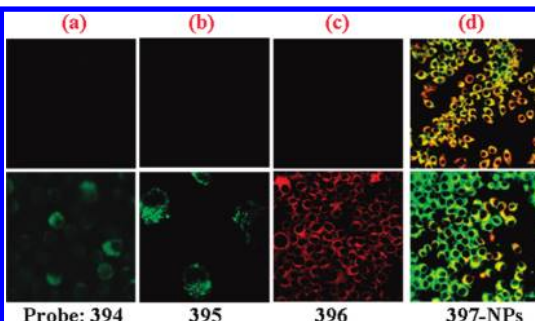
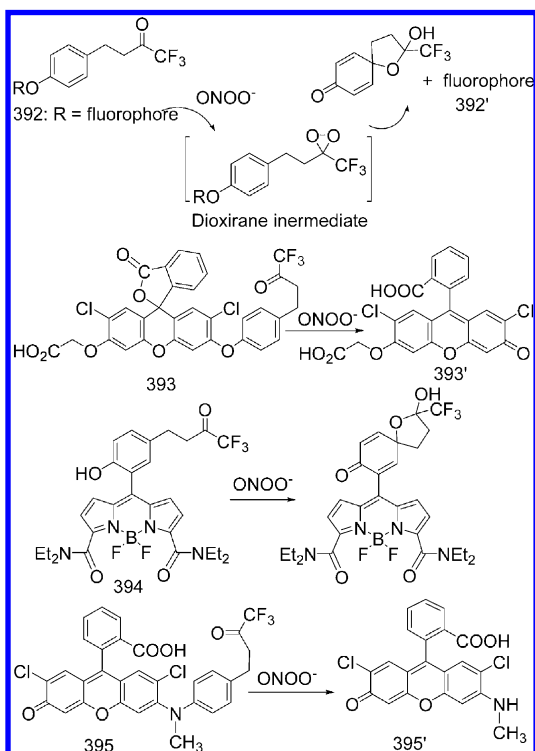
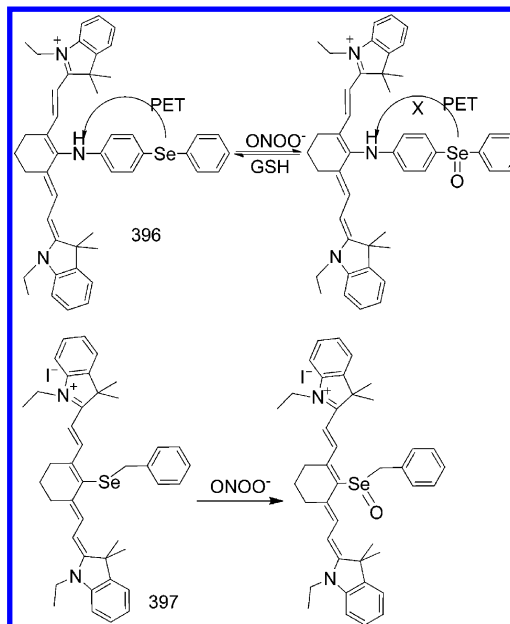


Figure 17. Selected examples of fluorescence imaging of living cells in the absence (upper) or presence (lower) of peroxynitrite using chemodosimeters (394–397) as fluorescent probes. (a) Reprinted with permission from ref 511. Copyright 2009 American Chemical Society. (b) Reprinted with permission from ref 512. Copyright 2010 American Chemical Society. (c) Reprinted with permission from ref 513. Copyright 2011 American Chemical Society. (d) Ratiometric imaging. $\lambda_{\text{ex}} = 532$ and 635 nm, $\lambda_{\text{em}} = 535$ – 600 and 700 – 800 nm. Reprinted with permission from ref 515. Copyright 2011 Wiley-VCH Verlag GmbH & Co. KgaA, Weinheim.

ONOO⁻. Moreover, 393 has successfully been applied for the highly selective detection of ONOO⁻ in living cells. The above mechanism has been utilized for the design of other chemodosimeters 394⁵¹¹ and 395.⁵¹² For 394, it is non-fluorescent because of the PET mechanism. The reaction of 394 with ONOO⁻ inhibits the PET mechanism and leads to a dramatic increase of the fluorescence signal. 394 has also been used for imaging the subcellular locations of endogenous ONOO⁻ in J774.1 macrophage cells (Figure 17). For 395, the reaction of ONOO⁻ with the trifluoromethyl ketone can lead to N-dearylation, along with the release of the highly

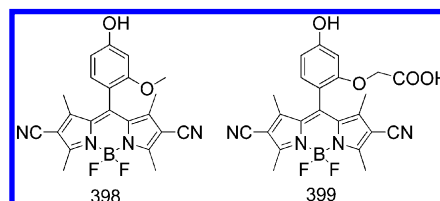
Scheme 93. Sensing Mechanism of 396 and 397 Based on ONOO⁻-Induced Se(II) Oxidation



fluorescent compound 395'. Moreover, 395 was also utilized for detecting ONOO⁻ in a biological system (Figure 17).⁵¹²

8.3.2. ONOO⁻-Induced Se(II) Oxidation. Utilizing the peroxynitrite-induced specific oxidation reaction of divalent selenium to quadrivalent selenium, two tricarbocyanine dyes have been developed as NIR luminescent chemodosimeters for ONOO⁻ (Scheme 93). Chemodosimeter 396⁵¹³ is non-fluorescent as a result of PET between the 4-(phenylselenyl)-aniline moiety and the cyanine dye. However, the Se(II)

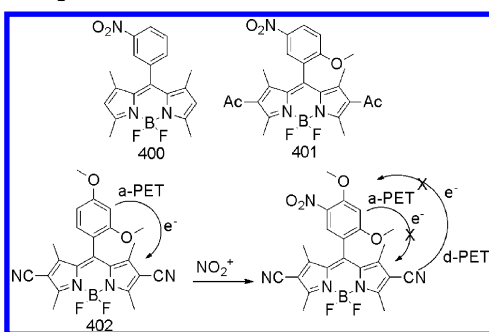
Chart 9. Chemodosimeters 398 and 399 Based on ONOO⁻-Induced Aromatic Nitration



oxidation induced by ONOO⁻ prevents the PET, causing the fluorescence turn-on response. 396 has also been used for imaging subcellular locations of endogenous ONOO⁻ and for monitoring ONOO⁻ oxidation and reduction events in RAW 264.7 cells (Figure 17). Recently, Tang and co-workers have devised another benzylselenide tricarbocyanine 397 as an ONOO⁻ indicator for fluorescence bioimaging.⁵¹⁴ Unlike 396, 397 exhibits strong fluorescence and the oxidation of Se results in a significant fluorescence decrease. Furthermore, 397 as an energy acceptor and isoprorthodamine B as an energy donor were codoped into a polymer nanoparticle to fabricate a FRET-based nanoprobe.⁵¹⁵ This nanoprobe can realize a ratiometric fluorescence response to ONOO⁻ in solution and in living cells (Figure 17).

8.3.3. ONOO⁻-Induced Aromatic Nitration. Peroxynitrite is a potent nitrating agent. Utilizing ONOO⁻-induced aromatic nitration, fluorescent chemodosimeters 398 and 399 for ONOO⁻ were designed (Chart 9).⁵¹⁶ The water-soluble

Scheme 94. Sensing Mechanism of Chemodosimeters 400–402 for NO_2^+

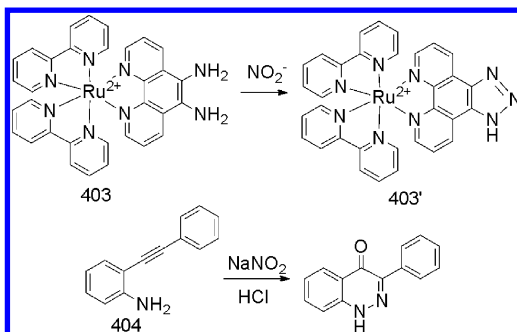


399 is nonemissive due to the PET process from the benzene moiety to the excited BODIPY fluorophore. Interestingly, the ONO^- -induced aromatic nitration leads to inhibition of PET process and formation of a highly fluorescent nitrated product, realizing a turn-on fluorescence response. The addition of other reactive oxygen species induces little fluorescence augmentation of 399.⁵¹⁶

8.4. Luminescent Chemodosimeters for NO_2^+

Nitration in biological samples has been implicated in various pathogenic processes, such as inflammatory events, ischemia-reperfusion, and neurodegenerative disorders. Therefore, it is important to monitor nitrative stress in biological samples. Nitronium (NO_2^+) is an important and active agent of nitration reaction. To date, only Nagano's group has reported three BODIPY derivatives as fluorescence turn-on probes for monitoring nitration (Scheme 94).⁵¹⁶ The nitro-containing BODIPY dye 400 is weakly emissive, due to an intramolecular photoinduced electron transfer (PET) process from the excited fluorophore to the electron-deficient benzene moiety (d-PET). Interestingly, when electro-drawing acetyl groups were

Scheme 95. Sensing Mechanism of Fluorescent NO_2^- Chemodosimeters 403 and 404



introduced into the BODIPY moiety, the fluorescence quantum yield of 401 is high, 0.529. The calculated relative free energy change of the PET process (ΔG_{ET}), with respect to the value for 400 as a standard, is +0.42 eV for 401, which is high enough to prevent a d-PET process. On basis of this strategy, BODIPY derivatives 398, 399, and 402 containing an electro-drawing nitrile group were reported as fluorescence turn-on chemodosimeters for monitoring nitration. For example, upon reaction with NO_2BF_4 , a rapid and drastic enhancement in fluorescent emission for 402 in CH_3CN was observed, and the nitration product 402' has a high quantum yield of 0.687.⁵¹⁶

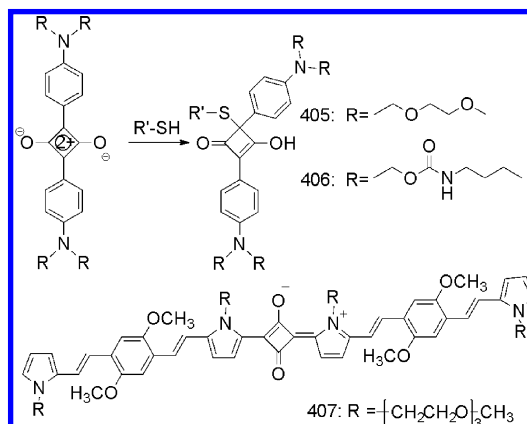
8.5. Luminescent Chemodosimeters for NO_2^-

Nitrite ion (NO_2^-) contamination in the environment is of growing concern. At high concentrations, NO_2^- can have an adverse influence on different biological processes.⁵¹⁷ To date, only two luminescent chemodosimeters for NO_2^- have been reported (Scheme 95). Recently, a Ru(II)-polypyridyl-based complex (403) that features a 9,10-diaminophenanthroline has been reported for the chemodosimetric detection of NO_2^- in aqueous solution.⁵¹⁸ The detection was based on the formation of a new triazole-based complex 403' in the presence of NO_2^- , with enhanced emission. Ranu and co-workers found that 2-arylethynyl aniline (404) can undergo a rapid reaction with NO_2^- in aqueous acidic media to form 4(1H)-cinnolones, leading to fluorescence enhancement.⁵¹⁹ Utilizing this reaction, the detection of NO_2^- was realized for 404.

9. LUMINESCENT CHEMOSIMETERS FOR REACTIVE SULFUR SPECIES

Reactive sulfur species (RSS) includes thiols, S-nitrosothiols, sulfenic acids, and sulfite, and it plays vital roles in regulating intracellular redox status and other fundamental signaling processes involved in human health and disease.^{378,520,521}

Scheme 96. Sensing Mechanism of Fluorescent Thiol Chemodosimeters 405–407 Based on Nucleophilic Addition of Squaraine

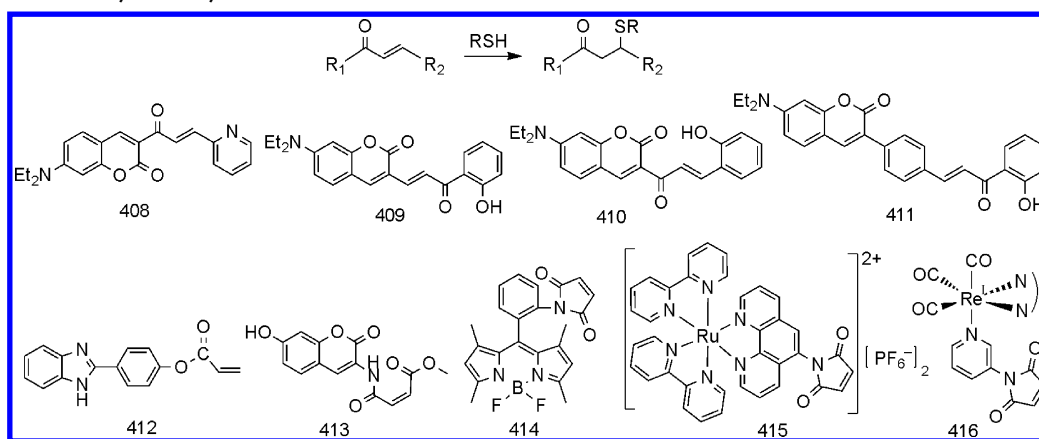


9.1. Luminescent Chemodosimeters for Thiol

Intracellular thiols play many crucial roles in physiological matrices. For example, glutathione, the most abundant intracellular nonproteinogenic thiol, plays a key role in maintaining the reducing environment of cells and acts as a redox regulator.⁵²² The selective detection and monitoring of thiol-containing molecules in biological samples is of great importance. To date, 25 fluorescent thiol-selective chemodosimeters have been generated by exploiting various mechanisms, including nucleophilic addition and bond-cleavage processes.

9.1.1. Nucleophilic Addition of Squaraine. Because of their electron-deficient central four-membered ring, squaraines are electrophiles and can react with thiols through nucleophilic addition. On the basis of this design strategy, squaraine derivatives 405 and 406⁵²³ and 407⁵²⁴ were developed as luminescent chemodosimeters for thiols (Scheme 96). Both 405 and 406 show a band at ~640 nm and have a quantum yield of 0.1 in acetonitrile/water (1:4, v/v).⁵²³ Their solutions

Scheme 97. Proposed Mechanism of Luminescent Chemodosimeters 408–416 Based on Michael Addition Reaction of Thiol to α,β -Unsaturated Carbonyl Moiety



become decolored and their fluorescence is quenched in the presence of thiol-containing compounds. Alcohols, phenols, amines (primary, secondary, and tertiary), and sulfides do not

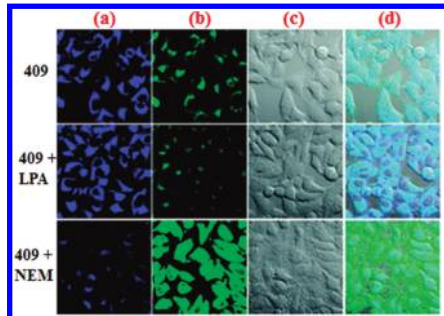


Figure 18. Confocal fluorescent images (a, b), bright-field imaging (c), and their overlay (d) of HeLa cells incubated with **409** ($2.5 \mu\text{M}$) upon pretreatment of LPA or NEM. Images at channel a and channel b were achieved at excitations at 405 and 488 nm, respectively. Reprinted with permission from ref 527. Copyright 2011 American Chemical Society.

induce this effect, which is attributed to the selective addition of thiols to the cyclobutene ring.

9.1.2. Michael Addition of Thiols to α,β -Unsaturated Carbonyl Moiety. Another strategy to generate thiol-selective luminescent chemodosimeters is based on Michael addition of thiols to α,β -unsaturated ketones or esters to form thioethers (Scheme 97).⁵²⁵ This process often results in a significant change in fluorescence emission.

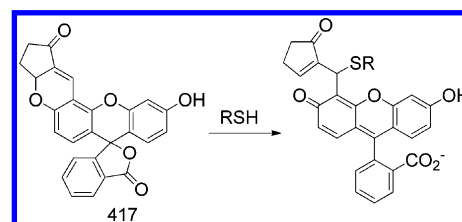
Lin and co-workers reported that **408** is a selective and sensitive luminescent chemodosimeter for thiol in water.⁵²⁶ Upon addition of GSH to a solution of **408**, a 35-fold enhancement in fluorescence intensity was observed, due to the inhibition of the ICT process. Following a similar mechanism, another three chemodosimeters **409**,⁵²⁷ **410**,⁵²⁸ and **411**⁵²⁹ containing phenylhydroxyl groups were reported for selective detection of thiols. For example, **409** exhibited rapid and ratiometric fluorescence responses for biothiols and has been successfully applied to intracellular imaging (Figure 18). If the HeLa cells are pretreated with R-lipoic acid (LPA, as biothiols enhancer, $500 \mu\text{M}$, 24 h) and then stained with **409** ($2.5 \mu\text{M}$, 0.5 h), the blue fluorescence is moderately enhanced. In contrast, when the cells are pretreated with *N*-ethylmaleimide (NEM, a scavenger of biothiols, $100 \mu\text{M}$, 0.5 h), and

subsequently incubated with **409** ($2.5 \mu\text{M}$, 0.5 h), the strong green fluorescence is observed (Figure 18).⁵²⁷

Chemodosimeter **412** shows weak fluorescence emission, due to the PET process that quenches the fluorophore by intramolecular interaction of the carbon–carbon double bond.⁵³⁰ However, significantly enhanced fluorescence was observed through the addition reaction of thiols to the α,β -unsaturated carbonyl moiety, which eliminates the PET process. **412** can also be applied to the detection of biothiols in human urine samples without interference from other biologically relevant analytes.

The thiol–maleimide bioconjugate reaction has been known for several decades. On the basis of this reaction, two luminescent thiol chemodosimeters **413** and **414** have been designed. Chemodosimeter **413** contains a coumarin as the fluorophore and a maleimide as the thiol acceptor.⁵³¹ It exhibits highly selective and very rapid detection of thiols with an excellent signal-to-noise ratio and sensitivity. Thus, **413** can be

Scheme 98. Sensing Mechanism of Fluorescent Thiol Chemodosimeter 417



used for real-time thiol quantification and has been used to develop a high-throughput fluorescence assay for glutathione reductase. Moreover, **413** can readily penetrate cell membranes, and the monitoring of thiol molecules (such as GSH) in living cells has been realized. For BODIPY-based chemodosimeter **414**, which contains a maleimide moiety,⁵³² thiols underwent nucleophilic addition to the maleimide unit, leading to a 350-fold fluorescence enhancement due to the destruction of the PET process. In addition, Duerkop and co-workers reported Ru(II) complex **415**⁵³³ for thiol bioconjugation. Lo and co-workers have demonstrated that the Re(I) complex **416**⁵³⁴ containing a maleimide moiety can be used as a luminescent biological label via the bioconjugation with reactive thiol groups of proteins.

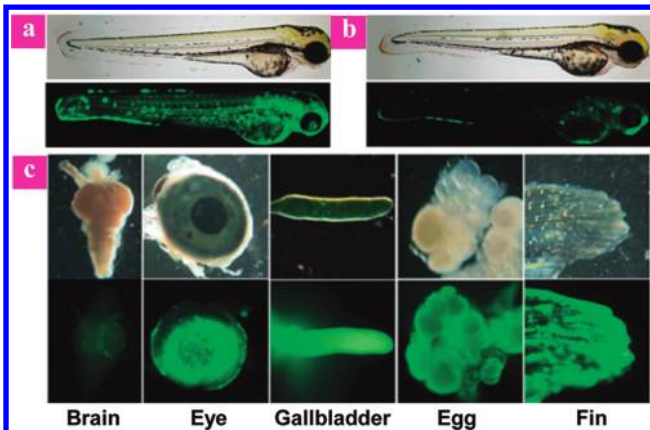
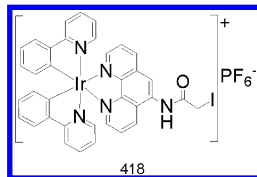


Figure 19. Phase-contrast and fluorescence images of zebrafish and their organs. (a) Three-day-old zebrafish was incubated with 20 mM of 417; (b) three-day-old zebrafish was preincubated with 40 mM NMM for 20 min and then treated with 20 mM of 417 for 1 h; (c) zebrafish organs treated with 5 mM of 417 (top, phase-contrast image; bottom, fluorescence image). Reprinted with permission from ref 535. Copyright 2010 The Royal Society of Chemistry.

Scheme 99. Luminescent Chemodosimeter 418 Based on the Reaction between Iodoacetamide and Thiol



9.1.3. Nucleophilic Addition and Spirolactam-Ring-Opening Processes. The nucleophilic addition of thiols can also induce the spiro-ring-opening of fluorescein, providing another mechanism for thiol detection (Scheme 98). Yoon and co-workers reported that chemodosimeter 417 can sense biological thiols with high selectivity and sensitivity based on spirolactam-ring-opening of fluorescein induced by nucleophilic attack of the thiol.⁵³⁵ Furthermore, 417 was used to detect

thiols in living murine P19 embryonic carcinoma cells (Figure 19) and to monitor thiol species in 3-day-old zebrafish for the first time by fluorescence imaging.

9.1.4. Reaction between Iodoacetamide and Thiol.

The iodoacetamide group can react with the thiol of biomolecules. On the basis of this mechanism, the detection of biothiols can be realized by introducing an iodoacetamide group into the chemodosimeter (Scheme 99). Lo and co-workers reported a cationic iridium(III) complex 418 containing the iodoacetamide group in N⁺N ligand.⁵³⁶ This complex 418 has successfully been used to label a universal M13 reverse sequencing primer modified with a thiol group via a C₆ linker at the 5' end, and the labeled product exhibits intense orange-yellow photoluminescence.

9.1.5. Sulfonethers or Sulfonamides Cleavage Process.

It is well-known that sulfonethers and sulfonamides can be readily cleaved by thiolate anions (Scheme 100). On the basis of this strategy, seven chemodosimeters 419–425 have been designed for thiol detection.

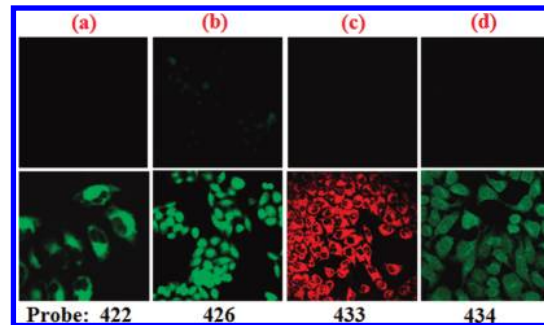
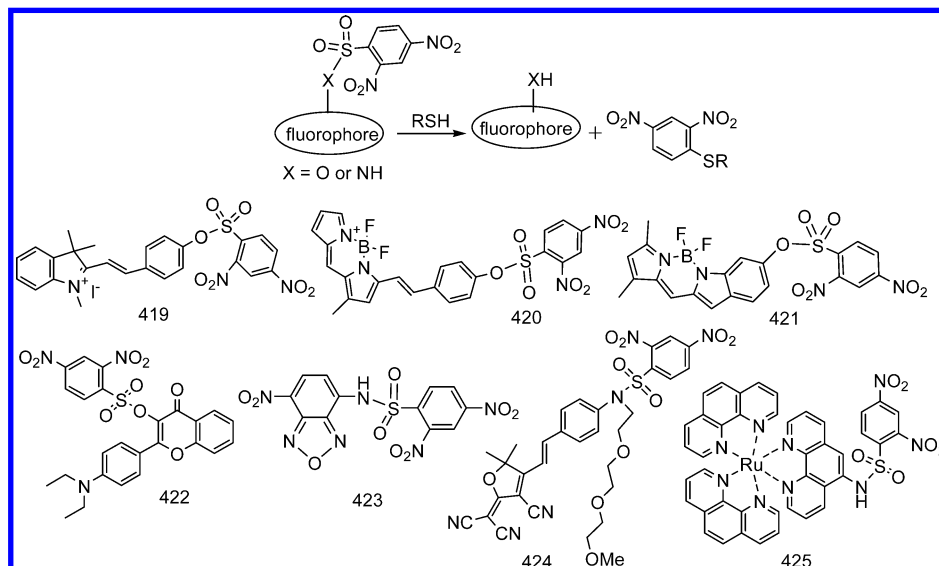


Figure 20. Selected examples of luminescent chemodosimeters (422, 426, 433, and 434) for imaging of biothiols in living cells pretreated with (upper) or without (lower) N-ethylmaleimide (NEM). (a) Reprinted with permission from ref 540. Copyright 2011 Elsevier B.V. (b) Reprinted with permission from ref 544. Copyright 2010 Royal Society of Chemistry. (c) Reprinted with permission from ref 550. Copyright 2007 American Chemical Society. (d) Reprinted with permission from ref 551. Copyright 2009 Royal Society of Chemistry.

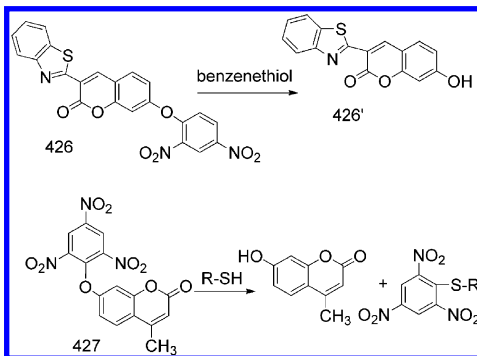
Scheme 100. Proposed Mechanism of Luminescent Chemodosimeters 419–425 Based on Thiol-Induced Cleavage of Dinitrobenzene Sulfonethers and Sulfonamides Moiety



(1). *Thiol-Induced Sulfonether Cleavage.* The first example based on a thiol-mediated nucleophilic reaction that involves a cleavage event is the merocyanine-containing chemodosimeter **419**.⁵³⁷ By masking the electron donor (phenol group) with an electron-withdrawing group of dinitrobenzenesulfonyl (DNS) moiety, sulfonether **419** is nonemissive due to weak intramolecular charge transfer (ICT). Upon addition of GSH into solutions of **419**, the DNS group can be removed by a thiol-mediated sulfonether cleavage process, producing a significantly enhanced fluorescence at 553 nm, with a detection limit of about 2.4×10^{-8} mol L⁻¹.⁵³⁷ On the basis of the same thiol-induced sulfonether cleavage, two BODIPY-based sulfonethers **420**⁵³⁸ and **421**⁵³⁹ were also developed as fluorescence turn-on chemodosimeters for thiol detection. Moreover, **420** was successfully applied to the detection of thiol species in the monkey renal fibroblast COS-7 cell line. Interestingly, the design of chemodosimeter **422**⁵⁴⁰ combines both PET and ESIPT mechanisms. It exhibits a turn-on fluorescence response to thiol with high sensitivity and selectivity. Moreover, **422** has also been used for imaging thiol in living cells (Figure 20).

(2). *Thiol-Induced Sulfonamide Cleavage.* Luminescent chemodosimeters **423**⁵⁴¹ and **424**⁵⁴² have been reported to detect thiols at physiological pH conditions, based on a thiol-induced sulfonamide-cleavage mechanism. For **423** and **424**, thiol-mediated cleavage of the electron-withdrawing sulfonyl group releases an aniline donor, increasing the push–pull

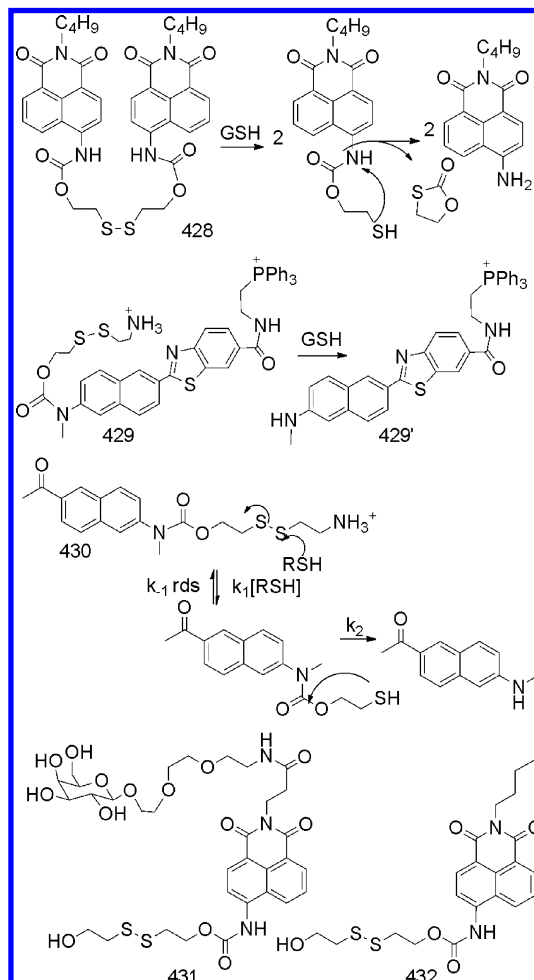
Scheme 101. Sensing Mechanism of **426 and **427** Based on Thiol-Induced Cleavage of Multi-Nitrobenzyl Ester**



character of the fluorophore, and results in a higher quantum yield and a large red-shift in the emission wavelength. Moreover, **424** could be successfully applied to the bioimaging of thiols in living cells.⁵⁴² In addition to purely organic probes, metal complex **425** as an interesting thiol-selective chemodosimeter was reported by Zhao and co-workers.⁵⁴³ Because of the efficient PET from Ru(II) to dinitrobenzenesulfonyl (DNS) unit, **425** is nonluminescent. Thiols cleave the DNS, and the MLCT is re-established, resulting in a 90-fold luminescence enhancement at 598 nm with a significant Stokes shift of 143 nm. Luminescent imaging showed that **425** is specific for thiols over other analytes in living NCI-H446 cells.

9.1.6. Multi-Nitrobenzyl Ester-Cleavage Process. Another strategy is based on nucleophilic attack of thiols on the ether carbon site of nitrophenyl ring. For example, two multi-nitrobenzyl ethers **426**⁵⁴⁴ and **427**⁵⁴⁵ were designed as thiol-selective chemodosimeters, by incorporating the strongly electron-withdrawing dinitrophenyl or trinitrophenyl group into the electron donor (phenol group) of a coumarin fluorophore (Scheme 101). **426** is nonfluorescent and is

Scheme 102. Sensing Mechanism of **428–**432** Based on Cleavage of Thiol-Induced Disulfide-Based Carbamate Protecting Group**



converted into phenolic hydroxyl **426'** by benzenethiols, with a 165-fold fluorescence enhancement. Interestingly, **426** can selectively sense benzenethiol over 2-mercaptoethanol, and the quantitative detection of benzenethiol in water samples was realized. Moreover, **426** is cell-membrane-permeable and able to respond to benzenethiol in living cells (Figure 20).⁵⁴⁴ Another thiol-selective chemodosimeter **427** displays high selectivity toward GSH, with a detection limit of 26.8 nmol L⁻¹. Moreover, **427** could also be used to detect biothiols in human serum samples.⁵⁴⁵

9.1.7. Cleavage of Disulfide-Based Carbamate Protecting Group. On the basis of the cleavage of a disulfide-based carbamate protecting group, naphthalimide derivative **428** was developed as a luminescent chemodosimeter for GSH detection at physiological levels (Scheme 102).⁵⁴⁶ The reaction of **428** with thiol triggers the cleavage of a disulfide-based carbamate protecting group, resulting in significant changes in internal charge transfer. Moreover, **428** was successfully applied to the bioimaging of thiols in living HeLa cells. Utilizing a similar mechanism, a two-photon fluorescent chemodosimeter **429**⁵⁴⁷ for ratiometric detection of mitochondrial thiol has been reported recently (Scheme 102). In **429**, the disulfide group is the reaction site and the triphenylphosphonium salt (TPP) is the mitochondrial-targeting site. The reaction between **429** and a thiol, such as GSH, produces **429'** as the only product. This

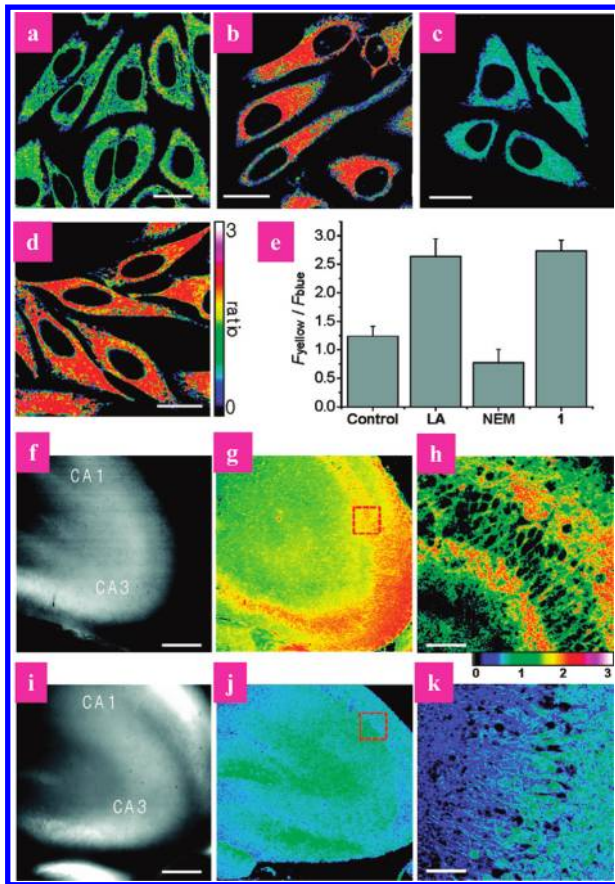
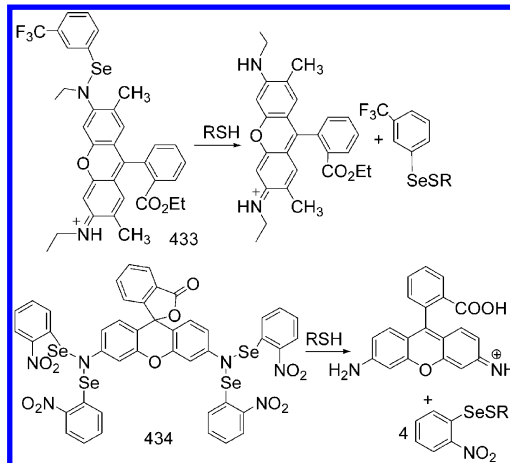


Figure 21. (a–d) Pseudocolored ratiometric two-photon fluorescence (TPM) images ($F_{\text{yellow}}/F_{\text{blue}}$) of HeLa cells incubated with 5 μM (a) 429 and (d) 429' and cells pretreated with (b) lipoic acid (500 μM) for 1 day and (c) NEM (100 μM) for 30 min before labeling with 429. (e) Average $F_{\text{yellow}}/F_{\text{blue}}$ intensity ratios in (a–d). (f–k) Images of a rat hippocampal slice stained with 20 μM 429 for 2 h. (f, i) Bright-field images of the CA1 and CA3 regions. (g, j) Ratiometric TPM images of fresh rat hippocampal slices that were (b) not treated and (e) pretreated with NEM (100 μM) for 30 min before labeling with 429. (h, k) Enlarged images of the red boxes in (g) and (j) at a depth of 120 μm . $\lambda_{\text{ex}} = 740 \text{ nm}$, $\lambda_{\text{em}} = 425\text{--}475 \text{ nm}$ (blue) and 525–575 nm (yellow). Reprinted with permission from ref 547. Copyright 2011 American Chemical Society.

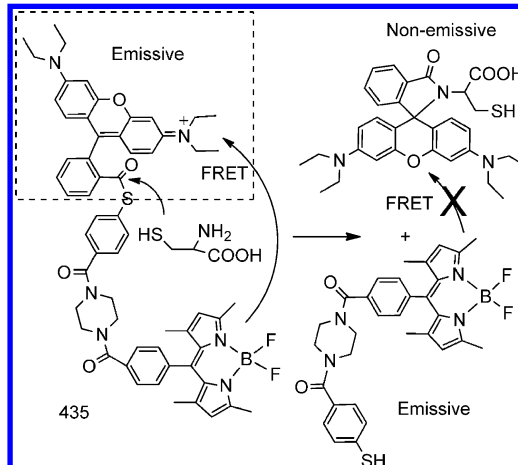
leads to a decrease of fluorescence intensity at 425–475 nm and an increase at 525–575 nm, resulting in a ratiometric fluorescence response. Considering its large two-photon cross section of 80 GM, 429 has been used for the ratiometric two-photon fluorescent imaging of mitochondrial RSH levels in live cells as well as in living tissues to depths of 90–190 μm (Figure 21).⁵⁴⁷ Similarly, another two-photon fluorescent chemodosimeter 430 for thiols has been reported most recently (Scheme 102).⁵⁴⁸

Recently, Kim, Kang, and co-workers used a single galactose-appended naphthalimide 431 as a probe for hepatic thiol imaging in living cells and animals (Scheme 102).⁵⁴⁹ The fluorescence intensity of 431 will be turned on after the cleavage of the disulfide bond, and 431 has a specific targeting effect toward hepatocyte because of the galactose species. The mechanism can be proved by the experiments applying the analogue 432 without galactose, which shows no selectivity (Scheme 102).

Scheme 103. Sensing Mechanism of 433 and 434 Based on Thiol-Induced Cleavage of Se–N Bond



Scheme 104. Sensing Mechanism of Fluorescent Chemodosimeter 435 for Cysteine



9.1.8. Cleavage of Se–N bond. On the basis of the strategy of strong nucleophilicity of the thiol to cleave the Se–N bond, Tang and co-workers reported two organoselenium compounds 433⁵⁵⁰ and 434⁵⁵¹ that acted as fluorescent turn-on chemodosimeters for thiols (Scheme 103). Upon selective reaction with thiols, the Se–N bond is cleaved, accompanied by a 170-fold fluorescence enhancement. Confocal microscopy experiments in both HL-7702 cells and HepG2 cells show that 433 and 434 can visualize differences and changes in thiol concentrations in normal and aberrant cell types, allowing a fluorescent method for intracellular thiol detection (Figure 20).^{550,551}

9.1.9. Native Chemical Ligation Reaction. The native chemical ligation reaction has been widely used in peptide synthesis. It involves the reaction between a peptide- α -thioester and an N-terminal cysteine (Cys) peptide (Scheme 104).⁵⁵² Utilizing this reaction, a FRET-based chemodosimeter 435 for Cys has been realized using a thiophenylester moiety as the reaction site.⁵⁵³ In 435, there exists efficient energy transfer from BODIPY (donor) to rhodamine (acceptor), and the emission of rhodamine at 590 nm was observed. After adding Cys, the thiol group of Cys attacks the electrophilic carbon of the thioester group, and further the *trans*-thioesterification and intramolecular rearrangement reactions result in the cleavage of

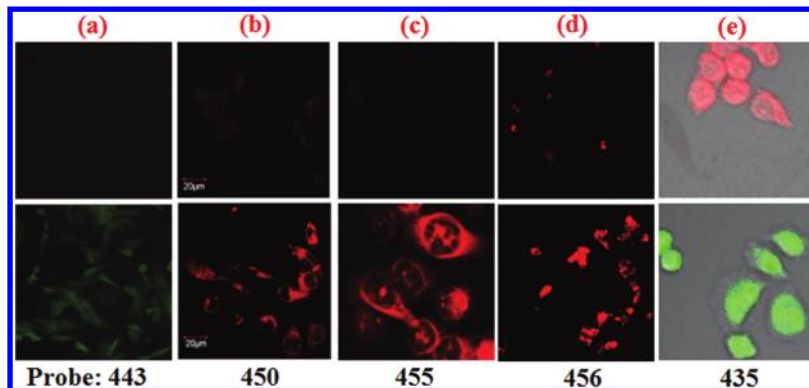
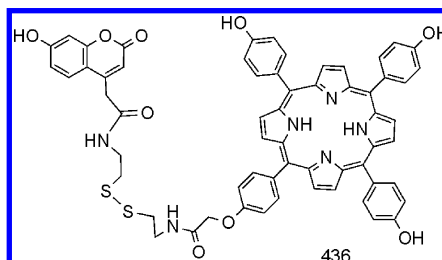


Figure 22. Selected examples of luminescent chemodosimeters (435, 443, 450, 455, and 456) for imaging of Cys/Hcy in living cells. Upper imagings were achieved for living cells pretreatment with *N*-ethylmaleimide (as a thio-reactive compound). (a) Reprinted with permission from ref 564. Copyright 2011 Royal Society of Chemistry. (b) Reprinted with permission from ref 569. Copyright 2011 Royal Society of Chemistry. (c) Reprinted with permission from ref 573. Copyright 2007 American Chemical Society. (d) Reprinted with permission from ref 574. Copyright 2011 American Chemical Society. (e) Ratiometric imaging. $\lambda_{\text{ex}} = 488 \text{ nm}$, $\lambda_{\text{em}} = 610 \pm 10 \text{ nm}$ (red) and $515 \pm 10 \text{ nm}$ (green). Reprinted with permission from ref 553. Copyright 2011 Royal Society of Chemistry.

Scheme 105. Fluorescent Chemodosimeter 436 for Cys

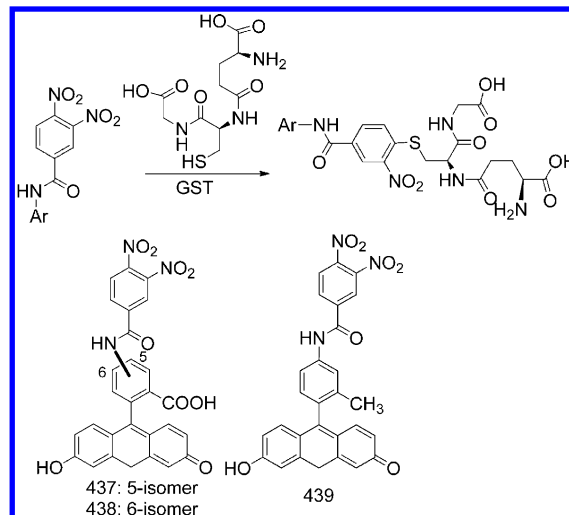


the FRET dyad and the switch-off of the FRET process. Finally, the N atom of the amide group further attacks the electrophilic 9-position carbon of the conjugated xanthene to form the nonfluorescent spirolactam. As a result, a new emission of BODIPY at 510 nm appeared. Importantly, the FRET-based ratiometric imaging of Cys in living cells has been realized using 435 (Figure 22).⁵⁵³

9.1.10. Cleavage Reaction of Disulfide Bond. Thiol/disulfide exchange reaction has been used for detecting thiols, such as Cys. For chemodosimeter 436,⁵⁵⁴ tetrakis(4-hydroxyphenyl)porphyrin and coumarin moiety act as energy donor and acceptor, respectively (Scheme 105). The energy donor is linked to the acceptor by a disulfide bond. There is a FRET process from donor to acceptor, leading to fluorescence quenching of the coumarin moiety. Upon addition of Cys, cleavage of S–S bonds takes place, which switches off the FRET process. Thus, the enhancement of porphyrin emission can be observed with constant porphyrin emission, realizing ratiometric fluorescence detection of Cys. Furthermore, ratiometric imaging of intracellular thiols has been demonstrated.⁵⁵⁴

9.1.11. Demetalization and Hydrolysis Processes. By taking advantage of the affinity of copper ions for thiols, Kim and co-workers have reported that Cu(II) complex 237 (Scheme 52) exhibits sensitive detection of biological thiols, such as GSH.⁵⁵⁵ 237 is nonluminescent, due to the heavy metal ion effect. The addition of thiols induces decomplexation of the Cu²⁺ ion from 237, followed by hydrolytic cleavage of the resulting Schiff base to give a strongly fluorescent coumarinaldehyde 237'. Thus, an off-on fluorescence change was realized.

Scheme 106. Sensing Mechanism of 437–439 Based on GST-Induced Denitration and Glutathionylation



9.1.12. Denitration and Glutathionylation. Glutathione S-transferase (GST) is of clinical interest, because it is often overexpressed in various types of cancer cells and is involved in drug resistance.⁵⁵⁶ However, the fluorescence probes for GST activity were lacking. Nagano and co-workers reported the excellent fluorescent chemodosimeters 437 and 438 for GST with an off-on fluorescence-switching mechanism based on the replacement of a nitro group with GST (Scheme 106).⁵⁵⁷ These chemodosimeters are highly sensitive and suitable for high-throughput screening. Furthermore, the membrane-permeable derivative 439 was synthesized, which was used for visualizing high GST activity in the nucleus of HuCCT1 cells.⁵⁵⁷

9.2. Luminescent Chemodosimeters for Cys/Hcy

Cysteine (Cys) and homocysteine (Hcy) play important roles in maintaining biological systems and are essential for the growth of cells and tissues in living systems. Cys deficiency is associated with retarded growth, hair depigmentation, edema, lethargy, liver damage, muscle and fat loss, skin lesions, and weakness.^{558–560} An elevated level of Hcy in human plasma is a risk factor for Alzheimer's disease, cardiovascular disease, neural

Scheme 107. Proposed Mechanism of Fluorescent Chemodosimeters 440–453 Based on Cyclization Reaction of Aldehyde with Cys and Hcy

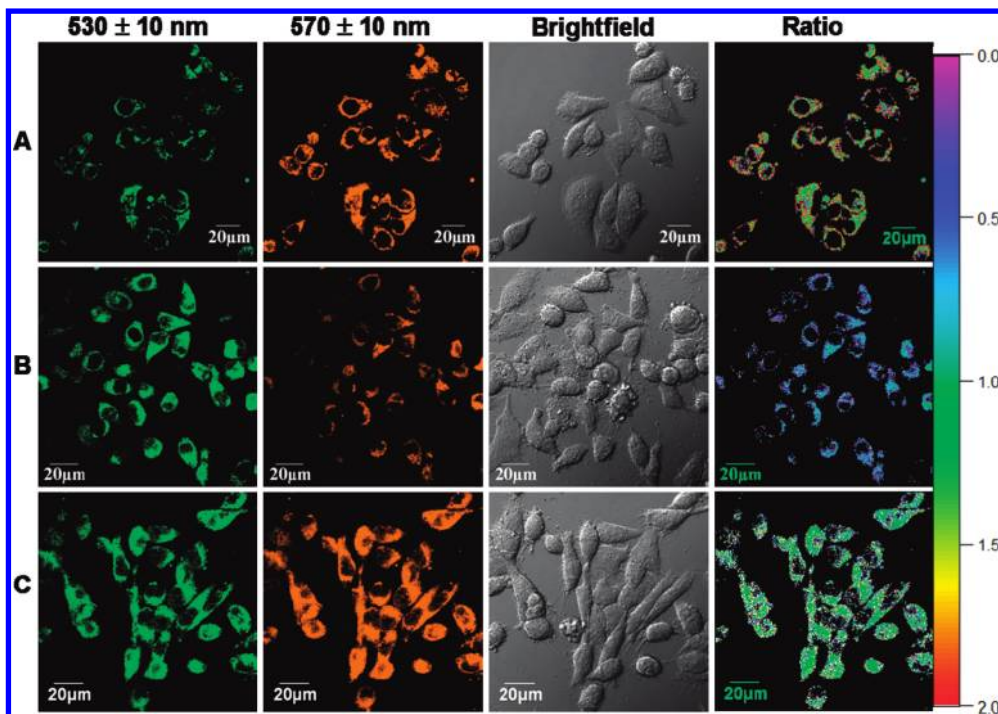
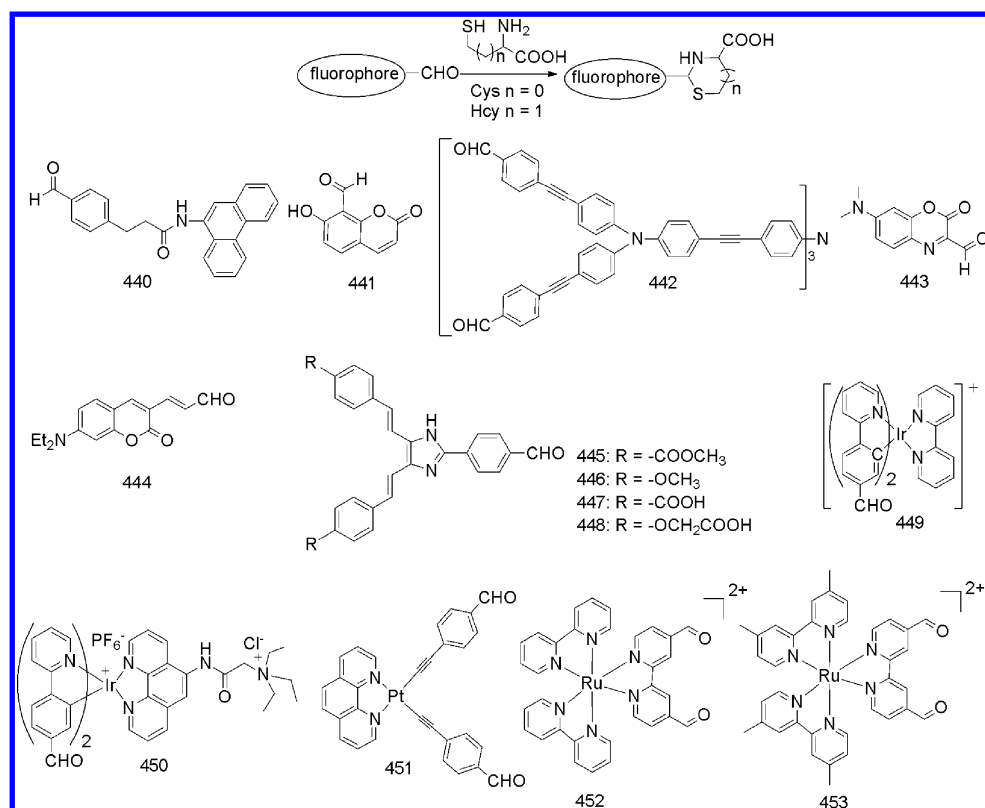


Figure 23. Ratio phosphorescence images of 449 in KB cells. (A) KB cells incubated with 20 μ M 449 for 30 min. (B) KB cells incubated with 200 μ M N-ethylmaleimide for 1 h and then further incubated with 20 μ M 449 for 30 min. (C) KB cells incubated with 200 μ M N-ethylmaleimide for 1 h and then further incubated with 20 μ M 449 for 1 h. Emission was collected by the green channel from 530 ± 10 nm and red channel from 570 ± 10 nm ($\lambda_{ex} = 405$ nm). Ratio of emission intensity at 570 ± 10 nm to 530 ± 10 nm is also shown. Reprinted with permission from ref 568. Copyright 2010 American Chemical Society.

tube defects, inflammatory bowel disease, and osteoporosis.^{558–560} Therefore, the selective detection of Hcy and Cys is

very important as they are disease-associated biomarkers. To date, 17 fluorescence chemodosimeters for Cys/Hcy have been

developed based on cyclization reaction of aldehyde, nucleophilic addition reaction, native chemical ligand reaction, and cleavage of disulfide bond.

9.2.1. Cyclization Process of Arylic Aldehyde. It is well-known that aldehydes can react with the thiol and amine groups of Cys or Hcy to form thiazolidine or thiazinane (Scheme 107). On the basis of this cyclization reaction, some arylic aldehydes have been developed as luminescent chemodosimeters for the selective detection for Cys and Hcy, accompanying an evident fluorescence change.

(1). *Organic Fluorescent Dyes.* The first example of luminescent chemodosimeters for cysteine based on cyclization process of aldehyde is **440**.⁵⁶¹ Accurate results could be obtained in a low Cys concentration range (20–100 μM) when the velocities of the increase in fluorescence were measured. A typical example is **441**, which contains a coumarin group as the fluorescent signaling unit and a salicylaldehyde functionality as the reactive aldehyde. **441** exhibits a high selectivity toward Hcy and Cys over other amino acids and glutathione in water under neutral conditions,⁵⁶² corresponding to 50-fold fluorescence enhancement. Furthermore, Chen and co-workers developed the dendritic chromophore **442** as a two-photon luminescent chemodosimeter for Hcy and Cys over other amino acids.⁵⁶³ After reacting with Cys/Hcy, the intramolecular charge transfer characteristics changed, resulting in 30-fold enhancement of the two-photon fluorescence and a blue-shift of 165 nm in the peak wavelength. **443** shows efficient intramolecular charge transfer and was designed as a fluorescent turn-on chemodosimeter for Cys and Hcy for monitoring the cellular distribution of Cys/Hcy by confocal fluorescence microscopy (Figure 22).⁵⁶⁴

Recently, another coumarin dye **444**, containing an α,β -unsaturated aldehyde, was reported to exhibit a specific fluorescence response to Cys compared with Hcy and glutathione.⁵⁶⁵ Treatment of Cys induces a marked fluorescence decrease at 557 nm (green channel) and concurrently a dramatic fluorescence enhancement at 487 nm (blue channel), allowing the ratiometric detection of Cys. The high selectivity for Cys over Hcy and GSH may be rationalized by the hypothesis that the “7-membered heterocycle” cyclization of Cys with **444** is more favorable.⁵⁶⁵ Furthermore, **444** can be used for the ratiometric imaging of variations of Cys levels in living cells.

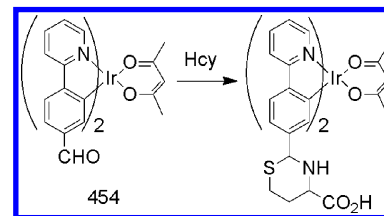
Following the mechanism-selective cyclization process of aldehyde with Cys/Hcy, we have developed a series of two-photon excited fluorescent chemodosimeters **445–448** for Cys and Hcy.^{566,567} **445** has a significant blue-shift (~ 30 nm) in two-photon excited fluorescence emission upon addition of Cys/Hcy.⁵⁶⁶ Compared to **445**, **446** shows a prominent enhancement in the fluorescence and ratiometric emission in the presence of Cys or Hcy. Two other chemodosimeters, **447** and **448**, having a carboxylic acid show excellent water solubility.

(2). *Phosphorescent Metal Complexes.* By introducing the aldehyde groups into the ligands, phosphorescent Ir(III), Pt(II), and Ru(II) complexes have been designed as chemodosimeters for Cys/Hcy detection, based on cyclization mechanisms. Such cyclization reactions often result in clear enhancement of the phosphorescence intensity or a change in the emission wavelength.

Recently, we have reported a cationic aldehyde-containing Ir(III) complex **449** that acts as a phosphorescent chemodosimeter for imaging of intracellular Hcy and Cys (Figure 23).⁵⁶⁸ Upon addition of Hcy or Cys to a semiaqueous solution

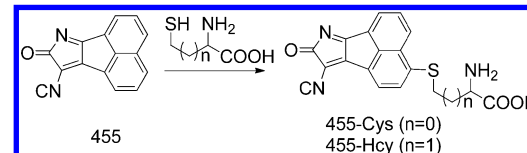
of **449**, a change in luminescence from yellow to red was visible to the naked eye. **449** is membrane-permeable with low cytotoxicity and can be used to monitor changes in Hcy/Cys concentration within living cells ratiometrically. Living KB cells incubated with **449** displayed both a brighter emission intensity

Scheme 108. Sensing Mechanism of Luminescent Hcy-Selective Chemodosimeter **454**



at 570 ± 10 nm over the region of 530 ± 10 nm. If the cells were pretreated with *N*-ethylmaleimide (NEM, as a thiol-blocking agent) and then loaded with **449**, an evident luminescent enhancement at 530 ± 10 nm was observed. These results demonstrate that **449** is suitable for ratiometric imaging of Hcy/Cys in living cells.⁵⁶⁸ Furthermore, by introducing a quaternary ammonium salt into the N⁺N ligand, we have designed and synthesized a completely water-soluble phosphorescent chemodosimeter **450**⁵⁶⁹ for Cys and Hcy.

Scheme 109. Sensing Mechanism of Fluorescent Chemodosimeter **455 for Cys/Hcy**



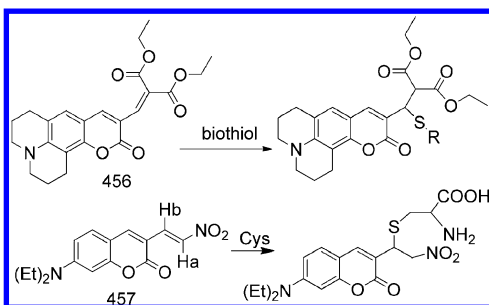
Moreover, **450** can be used to image Cys and Hcy in living cells with its turn-on phosphorescent response (Figure 22).

Similarly, the Pt(II) complex **451**⁵⁷⁰ and Ru(II) complexes **452** and **453**⁵⁷¹ were also reported as chemodosimeters for Cys and Hcy. For example, we have reported that platinum(II) complex **451** exhibits high selectivity toward Cys and Hcy in the presence of other amino acids, resulting in a luminescent color change from green to orange.

It is very important to design fluorescent probes that can distinguish Hcy from Cys. In 2007, we devised the neutral iridium(III) complex **454** as a Hcy-selective chemodosimeter that can distinguish Hcy from Cys and other thiol-related peptides (Scheme 108).⁵⁷² Upon addition of increasing amounts of Hcy to a solution of **454**, a new emission band at 525 nm gradually appeared, corresponding to a blue-shift of ~ 90 nm. Both surface-charge analysis and electrochemical measurement indicated that a photoinduced electron-transfer process for the adduct **454–Cys** with weak emission might be responsible for the phosphorescence enhancement observed for **454** toward Hcy over Cys.

9.2.2. Nucleophilic Addition Process. In 2007, we reported the first Cys/Hcy chemodosimeter **455** (Scheme 109) for fluorescence imaging of Cys/Hcy distribution in living cells.⁵⁷³ In a mixture of methanol and HEPES (7:3, v/v) solution at pH 7, the emission peak of **455** at 588 nm increased rapidly (75-fold) upon addition of Cys or Hcy, which is

Scheme 110. Sensing Mechanism of Fluorescent Chemodosimeters **456 and **457** for Cys/Hcy**



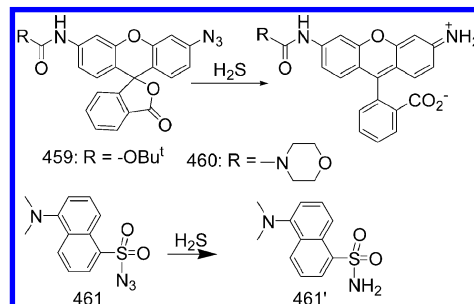
attributed to the nucleophilic addition process of Cys/Hcy. Competition experiments indicated that **455** displays a high selectivity for Cys/Hcy over various other amino acids and thiol biomacromolecules. Furthermore, the practical application of **455** toward Cys and Hcy detection in biological samples was demonstrated through confocal fluorescence microscopy and two-photon fluorescence microscopy (Figure 22), indicating that **455** can be used for bioimaging the subcellular distribution of Cys/Hcy, with excitation in the visible region and turn-on fluorescence response.⁵⁷³

9.2.3. Michael Addition Process. The design of a chemodosimeter for Cys/Hcy has also been based on a Michael addition reaction between Cys/Hcy and the α,β -unsaturated carbonyl to form a new adduct (Scheme 110). For example, **456** did not exhibit fluorescence due to the ICT from the fluorophore (coumarin) to the nearby conjugated diester.⁵⁷⁴ However, conjugation of the coumarin ring system to the α,β -unsaturated carbonyl group changed significantly after an addition reaction with Cys/Hcy, resulting in a hypsochromic absorption shift and fluorescence enhancement.⁵⁷⁴ Another example of a turn-on fluorescent chemodosimeter for Cys/Hcy is compound **457** containing a nitroolefin moiety as electron acceptor.⁵⁷⁵ Furthermore, **456** (Figure 22) and **457** have been applied for imaging the intracellular thiols through confocal microscopic analysis. It should be noticed that the selectivity of chemodosimeters designed based on the Michael reaction for Cys/Hcy over other biothiols, such as GSH, is not high.

9.2.4. Michael Addition and Intramolecular Cyclization Reactions. The Michael addition of Cys to acrylates can generate thioethers, which can subsequently undergo the intramolecular cyclization to yield lactam (Scheme 111). Utilizing this reaction, the discrimination of Cys over Hcy can be realized, because the intramolecular cyclization reaction to form a seven-membered ring for Cys is kinetically favored relative to the formation of an eight-membered ring for Hcy. A representative example is compound **458**.⁵⁷⁶ The addition of

Cys into the ethanol/phosphate buffer of **458** leads to the formation of 2-(2'-hydroxy-3'-methoxyphenyl)benzothiazole (HMBT) with emission at 487 nm and lactam. In the case of Hcy, however, the cyclization reaction for the formation of eight-membered-ring lactam is relatively slow, and only conjugate addition adduct **458b** with emission at 377 nm was formed. Interestingly, cetyltrimethylammonium bromide (CTAB) micellar media can significantly enhance the reaction rates. The response of **458** to Cys in CTAB micellar media reaches saturation within 9 min. Hcy, however, can still cause a proportional change of the emission signals at 377 and 487 nm

Scheme 112. Mechanism of **459–461 Based on H_2S -Mediated Reduction of Azide to Amine**



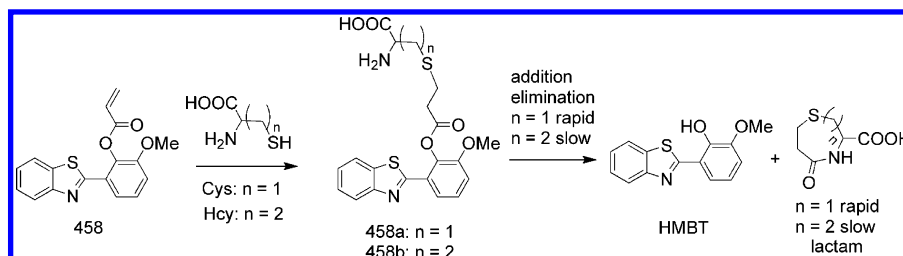
after 9 min. Thus, simultaneous detection of Cys and Hcy over non-aminothiols in CTAB micellar media can be realized by spectral and kinetic modes. In addition, the detection of Cys in diluted (10%) deproteinized human plasma was successfully carried out, suggesting its potential utility in clinical diagnosis.

9.3. Luminescent Chemodosimeters for $\text{H}_2\text{S}/\text{S}^{2-}$

Hydrogen sulfide (H_2S) and sulfide (S^{2-}) are important reactive sulfur species. H_2S is a colorless and flammable gas and plays an important role in many physiological processes, such as angiogenesis, vasodilation, neuromodulation, apoptosis, and inflammation.^{577,578} In addition, some diseases, including Alzheimer's disease, Down's syndrome, diabetes, and liver cirrhosis, can result in a change of H_2S levels.^{579,580} H_2S can dissociate into S^{2-} . S^{2-} is toxic and presents in many environments as a byproduct of manufacturing and industrial processes.⁵⁸¹ To elucidate the influence of H_2S levels on healthy and diseased states, it is important to selectively track H_2S within living biological specimens by a fluorescent method.

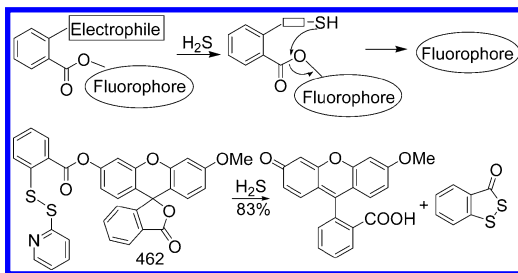
9.3.1. H_2S -Mediated Reduction of Azide to Amine. Recently, Chang and co-workers reported a new strategy for designing H_2S -selective luminescent chemodosimeters **459** and **460** based on H_2S -mediated reduction of azides to amines (Scheme 112).⁵⁸² The reduction of the azide group with H_2S results in a spirolactam ring-opening process, generating 7- and

Scheme 111. Sensing Mechanism of Chemodosimeter **458 for Cys/Hcy Based on Michael Addition and Intramolecular Cyclization Reactions**



9-fold fluorescence turn-on responses for **459** and **460**, respectively, in aqueous media at physiological pH values.

Scheme 113. Proposed Mechanism for **462 Based on H₂S-Induced Nucleophilic Reaction**

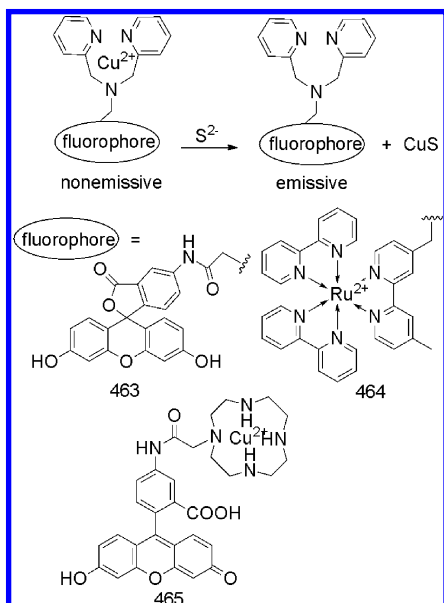


This fluorescence turn-on response was found to be selective for H₂S over other biologically relevant reactive sulfur species, reactive nitrogen species, and reactive oxygen species. Importantly, **459** and **460** can show changes in H₂S levels in live-cell imaging using confocal microscopy. When HEK 293T cells were preincubated with 5 μM **459** or **460** for 30 min, a significant increase in intracellular fluorescence intensity was observed. **459** gave a greater turn-on response to H₂S than **460**, due to the increased lipophilicity and cellular retention of **459**. Such fluorescent chemodosimetric detection provides an effective tool for studying the endogenous production of H₂S in living cells.⁵⁸²

Another example is nonfluorescent probe **461**, which was transformed to fluorescent **461'** after H₂S-mediated reduction of azides to amines (Scheme 112).⁵⁸³ This probe can be used for detecting H₂S in aqueous solutions, including blood serum and whole blood.

9.3.2. H₂S-Induced Nucleophilic Reaction. H₂S can be considered as a nonsubstituted thiol and can participate in nucleophilic reaction twice, which is different from thiols. If the fluorescent probe contains bis-electrophilic sites, as shown in Scheme 113, H₂S can react with the most electrophilic component to form a thiol intermediate. Subsequently, the

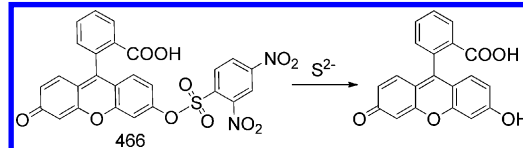
Scheme 114. Sensing Mechanism of **463–**465** Based on High Affinity of S^{2−} to Cu(II)**



thiol group can attack another electrophile, such as the ester group, and undergo a spontaneous cyclization to release the fluorophore. Thus, the fluorescent detection of H₂S can be realized. On the basis of this mechanism, a reactive disulfide-containing chemodosimeter **462** was designed, which can react rapidly with H₂S to generate fluorophore, realizing turn-on fluorescent detection.⁵⁸⁴ Furthermore, **462** was used for detecting H₂S in plasma and COS7 cells.

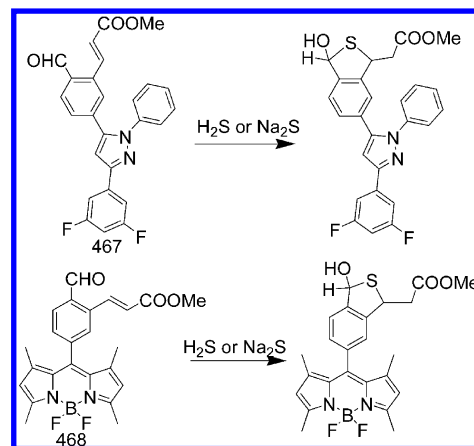
9.3.3. High Affinity of S^{2−} to Cu(II). A general and effective design principle of sulfide chemodosimeter is based on

Scheme 115. Sensing Mechanism of **466 Based on Nucleophilic Reaction of S^{2−}**



the high affinity of sulfide to Cu(II). By introducing the di(2-picoly)amine–Cu(II) complex moiety into a fluorophore, its fluorescence can be effectively quenched due to coordination to a paramagnetic Cu²⁺ center. After adding sulfide, the nonluminescent Cu(II) complex can specifically and rapidly react with sulfide to yield the corresponding fluorescent product, exhibiting a turn-on signaling behavior (Scheme 114). On the basis of this principle, **463**,⁵⁸⁵ **464**,⁵⁸⁶ and **465**⁵⁸⁷ using fluorescein and Ru(II) complex as fluorophores, respectively, were demonstrated as successful luminescent chemodosimeters for the S^{2−} detection. Among them, **465** was used successfully

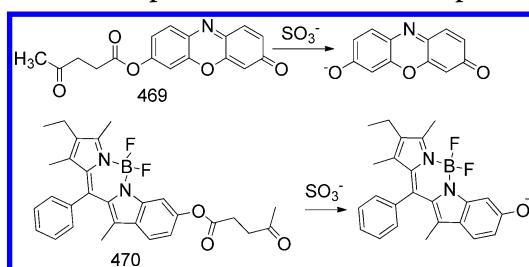
Scheme 116. Sensing Mechanism of **467 and **468** Based on Addition Reaction of S^{2−} and Michael Addition**



for real-time fluorescence imaging of intracellular H₂S in live HeLa cells.

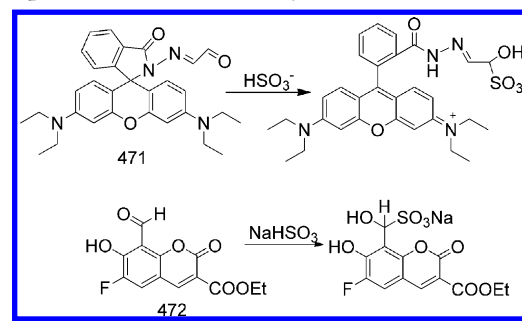
9.3.4. Nucleophilic Reaction of S^{2−}. Another design principle for S^{2−} chemodosimeter is based on the nucleophilicity of S^{2−}. 2,4-Dinitrobenzenesulfonylfluorescein **466**⁵⁸⁸ is weakly emissive. Upon addition of S^{2−}, the 2,4-dinitrobenzenesulfonyl group of **466** is efficiently removed, resulting in the formation of a fluorescein unit and a dramatic increase in the fluorescence intensity (Scheme 115). Other anions do not produce any changes under the same conditions. Importantly, **466** has been successfully applied to the determination of sulfide anion in wastewater samples.

Scheme 117. Sensing Mechanism of 469 and 470 Based on SO_3^{2-} -Induced Deprotection of Phenolic Group



9.3.5. Addition Reaction of S^{2-} and Michael Addition. Recently, the fluorophores 467 and 468 substituted by α,β -unsaturated acrylate methyl ester and aldehyde ortho to each other have been demonstrated for the selective fluorescent detection of S^{2-} with turn-on fluorescence response.⁵⁸⁹ The sulfide can first react with the aldehyde to form a hemithioacetal intermediate with a free thiol, which performs the subsequent Michael addition with α,β -unsaturated acrylate methyl ester to produce the original probe (Scheme 116). Furthermore, 467 and 468 have been used to monitor sulfide generation from enzymes and for cell-based sulfide imaging in live cells in the presence of large excess of thiols.

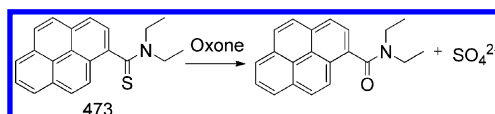
Scheme 118. Sensing Mechanism of 471 and 472 Based on Nucleophilic Addition of Aldehyde and HSO_3^-



9.4. Fluorescent Chemodosimeters for $\text{HSO}_3^-/\text{SO}_3^{2-}$

Sulfite (SO_3^{2-}) is widely used as a preservative in beverages and food. It is potentially toxic and is associated with allergic reactions and food-intolerance symptoms.^{590,591} On the basis of SO_3^{2-} -induced selective deprotection of resorufin levulinate (Scheme 117), Chang and co-workers reported a SO_3^{2-} -selective chemodosimeter 469⁵⁹² in an aqueous environment. Levulinate 469 showed a weak emission at 584 nm. Upon treatment with 100 equiv of SO_3^{2-} , however, intense emission appeared at 588 nm, which was assigned to the generated resorufin. The signaling of 469 toward SO_3^{2-} was not affected by other anions, demonstrating its high selectivity. On the basis of a similar mechanism, a BODIPY derivative 470 was also used for ratiometric fluorescent detection of SO_3^{2-} (Scheme 117).⁵⁹³

Scheme 119. Sensing Mechanism of 473 Based on Oxone-Induced Desulfurization Process

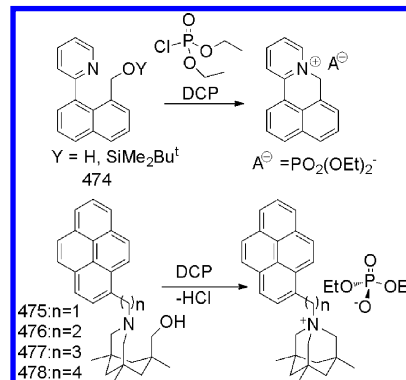


Like sulfites, bisulfite (HSO_3^-) is also a common preservative added to foodstuffs to inhibit development of both enzymatic and nonenzymatic browning in various processing and storage situations.⁵⁹⁴ The design of chemodosimeters for HSO_3^- is usually based on the nucleophilic addition reaction between HSO_3^- and aldehyde group to form an aldehyde–bisulfite adduct. On the basis of this mechanism, two fluorescent turn-on chemodosimeters 471⁵⁹⁵ and 472⁵⁹⁶ have been developed for HSO_3^- detection in aqueous media (Scheme 118). Upon reaction of HSO_3^- with aldehyde, the spriolactam ring-opening process of the rhodamine unit takes place, resulting in the turn-on fluorescence response of 471 to HSO_3^- . Such fluorescent turn-on response to HSO_3^- is hardly influenced by other anions, therefore showing excellent selectivity.⁵⁹⁵

9.5. Luminescent Chemodosimeters for Oxone

Oxone is a component of a triple salt with the formula $2\text{KHSO}_5 \cdot \text{KHSO}_4 \cdot \text{K}_2\text{SO}_4$.⁵⁹⁷ Oxone is a versatile oxidant in synthetic chemistry and can convert thiocarbonyl to the oxo derivatives.⁵⁹⁸ On the basis of this reaction, Chang and co-workers reported a fluorescent turn-on chemodosimeter for oxone by selective desulfurization of a pyrene thioamide

Scheme 120. Sensing Mechanism of 474–478 Based on DCP-Induced Intramolecular Cyclization Process



derivative 473⁵⁹⁹ to the amide derivative (Scheme 119). Such a turn-on fluorescence signaling of 473 by oxone was rapid (<10 min). No interference from common metal ions, anions, and hydrogen peroxide was observed for the signaling of oxone by 473.

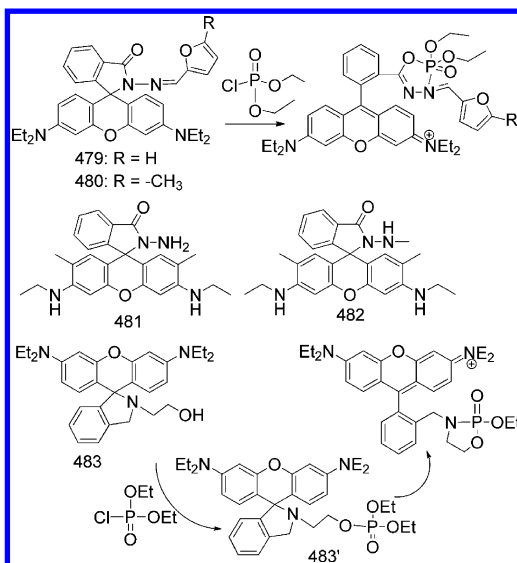
10. LUMINESCENT CHEMOSIMETERS FOR NERVE GAS DCP

Nerve gas agent diethyl chlorophosphate (DCP) is a highly toxic organophosphonate and can irreversibly inhibit the serine esterase activity of acetylcholinesterase, a highly critical enzyme in nerve function, via the phosphorylation of the serine residue at the active site.^{600,601} Recently, two design principles, the DCP-induced intramolecular cyclization mechanism and the DCP-induced spriolactam ring-opening process of rhodamine dyes, have been developed for fluorescent chemodosimetric detection of DCP.

10.1. DCP-Induced Intramolecular Cyclization Process

The first luminescent chemodosimeter based on this mechanism is the flexible chromophore 474, synthesized by Zhang and Swager.⁶⁰² The DCP-induced intramolecular cyclization reaction of 474 can transform it to a rigid extended

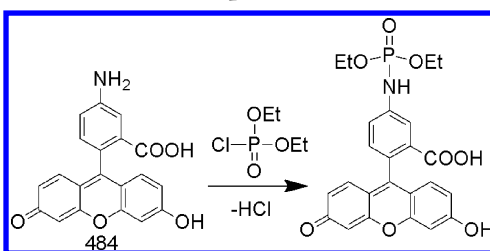
Scheme 121. Sensing Mechanism of 479–483 Based on the DCP-Induced Spirolactam Ring-Opening Process



one and result in a significant fluorescence enhancement by reducing the nonradiative rate (Scheme 120).

On the basis of a similar mechanism, Dale and Rebek reported another class of fluorescent chemodosimeters (475–478)⁶⁰³ for DCP with different aliphatic chains (Scheme 120). The fluorescence of pyrene is quenched via PET of the nonbonding electrons of the nitrogen atom. Compounds 475–478 can react with 1 equiv of DCP to produce the aza adamantane quaternary ammonium, which inhibits the PET process and restores the fluorescence of pyrene. Thus, the fluorescence turn-on detection of DCP was achieved. Among this group, 475, with the shortest distance between the pyrene

Scheme 122. Sensing Mechanism of 484 Based on DCP-Induced Formation of Phosphoramides



and amine moieties, exhibited the most significant increase in fluorescence intensity upon reaction with DCP.⁶⁰³

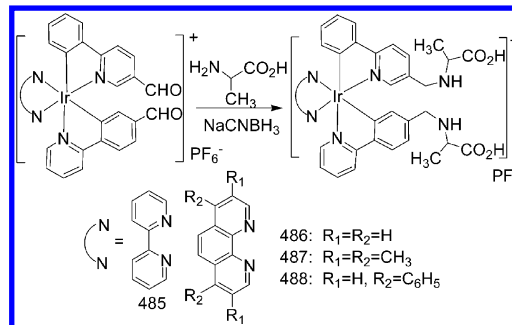
10.2. DCP-Induced Spirolactam Ring-Opening Process

To date, four rhodamine derivatives 479 and 480⁶⁰⁴ and 481 and 482⁶⁰⁵ have been reported as fluorescence turn-on chemodosimeters for the detection of DCP (Scheme 121). Upon DCP binding, significant fluorescent enhancement was observed for 479 and 480, which is attributed to the DCP-induced formation of the highly fluorescent open-ring form involving carbonyl oxygen and imine nitrogen, accompanied by the loss of the chlorine group. 479 and 480 also show very high selectivity toward DCP over the common interferences, such as dimethylmethylphosphonate, HCl, and metal ions.

10.3. DCP-Induced Spirolactam Ring-Opening and Intramolecular Cyclization Processes

Compound 483 can be used as a turn-on luminescent chemodosimeter for DCP (Scheme 121).⁶⁰⁶ Upon addition

Scheme 123. Sensing Mechanism of Luminescent Chemodosimeters 485–488 for Alanine



of DCP, the fluorescence emission intensity peak at 590 nm increased, which can be attributed to the nucleophilic attack of the deoxylactam amine of 483 on the phosphate group of intermediate 483' and subsequent opening of the deoxylactam and intramolecular cyclization reaction.

10.4. DCP-Induced Formation of Phosphoramide

The phosphoryl halides of DCP can also react with an amino group to form phosphoramides. Utilizing this reaction, chemodosimeter 484 for DCP was reported (Scheme 122).⁶⁰⁷ For 484, the lone pair nitrogen of the amine group can quench the fluorescence from fluorescein via PET process. Upon reaction between the amino group and DCP, the fluorescence from fluorescein was recovered, realizing off-on fluorescence response.

11. LUMINESCENT CHEMOSIMETERS FOR AMINO ACIDS

11.1. Luminescent Chemodosimeters for Alanine

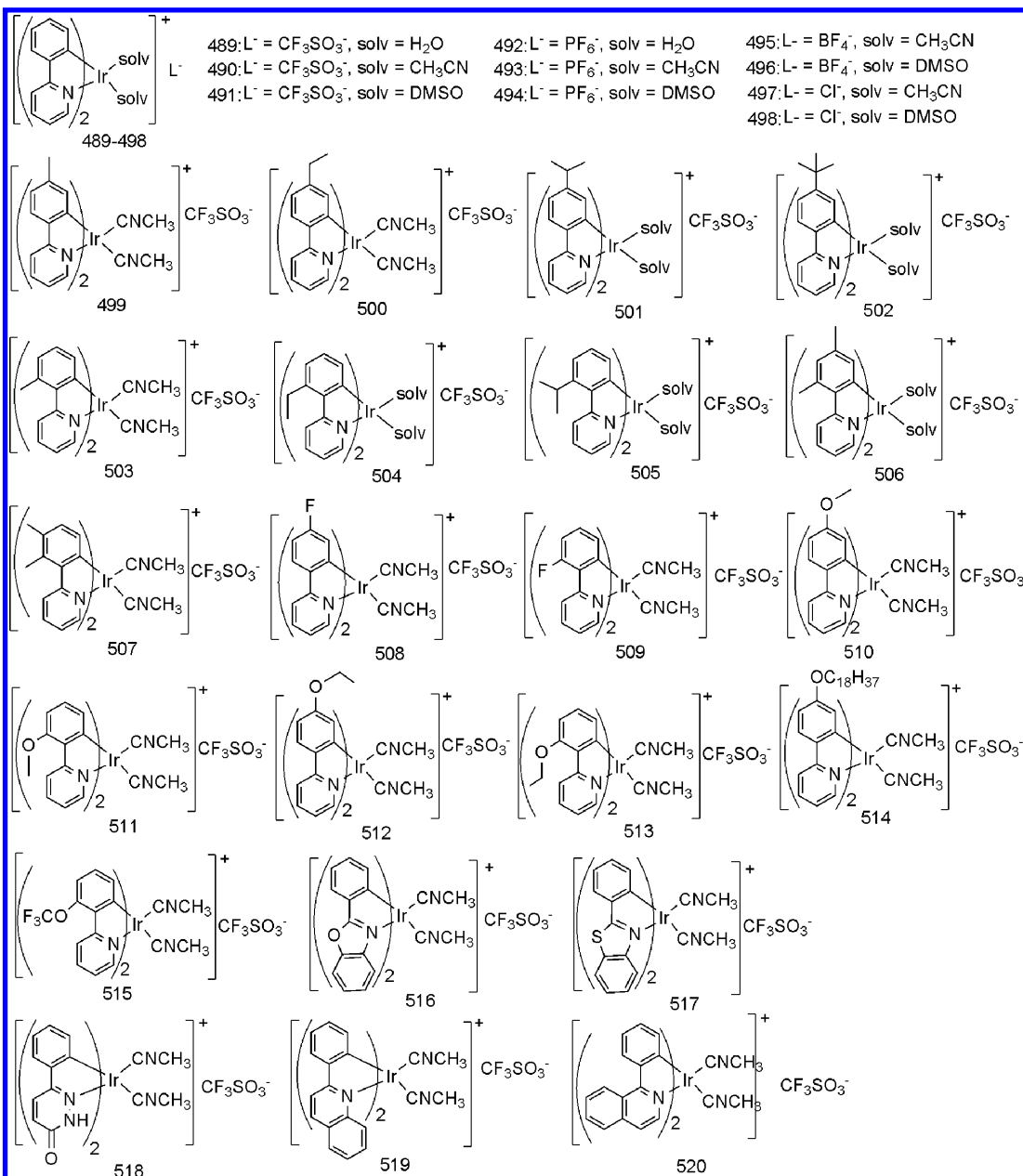
Utilizing the reaction between the aldehyde and amino groups, Lo and co-workers have developed a series of phosphorescent chemodosimeters for alanine based on heavy-metal complexes. For iridium(III) complexes 485–488,⁶⁰⁸ the two aldehyde groups in C^N ligands react with two primary amine groups of alanine to form two imine moieties, which can be reduced to form stable secondary amines by sodium cyanoborohydride (Scheme 123). Thus, the excited-state properties of 485–488 were changed and the detection of alanine can be realized.

11.2. Luminescent Chemodosimeters for Histidine and Histidine-Rich Protein

Abnormal levels of histidine-rich proteins are indicators for many diseases, including advanced liver cirrhosis, asthma, pulmonary disorders, AIDS, renal disease, thrombotic disorders, and malaria.^{609–611} Wong and co-workers reported the iridium(III) solvent complexes 489 and 490 as chemodosimeters for histidine/histidine-rich protein detection (Chart 10). Complex 490 exhibits a 180-fold fluorescence enhancement in the presence of histidine.⁶¹² It displays high selectivity for histidine over other natural amino acids through coordination attachment of the imidazole moiety of histidine.

Recently, we have reported two nonemissive cyclometalated iridium(III) solvent complexes, without conjugation with a cell-

Chart 10. Chemical Structures of Chemodosimeters 489–520 for Histidine and Histidine-Rich Protein



penetrating molecular transporter, $[\text{Ir}(\text{ppy})_2(\text{H}_2\text{O})_2]^+\text{PF}_6^-$ (**492**) and $[\text{Ir}(\text{ppy})_2(\text{DMSO})_2]^+\text{PF}_6^-$ (**494**), as reaction-based luminescence-turn-on agents for the nuclei of living cells (Chart 10).⁶¹³ Unlike the reported nuclear stains (DAPI and Hoechst dyes)⁶¹⁴⁻⁶¹⁵ that are based on luminescence enhancement through intercalation among the stacked base pairs of nucleic acids, **494** as a luminescence-turn-on nuclear stain has a chemical reaction-based mode of action, which relies on its rapid coordination reaction with the imidazole moiety of intracellular histidine/histidine-containing proteins.⁶¹⁶ Interestingly, **494** can rapidly and selectively light up the nuclei of living cells over fixed cells, giving rise to a ~200-fold luminescence enhancement (Figure 24). The detailed cellular uptake investigations under different conditions, such as at various temperatures, with hypertonic treatment, and in the presence of metabolic and endocytic inhibitors, indicate that **494** permeates the outer and nuclear membranes of living cells

through an energy-dependent entry pathway within 6 min and is further accumulated in the nuclei and converted into an intensely emissive adduct. Such novel reaction-based nuclear staining provides a new strategy for visualizing exclusively the nuclei of living cells.

To further understand the structure-activity relationship, we designed and synthesized a series of such a type of cyclometalated iridium(III) solvent complexes [$\text{Ir}(\text{C}^{\text{N}}\text{N})_2(\text{solv})_2]^+\text{L}^-$ (491, 493, and 495–523; Chart 10) through changing the counteranions (L^-), solvent molecules (solv), and cyclometalated C^{N} ligands.⁶¹⁶ All of these solvent complexes exhibit negligible luminescence in both solution and the solid state at room temperature, with a luminescence quantum yield of <0.1%. Moreover, all of them can enter living cells with significant luminescence enhancement. Interestingly, variations of counteranions ($\text{L}^- = \text{PF}_6^-$ or CF_3SO_3^-) and solvent ligands ($\text{solv} = \text{DMSO}$, H_2O , or CH_3CN) of

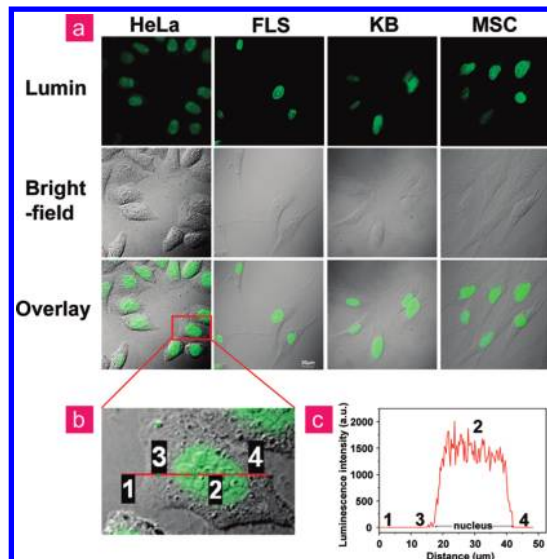


Figure 24. (a) Confocal luminescence images of living HeLa, FLS, KB, and MSC cells incubated with 10 μM chemodosimeter 494 in PBS for 10 min at 37 °C ($\lambda_{\text{ex}} = 488 \text{ nm}$, $\lambda_{\text{em}} = 520 \pm 20 \text{ nm}$). (b) Amplified confocal luminescence imaging of living HeLa cells incubated with 10 μM 494 in PBS for 10 min at 37 °C. (c) Luminescence intensity profile across the line shown in (b) corresponding to extracellular region (1), nuclear region (2), and cytoplasm (3 and 4). Reprinted with permission from ref 613. Copyright 2011 American Chemical Society.

iridium(III) complexes cannot affect cellular staining behaviors. However, their cellular uptake behavior is significant dependent on the change in chemical structure of cyclometalated C^N ligands. In particular, the length of the side carbon chain, the replacement position, and the spatial separation in the C^N ligands have a drastic effect on the cellular uptake and localization accumulation of these iridium complexes in living cells.

12. SUMMARY AND PROSPECTS

Chemodosimeters are a class of sensing system based on analyte-induced irreversible chemical reactions. They exhibit high selectivity, sensitivity, and rapid response. Significant advances have been achieved in the design of chemodosimeters, and many fluorophores have been successfully used as the basis of luminescent chemodosimeters. In addition to the well-known rhodamine compounds, other fluorophores, such as fluorescein, cyanine, coumarin, thiadiazole, 1,8-naphthalimide, pyrene, porphyrin, BODIPY, squaraine, and metal complexes, have also been widely used for detection based on a variety of mechanisms including PET, ICT, ESIPT, and FRET. The most reported luminescent chemodosimeters have been based on fluorescence turn-on, or emission wavelength shifts, which makes them ideal for application in bioimaging. In this review, we have presented the general design principles of luminescent chemodosimeters for bioimaging and summarized recent advances in the detection of metal cations, anions, thiols, reactive oxygen species, reactive nitrogen species, reactive sulfur species, DCP, and amino acids in vitro and in vivo, developed by us and other groups.

On the basis of the advantages and disadvantages of the present luminescent chemodosimeters used for bioimaging, several future directions in this field should be followed to

develop better luminescent chemodosimeters and to exploit their further application:

- (i) Although there are a few principles used in the design of luminescent chemodosimeters, such as analyte-induced rhodamine spirolactam ring-opening, effective and general principles remain few. Hence, exploiting new design principles and sensing systems with excellent optical and biological properties should be the first research direction in the field of luminescent chemodosimeters.
- (ii) For real applications of luminescent chemodosimeters, especially in bioimaging, water solubility is essential. Although most reported chemodosimeters can function well in organic solvents, their water solubility is often poor, which limits their application to real systems. Hence, the development of water-soluble luminescent chemodosimeters with good sensing performances in vitro and in vivo is another important research direction.
- (iii) The long lifetime of phosphorescence can eliminate interference from short-lived background fluorescence by using time-resolved luminescence technology, leading to improved signal-to-noise ratios. Hence, the design and synthesis of phosphorescent chemodosimeters based on heavy-metal complexes for application in time-resolved luminescence bioimaging will be a very important research topic.
- (iv) The optimal excitation and emission wavelengths of a bioimaging material are in the deep red or near-infrared range (650–950 nm) because of the combined virtues of good tissue penetration and low autofluorescence. Hence, NIR luminescent chemodosimeters should be exploited.
- (v) Two-photon fluorescence microscopy and upconversion luminescence microscopy employ near-infrared photons of lower energy as the excitation source. This has the advantage of increased penetration depth (>500 μm), and prolonged observation time, thereby allowing tissue imaging. In particular, the exploitation of upconversion luminescent chemodosimeters with high responsive ratio and their application to upconversion luminescence bioimaging will generate significant interest.
- (vi) Besides molecular design, it is also important to understand better the cellular uptake behavior of luminescent chemodosimeters for bioimaging application.

In summary, luminescent chemodosimeters have become a very attractive sensing system, especially for intracellular detection. It can be anticipated that ongoing research in the area in years to come will lead to further improvements in the luminescent chemodosimeters available for bioimaging.

13. APPENDIX I: SUMMARY OF PHYSICOCHEMICAL PROPERTIES OF LUMINESCENT CHEMOSIMETERS FOR BIOIMAGING

Table A1 shows a summary of physicochemical properties of luminescent chemodosimeters for bioimaging.

Table A1

dye	analyte	physicochemical properties for solution detection						physicochemical properties for biotiming		
		$\lambda_{\text{abs}}^{\text{B}} \rightarrow \lambda_{\text{abs}}^{\text{A}}$ /nm	$\lambda_{\text{em}}^{\text{B}} \rightarrow \lambda_{\text{em}}^{\text{A}}$ /nm	$\varphi^{\text{B}} \rightarrow \varphi^{\text{A}}$ or φ ratio	limit	media	$\lambda_{\text{em}}^{\text{B}}/\text{nm}$ ($\lambda_{\text{ex}}/\text{nm}$)	media	biosamples	ref
6	Hg ²⁺	430→350	548→496	0.35→0.48	0.37 μM	H ₂ O	CH ₃ CN-H ₂ O (1:9, v/v)	505→550 (405, 800)	YPD plate	77
15	Hg ²⁺	668→830	780→830	↓		CH ₃ OH-H ₂ O (4:1, v/v)			H ₂ O	87
23	Hg ²⁺	664→840	780→830	↓		CH ₃ OH-H ₂ O (4:1, v/v)			PBS	SW1116
24	Hg ²⁺	670→830	780→830	↓		CH ₃ OH-H ₂ O (4:1, v/v)			PBS	SW1116
25	Hg ²⁺	390→390	458→	20-fold ↓	<2 μM	H ₂ O-CH ₃ OH (99: 1, v/v)	420→520 (760)		PBS	SW1116
26e	Hg ²⁺	→560	→580	105-fold ↑		C ₂ H ₅ OH-HEPES (1:1, v/v, pH 7.2)	570→625 (515)	C ₂ H ₅ OH-PBS (1:49, v/v)	H9C2(2-)	95
47	Hg ²⁺	→561	→585	100-fold ↑		CH ₃ CN-HEPES (1:2, v/v, pH 7.2)	560→620 (543)	CH ₃ CN-PBS (1:49, v/v)	Caov-3	115
48	Hg ²⁺	→535	→545	23-fold ↑	0.487 μM	CH ₃ CN-HEPES (1:1, v/v, pH 7.0)	480→640 (780)	DMEM	HeLa	116
51	Hg ²⁺	→563	→586	1200-fold ↑	1.14 ppb	CH ₃ CN-H ₂ O (19:1, v/v, pH 7.2)			HeLa	118
52	Hg ²⁺	→562	→575	300-fold ↑	2 ppb	CH ₃ OH	560→600 (546)	DMEM-DMSO (9:1, v/v)	HeLa	119
53	Hg ²⁺	→560	→580	→0.51↑		C ₂ H ₅ OH-H ₂ O (1:4, v/v)	550 (514)	PBS	HeK 293	120
54	Hg ²⁺		→545	200-fold ↑		CH ₃ CN-HEPES (1:99, v/v, pH 7.4)		NGM	C. elegans	121
57	Hg ²⁺	→567	→593	442-fold ↑	1.72 nM	HEPES-C ₂ H ₅ OH (1:1, v/v, pH 7.0)			MCF-7	123
61	Hg ²⁺	→563	→591	383-fold ↑		HEPES-C ₂ H ₅ OH (1:1, v/v)	560→610 (515)	DMEM	A549	126
62	Hg ²⁺	→537	→564	120-fold ↑	0.1 μM	(NaAc-HAc)-DMF (1/1, v/v, pH 7.0)		DMEM	RSC ²⁶	127
63	Hg ²⁺								HeLa	128
64	Hg ²⁺	→535	553→557	26-fold ↑	0.1 μM	H ₂ O-CH ₃ OH (4:1, v/v)	557 (500)	DMEM	C2C12, PC 12, human muscle precursor cells, zebrafish	130
66	Hg ²⁺	→560	→580	50-fold ↑		C ₂ H ₅ OH-H ₂ O (4:1,v/v)		DMEM	HK-2	133
67	Hg ²⁺	→534	→566	140-fold ↑	39 nM	PBS-DMF (4:1,v/v)		DMEM	Tca-8113	134
68	Hg ²⁺	→554	→580	370-fold ↑	0.91 ppb	C ₂ H ₅ OH-H ₂ O (1:1, v/v)	(510→570)	PBS	HeLa	135
78	Hg ²⁺	438→398	560→520			CH ₃ CN	500→530, 560→580 (405)	PBS	KB	147
84	Hg ²⁺	500→562	510→584	↑	ppm level	C ₂ H ₅ OH-H ₂ O (4:1, v/v)	500→530, 565→615 (488)	PBS	HeLa, MCF-7	158
85	Hg ²⁺	500→557	510→584	↑	ppb level	CH ₃ CN-H ₂ O (4:1, v/v)	500→530, 565→615 (488)	PBS	HeLa, MCF-7	158
86	Hg ²⁺	485→557	518→586	0.39→0.07	10 nM	HEPES		RPMI 1640	HeLa L929	159
87	Hg ²⁺	541→485	541→541	~2-fold ↑	1.95 ppb	H ₂ O	520→560 (980)	DMEM	HeLa	173
89	Hg ²⁺		→520	↑	<1 ppb	PBS-DMSO (19:1, v/v, pH 7.4)		DMEM	AS49, zebrafish	177
90	Hg ²⁺	→560	→580	↑	20 nM	HEPES-CH ₃ CN (99:1, v/v, pH 7.4)	590 (510→560)	RPMI 1640-FBS-DMSO	HeLa	178
95	Cu ²⁺	→529	→550	80-fold ↑	0.3 μM	Tris-HCl-C ₂ H ₅ OH (4:1, v/v)	(500)	PBS	HeLa	188
98	Cu ²⁺	→556	→572	0.07→0.45		HEPES-CH ₃ CN (199:1, v/v, pH 7.4)		DMEM	P19, zebrafish	190

Table A1. continued

dye	analyte	physicochemical properties for solution detection						physicochemical properties for biotiming		
		$\lambda_{\text{abs}}^{\text{B}} \rightarrow \lambda_{\text{abs}}^{\text{A}}$ /nm	$\lambda_{\text{em}}^{\text{B}} \rightarrow \lambda_{\text{abs}}^{\text{A}}$ /nm	$\phi^{\text{B}} \rightarrow \phi^{\text{A}}$ or ϕ ratio	limit	media	$\lambda_{\text{em}}^{\text{B}}/\text{nm}$ ($\lambda_{\text{ex}}^{\text{B}}$)	media	biosamples	ref
105	Cu ²⁺	→528	→545	22-fold ↑	<2 ppb	HEPES-CH ₃ CN (1:1, v/v, pH 7.0)	570–625 (515)	DMSO-PBS (1:49, v/v)	SPC-A-1	197
106	Cu ²⁺	→531	→550	↑	CH ₃ CN-H ₂ O (1:1, v/v)	570–625 (515)	DMF-PBS (1:49, v/v)	EJ	198	
107	Cu ²⁺	→558	→582	400-fold ↑	CH ₃ CN-H ₂ O (1:1, v/v)	DMEM	HeLa	199		
108	Cu ²⁺	→556	→585	↑	CH ₃ CN-H ₂ O (1:1, v/v)	DMEM	E. coli	200		
109	Cu ²⁺	→554	→580	40-fold ↑	CH ₃ CN-HEPES (3:7, v/v, pH 7.2)	DMEM	HeLa	201		
110	Cu ²⁺	→556	→580	↑	C ₂ H ₅ OH-HEPES (1:9, v/v, pH 7.0)	(559)	PBS	HeLa	202	
123	Cu ²⁺	→556	→580	100-fold†	7.0 nM	H ₂ O-CH ₃ OH (1:4, v/v, pH 7.0)	570–670 (559)	PBS	HeLa	215
124	Cu ²⁺	→556	508→586	27-fold†	20 nM	CH ₃ CN-HEPES (4:1, v/v)	500–540, 550–590 (488)	RPMI 1640	PC3	216
125	Cu ²⁺	→555	→580	470-fold †	10 ppb	CH ₃ CN-HEPES (3:7, v/v, pH 7.2)	550–650 (543, 880)	DMEM	HeLa	217
126	Cu ²⁺	→529	→554	180-fold †	<3 ppb	Tris-HCl-CH ₃ CN (1:1, v/ v)	570–625 (488)	DMEM	EJ	218
127	Cu ²⁺	→552	→580	105-fold†	2 μM	CH ₃ CN-HEPES	560–620 (543)	RPMI 1640	KB	219
128	Cu ²⁺	→492	→516	350-fold †	0.19 μM	HEPES-CH ₃ CN (4:1, v/v)	590–650 (528–553)	HEPES-CH ₃ CN (9:7, 3, v/v) DMEM	HeLa	220
132	Cu ²⁺	→558	→580	100-fold †	0.261 μM	HEPES-CH ₃ CN (3:2, v/v, pH 7.4)	590–650 (528–553)	HEPES-CH ₃ CN (9:7, 3, v/v) DMEM	nasopharyngeal carcinoma	224
142	Fe ³⁺	→561	→583	112-fold †	CH ₃ CN-HEPES (1:19, v/v, pH 7.0)	PBS	PIEC	PBS	PIEC	235
143	Fe ³⁺		→582	↑	CH ₃ CN-H ₂ O (1:4, v/v)	500–550 (488, 570– 620 (561))	PBS-DMSO (199:1, v/v)	HeLa	236	
145	Fe ³⁺	→563	→575	↑	CH ₃ CN-H ₂ O (1:1, v/v)	CH ₃ CN-H ₂ O (1:1, v/v)	E. coli	238		
149	Fe ³⁺	400→526	→551	↑	H ₂ O-CH ₃ CN (19: 1, v/v)	>560 (543)	DMEM	Hep G2	242	
156	Cr ³⁺	→565	→587	15-fold †	C ₂ H ₅ OH-H ₂ O (1:1, v/v, pH 7.4)	570–625 (543)	C ₂ H ₅ OH-PBS (1:99, v/v)	HeLa	249	
157	Cr ³⁺	380→568	544→592	15-fold †	C ₂ H ₅ OH-H ₂ O (2:1, v/v)	510–550, 570–650 (405)	PBS	HeLa	250	
159	Zn ²⁺	→569	→595	220-fold †	PIPES (pH 7.0)	DMEM	HeLa	257		
160	Zn ²⁺	371→430	→508	13-fold †	Tris-HCl (pH 7.2)	500–550 (405)	Trits-HCl, DMEM	yeast, HeLa	258	
161	Zn ²⁺	378→428	→505	15-fold †	C ₂ H ₅ OH	PBS	MCF-7	259		
166	Au ³⁺	→562	→579	250-fold †	63 ppb	PBS	HeCaT	269		
167	Au ³⁺	→524	→545	↑	50 nM	PBS (pH 7.4)	HeLa	271		
168	Au ³⁺		→556	100-fold †	48 nM	MEM	HeLa	268		
169	Au ³⁺		→549	233-fold †	290 nM	PBS-DMF (997:3, v/v)	Hela	272		
172	Ag ⁺	→560	→580	10-fold †	52 nM	HEPES	zebrafish	276		
174	Pd ²⁺		→520	→0.89	30 nM	DMEM	zebrafish	280		
176	Pd ²⁺	364→453	480→553	10.3-fold †	70 nM	H ₂ O-CH ₃ CN (9:1, v/v) PBS (pH 7.4)	E3 embryo	RAW 264.7	282	
190	F ⁻		→461	>4-fold †		PBS	PBS	RPMI 1640	A549	318

Table A1. continued

dye	analyte	physicochemical properties for solution detection						physicochemical properties for biotiming		
		$\lambda_{\text{abs}}^{\text{B}} \rightarrow \lambda_{\text{abs}}^{\text{A}}$ /nm	$\lambda_{\text{em}}^{\text{B}} \rightarrow \lambda_{\text{abs}}^{\text{A}}$ /nm	$\varphi^{\text{B}} \rightarrow \varphi^{\text{A}}$ or φ ratio	limit	media	$\lambda_{\text{em}}^{\text{B}}/\text{nm}$ ($\lambda_{\text{ex}}^{\text{B}}$)/nm	media	biosamples	ref
191	F ⁻	407→517	500→558	↑	80 μM	C ₂ H ₅ OH–PBS (3:7, v/v, pH 7.4)	470→510, 540→580 (405)	DMEM	RAW 264.7	319
216	CN ⁻	505→	540→540	↑	0.18 μM	DMF/H ₂ O (9:1, v/v)	515→560, 635→680 (980)	DMEM	HeLa	352
221	CN ⁻		→520	>200-fold†		CH ₃ CN–HEPES (9:1, v/v, pH 7.4)	505→530 (488)	PBS	HaCaT	358
237	CN ⁻	521→464	→514	0.02→0.65		PBS–DMSO (99:1, v/v, pH 7.4)	>505 (488)	PBS	Hep G2	368
240	H ₂ O ₂		→524	↑	100 nM	HEPES (pH 7)	505→580 (488)	PBS	HEK	379, 380
241	H ₂ O ₂		→584	>1000-fold †	100 nM	HEPES (pH 7)	548→644 (543)	PBS	HEK	380
242	H ₂ O ₂	→350	400→450	52-fold †	100 nM	HEPES (pH 7)	420→500 (704)	PBS	HEK	380
245	H ₂ O ₂	→460	→510	10-fold †		HEPES (pH 7)	495→559 (488)	DMEM	HEK293 A431	384
246	H ₂ O ₂	→480	→584	40-fold †		HEPES (pH 7)	548→644 (543)	DMEM	HEK293	384
247	H ₂ O ₂	→475	→511	→0.27		HEPES (pH 7)	495→581 (488)	DMEM	RAW264.7	385
248	H ₂ O ₂	454→492	521→515	0.1→0.94		HEPES (pH 7)	495→581 (488)	DMEM	A431, RAW264.7	385
250	H ₂ O ₂	494→519	558→548	0.01→0.12		HEPES (pH 7)	516→581 (514)	DMEM	A431, RAW264.7	385
251	H ₂ O ₂	507→540	574→565	0.07→0.46		HEPES (pH 7)	548→613 (543)	DMEM	A431, RAW264.7	385
252	H ₂ O ₂	490→505	→530	0.117→0.626		HEPES (pH 7.0)	522→554 (514)	DPBS	HEK293, HeLa	386
255	H ₂ O ₂	465→495	515→513	0.10→0.12		HEPES (pH 7.0)	500→550 (488)	DMEM	HEK 293T	389
256	H ₂ O ₂	465→495	515→513	0.09→>0.87		HEPES (pH 7.0)	500→550 (488)	DMEM	HEK 293T	389
257	H ₂ O ₂	489,	540→528	0.019→0.405		HEPES (pH 7)	527→601 (510)	DPBS	HeLa	390
258	H ₂ O ₂	510→510				CH ₃ CN–PBS (1:4, v/v, pH 7.4)	(405, 540)		HeLa, RAW 264.7	391
260	H ₂ O ₂	400→550	460→586	↑		HEPES (pH 7.4)	(405, 540)	DMEM	RAW 264.7	393
261	H ₂ O ₂	375→435	475→540	0.38→0.11		HEPES (pH 7.1)	430→495, 535→600 (820)	DMEM	RAW 264.7	393
262	H ₂ O ₂	321→338	453→500	0.7→0.4		HEPES (pH 7.4)	390→465, 500→550 (750)	DPBS	RAW 264.7	394
263	H ₂ O ₂	→590	→720	↑	0.006→0.051	HEPES (pH 7.4)	(280)	DMEM	RAW 264.7	388
264	H ₂ O ₂		→602	1.5-fold†	46.0 ppm	PBS (pH 7.4)	>635 (595)	PBS	mice	395
267	H ₂ O ₂	→491	→662	15.5-fold†	81.5 pM	HEPES (pH 7.4)	505→555 (485 ± 20)	MBM	IM C-238	396
269	H ₂ O ₂	→493	→520	1.1-fold†	26 nM	HEPES (pH 7.4)	>550 (633)	HEPES	PM	397
270	H ₂ O ₂	495→490	→519	10.7-fold†	8.9 nM	HEPES (pH 7.4)	505→550 (488)	DMSO–HEPES	PM	398
271	H ₂ O ₂	402→418	→542	15.0-fold†	PBS (pH 7.4)	PBS (pH 7.4)	505→540 (495)	DPBS	Tobacco leaf epidermal tissues	398
277	H ₂ O ₂	→360	→441	39-fold†	3.7 nM	Tris–HCl (pH 7.4)	545	Tris–KCl (pH 7.2)	RAW 264.7, A431	400
279	ClO ⁻		→541	1079-fold†	0.3 μM	PBS–THF (1:1, v/v, pH 7.4)	(330–385)	DMEM–THF (19:1, v/v)	HeLa	404
281	ClO ⁻		→541	0.01→0.65		PBS (pH 7.5)		DPBS	RAW264.7	408
283	ClO ⁻		→530			HEPES–DMSO (9:1, v/v, pH 7.05)		PBS	HeLa	410
285	ClO ⁻	540→464	585→505	0.02→0.59	0.2 μM	PBS–DMF (4:1, v/v, pH 7.4)	560 (543)	MEM	MCF-7	415
286	ClO ⁻	→555	→575	~0→0.34		PBS		DMEM	neutrophil	416

Table A1. continued

dye	analyte	physicochemical properties for solution detection						physicochemical properties for biomimaging		
		$\lambda_{\text{abs}}^{\text{B}} \rightarrow \lambda_{\text{abs}}^{\text{A}}$ /nm	$\lambda_{\text{em}}^{\text{B}} \rightarrow \lambda_{\text{em}}^{\text{A}}$ /nm	$\varphi^{\text{B}} \rightarrow \varphi^{\text{A}}$ or φ ratio	limit	media	$\lambda_{\text{em}}^{\text{B}}/\text{nm}$ ($\lambda_{\text{ex}}^{\text{B}}$)/nm	media	biosamples	ref
287	ClO^-	$\rightarrow 652$	$\rightarrow 670$	$\sim 0 \rightarrow 0.31$		PBS–DMF (99:1, v/v, pH 7.4)	>660 (633)	KRP	neutrophil	417
288	ClO^-	$\rightarrow 750$	$\rightarrow 546$	\uparrow	25 nM	PBS–DMF (99:1, v/v, pH 7.4)	670–750 (590–650) (546)	saline RPMI 1640	C57BL/6 mice A549, zebrafish	417 418
289	ClO^-	$\rightarrow 561$	$\rightarrow 579$	$\sim 0 \rightarrow 0.24\uparrow$	0.3 μM	PBS–DMSO (99:1, v/v)	530–600 (514)	PBS–DMSO (99:1, v/v)	neutrophil, kidney sections of nude mouse	419
291	ClO^-		$\rightarrow 550$	\uparrow		PBS–DMF (99:1, v/v, pH 5.5)		neutrophil		420
295	ClO^-		$\rightarrow 574$	7.6-fold \uparrow	3.8 nM	PBS (pH 7.4)	>560 (543)	DMEM	HeLa	422
306	${}^1\text{O}_2$	$\rightarrow 294$	614→614	15.3-fold \uparrow	7.9 nM	borate buffer (pH 9.1) Tris–HCl (pH 7.4)	>520 (450–490) 700–800 (633)	saline DMEM	HeLa RAW264.7	431 435
310	${}^1\text{O}_2$		$\rightarrow 794$	\uparrow		DMSO	(405, 514)	supplemented L15	oligodendrocyte	440
312	$\text{O}_2^{\bullet-}$	$\rightarrow 396$	$\rightarrow 579$	20-fold \uparrow	1.68 nM	HEPES (pH 7.4)	(488)	DMEM	RAW264.7	443
315	$\text{O}_2^{\bullet-}$		$\rightarrow 559$	\uparrow		PBS (pH 7.4)	550–580 (543)	HEPES	RASM	444
317	$\text{O}_2^{\bullet-}$		$\rightarrow 560$	11.8-fold \uparrow		PBS (pH 7.4)	790 (700)	HEPES	C57Bl/6 mice	444
319	$\text{O}_2^{\bullet-}$		$\rightarrow 760$	104-fold \uparrow		PBS (pH 7.4)	450–480 (515)	RPMI 1640	Jurkat T	447
324	$\text{O}_2^{\bullet-}$		$\rightarrow 544$	\uparrow	0.1 pmol/well	HEPES (pH 7.4)				
325	$\text{O}_2^{\bullet-}$		$\rightarrow 530$	\uparrow	4.6 pM	PBS (pH 7.4)	505–550 (488)	RPMI 1640	peritoneal macrophages	448
326	$\text{O}_2^{\bullet-}$		$\rightarrow 662$	\uparrow	0.1 nM	PBS (pH 7.4)	>550 (633)	DMEM	RAW264.7	449
330	$\bullet\text{OH}$	$\rightarrow 560$	$\rightarrow 601$	$0.03 \rightarrow 0.2$	18 pM	HEPES (pH 7.4)	(532)	PBS	RAW264.7, HL-7702, Hep G2.	453
331	$\bullet\text{OH}$	$\rightarrow 560$	$\rightarrow 588$	\uparrow		0.1% DMSO (pH 4)			ARPE-19, Hep G2, SW-620	454
332	$\bullet\text{OH}$	$\rightarrow 560$	$\rightarrow 585$	\uparrow		0.1% DMSO (pH 4)			ARPE-19, Hep G2, SW-620	454
333	$\bullet\text{OH}$	$\rightarrow 550$	$\rightarrow 590$	\uparrow		0.1% DMSO (pH 4)			ARPE-19, Hep G2, SW-620	454
335	$\bullet\text{OH}$	$\rightarrow 490$	$\rightarrow 517$	\uparrow	2.4 nM	PBS (pH 7.4)	(488)	PBS (pH 7.4)	Hep G2	456
339	O_3		$\rightarrow 531$	\uparrow	<50 nM	CH_3OH –PBS (1:19, v/v, pH 7)	523 (497)	RPMI 1640	BECs	461
340	O_3			\uparrow		PBS–DMSO	523 (497)	RPMI 1640	BECs	461
341	ROS			\uparrow			535 (470)	MEM	LS174T, Hep G2	463
342	hypoxia	324→361	$\rightarrow 526$	\uparrow		CH_3OH	(359, 410)	MEM	V79	466
343	hypoxia	→437		\uparrow		CH_3OH	(359, 410)	MEM	V79	466
344	hypoxia	→324		\uparrow		CH_3OH	(359, 410)	MEM	V79	466
346	hypoxia	412→	500→	\rightarrow		CH_3OH	(359, 410)	MEM	V79	467
347	hypoxia	421→	→550	\rightarrow		CH_3OH	(359, 410)	MEM	V79	467
349	hypoxia	370→435	475→550	\uparrow		PBS–DMSO (99:1, v/v, pH 7.0)	430–495, 540–580	Ham–DMSO (199:1, v/v)	A549	468
350	hypoxia	→595		\uparrow		PBS	670–720 (650)	DMEM–DMSO (99:1, v/v)	MCF-7	469
351	hypoxia	→606		\uparrow		PBS	690–740 (670)	DMEM–DMSO (99:1, v/v)	MCF-7	469
352	hypoxia	→623		\uparrow		PBS	710–760 (670)	DMEM–DMSO (99:1, v/v)	MCF-7	469
354	NO	505→506	$\rightarrow 528$	0.003→0.53		PBS	>515 (490)	DMEM	smooth muscle cells	480
355	NO	501→505	$\rightarrow 530$	0.002→0.75	3 nM	PBS	515 (500)	PBS	smooth muscle cells	481
356	NO	543→554	$\rightarrow 572$	0.0005→0.42	7 nM	PBS (pH 7.4)	>580 (520–550)	DMEM–DMSO (499:1, v/v)	bovine aortic endothelial cells	482
360	NO		$\rightarrow 479$	\uparrow	nM level			HEPES (pH 7.4)	RAW 264.7	485

Table A1. continued

dye	analyte	physicochemical properties for solution detection						physicochemical properties for biotimaging			
		$\lambda_{\text{abs}}^{\text{B}} \rightarrow \lambda_{\text{abs}}^{\text{A}}$ /nm	$\lambda_{\text{em}}^{\text{B}} \rightarrow \lambda_{\text{abs}}^{\text{A}}$ /nm	$\phi^{\text{B}} \rightarrow \phi^{\text{A}}$ or ϕ ratio	limit	media	$\lambda_{\text{em}}^{\text{B}}/\text{nm}$ ($\lambda_{\text{ex}}^{\text{B}}$)	media	biosamples	ref	
361	NO	450→500	580→	↓		DMSO-THF	(543, 488)		RAW 264.7	487	
362	NO	→760	→790	14-fold ↑		PBS		Krebs-Henseleit	rat kidney	488	
363	NO	→760	→790	14-fold ↑		PBS		Krebs-Henseleit	rat kidney	488	
364	NO	455→	610→616	16.9-fold ↑	0.27 μM	borate buffer (pH 7.4)	>520 (450–490)	isotonic saline	mouse macrophage	489	
365	NO	352→450	→550	1500-fold ↑	~30 nM	PBS-DMSO (4:1, v/v)	>520 (450–490)	PBS	PC12	490	
367	NO	→560	→580	↑	38 nM	$\text{C}_2\text{H}_5\text{OH}$ -HEPES (20:80, v/v)		PBS	HeLa	492	
380	NO	499→504	→520	16-fold ↑	5 nM	PIPES-KCl (pH 7.0)		DMEM	RAW264.7	500	
384	NO	→506	520→527	0.028→0.37		PIPES-KCl		DMEM	RAW264.7	504	
385	NO	→504	520→526	0.0337→0.22		PIPES-KCl		DMEM	RAW264.7	504	
386	NO	→496	53.8→548	0.021→0.22		PIPES-KCl	>550 (500–530)		RAW264.7	503	
387	NO	→505	542→548	0.0034→0.14		PIPES-KCl	>550 (500–530)		RAW264.7	503	
388	NO	→496	53.8→549	0.0092→0.24		PIPES-KCl	>550 (500–530)		RAW264.7	503	
389	NO	→501	→549	0.006→0.13	1 nM	PIPES-KCl	>550 (500–530)		RAW264.7	503	
390	NO	→560	→590	0→0.13		PBS		PBS	MCF-7	505	
391	HNO	→518	→526	4.3-fold †		PIPES-KCl (pH 7)		PBS	HeLa	507	
393	ONO [−]	→521	8-fold ↑			PBS (pH 7.3)		DMEM	neuronal	510	
394	ONO [−]	→539	21-fold ↑			PBS (pH 7.4)	585–650 (543)	DMEM	J774.1	511	
395	ONO [−]	→535	140-fold ↑			PBS (pH 7.4)	530–580 (488)	DMEM	RAW 264.7	512	
396	ONO [−]	758→758	800→775	0.05→0.12 (23.3-fold †)		PBS (pH 7.4)	(633)	PBS	RAW264.7	513	
397	ONO [−]	810→	↓		50 nM	PBS (pH 7.4)	700–800 (635)	DMEM	RAW 264.7	515	
399	ONO [−]	485→398	553→466	0→0.687		PBS/1% DMF (pH 7.4)	(470–490)	DMEM	HeLa	516	
409	R-SH	485→398	630-fold ↑	630-fold ↑	37 μM	DMSO-HEPES (4:1, v/v, pH 7.4)	410–460, 490–540 (405)	DMEM	HeLa	527	
411	R-SH	434→404	→480	22-fold ↑	0.18 mM	DMF-HEPES (3:1, v/v, pH 7.4)	>450 (380)	RPMI 1640	HeLa	529	
413	R-SH	→400	→465	470-fold †	0.5 nM	Tris-HCl (pH 7.4)		PBS	HEK293	531	
417	R-SH	454→500	→520	61-fold †	50 nM	HEPES-CH ₃ CN (99:1, pH 7.4)		DMEM	P19	535	
420	R-SH	325→550	500→570	0.03→0.69		PBS-C ₂ H ₅ OH (99:1, v/v, pH 7.3)		DMSO-PBS (1:1000, v/v)	COS-7	538	
422	R-SH	405→420	→534	180-fold ↑	50 nM	C ₂ H ₅ OH-PBS (2:3, v/v, pH 7.4)		DMEM	HeLa	540	
424	R-SH	405→563	560→623	120-fold †	1.8 nM	glycerol-CH ₃ OH (9:1, v/v, pH 7.0)		DMSO-PBS (1:100, v/v)	3T3	542	
426	R-SH	→494	165-fold †		28 μM	PBS-DMF (11:9, v/v, pH 7.0)		DMEM	HeLa	544	
428	R-SH	485→533	11.4-fold †			$\text{C}_2\text{H}_5\text{OH}$ -PBS (1:9, v/v)	415–485, 485–545 (408)	DMEM	HeLa	546	
429	R-SH	338→383	462→545	0.82→0.12		MOPS (pH 7.4)	425–475, 525–575 (740)	MEM	HeLa	547	
430	R-SH	293→370	448→427	0.002→0.21	↑	MOPS (pH 7.4)	500–620 (780)	DMEM	HeLa	548	
431	R-SH	367→428	473→540			PBS (pH 7.4)	530–600 (458)	PBS	Hep G2, C2C12 HaCaT, N2a	549	

Table A1. continued

physicochemical properties for solution detection										physicochemical properties for biomonitoring		
dye	analyte	$\lambda_{\text{abs}}^{\text{A}} \rightarrow \lambda_{\text{abs}}^{\text{B}}$ /nm	$\lambda_{\text{em}}^{\text{B}} \rightarrow \lambda_{\text{abs}}^{\text{A}}$ /nm	$\phi^{\text{B}} \rightarrow \phi^{\text{A}}$ or φ ratio	limit	media	$\lambda_{\text{em}}^{\text{B}}/\text{nm}$ ($\lambda_{\text{ex}}^{\text{B}}$)/nm	media	biosamples	ref		
432	R-SH	→525	470→541	↑	1.4 nM	PBS (pH 7.4)	530–600 (458)	PBS	Hep G2, C2C12 HaCaT, N2a	549		
433	R-SH	→525	→550	170-fold ↑	144 pM	PBS (pH 7.4)	550 (525)	DMEM	Hep G2 HL-7702	550		
434	R-SH	→522	→522	275-fold ↑	82 nM	PBS-CH ₃ CN (11:9, v/v, pH 7.4)	505–525, 610–620 (488)	DMEM	Hep G2 HL-7702	551		
435	R-SH	562→	590→510	60-fold ↑	0.73 μM	PBS-C ₂ H ₅ OH (1:1, v/v, pH 7.4)		DMEM	HeLa	553		
436	R-SH	—	→459	60-fold ↑	0.73 μM	PBS-C ₂ H ₅ OH (1:1, v/v, pH 7.4)		DMEM	HeLa	554		
439	GST	493→492	→513	↑	0.68 μM	CH ₃ CN-HEPES (3:7, v/v, pH 7.4)	510–550 (480) (365)	RPMI1640	HuCCT1	557		
443	Cys/Hcy	500→430	→560	5-fold ↑	0.75 μM	PBS-CH ₃ CN (9:1,v/v, pH 7.4)		DMEM	osteoblasts	564		
444	Cys	470→408	557→487	115-fold ↑		DMSO-HEPES (9:1, v/v, pH 7.2)			MCF-7	565		
449	Cys/Hcy	430→390	547→586			HEPES (pH 7.2)	520–540, 560–580 (405)	RPMI1640	KB	568		
450	Cys/Hcy	428→	→565	↑		CH ₃ OH-HEPES (7:3, v/v, pH 7)	520–620 (405)	PBS	KB	569		
455	Cys/Hcy	430→580	→588	75-fold ↑		PBS-DMSO (9:1, v/v, pH 7.4)	555–655 (543, 880)	DMSO-PBS (1:49, v/v)	ACCM, PANC, Caov-3	573		
456	Cys/Hcy	488→426	→502	107-fold ↑	30 nM		>560 (488)	PBS				
457	Cys/Hcy	483→400	→480	6-fold ↑		CH ₃ CN-HEPES (1:1, v/v, pH 7.4)		1 × SPP	Tetrahymena thermophila	575		
459	H ₂ S	→490	→525	7-fold ↑	10 μM	HEPES	500–650 (488)	DMEM	HEK293T	582		
460	H ₂ S	→492	→525	9-fold ↑	10 μM	PBS-CH ₃ CN (pH 7.4)	500–650 (488)	DMEM	HEK293T	582		
462	HS ⁻ /H ₂ S	→515	0.003→0.392	50-fold ↑		HEPES (pH 7.4)	500–550 (450–490)	DMEM	COS-7	584		
465	H ₂ S/S ²⁻	→516	428→391	10-fold ↑		PBS (pH 7.4)	515–550 (470–490)	DMEM	HeLa	587		
467	H ₂ S/S ²⁻	→510	13-fold ↑			PBS (pH 7.0)	400–480 (376–398)	DMEM	HeLa	589		
468	H ₂ S/S ²⁻	387→	→512	>300-fold ↑		PBS-DMSO (99:1, v/v, pH 7.4)	495–555 (465–505)	DMSO	HeLa, FLS, KB, MSC	589		
492	His					PBS-DMSO (99:1, v/v, pH 7.4)	500–540 (488)	PBS-DMSO (99:1, v/v, pH 7.4)	HeLa, FLS, KB, MSC	613		
494	His					PBS-DMSO (99:1, v/v, pH 7.4)	500–540 (488)	PBS-DMSO (99:1, v/v, pH 7.4)	HeLa, FLS, KB, MSC	613		
259												

^a $\lambda_{\text{abs}}^{\text{A}}$ is the maximum absorption wavelength of the chemodosimeter in the absence of the analyte. $\lambda_{\text{abs}}^{\text{B}}$ is the maximum absorption wavelength of the chemodosimeter in the presence of the analyte. $\lambda_{\text{em}}^{\text{A}}$ is the maximum emission wavelength of the chemodosimeter in the absence of the analyte. $\lambda_{\text{em}}^{\text{B}}$ is the maximum emission wavelength of the chemodosimeter in the presence of the analyte. φ^{A} is the emission quantum yield of the chemodosimeter in the absence of the analyte. φ^{B} is the emission quantum yield of the chemodosimeter in the presence of the analyte. φ ratio is the change ratio of the emission intensity of the chemodosimeter upon addition of the analyte. Limit is the detection limit of the chemodosimeter for detecting the analyte. λ_{em} (λ_{ex}) is the excitation wavelength and emission collection channel for biomonitoring.

ASSOCIATED CONTENT**S Supporting Information**

Summaries of physiochemical properties of luminescent chemodosimeters. This information is available free of charge via the Internet at <http://pubs.acs.org/>.

AUTHOR INFORMATION**Corresponding Author**

*Fax: 86-21-55664621. Tel.: 86-21-55664185. E-mail: fyli@fudan.edu.cn.

Author Contributions

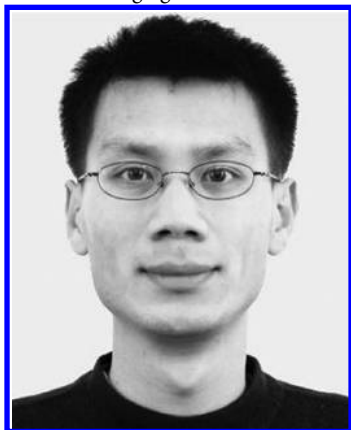
[§]These authors contributed equally to this work.

Notes

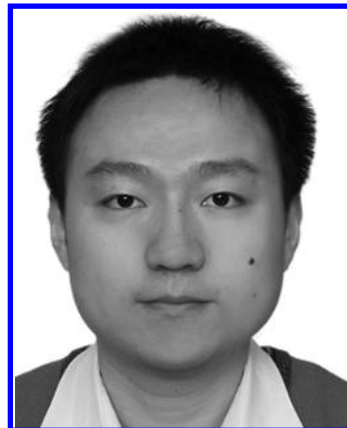
The authors declare no competing financial interest.

Biographies

Yuming Yang was born in 1981 in Changchun, China. In 2009, she received her Ph.D. degree in inorganic chemistry from Jilin University, and went to Fudan University as postdoctoral fellow in the group of Professor Fuyou Li. Her main task involved the development of fluorescent probes for bioimaging.



Prof. Qiang Zhao received his Ph.D. degree in inorganic chemistry from Fudan University in 2007 under the direction of Professor Chunhui Huang and Professor Fuyou Li. He then became a postdoctoral fellow in the group of Professor Shigehiro Yamaguchi at Nagoya University of Japan. He joined the Institute of Advanced Materials, Nanjing University of Posts & Telecommunications, in 2008. He was promoted as a full professor in 2010. His research interests focus on the fluorescent and phosphorescent probes for sensing and bioimaging.



Wei Feng received his B.S. degree in 2004 and Ph.D. degree in 2009, both in chemistry from Peking University. He subsequently worked as a postdoctoral on the synthesis and applications of upconversion nanomaterials with Prof. Chun-Hua Yan in Peking University for two years. He is currently a lecturer in the Department of Chemistry at Fudan University. His research interests lie in design and synthesis of luminescent nanomaterials with focus on their biological applications.



Fuyou Li was born in Zhejiang, China, in 1973. He received his Ph.D. degree (2000) from Beijing Normal University. He worked as a postdoctoral researcher at Peking University from 2000 to 2002. He worked as an associate professor at Peking University from 2002 to 2003 and Fudan University from 2003 to 2006. He has been working as a full professor at Fudan University since 2006. His current research interests involve fluorescent probes, phosphorescent metal complexes, and multifunctional rare-earth nanomaterials for sensing and bioimaging. To date, his research records 160 scientific publications.

ACKNOWLEDGMENTS

The authors thank NSFC (20825101, 21171098, and 91027004), the State Key Basic Research Program of China (2011AA03A407 and 2012CB932403), Shanghai Sci. Tech. Comm. (11XD1400200 and 1052 nm03400), IRT0911, B108, and the CAS/SAFEA International Partnership Program for Creative Research Teams for financial support.

DEDICATION

[¶]This review is dedicated to one of the most inspirational leaders in the field of fluorescent material, Prof. Chunhui Huang, on the occasion of her 80th birthday.

ABBREVIATIONS

1 × SPP medium	1% proteose peptone, 0.2% glucose, 0.1% yeast extract, 0.003% EDTA ferric sodium salt	J774.1	murine macrophage cell
3T3	albino Swiss mouse embryo fibroblast cells	KRP buffer	Krebs–Ringer–phosphate buffer
5-TAMRA	5-carboxytetramethyl rhodamine	LPA	lipoic acid
6-FAM	6-carboxyfluorescein	LRET	luminescence resonance energy transfer
A431	epidermoid carcinoma cell	LS174T	human Caucasian colon adenocarcinoma
A549	human lung cancer cell	LSUCLM	laser scanning upconversion luminescence microscopy
ACCM	metastatic adenoid cystic carcinoma cell	LUMO	lowest unoccupied molecular orbital
AIDS	acquired immune deficiency syndrome	MBM	modified Bristol medium
Au NP	gold nanoparticle	MC	metal-centered
BAECs	bovine aortic endothelial cells	MCF-7	human breast carcinoma cells
BECs	blood vessel endothelial cells	MLCT	metal-to-ligand charge transfer
BHQ3	black hole quencher	MLLCT	metal-to-ligand–ligand charge transfer
BMes ₂	dimesitylboryl group	MMLCT	metal–metal-to-ligand charge transfer
BODIPY	borondipyrromethene dyes	N2a	mouse neuroblastoma cell
<i>C. elegans</i>	<i>Caenorhabditis elegans</i>	NEM	<i>N</i> -ethylmaleimide
C2C12	mouse myoblast cell	NGM	nematode growth medium
Caov-3	ovarian carcinoma cells	NIR	near-infrared
CH ₃ HgX	methylmercury species	P19	murine embryonic carcinoma cells
COS-7	monkey renal fibroblast cell	PANC	pancreatic cancer cells
Cys	cysteine	PBS	phosphate-buffered saline
D-π-A	electron donor–π-conjugation bridge–electron acceptor	PC3	prostate cancer cells
DAC	1,8-bis(9-anthracylmethyl)	PC12	rat adrenal medulla pheochromocytoma cell
DAFs	diaminofluoresceins	PET	photoinduced electron transfer
DCP	diethyl chlorophosphate	PIEC	pig endothelial cell
DMEM	Dulbecco's modified Eagle's medium	PIPES	piperazine-1,4-bisethanesulfonic acid
DNS	dinitrobenzenesulfonyl	PM	peritoneal macrophages
Dobz	<i>p</i> -dihydroxyborylbenzyloxycarbonyl	RASM	rat aortic smooth muscle cell
DPA	9,10-diphenylanthracene	RNS	reactive nitrogen species
DPPP	diphenyl-1-pyrenylphosphine	ROONS	reactive oxygen and nitrogen species
Ds-im	dansylimidazole	RSC 96	reactive oxygen species
Ds-pip	dansyliptoprazine	RSS	rat schwann cells
E3	embryo media	SPC-A-1	reactive sulfur species
EG 277	ruglena gracilis 277 living cells	SubPc	lung cancer cells
EJ	lung cancer cells	SW1116	subphthalocyanine
ESIPT	excited-state intramolecular proton transfer	SW-620	human colon cancer cells
FITC	fluorescein isothiocyanate	TFA	human colonic adenocarcinoma cell
FLS	fibroblast-like synoviocyte cell	TPM	trifluoroacetyl group
FRET	Förster resonance energy transfer	TPP	two-photon fluorescence microscopy
GSH	glutathione	tren	triphenylphosphonium salt
GST	glutathione S-transferase	TTF	tris(2-aminoethyl)amine
H9C2(2-)	rat myocardial cells	UCL	tetrathiafulvalene
HaCat	human keratinocyte cell	UCNPs	upconversion luminescence
Ham	nutrient mixture	V79	upconversion nanophosphors
Hcy	homocysteine	WHO	Chinese hamster cells
HEK	human embryonic kidney cells	YPD plate	World Health Organization
HEK293	human embryonic kidney 293 cells		yeast extract peptone dextrose plate
HeLa	human cervical carcinoma cells		
HEPES	4-(2-hydroxyethyl)-1-piperazineethanesulfonic acid		
Hep G2	human liver carcinoma cell		
HL-7702	culture human normal liver cells		
HOMO	highest occupied molecular orbital		
H ^R DATI	dansylaminotroponimine		
hROS	highly reactive oxygen species		
HuCCT1	human cholangiocarcinoma cell		
IAM C-238	<i>Chlamydomonas reinhardtii</i>		
ICT	intramolecular charge transfer		
ILCT	intraligand charge transfer		

REFERENCES

- (1) Stephens, D. J.; Allan, V. J. *Science* **2003**, *300*, 82.
- (2) Zipfel, W. R.; Williams, R. M.; Webb, W. W. *Nat. Biotechnol.* **2003**, *21*, 1368.
- (3) Kobayashi, H.; Ogawa, M.; Alford, R.; Choyke, P. L.; Urano, Y. *Chem. Rev.* **2010**, *110*, 2620.
- (4) Yu, M. X.; Li, F. Y.; Chen, Z. G.; Hu, H.; Zhan, C.; Yang, H.; Huang, C. H. *Anal. Chem.* **2009**, *81*, 930.
- (5) Xiong, L. Q.; Chen, Z. G.; Tian, Q. W.; Cao, T. Y.; Xu, C. J.; Li, F. Y. *Anal. Chem.* **2009**, *81*, 8687.
- (6) Chalfie, M.; Tu, Y.; Euskirchen, G.; Ward, W. W.; Prasher, D. C. *Science* **1994**, *263*, 802.
- (7) Tsien, R. Y. *Annu. Rev. Biochem.* **1998**, *67*, 509.
- (8) Terai, T.; Nagano, T. *Curr. Opin. Chem. Biol.* **2008**, *12*, 515.
- (9) Kim, H. M.; Cho, B. R. *Acc. Chem. Res.* **2009**, *42*, 863.

- (10) Lu, X. Y.; Zhu, W. H.; Xie, Y. S.; Li, X.; Gao, Y. A.; Li, F. Y.; Tian, H. *Chem.—Eur. J.* **2010**, *16*, 8355.
- (11) Lu, H.; Xiong, L. Q.; Liu, H. Z.; Yu, M. X.; Shen, Z.; Li, F. Y.; You, X. Z. *Org. Biomol. Chem.* **2009**, *7*, 2554.
- (12) Zou, Y.; Yi, T.; Xiao, S. Z.; Li, F. Y.; Li, C. Y.; Gao, X.; Wu, J. C.; Yu, M. X.; Huang, C. H. *J. Am. Chem. Soc.* **2008**, *130*, 15750.
- (13) Montgomery, C. P.; Murray, B. S.; New, E. J.; Pal, R.; Parker, D. *Acc. Chem. Res.* **2009**, *42*, 925.
- (14) New, E. J.; Parker, D.; Smith, D. G.; Walton, J. W. *Curr. Opin. Chem. Biol.* **2010**, *14*, 238.
- (15) Fernandez-Moreira, V.; Thorp-Greenwood, F. L.; Coogan, M. P. *Chem. Commun.* **2010**, *46*, 186.
- (16) Lo, K. K. W.; Li, S. P. Y.; Zhang, K. Y. *New J. Chem.* **2011**, *35*, 265.
- (17) Bunzli, J. C. G. *Chem. Rev.* **2010**, *110*, 2729.
- (18) Zhao, Q.; Li, F. Y.; Huang, C. H. *Chem. Soc. Rev.* **2010**, *39*, 3007.
- (19) Zhao, Q.; Huang, C. H.; Li, F. Y. *Chem. Soc. Rev.* **2011**, *40*, 2508.
- (20) Yu, M. X.; Zhao, Q.; Shi, L. X.; Li, F. Y.; Zhou, Z. G.; Yang, H.; Yi, T.; Huang, C. H. *Chem. Commun.* **2008**, *44*, 2115.
- (21) Michalet, X.; Pinaud, F. F.; Bentolila, L. A.; Tsay, J. M.; Doose, S.; Li, J. J.; Sundaresan, G.; Wu, A. M.; Gambhir, S. S.; Weiss, S. *Science* **2005**, *307*, 538.
- (22) Wang, F.; Banerjee, D.; Liu, Y. S.; Chen, X. Y.; Liu, X. G. *Analyst* **2010**, *135*, 1839.
- (23) Zhou, J.; Liu, Z.; Li, F. Y. *Chem. Soc. Rev.* **2012**, *41*, 1323.
- (24) Xie, J.; Liu, G.; Eden, H. S.; Ai, H. B.; Chen, X. Y. *Acc. Chem. Res.* **2011**, *44*, 883.
- (25) He, Y.; Fan, C. H.; Lee, S. T. *Nano Today* **2010**, *5*, 282.
- (26) Welsher, K.; Liu, Z.; Sherlock, S. P.; Robinson, J. T.; Chen, Z.; Daranciang, D.; Dai, H. J. *Nat. Nanotechnol.* **2009**, *4*, 773.
- (27) Giepmans, B. N. G.; Adams, S. R.; Ellisman, M. H.; Tsien, R. Y. *Science* **2006**, *312*, 217.
- (28) Desvergne, J. P.; Czarnik, A. W. *Chemosensors for Ion and Molecule Recognition*; Kluwer Academic Publishers: London, 1997.
- (29) Suksai, C.; Tuntulani, T. *Chem. Soc. Rev.* **2003**, *32*, 192.
- (30) Kim, H. N.; Guo, Z. Q.; Zhu, W. H.; Yoon, J.; Tian, H. *Chem. Soc. Rev.* **2011**, *40*, 79.
- (31) Martínez-Máñez, R.; Sancenón, F. *Chem. Rev.* **2003**, *103*, 4419.
- (32) Cho, D. G.; Sessler, J. L. *Chem. Soc. Rev.* **2009**, *38*, 1647.
- (33) Duong, T. Q.; Kim, J. S. *Chem. Rev.* **2010**, *110*, 6280.
- (34) Chen, X. Q.; Zhou, Y.; Peng, X. J.; Yoon, J. Y. *Chem. Soc. Rev.* **2010**, *39*, 2120.
- (35) Xu, Z. C.; Chen, X. Q.; Kim, H. N.; Yoon, J. Y. *Chem. Soc. Rev.* **2010**, *39*, 127.
- (36) Chen, X. Q.; Tian, X. Z.; Shin, I.; Yoon, J. Y. *Chem. Soc. Rev.* **2011**, *40*, 4783.
- (37) Mohr, G. J. *Chem.—Eur. J.* **2004**, *10*, 1082.
- (38) Lakowicz, J. R. *Principles of fluorescence spectroscopy*, 1st ed.; Plenum: New York, 1983.
- (39) Guilbault, G. G. *Practical Fluorescence*, 2nd ed.; Marcel Dekker: New York, 1990.
- (40) Grabowski, Z. R.; Dobkowski, J. *Pure Appl. Chem.* **1983**, *55*, 245.
- (41) de Silva, A. P.; Gunaratne, H. Q. N.; Gunnlaugsson, T.; Huxley, A. J. M.; McCoy, C. P.; Rademacher, J. T.; Rice, T. E. *Chem. Rev.* **1997**, *97*, 1515.
- (42) Kim, J. S.; Quang, D. T. *Chem. Rev.* **2007**, *107*, 3780.
- (43) Sytnik, A.; Kasha, M. *Proc. Natl. Acad. Sci. U.S.A.* **1994**, *91*, 8627.
- (44) Zhao, Q.; Liu, S. J.; Shi, M.; Wang, C. M.; Yu, M. X.; Li, L.; Li, F. Y.; Yi, T.; Huang, C. H. *Inorg. Chem.* **2006**, *45*, 6152.
- (45) Zhao, Q.; Jiang, C. Y.; Shi, M.; Li, F. Y.; Yi, T.; Cao, Y.; Huang, C. H. *Organometallics* **2006**, *25*, 3631.
- (46) Li, X. H.; Chen, Z.; Zhao, Q.; Shen, L.; Li, F. Y.; Yi, T.; Cao, Y.; Huang, C. H. *Inorg. Chem.* **2007**, *46*, 5518.
- (47) Yang, T. S.; Xia, A.; Liu, Q.; Shi, M.; Wu, H. Z.; Xiong, L. Q.; Huang, C. H.; Li, F. Y. *J. Mater. Chem.* **2011**, *21*, 5360.
- (48) Wong, K. M. C.; Yam, V. W. W. *Acc. Chem. Res.* **2011**, *44*, 424.
- (49) Chi, Y.; Chou, P. T. *Chem. Soc. Rev.* **2007**, *36*, 1421.
- (50) Chen, Z. Q.; Bian, Z. Q.; Huang, C. H. *Adv. Mater.* **2010**, *22*, 1534.
- (51) Wong, W. Y.; Ho, C. L. *Coord. Chem. Rev.* **2009**, *253*, 1709.
- (52) Ulbricht, C.; Beyer, B.; Fribe, C.; Winter, A.; Schubert, U. S. *Adv. Mater.* **2009**, *21*, 4418.
- (53) Ferrer-Sueta, G.; Radi, R. *ACS Chem. Biol.* **2009**, *4*, 161.
- (54) Yam, V. W. W.; Lo, K. K. W. *Chem. Soc. Rev.* **1999**, *28*, 323.
- (55) Zhao, Q.; Li, L.; Li, F. Y.; Yu, M. X.; Liu, Z. P.; Yi, T.; Huang, C. H. *Chem. Commun.* **2008**, *44*, 685.
- (56) Huang, K. W.; Wu, H. Z.; Shi, M.; Li, F. Y.; Yi, T.; Huang, C. H. *Chem. Commun.* **2009**, *45*, 1243.
- (57) Wu, H. Z.; Yang, T. S.; Zhao, Q.; Zhou, J.; Li, C. Y.; Li, F. Y. *Dalton Trans.* **2011**, *40*, 1969.
- (58) Eliseeva, S. V.; Bunzli, J. C. G. *Chem. Soc. Rev.* **2010**, *39*, 189.
- (59) Shi, M.; Li, F. Y.; Yi, T.; Zhang, D. Q.; Hu, H. M.; Huang, C. H. *Inorg. Chem.* **2005**, *44*, 8929.
- (60) Förster, T. Z. *Ann. Phys.* **1948**, *437*, 55.
- (61) Sevick-Muraca, E. M.; Houston, J. P.; Gurfinkel, M. *Curr. Opin. Chem. Biol.* **2002**, *6*, 642.
- (62) Hilderbrand, S. A.; Weissleder, R. *Curr. Opin. Chem. Biol.* **2010**, *14*, 71.
- (63) Boening, D. W. *Chemosphere* **2000**, *40*, 1335.
- (64) Renzoni, A.; Zino, F.; Franchi, E. *Environ. Res.* **1998**, *77*, 68.
- (65) Zhang, D.; Su, J. H.; Ma, X.; Tian, H. *Tetrahedron* **2008**, *64*, 8515.
- (66) Zalups, R. K.; Lash, L. H. *Toxicol. Appl. Pharmacol.* **2006**, *214*, 88.
- (67) Zalups, R. K.; Ahmad, S. *J. Am. Soc. Nephrol.* **2004**, *15*, 2023.
- (68) Silbergeld, E. K.; Silva, I. A.; Nyland, J. F. *Toxicol. Appl. Pharmacol.* **2005**, *207*, s282.
- (69) Nolan, E. M.; Lippard, S. J. *Chem. Rev.* **2008**, *108*, 3443.
- (70) Que, E. L.; Domaille, D. W.; Chang, C. J. *Chem. Rev.* **2008**, *108*, 1517.
- (71) Zou, Q.; Jin, J. Y.; Xu, B.; Ding, L.; Tian, H. *Tetrahedron* **2011**, *67*, 915.
- (72) Hennrich, G.; Walther, W.; Resch-Genger, U.; Sonnenschein, H. *Inorg. Chem.* **2001**, *40*, 641.
- (73) Li, H. B.; Yan, H. J. *J. Phys. Chem. C* **2009**, *113*, 7526.
- (74) Ma, W. H.; Xu, Q.; Du, J. J.; Song, B.; Peng, X. J.; Wang, Z.; Li, G. D.; Wang, X. F. *Spectrochim. Acta, Part A* **2010**, *76*, 248.
- (75) Misra, A.; Shahid, M.; Srivastava, P.; Dwivedi, P. J. *Inclusion Phenom. Macrocyclic Chem.* **2011**, *69*, 119.
- (76) Tsukamoto, K.; Shinohara, Y.; Iwasaki, S.; Maeda, H. *Chem. Commun.* **2011**, *47*, 5073.
- (77) Chen, Y.; Sun, Z. H.; Song, B. E.; Liu, Y. *Org. Biomol. Chem.* **2011**, *9*, 5530.
- (78) Song, K. C.; Kim, J. S.; Park, S. M.; Chung, K. C.; Ahn, S.; Chang, S. K. *Org. Lett.* **2006**, *8*, 3413.
- (79) Jadhay, S. R.; Jyothish, K.; John, G. *Green Chem.* **2010**, *12*, 1345.
- (80) Choi, M. G.; Kim, Y. H.; Namgoong, J. E.; Chang, S. K. *Chem. Commun.* **2009**, *45*, 3560.
- (81) Zhang, G. X.; Zhang, D. Q.; Yin, S. W.; Yang, X. D.; Shuai, Z. G.; Zhu, D. B. *Chem. Commun.* **2005**, *41*, 2161.
- (82) Namgoong, J. E.; Jeon, H. L.; Kim, Y. H.; Choi, M. G.; Chang, S. K. *Tetrahedron Lett.* **2010**, *51*, 167.
- (83) Arai, T.; Ikemoto, T.; Hokura, A.; Terada, Y.; Kunito, T.; Tanabe, S.; Nakai, I. *Environ. Sci. Technol.* **2004**, *38*, 6468.
- (84) Samb, I.; Bell, J.; Toullec, P. Y.; Michelet, V.; Leray, I. *Org. Lett.* **2011**, *13*, 1182.
- (85) Liu, B.; Tian, H. *Chem. Commun.* **2005**, *41*, 3156.
- (86) Leng, B.; Zou, L.; Jiang, J. B.; Tian, H. *Sens. Actuators, B* **2009**, *140*, 162.
- (87) Lu, Z. J.; Wang, P. N.; Zhang, Y.; Chen, J. Y.; Zhen, S.; Leng, B.; Tian, H. *Anal. Chim. Acta* **2007**, *597*, 306.
- (88) Leng, B.; Jiang, J. B.; Tian, H. *AIChE J.* **2010**, *56*, 2957.
- (89) Zou, Q.; Zou, L.; Tian, H. *J. Mater. Chem.* **2011**, *21*, 14441.
- (90) Shiraishi, Y.; Sumiya, S.; Hirai, T. *Org. Biomol. Chem.* **2010**, *8*, 1310.
- (91) Sumiya, S.; Sugii, T.; Shiraishi, Y.; Hirai, T. *J. Photochem. Photobiol., A* **2011**, *219*, 154.

- (92) Lee, M. H.; Lee, S. W.; Kim, S. H.; Kang, C.; Kim, J. S. *Org. Lett.* **2009**, *11*, 2101.
- (93) Guo, Z. Q.; Zhu, W. H.; Zhu, M. M.; Wu, X. M.; Tian, H. *Chem.—Eur. J.* **2010**, *16*, 14424.
- (94) Wan, X. J.; Liu, T.; Liu, S. Y. *Langmuir* **2011**, *27*, 4082.
- (95) Koteeswari, R.; Ashokkumar, P.; Malar, E. J. P.; Ramakrishnan, V. T.; Ramamurthy, P. *Chem. Commun.* **2011**, *47*, 7695.
- (96) Zhao, Y. G.; Lin, Z. H.; He, C.; Wu, H. M.; Duan, C. Y. *Inorg. Chem.* **2006**, *45*, 10013.
- (97) Jiang, W.; Wang, W. *Chem. Commun.* **2009**, *45*, 3913.
- (98) Cheng, X. H.; Li, Q. Q.; Qin, J. G.; Li, Z. *ACS Appl. Mater. Interfaces* **2010**, *2*, 1066.
- (99) Cheng, X. H.; Li, S.; Zhong, A. S.; Qin, J. G.; Li, Z. *Sens. Actuators, B* **2011**, *157*, 57.
- (100) Ren, W. X.; Bhuniya, S.; Zhang, J. F.; Lee, Y. H.; Lee, S. J.; Kim, J. S. *Tetrahedron Lett.* **2010**, *51*, 5784.
- (101) Ros-Lis, J. V.; Marcos, M. D.; Martínez-Máñez, R.; Rurack, K.; Soto, J. *Angew. Chem., Int. Ed.* **2005**, *44*, 4405.
- (102) Beija, M.; Afonso, C. A. M.; Martinho, J. M. G. *Chem. Soc. Rev.* **2009**, *38*, 2410.
- (103) Chen, X. Q.; Pradhan, T.; Wang, F.; Kim, J. S.; Yoon, J. *Chem. Rev.* **2012**, *112*, 1910.
- (104) Kim, H. N.; Lee, M. H.; Kim, H. J.; Kim, J. S.; Yoon, J. *Chem. Soc. Rev.* **2008**, *37*, 1465.
- (105) Huang, J. H.; Xu, Y. F.; Qian, X. H. *J. Org. Chem.* **2009**, *74*, 2167.
- (106) Wanichacheva, N.; Setthakarn, K.; Prapawattanapol, N.; Hammeng, O.; Sanghiran Lee, V.; Grudpan, K. *J. Lumin.* **2012**, *132*, 35.
- (107) Lee, M. H.; Wu, J. S.; Lee, J. W.; Jung, J. H.; Kim, J. S. *Org. Lett.* **2007**, *9*, 2501.
- (108) Xu, J.; Sun, Y. H.; Zhang, H. *Chin. J. Inorg. Chem.* **2010**, *26*, 2189.
- (109) Ahamed, B. N.; Ghosh, P. *Inorg. Chim. Acta* **2011**, *372*, 100.
- (110) Duong, T. Q.; Wu, J. S.; Nguyen, D. L.; Tran, D.; Nguyen, D. D.; Nguyen, C. B.; Phan, T. Q. *Spectrochim. Acta, Part A* **2011**, *78*, 753.
- (111) Kim, S. K.; Swamy, K. M. K.; Chung, S. Y.; Kim, H. N.; Kim, M. J.; Jeong, Y.; Yoon, J. *Tetrahedron Lett.* **2010**, *51*, 3286.
- (112) Huang, W.; Zhou, P.; Yan, W. B.; He, C.; Xiong, L. Q.; Li, F. Y.; Duan, C. Y. *J. Environ. Monit.* **2009**, *11*, 330.
- (113) Tang, L. J.; Li, F. F.; Liu, M. H.; Nandhakumar, R. *Spectrochim. Acta, Part A* **2011**, *78*, 1168.
- (114) Lu, H.; Qi, S. L.; Mack, J.; Li, Z. F.; Lei, J. P.; Kobayashi, N.; Shen, Z. *J. Mater. Chem.* **2011**, *21*, 10878.
- (115) Yang, H.; Zhou, Z. G.; Huang, K. W.; Yu, M. X.; Li, F. Y.; Yi, T.; Huang, C. H. *Org. Lett.* **2007**, *9*, 4729.
- (116) Liu, C.; Zhou, Z. G.; Gao, Y.; Yang, H.; Li, B. G.; Li, F. Y.; Huang, C. H. *Sci. China, Ser. B* **2009**, *52*, 760.
- (117) Kim, H. N.; Nam, S. W.; Swamy, K. M. K.; Jin, Y.; Chen, X. Q.; Kim, Y.; Kim, S. J.; Park, S.; Yoon, J. *Analyst* **2011**, *136*, 1339.
- (118) Zhang, J. F.; Lim, C. S.; Cho, B. R.; Kim, J. S. *Talanta* **2010**, *83*, 658.
- (119) Zhao, Y.; Sun, Y.; Lv, X.; Liu, Y. L.; Chen, M. L.; Guo, W. *Org. Biomol. Chem.* **2010**, *8*, 4143.
- (120) Jiang, L.; Wang, L.; Zhang, B.; Yin, G.; Wang, R. Y. *Eur. J. Inorg. Chem.* **2010**, *28*, 4438.
- (121) Jana, A.; Kim, J. S.; Jung, H. S.; Bharadwaj, P. K. *Chem. Commun.* **2009**, *45*, 4417.
- (122) Huang, W.; Song, C. X.; He, C.; Lv, G. J.; Hu, X. Y.; Zhu, X.; Duan, C. Y. *Inorg. Chem.* **2009**, *48*, 5061.
- (123) Chen, X. Q.; Nam, S. W.; Jou, M. J.; Kim, Y. M.; Kim, S. J.; Park, S. S.; Yoon, J. Y. *Org. Lett.* **2008**, *10*, 5235.
- (124) Zheng, H.; Qian, Z. H.; Xu, L.; Yuan, F. F.; Lan, L. D.; Xu, J. G. *Org. Lett.* **2006**, *8*, 859.
- (125) Ma, Q. J.; Zhang, X. B.; Zhao, X. H.; Jin, Z.; Mao, G. J.; Shen, G. L.; Yu, R. Q. *Anal. Chim. Acta* **2010**, *663*, 85.
- (126) Zhou, Y.; You, X. Y.; Fang, Y.; Li, J. Y.; Liu, K.; Yao, C. *Org. Biomol. Chem.* **2010**, *8*, 4819.
- (127) Wang, H. H.; Xue, L.; Yu, C. L.; Qian, Y. Y.; Jiang, H. *Dyes Pigm.* **2011**, *91*, 350.
- (128) Wang, H. G.; Li, Y. P.; Xu, S. F.; Li, Y. C.; Zhou, C.; Fei, X. L.; Sun, L.; Zhang, C. Q.; Li, Y. X.; Yang, Q. B.; Xu, X. Y. *Org. Biomol. Chem.* **2011**, *9*, 2850.
- (129) Yang, Y. K.; Yook, K. J.; Tae, J. *J. Am. Chem. Soc.* **2005**, *127*, 16760.
- (130) Ko, S. K.; Yang, Y. K.; Tae, J. S.; Shin, I. *J. Am. Chem. Soc.* **2006**, *128*, 14150.
- (131) Yang, Y. K.; Ko, S. K.; Shin, I.; Tae, J. *Nat. Protoc.* **2007**, *2*, 1740.
- (132) Wu, J. S.; Hwang, I. C.; Kim, K. S.; Kim, J. S. *Org. Lett.* **2007**, *9*, 907.
- (133) Liu, W. M.; Xu, L. W.; Zhang, H. Y.; You, J. J.; Zhang, X. L.; Sheng, R. L.; Li, H. P.; Wu, S. K.; Wang, P. F. *Org. Biomol. Chem.* **2009**, *7*, 660.
- (134) Lin, W. Y.; Cao, X. W.; Ding, Y. D.; Yuan, L.; Long, L. L. *Chem. Commun.* **2010**, *46*, 3529.
- (135) Du, J. J.; Fan, J. L.; Peng, X. J.; Sun, P. P.; Wang, J. Y.; Li, H. L.; Sun, S. G. *Org. Lett.* **2010**, *12*, 476.
- (136) Hintermann, L.; Labonne, A. *Synthesis* **2007**, *8*, 1121.
- (137) Song, F. L.; Watanabe, S. J.; Floreancig, P. E.; Koide, K. *J. Am. Chem. Soc.* **2008**, *130*, 16460.
- (138) Ando, S.; Koide, K. *J. Am. Chem. Soc.* **2011**, *133*, 2556.
- (139) Santra, M.; Roy, B.; Ahn, K. H. *Org. Lett.* **2011**, *13*, 3422.
- (140) Cho, Y. S.; Ahn, K. H. *Tetrahedron Lett.* **2010**, *51*, 3852.
- (141) Lee, H.; Kim, H. J. *Tetrahedron Lett.* **2011**, *52*, 4775.
- (142) Lee, H.; Choi, M. G.; Yu, H. Y.; Ahn, S.; Chang, S. K. *Bull. Korean Chem. Soc.* **2010**, *31*, 3539.
- (143) Zhao, Q.; Yu, M. X.; Shi, L. X.; Liu, S. J.; Li, C. Y.; Shi, M.; Zhou, Z. G.; Huang, C. H.; Li, F. Y. *Organometallics* **2010**, *29*, 1085.
- (144) Jiang, W. L.; Gao, Y.; Sun, Y.; Ding, F.; Xu, Y.; Bian, Z. Q.; Li, F. Y.; Bian, J.; Huang, C. H. *Inorg. Chem.* **2010**, *49*, 3252.
- (145) Liu, Y.; Li, M. Y.; Zhao, Q.; Wu, H. Z.; Huang, K. W.; Li, F. Y. *Inorg. Chem.* **2011**, *50*, 5969.
- (146) Yang, H.; Qian, J. J.; Li, L. T.; Zhou, Z. G.; Li, D. R.; Wu, H. X.; Yang, S. P. *Inorg. Chim. Acta* **2010**, *363*, 1755.
- (147) Wu, Y. Q.; Jing, H.; Dong, Z. S.; Zhao, Q.; Wu, H. Z.; Li, F. Y. *Inorg. Chem.* **2011**, *50*, 7412.
- (148) Thomas, S. W.; Joly, G. D.; Swager, T. M. *Chem. Rev.* **2007**, *107*, 1339.
- (149) Shi, H. F.; Liu, S. J.; Sun, H. B.; Xu, W. J.; An, Z. F.; Chen, J.; Sun, S.; Lu, X. M.; Zhao, Q.; Huang, C. H. *Chem.—Eur. J.* **2010**, *16*, 12158.
- (150) Zhao, Q.; Liu, S. J.; Li, F. Y.; Yi, T.; Huang, C. H. *Dalton Trans.* **2008**, *29*, 3836.
- (151) Zhao, Q.; Cao, T. Y.; Li, F. Y.; Li, X. H.; Jing, H.; Yi, T.; Huang, C. H. *Organometallics* **2007**, *26*, 2077.
- (152) Kubo, Y.; Yamamoto, M.; Ikeda, M.; Takeuchi, M.; Shinkai, S.; Yamaguchi, S.; Tamao, K. *Angew. Chem., Int. Ed.* **2003**, *42*, 2036.
- (153) Maruyama, S.; Kikuchi, K.; Hirano, T.; Urano, Y.; Nagano, T. *J. Am. Chem. Soc.* **2002**, *124*, 10650.
- (154) Othman, A. B.; Lee, J. W.; Wu, J. S.; Kim, J. S.; Abidi, R.; Thuery, P.; Strub, J. M.; Dorsselaer, A. V.; Vicens, J. *J. Org. Chem.* **2007**, *72*, 7634.
- (155) Yuan, M. J.; Zhou, W. D.; Liu, X. F.; Zhu, M.; Li, J. B.; Yin, X. D.; Zheng, H. Y.; Zuo, Z. C.; Ouyang, C. B.; Liu, H. B.; Li, Y. L.; Zhu, D. B. *J. Org. Chem.* **2008**, *73*, 5008.
- (156) Shang, G. Q.; Gao, X.; Chen, M. X.; Zheng, H.; Xu, J. G. *J. Fluoresc.* **2008**, *18*, 1187.
- (157) Lee, Y. H.; Lee, M. H.; Zhang, J. F.; Kim, J. S. *J. Org. Chem.* **2010**, *75*, 7159.
- (158) Yu, H. B.; Xiao, Y.; Guo, H. Y.; Qian, X. H. *Chem.—Eur. J.* **2011**, *17*, 3179.
- (159) Fang, G.; Xu, M. Y.; Zeng, F.; Wu, S. Z. *Langmuir* **2010**, *26*, 17764.
- (160) Hu, H.; Yu, M. X.; Li, F. Y.; Chen, Z. G.; Gao, X.; Xiong, L. Q.; Huang, C. H. *Chem. Mater.* **2008**, *20*, 7003.
- (161) Xiong, L. Q.; Chen, Z. G.; Yu, M. X.; Li, F. Y.; Liu, C.; Huang, C. H. *Biomaterials* **2009**, *30*, 5592.

- (162) Hu, H.; Xiong, L. Q.; Zhou, J.; Li, F. Y.; Cao, T. Y.; Huang, C. H. *Chem.—Eur. J.* **2009**, *15*, 3577.
- (163) Zhou, J.; Sun, Y.; Du, X. X.; Xiong, L. Q.; Hu, H.; Li, F. Y. *Biomaterials* **2010**, *31*, 3287.
- (164) Xiong, L. Q.; Yang, T. S.; Yang, Y.; Xu, C. J.; Li, F. Y. *Biomaterials* **2010**, *31*, 7078.
- (165) Sun, Y.; Yu, M. X.; Liang, S.; Zhang, Y. J.; Li, C. G.; Mou, T. T.; Yang, W. J.; Zhang, X. Z.; Li, B. A.; Huang, C. H.; Li, F. Y. *Biomaterials* **2011**, *32*, 2999.
- (166) Xia, A.; Gao, Y.; Zhou, J.; Li, C. Y.; Yang, T. S.; Wu, D. M.; Wu, L. M.; Li, F. Y. *Biomaterials* **2011**, *32*, 7200.
- (167) Liu, Q.; Chen, M.; Sun, Y.; Chen, G. Y.; Yang, T. S.; Gao, Y.; Zhang, X. Z.; Li, F. Y. *Biomaterials* **2011**, *32*, 8243.
- (168) Liu, Q.; Sun, Y.; Yang, T. S.; Feng, W.; Li, C. G.; Li, F. Y. *J. Am. Chem. Soc.* **2011**, *133*, 17122.
- (169) Liu, Q.; Sun, Y.; Li, C. G.; Zhou, J.; Li, C. Y.; Yang, T. S.; Zhang, X. Z.; Yi, T.; Wu, D. M.; Li, F. Y. *ACS Nano* **2011**, *5*, 3146.
- (170) Zhou, J.; Yu, M. X.; Sun, Y.; Zhang, X. Z.; Zhu, X. J.; Wu, Z. H.; Wu, D. M.; Li, F. Y. *Biomaterials* **2011**, *32*, 1148.
- (171) Chen, Z. G.; Chen, H. L.; Hu, H.; Yu, M. X.; Li, F. Y.; Zhang, Q.; Zhou, Z. G.; Yi, T.; Huang, C. H. *J. Am. Chem. Soc.* **2008**, *130*, 3023.
- (172) Wang, F.; Deng, R. R.; Wang, J.; Wang, Q. X.; Han, Y.; Zhu, H. M.; Chen, X. Y.; Liu, X. G. *Nat. Mater.* **2011**, *10*, 968.
- (173) Liu, Q.; Peng, J. J.; Sun, L. N.; Li, F. Y. *ACS Nano* **2011**, *5*, 8040.
- (174) Davidson, P. W.; Myers, G. J.; Cox, C.; Shamlaye, C. F.; Marsh, D. O.; Tanner, M. A.; Berlin, M.; Sloane-Reeves, J.; Cernichiari, E.; Choisy, O.; Choi, A.; Clarkson, T. W. *Neurotoxicology* **1995**, *16*, 677.
- (175) Counter, S. A.; Buchanan, L. H. *Toxicol. Appl. Pharmacol.* **2004**, *198*, 209.
- (176) Campo, O. D.; Carbayo, A.; Cuevas, J. V.; Muñoz, A.; García-Herbosa, G.; Moreno, D.; Ballesteros, E.; Basurto, S.; Gómez, T.; Torroba, T. *Chem. Commun.* **2008**, *44*, 4576.
- (177) Santra, M.; Ryu, D.; Chatterjee, A.; Ko, S. K.; Shin, I.; Ahn, K. H. *Chem. Commun.* **2009**, *45*, 2115.
- (178) Chen, X. Q.; Baek, K. H.; Kim, Y. M.; Kim, S. J.; Shin, I.; Yoon, J. Y. *Tetrahedron* **2010**, *66*, 4016.
- (179) Zou, Q.; Tian, H. *Sens. Actuators, B* **2010**, *149*, 20.
- (180) Tapiero, H.; Townsend, D. M.; Tew, K. D. *Biomed. Pharmacother.* **2003**, *57*, 386.
- (181) Uauy, R.; Olivares, M.; Gonzalez, M. *Am. J. Clin. Nutr.* **1998**, *67*, 952S.
- (182) Valentine, J. S.; Hart, P. J. *Proc. Natl. Acad. Sci. U.S.A.* **2003**, *100*, 3617.
- (183) Guo, Z. Q.; Zhu, W. H.; Tian, H. *Macromolecules* **2010**, *43*, 739.
- (184) Yang, H.; Liu, Z. Q.; Zhou, Z. G.; Shi, E. X.; Li, F. Y.; Du, Y. K.; Yi, T.; Huang, C. H. *Tetrahedron Lett.* **2006**, *47*, 2911.
- (185) Zhang, X.; Shiraishi, Y.; Hirai, T. *Org. Lett.* **2007**, *9*, 5039.
- (186) Zhang, X.; Sumiya, S.; Shiraishi, Y.; Hirai, T. *J. Photochem. Photobiol., A* **2009**, *205*, 215.
- (187) Xiang, Y.; Li, Z. F.; Chen, X. T.; Tong, A. J. *Talanta* **2008**, *74*, 1148.
- (188) Zhao, Y.; Zhang, X. B.; Han, Z. X.; Qiao, L.; Li, C. Y.; Jian, L. X.; Shen, G. L.; Yu, R. Q. *Anal. Chem.* **2009**, *81*, 7022.
- (189) Zhao, M. L.; Yang, X. F.; He, S. H.; Wang, L. P. *Sens. Actuators, B* **2009**, *135*, 625.
- (190) Swamy, K.; Ko, S. K.; Kwon, S. K.; Lee, H. N.; Mao, C.; Kim, J. M.; Lee, K. H.; Kim, J. H.; Shin, I.; Yoon, J. Y. *Chem. Commun.* **2008**, *44*, 5915.
- (191) Zhou, Y.; Wang, F.; Kim, Y. M.; Kim, S. J.; Yoon, J. Y. *Org. Lett.* **2009**, *11*, 4442.
- (192) Tang, R. R.; Lei, K.; Chen, K.; Zhao, H.; Chen, J. W. *J. Fluoresc.* **2011**, *21*, 141.
- (193) Sun, C. D.; Chen, J. M.; Ma, H. M.; Liu, Y.; Zhang, J. H.; Liu, Q. *J. Sci. China, Ser. B* **2011**, *54*, 1101.
- (194) Yu, C. W.; Zhang, J.; Wang, R.; Chen, L. X. *Org. Biomol. Chem.* **2010**, *8*, 5277.
- (195) Xu, Z. H.; Zhang, L. K.; Guo, R.; Xiang, T. C.; Wu, C. Z.; Zheng, Z.; Yang, F. L. *Sens. Actuators, B* **2011**, *156*, 546.
- (196) Zhang, J. F.; Zhou, Y.; Yoon, J.; Kim, Y.; Kim, S. J.; Kim, J. S. *Org. Lett.* **2010**, *12*, 3852.
- (197) Xi, P. X.; Dou, J. Y.; Huang, L.; Xu, M.; Chen, F. J.; Wu, Y. J.; Bai, D. C.; Li, W. G.; Zeng, Z. Z. *Sens. Actuators, B* **2010**, *148*, 337.
- (198) Huang, L.; Chen, F. J.; Xi, P. X.; Xie, G. Q.; Li, Z. P.; Shi, Y. J.; Xu, M.; Liu, H. Y.; Ma, Z. R.; Bai, D. C.; Zeng, Z. Z. *Dyes Pigm.* **2011**, *90*, 265.
- (199) Jiang, L.; Zhang, B.; Sun, J.; Yin, G.; Shang, T. M.; Wang, L.; Wang, R. Y. *Chin. J. Inorg. Chem.* **2010**, *26*, 1750.
- (200) Cherreddy, N. R.; Thennarasu, S. *Dyes Pigm.* **2011**, *91*, 378.
- (201) Liu, W. Y.; Li, H. Y.; Zhao, B. X.; Miao, J. Y. *Org. Biomol. Chem.* **2011**, *9*, 4802.
- (202) Yu, C. W.; Chen, L. X.; Zhang, J.; Li, J. H.; Liu, P.; Wang, W. H.; Yan, B. *Talanta* **2011**, *85*, 1627.
- (203) Mei, L.; Xiang, Y.; Li, N.; Tong, A. J. *Talanta* **2007**, *72*, 1717.
- (204) Zeng, X.; Wu, C.; Dong, L.; Mu, L.; Xue, S. F.; Tao, Z. *Sci. China, Ser. B* **2009**, *52*, 523.
- (205) Kovács, J.; Mokhir, A. *Inorg. Chem.* **2008**, *47*, 1880.
- (206) Qi, X.; Jun, E. J.; Xu, L.; Kim, S. J.; Hong, J. S. J.; Yoon, Y. J.; Yoon, J. Y. *J. Org. Chem.* **2006**, *71*, 2881.
- (207) Zhou, Z. J.; Li, N.; Tong, A. J. *Anal. Chim. Acta* **2011**, *702*, 81.
- (208) Li, N.; Xiang, Y.; Tong, A. J. *Chem. Commun.* **2010**, *46*, 3363.
- (209) Kim, M. H.; Jang, H. H.; Yi, S. J.; Chang, S. K.; Han, M. S. *Chem. Commun.* **2009**, *45*, 4838.
- (210) Dujols, V.; Ford, F.; Czarnik, A. W. *J. Am. Chem. Soc.* **1997**, *119*, 7386.
- (211) Xie, P. H.; Guo, F. Q.; Li, D.; Liu, X. Y.; Liu, L. *J. Lumin.* **2011**, *131*, 104.
- (212) Chen, X. Q.; Jia, J. J.; Ma, H. M.; Wang, S. J.; Wang, X. C. *Anal. Chim. Acta* **2009**, *632*, 9.
- (213) Hu, Z. Q.; Wang, X. M.; Feng, Y. C.; Ding, L.; Lu, H. Y. *Dyes Pigm.* **2011**, *88*, 257.
- (214) Xiang, Y.; Tong, A. J. *Luminescence* **2008**, *23*, 28.
- (215) Yu, C. W.; Zhang, J.; Li, J. H.; Liu, P.; Wei, P. H.; Chen, L. X. *Microchim. Acta* **2011**, *174*, 247.
- (216) Kumar, M.; Kumar, N.; Bhalla, V.; Sharma, P. R.; Kaur, T. *Org. Lett.* **2012**, *14*, 406.
- (217) Yu, M. X.; Shi, M.; Chen, Z. G.; Li, F. Y.; Li, X. X.; Gao, Y. H.; Xu, J.; Yang, H.; Zhou, Z. G.; Yi, T.; Huang, C. H. *Chem.—Eur. J.* **2008**, *14*, 6892.
- (218) Huang, L.; Hou, F. P.; Xi, P. X.; Bai, D. C.; Xu, M.; Li, Z. P.; Xie, G. Q.; Shi, Y. J.; Liu, H. Y.; Zeng, Z. Z. *J. Inorg. Biochem.* **2011**, *105*, 800.
- (219) Liu, J. L.; Li, C. Y.; Li, F. Y. *J. Mater. Chem.* **2011**, *21*, 7175.
- (220) Yuan, L.; Lin, W. Y.; Cao, Z. M.; Long, L. L.; Song, J. Z. *Chem.—Eur. J.* **2011**, *17*, 689.
- (221) Ajayakumar, G.; Sreenath, K.; Gopidas, K. R. *Dalton Trans.* **2009**, *7*, 1180.
- (222) Wang, D. P.; Shiraishi, Y.; Hirai, T. *Chem. Commun.* **2011**, *47*, 2673.
- (223) Bricks, J. L.; Rurack, K.; Radeglia, R.; Reck, G.; Schulz, B.; Sonnenschein, H.; Resch-Genger, U. *J. Chem. Soc., Perkin Trans. 2000*, *6*, 1209.
- (224) Lin, W. Y.; Long, L. L.; Chen, B. B.; Tan, W.; Gao, W. S. *Chem. Commun.* **2010**, *46*, 1311.
- (225) Liu, Z.; Lin, L. R.; Huang, R. B.; Zheng, L. S. *Spectrochim. Acta, Part A* **2008**, *71*, 1212.
- (226) Basu, A.; Das, G. *Dalton Trans.* **2011**, *40*, 2837.
- (227) Kim, H. J.; Lee, S. J.; Park, S. Y.; Jung, J. H.; Kim, J. S. *Adv. Mater.* **2008**, *20*, 3229.
- (228) Li, A. F.; He, H.; Ruan, Y. B.; Wen, Z. C.; Zhao, J. S.; Jiang, Q. J.; Jiang, Y. B. *Org. Biomol. Chem.* **2008**, *7*, 193.
- (229) Mashraqui, S. H.; Poonia, K.; Betkar, R.; Chandiramani, M. *Tetrahedron Lett.* **2010**, *51*, 4336.
- (230) Lin, W. Y.; Yuan, L.; Tan, W.; Feng, J. B.; Long, L. L. *Chem.—Eur. J.* **2009**, *15*, 1030.
- (231) Haas, J. D.; Brownlie, T. J. *Nutr.* **2001**, *131*, 676s.

- (232) Burdo, J. R.; Connor, J. R. *BioMetals* **2003**, *16*, 63.
- (233) Moon, K.-S.; Yang, Y.-K.; Ji, S.; Tae, J. *Tetrahedron Lett.* **2010**, *S1*, 3290.
- (234) Tang, L. J.; Li, Y.; Nandhakumar, R.; Qian, J. H. *Monatsh. Chem.* **2010**, *141*, 615.
- (235) Zhang, M.; Gao, Y. H.; Li, M. Y.; Yu, M. X.; Li, F. Y.; Li, L.; Zhu, M. W.; Zhang, J. P.; Yi, T.; Huang, C. H. *Tetrahedron Lett.* **2007**, *48*, 3709.
- (236) Chartres, J. D.; Busby, M.; Riley, M. J.; Davis, J. J.; Bernhardt, P. V. *Inorg. Chem.* **2011**, *50*, 9178.
- (237) Yin, W. T.; Cui, H.; Yang, Z.; Li, C.; She, M. Y.; Yin, B.; Li, J. L.; Zhao, G. F.; Shi, Z. *Sens. Actuators, B* **2011**, *157*, 675.
- (238) Hu, Z. Q.; Feng, Y. C.; Huang, H. Q.; Ding, L.; Wang, X. M.; Lin, C. S.; Li, M.; Ma, C. P. *Sens. Actuators, B* **2011**, *156*, 428.
- (239) Xiang, Y.; Tong, A. J. *Org. Lett.* **2006**, *8*, 1549.
- (240) Li, J. B.; Hu, Q. H.; Yu, X. L.; Zeng, Y.; Cao, C. C.; Liu, X. W.; Guo, J.; Pan, Z. Q. *J. Fluoresc.* **2011**, *21*, 2005.
- (241) Lin, W. Y.; Yuan, L.; Feng, J. B.; Cao, X. W. *Eur. J. Org. Chem.* **2008**, *16*, 2689.
- (242) Lee, M. H.; Giap, T. V.; Kim, S. H.; Lee, Y. H.; Kang, C.; Kim, J. S. *Chem. Commun.* **2010**, *46*, 1407.
- (243) Jackson, R. K.; Shi, Y.; Yao, X. D.; Burdette, S. C. *Dalton Trans.* **2010**, *39*, 4155.
- (244) Lim, N. C.; Pavlova, S. V.; Brückner, C. *Inorg. Chem.* **2009**, *48*, 1173.
- (245) Vincent, J. B. *Nutr. Rev.* **2000**, *58*, 67.
- (246) Mao, J.; Wang, L. N.; Dou, W.; Tang, X. L.; Yan, Y.; Liu, W. S. *Org. Lett.* **2007**, *9*, 4567.
- (247) Zheng, X. Y.; Zhang, W. J.; Mu, L.; Zeng, X.; Xue, S. F.; Tao, Z.; Yamatob, T. *J. Inclusion Phenom. Macrocyclic Chem.* **2010**, *68*, 139.
- (248) Mao, J.; He, Q.; Liu, W. S. *Anal. Bioanal. Chem.* **2010**, *396*, 1197.
- (249) Huang, K. W.; Yang, H.; Zhou, Z. G.; Yu, M. X.; Li, F. Y.; Gao, X.; Yi, T.; Huang, C. H. *Org. Lett.* **2008**, *10*, 2557.
- (250) Zhou, Z. G.; Yu, M. X.; Yang, H.; Huang, K. W.; Li, F. Y.; Yi, T.; Huang, C. H. *Chem. Commun.* **2008**, *44*, 3387.
- (251) Berg, J. M.; Shi, Y. G. *Science* **1996**, *271*, 1081.
- (252) Takeda, A. *Brain Res. Rev.* **2000**, *34*, 137.
- (253) Frederickson, C. J.; Koh, J. Y.; Bush, A. I. *Nat. Rev. Neurosci.* **2005**, *6*, 449.
- (254) Tomat, E.; Lippard, S. J. *Curr. Opin. Chem. Biol.* **2010**, *14*, 225.
- (255) Zhang, D.; Zhang, Q.; Sua, J. H.; Tian, H. *Chem. Commun.* **2009**, *45*, 1700.
- (256) Li, N.; Tang, W. X.; Xiang, Y.; Tong, A. J.; Jin, P. Y.; Ju, Y. *Luminescence* **2010**, *25*, 445.
- (257) Du, P. W.; Lippard, S. J. *Inorg. Chem.* **2010**, *49*, 10753.
- (258) Jiang, L.; Wang, L.; Guo, M.; Yin, G.; Wang, R. Y. *Sens. Actuators, B* **2011**, *156*, 825.
- (259) Li, Z. X.; Yu, M. M.; Zhang, L. F.; Yu, M.; Liu, J. X.; Wei, L. H.; Zhang, H. Y. *Chem. Commun.* **2010**, *46*, 7169.
- (260) Waalkes, M. P.; Coogan, T. P.; Barter, R. A. *Crit. Rev. Toxicol.* **1992**, *22*, 175.
- (261) Satarug, S.; Moore, M. R. *Environ. Health Perspect.* **2004**, *112*, 1099.
- (262) Mahapatra, A. K.; Roy, J.; Sahoo, P. *Tetrahedron Lett.* **2011**, *52*, 2965.
- (263) Chen, L. J.; Yang, X. Q.; Jiao, H. L.; Zhao, B. L. *Chem. Res. Toxicol.* **2004**, *17*, 922.
- (264) Kwon, J. Y.; Jang, Y. J.; Lee, Y. J.; Kim, K. M.; Seo, M. S.; Nam, W.; Yoon, J. Y. *J. Am. Chem. Soc.* **2005**, *127*, 10107.
- (265) Ju, H.; Lee, M. H.; Kim, J.; Kim, J. S.; Kim, J. *Talanta* **2011**, *83*, 1359.
- (266) Habib, A.; Tabata, M. *J. Inorg. Biochem.* **2004**, *98*, 1696.
- (267) Nyarko, E.; Hara, T.; Grab, D. J.; Habib, A.; Kim, Y.; Nikolskaia, O.; Fukuma, T.; Tabata, M. *Chem. Biol. Interact.* **2004**, *148*, 19.
- (268) Wang, J. L.; Lin, W. Y.; Yuan, L.; Song, J. Z.; Gao, W. S. *Chem. Commun.* **2011**, *47*, 12506.
- (269) Jou, M. J.; Chen, X. Q.; Swamy, K. M. K.; Kim, H. N.; Kim, H. J.; Lee, S.; Yoon, J. *Chem. Commun.* **2009**, *45*, 7218.
- (270) Egorova, O. A.; Seo, H.; Chatterjee, A.; Ahn, K. H. *Org. Lett.* **2010**, *12*, 401.
- (271) Yang, Y. K.; Lee, S.; Tae, J. *Org. Lett.* **2009**, *11*, 5610.
- (272) Yuan, L.; Lin, W.; Yang, Y.; Song, J. *Chem. Commun.* **2011**, *47*, 4703.
- (273) Dong, M.; Wang, Y. W.; Peng, Y. *Org. Lett.* **2010**, *12*, 5310.
- (274) Ratte, H. T. *Environ. Toxicol. Chem.* **1999**, *18*, 89.
- (275) Chatterjee, A.; Santra, M.; Won, N.; Kim, S.; Kim, J. K.; Kim, S. B.; Ahn, K. H. *J. Am. Chem. Soc.* **2009**, *131*, 2040.
- (276) Shi, W.; Sun, S. N.; Li, X. H.; Ma, H. M. *Inorg. Chem.* **2010**, *49*, 1206.
- (277) Liu, T. Z.; Lee, S. D.; Bhatnagar, R. S. *Toxicol. Lett.* **1979**, *4*, 469.
- (278) Garner, A. L.; Koide, K. *Chem. Commun.* **2009**, *45*, 83.
- (279) Garner, A. L.; Koide, K. *Chem. Commun.* **2009**, *45*, 86.
- (280) Santra, M.; Ko, S. K.; Shin, I.; Ahn, K. H. *Chem. Commun.* **2010**, *46*, 3964.
- (281) Jiang, J.; Jiang, H. E.; Liu, W.; Tang, X. L.; Zhou, X.; Liu, W. S.; Liu, R. T. *Org. Lett.* **2011**, *13*, 4922.
- (282) Zhu, B. C.; Gao, C. C.; Zhao, Y. Z.; Liu, C. Y.; Li, Y. M.; Wei, Q.; Ma, Z. M.; Du, B.; Zhang, X. L. *Chem. Commun.* **2011**, *47*, 8656.
- (283) Li, H. L.; Fan, J. L.; Du, J. J.; Guo, K. X.; Sun, S. G.; Liu, X. J.; Peng, X. *J. Chem. Commun.* **2010**, *46*, 1079.
- (284) Li, H. L.; Fan, J. L.; Liu, X. J.; Sun, S. G.; Peng, X. *J. Chem. J. Chin. Univ.* **2010**, *31*, 1725.
- (285) Kim, H.; Moon, K. S.; Shim, S.; Tae, J. *Chem. Asian J.* **2011**, *6*, 1987.
- (286) Thompson, K. H.; McNeill, J. H.; Orvig, C. *Chem. Rev.* **1999**, *99*, 2561.
- (287) Huo, F. J.; Su, J.; Sun, Y. Q.; Yin, C. X.; Tong, H. B.; Nie, Z. X. *Dyes Pigm.* **2010**, *86*, 50.
- (288) Connell, P. *Fluoride* **2007**, *40*, 155.
- (289) Xu, W. J.; Liu, S. J.; Sun, H. B.; Zhao, X. Y.; Zhao, Q.; Sun, S.; Cheng, S.; Ma, T. C.; Zhou, L. X.; Huang, W. *J. Mater. Chem.* **2011**, *21*, 7572.
- (290) Zhao, Q.; Li, F. Y.; Liu, S. J.; Yu, M. X.; Liu, Z. Q.; Yi, T.; Huang, C. H. *Inorg. Chem.* **2008**, *47*, 9256.
- (291) Ayoob, S.; Gupta, A. K. *Crit. Rev. Environ. Sci. Technol.* **2006**, *36*, 433.
- (292) Sessler, J. L.; Camiolo, S.; Gale, P. A. *Coord. Chem. Rev.* **2003**, *240*, 17.
- (293) Gale, P. A. *Acc. Chem. Res.* **2011**, *44*, 216.
- (294) Jiang, J. B.; Xiao, X.; Zhao, P.; Tian, H. *J. Polym. Sci., Part A: Polym. Chem.* **2010**, *48*, 1551.
- (295) Liu, B.; Tian, H. *Chem. Lett.* **2005**, *34*, 686.
- (296) Yang, H.; Yi, T.; Zhou, Z. G.; Zhou, Y. F.; Wu, J. C.; Xu, M.; Li, F. Y.; Huang, C. H. *Langmuir* **2007**, *23*, 8224.
- (297) Qu, Y.; Hua, J. L.; Tian, H. *Org. Lett.* **2010**, *12*, 3320.
- (298) Helal, A.; Thao, N.; Lee, S.; Kim, H. S. *J. Inclusion Phenom. Macrocyclic Chem.* **2010**, *66*, 87.
- (299) Gale, P. A. *Acc. Chem. Res.* **2006**, *39*, 465.
- (300) Zhao, P.; Jiang, J. B.; Leng, B.; Tian, H. *Macromol. Rapid Commun.* **2009**, *30*, 1715.
- (301) Qu, Y.; Hua, J. L.; Jiang, Y. H.; Tian, H. *J. Polym. Sci., Part A: Polym. Chem.* **2009**, *47*, 1544.
- (302) Li, Y.; Cao, L. F.; Tian, H. *J. Org. Chem.* **2006**, *71*, 8279.
- (303) Liu, B.; Tian, H. *J. Mater. Chem.* **2005**, *15*, 2681.
- (304) Plitt, P.; Gross, D. E.; Lynch, V. M.; Sessler, J. L. *Chem.—Eur. J.* **2007**, *13*, 1374.
- (305) Zhao, Q.; Liu, S. J.; Shi, M.; Li, F. Y.; Jing, H.; Yi, T.; Huang, C. H. *Organometallics* **2007**, *26*, 5922.
- (306) Yoon, J.; Kim, S. K.; Singh, N. J.; Kim, K. S. *Chem. Soc. Rev.* **2006**, *35*, 355.
- (307) Xu, Z. W.; Tang, J.; Tian, H. *Chin. Chem. Lett.* **2008**, *19*, 1353.
- (308) Peng, X. J.; Wu, Y. K.; Fan, J. L.; Tian, M. Z.; Han, K. L. *J. Org. Chem.* **2005**, *70*, 10524.

- (309) Wu, Y. K.; Peng, X. J.; Fan, J. L.; Gao, S.; Tian, M. Z.; Zhao, J. Z.; Sun, S. *J. Org. Chem.* **2007**, *72*, 62.
- (310) Kim, S. Y.; Hong, J. I. *Org. Lett.* **2007**, *9*, 3109.
- (311) Bozdemir, O. A.; Sozmen, F.; Buyukcakir, O.; Guliyev, R.; Cakmak, Y.; Akkaya, E. U. *Org. Lett.* **2010**, *12*, 1400.
- (312) Cao, X. W.; Lin, W. Y.; Yu, Q. X.; Wang, J. L. *Org. Lett.* **2011**, *13*, 6098.
- (313) Yang, X. F. *Spectrochim. Acta, Part A* **2007**, *67*, 321.
- (314) Zhang, J. F.; Lim, C. S.; Bhuniya, S.; Cho, B. R.; Kim, J. S. *Org. Lett.* **2011**, *13*, 1190.
- (315) Li, Y. M.; Zhang, X. L.; Zhu, B. C.; Yan, J. L.; Xu, W. P. *Anal. Sci.* **2010**, *26*, 1077.
- (316) Hu, R.; Feng, J.; Hu, D. H.; Wang, S. Q.; Li, S. Y.; Li, Y.; Yang, G. *Angew. Chem., Int. Ed.* **2010**, *49*, 4915.
- (317) Bao, Y. Y.; Liu, B.; Wang, H.; Tian, J.; Bai, R. K. *Chem. Commun.* **2011**, *47*, 3957.
- (318) Park, J.; Koh, M.; Park, S. B.; Hong, J. I. *Chem. Commun.* **2009**, *45*, 4735.
- (319) Zhu, B.; Yuan, F.; Li, R.; Li, Y.; Wei, Q.; Ma, Z.; Du, B.; Zhang, X. *Chem. Commun.* **2011**, *47*, 7098.
- (320) Fu, L.; Jiang, F. L.; Fortin, D.; Harvey, P. D.; Liu, Y. *Chem. Commun.* **2011**, *47*, 5503.
- (321) Rao, M. R.; Mobin, S. M.; Ravikanth, M. *Tetrahedron* **2010**, *66*, 1728.
- (322) Lu, H.; Wang, Q.; Li, Z.; Lai, G.; Jiang, J.; Shen, Z. *Org. Biomol. Chem.* **2011**, *9*, 4558.
- (323) Buckland, D.; Bhosale, S. V.; Langford, S. J. *Tetrahedron Lett.* **2011**, *52*, 1990.
- (324) Yu, H. B.; Fu, M. Y.; Xiao, Y. *Phys. Chem. Chem. Phys.* **2010**, *12*, 7386.
- (325) Padie, C.; Zeitler, K. *New J. Chem.* **2011**, *35*, 994.
- (326) Bhalla, V.; Singh, H.; Kumar, M. *Org. Lett.* **2010**, *12*, 628.
- (327) Li, G.; Gong, W. T.; Ye, J. W.; Lin, Y.; Ning, G. L. *Tetrahedron Lett.* **2011**, *52*, 1313.
- (328) Kim, T. H.; Swager, T. M. *Angew. Chem., Int. Ed.* **2003**, *42*, 4803.
- (329) Galbraith, E.; James, T. D. *Chem. Soc. Rev.* **2010**, *39*, 3831.
- (330) Yamaguchi, S.; Akiyama, S.; Tamao, K. *J. Am. Chem. Soc.* **2001**, *123*, 11372.
- (331) Liu, Z. Q.; Shi, M.; Li, F. Y.; Fang, Q.; Chen, Z. H.; Yi, T.; Huang, C. H. *Org. Lett.* **2005**, *7*, 5481.
- (332) Zhou, Z. G.; Xiao, S. Z.; Xu, J.; Liu, Z. Q.; Shi, M.; Li, F. Y.; Yi, T.; Huang, C. H. *Org. Lett.* **2006**, *8*, 3911.
- (333) Zhou, Z. G.; Yang, H.; Shi, M.; Xiao, S. Z.; Li, F. Y.; Yi, T.; Huang, C. H. *ChemPhysChem* **2007**, *8*, 1289.
- (334) Zhou, Z. G.; Li, F. Y.; Yi, T.; Huang, C. H. *Tetrahedron Lett.* **2007**, *48*, 6633.
- (335) Wade, C. R.; Broomsgrove, A. E.; Aldridge, S.; Gabbai, F. P. *Chem. Rev.* **2010**, *110*, 3958.
- (336) Hudson, Z. M.; Wang, S. N. *Acc. Chem. Res.* **2009**, *42*, 1584.
- (337) Hudnall, T. W.; Chiu, C. W.; Gabbai, F. P. *Acc. Chem. Res.* **2009**, *42*, 388.
- (338) Sole, S.; Gabbai, F. P. *Chem. Commun.* **2004**, *40*, 1284.
- (339) Melaimi, M.; Gabbai, F. P. *J. Am. Chem. Soc.* **2005**, *127*, 9680.
- (340) Kim, Y.; Gabbai, F. P. *J. Am. Chem. Soc.* **2009**, *131*, 3363.
- (341) Xu, S.; Chen, K. C.; Tian, H. *J. Mater. Chem.* **2005**, *15*, 2676.
- (342) Li, Y.; Xu, S.; Li, X.; Chen, K. C.; Tian, H. *Chem. Lett.* **2007**, *36*, 664.
- (343) Swamy, K. M. K.; Lee, Y. J.; Lee, H. N.; Chun, J.; Kim, Y.; Kim, S. J.; Yoon, J. *J. Org. Chem.* **2006**, *71*, 8626.
- (344) Holland, M. A.; Kozlowski, L. M. *Clin. Pharm.* **1986**, *5*, 737.
- (345) Yang, Y. K.; Tae, J. *Org. Lett.* **2006**, *8*, 5721.
- (346) Mashraqui, S. H.; Betkar, R.; Chandiramani, M.; Estarellas, C.; Frontera, A. *New J. Chem.* **2011**, *35*, 57.
- (347) Kim, G.-J.; Kim, H.-J. *Tetrahedron Lett.* **2010**, *51*, 185.
- (348) Kim, G.-J.; Kim, H.-J. *Tetrahedron Lett.* **2010**, *51*, 2914.
- (349) Park, S.; Kim, H. *J. Chem. Commun.* **2010**, *46*, 9197.
- (350) Dong, Y. M.; Peng, Y.; Dong, M.; Wang, Y. W. *J. Org. Chem.* **2011**, *76*, 6962.
- (351) Lou, B.; Chen, Z. Q.; Bian, Z. Q.; Huang, C. H. *New J. Chem.* **2010**, *34*, 132.
- (352) Liu, J. L.; Liu, Y.; Liu, Q.; Li, C. Y.; Sun, L. N.; Li, F. Y. *J. Am. Chem. Soc.* **2011**, *133*, 15276.
- (353) Yao, L. M.; Zhou, J.; Liu, J. L.; Feng, W.; Li, F. Y. *Adv. Funct. Mater.* **2012**, DOI: 10.1002/adfm.201102981.
- (354) Ekmekci, Z.; Yilmaz, M. D.; Akkaya, E. U. *Org. Lett.* **2008**, *10*, 461.
- (355) Lv, X.; Liu, J.; Liu, Y. L.; Zhao, Y.; Chen, M. L.; Wang, P.; Guo, W. *Sens. Actuators, B* **2011**, *158*, 405.
- (356) Li, H. D.; Li, B.; Jin, L. Y.; Kan, Y. H.; Yin, B. Z. *Tetrahedron* **2011**, *67*, 7348.
- (357) Chung, Y. M.; Raman, B.; Kim, D. S.; Ahn, K. H. *Chem. Commun.* **2006**, *42*, 186.
- (358) Kwon, S. K.; Kou, S.; Kim, H. N.; Chen, X. Q.; Hwang, H.; Nam, S. W.; Kim, S. H.; Swamy, K. M. K.; Park, S.; Yoon, J. Y. *Tetrahedron Lett.* **2008**, *49*, 4102.
- (359) Lee, K. S.; Kim, H. J.; Kim, G. H.; Shin, I.; Hong, J. I. *Org. Lett.* **2008**, *10*, 49.
- (360) Kim, H. J.; Ko, K. C.; Lee, J. H.; Lee, J. Y.; Kim, J. S. *Chem. Commun.* **2011**, *47*, 2886.
- (361) Ren, J. Q.; Zhu, W. H.; Tian, H. *Talanta* **2008**, *75*, 760.
- (362) Lee, J. H.; Jeong, A. R.; Shin, I. S.; Kim, H. J.; Hong, J. I. *Org. Lett.* **2010**, *12*, 764.
- (363) Badugu, R.; Lakowicz, J. R.; Geddes, C. D. *Anal. Biochem.* **2004**, *327*, 82.
- (364) Badugu, R.; Lakowicz, J. R.; Geddes, C. D. *Dyes Pigm.* **2005**, *64*, 49.
- (365) Palomares, E.; Martínez-Díaz, M. V.; Torres, T.; Coronado, E. *Adv. Funct. Mater.* **2006**, *16*, 1166.
- (366) Kim, Y. M.; Zhao, H. Y.; Gabba, F. P. *Angew. Chem., Int. Ed.* **2009**, *48*, 4957.
- (367) Chiu, C. W.; Kim, Y.; Gabbai, F. P. *J. Am. Chem. Soc.* **2009**, *131*, 60.
- (368) Jung, H. S.; Han, J. H.; Kim, Z. H.; Kang, C.; Kim, J. S. *Org. Lett.* **2011**, *13*, 5056.
- (369) Seiler, J. P. *Mutat. Res.* **1989**, *224*, 219.
- (370) Choi, M. G.; Cha, S.; Park, J. E.; Lee, H.; Jeon, H. L.; Chang, S.-K. *Org. Lett.* **2010**, *12*, 1468.
- (371) Dickinson, B. C.; Srikun, D.; Chang, C. *J. Curr. Opin. Chem. Biol.* **2010**, *14*, 50.
- (372) Zhang, W.; Wang, T. G.; Qin, L. Y.; Gao, H. M.; Wilson, B.; Ali, S. F.; Zhang, W. Q.; Hong, J. S.; Liu, B. *FASEB J.* **2004**, *18*, 589.
- (373) Andersen, J. K. *Nat. Med.* **2004**, *10* (Suppl), S18.
- (374) Barnham, K. J.; Masters, C. L.; Bush, A. I. *Nat. Rev. Drug Discovery* **2004**, *3*, 205.
- (375) Wood, Z. A.; Poole, L. B.; Karplus, P. A. *Science* **2003**, *300*, 650.
- (376) Woo, H. A.; Chae, H. Z.; Hwang, S. C.; Yang, K. S.; Kang, S. W.; Kim, K.; Rhee, S. G. *Science* **2003**, *300*, 653.
- (377) Budanov, A. V.; Sablina, A. A.; Feinstein, E.; Koonin, E. V.; Chumakov, P. M. *Science* **2004**, *304*, 596.
- (378) Paulsen, C. E.; Carroll, K. S. *ACS Chem. Biol.* **2010**, *5*, 47.
- (379) Chang, M. C. Y.; Pralle, A.; Isacoff, E. Y.; Chang, C. *J. Am. Chem. Soc.* **2004**, *126*, 15392.
- (380) Miller, E. W.; Albers, A. E.; Pralle, A.; Isacoff, E. Y.; Chang, C. *J. Am. Chem. Soc.* **2005**, *127*, 16652.
- (381) Albers, A. E.; Dickinson, B. C.; Miller, E. W.; Chang, C. *J. Bioorg. Med. Chem. Lett.* **2008**, *18*, 5948.
- (382) Srikun, D.; Albers, A. E.; Chang, C. *J. Chem. Sci.* **2011**, *2*, 1156.
- (383) Albers, A. E.; Okreglak, V. S.; Chang, C. *J. Am. Chem. Soc.* **2006**, *128*, 9640.
- (384) Miller, E. W.; Tulyathan, O.; Isacoff, E. Y.; Chang, C. *J. Nat. Chem. Biol.* **2007**, *3*, 263.
- (385) Dickinson, B. C.; Huynh, C.; Chang, C. *J. Am. Chem. Soc.* **2010**, *132*, 5906.
- (386) Dickinson, B. C.; Tang, Y.; Chang, Z. Y.; Chang, C. *J. Chem. Biol.* **2011**, *18*, 943.

- (387) Du, L. P.; Ni, N. T.; Li, M. Y.; Wang, B. H. *Tetrahedron Lett.* **2010**, *51*, 1152.
- (388) Lippert, A. R.; Gschneidner, T.; Chang, C. J. *Chem. Commun.* **2010**, *46*, 7510.
- (389) Srikun, D.; Albers, A. E.; Nam, C. I.; Iavarone, A. T.; Chang, C. J. *J. Am. Chem. Soc.* **2010**, *132*, 4455.
- (390) Dickinson, B. C.; Chang, C. J. *J. Am. Chem. Soc.* **2008**, *130*, 9638.
- (391) Yuan, L.; Lin, W. Y.; Xie, Y. N.; Chen, B.; Zhu, S. S. *J. Am. Chem. Soc.* **2012**, *134*, 1305.
- (392) Lo, L. C.; Chu, C. Y. *Chem. Commun.* **2003**, *39*, 2728.
- (393) Srikun, D.; Miller, E. W.; Domaille, D. W.; Chang, C. J. *J. Am. Chem. Soc.* **2008**, *130*, 4596.
- (394) Chung, C.; Srikun, D.; Lim, C. S.; Chang, C. J.; Cho, B. R. *Chem. Commun.* **2011**, *47*, 9618.
- (395) Karton Lifshin, N.; Segal, E.; Omer, L.; Portnoy, M.; Satchi Fainaro, R.; Shabat, D. *J. Am. Chem. Soc.* **2011**, *133*, 10960.
- (396) Maeda, H.; Fukuyasu, Y.; Yoshida, S.; Fukuda, M.; Saeki, K.; Matsuno, H.; Yamauchi, Y.; Yoshida, K.; Hirata, K.; Miyamoto, K. *Angew. Chem., Int. Ed.* **2004**, *43*, 2389.
- (397) Xu, K. H.; Tang, B.; Huang, H.; Yang, G. W.; Chen, Z. Z.; Li, P.; An, L. G. *Chem. Commun.* **2005**, *48*, 5974.
- (398) Xu, K. H.; Liu, F.; Wang, H. X.; Wang, S. S.; Wang, L. L.; Tang, B. *Sci. China, Ser. B* **2009**, *52*, 734.
- (399) Sawaki, Y.; Foote, C. S. *J. Am. Chem. Soc.* **1979**, *101*, 6292.
- (400) Abo, M.; Urano, Y.; Hanaoka, K.; Terai, T.; Komatsu, T.; Nagano, T. *J. Am. Chem. Soc.* **2011**, *133*, 10629.
- (401) Onoda, M.; Tokuyama, H.; Uchiyama, S.; Mawatari, K. I.; Santa, T.; Kaneko, K.; Imai, K.; Nakagomi, K. *Chem. Commun.* **2005**, *41*, 1848.
- (402) Soh, N.; Sakaway, O.; Makihara, K.; Odo, Y.; Fukaminato, T.; Kawai, T.; Irie, M.; Imato, T. *Bioorg. Med. Chem.* **2005**, *13*, 1131.
- (403) Onoda, M.; Uchiyama, S.; Endo, A.; Tokuyama, H.; Santa, T.; Imai, K. *Org. Lett.* **2003**, *5*, 1459.
- (404) Ye, Z. Q.; Chen, J. X.; Wang, G. L.; Yuan, J. L. *Anal. Chem.* **2011**, *83*, 4163.
- (405) Hitomi, Y.; Takeyasu, T.; Funabiki, T.; Kodera, M. *Anal. Chem.* **2011**, *83*, 9213.
- (406) Kettle, A. J.; Winterburn, C. C. *Redox Rep.* **1997**, *3*, 3.
- (407) Yap, Y. W.; Whiteman, M.; Cheung, N. S. *Cell. Signalling* **2007**, *19*, 219.
- (408) Chen, S. M.; Lu, J. X.; Sun, C. D.; Ma, H. M. *Analyst* **2010**, *135*, 577.
- (409) Zhang, W. J.; Guo, C.; Liu, L. H.; Qin, J. G.; Yang, C. L. *Org. Biomol. Chem.* **2011**, *9*, 5560.
- (410) Sun, Z. N.; Liu, F. Q.; Chen, Y.; Tam, P. K. H.; Yang, D. *Org. Lett.* **2008**, *10*, 2171.
- (411) Khurana, J. M.; Ray, A.; Sahoo, P. K. *Bull. Chem. Soc. Jpn.* **1994**, *67*, 1091.
- (412) Lin, W. Y.; Long, L. L.; Chen, B. B.; Tan, W. *Chem.—Eur. J.* **2009**, *15*, 2305.
- (413) Cheng, X. H.; Jia, H. Z.; Long, T.; Feng, J.; Qin, J. G.; Li, Z. *Chem. Commun.* **2011**, *47*, 11978.
- (414) Zhao, N.; Wu, Y. H.; Wang, R. M.; Shi, L. X.; Chen, Z. N. *Analyst* **2011**, *136*, 2277.
- (415) Yuan, L.; Lin, W. Y.; Song, J. Z.; Yang, Y. T. *Chem. Commun.* **2011**, *47*, 12691.
- (416) Kenmoku, S.; Urano, Y.; Kojima, H.; Nagano, T. *J. Am. Chem. Soc.* **2007**, *129*, 7313.
- (417) Koide, Y.; Urano, Y.; Hanaoka, K.; Terai, T.; Nagano, T. *J. Am. Chem. Soc.* **2011**, *133*, 5680.
- (418) Yang, Y. K.; Cho, H. J.; Lee, J.; Shin, I.; Tae, J. *Org. Lett.* **2009**, *11*, 859.
- (419) Zhan, X. Q.; Yan, J. H.; Su, J. H.; Wang, Y. C.; He, J.; Wang, S. Y.; Zheng, H.; Xu, J. G. *Sens. Actuators, B* **2010**, *150*, 774.
- (420) Chen, X. Q.; Lee, K. A.; Ha, E. M.; Lee, K. M.; Seo, Y. Y.; Choi, H. K.; Kim, H. N.; Kim, M. J.; Cho, C. S.; Lee, S. Y.; Lee, W. J.; Yoon, J. *Chem. Commun.* **2011**, *47*, 4373.
- (421) Chen, X. Q.; Wang, X. C.; Wang, S. J.; Shi, W.; Wang, K.; Ma, H. M. *Chem.—Eur. J.* **2008**, *14*, 4719.
- (422) Koide, Y.; Urano, Y.; Kenmoku, S.; Kojima, H.; Nagano, T. *J. Am. Chem. Soc.* **2007**, *129*, 10324.
- (423) Kang, P.; Foote, C. S. *J. Am. Chem. Soc.* **2002**, *124*, 4865.
- (424) Davies, M. J. *Biochem. Biophys. Res. Commun.* **2003**, *305*, 761.
- (425) Steinbeck, M. J.; Khan, A. U.; Karnovsky, M. J. *J. Biol. Chem.* **1992**, *267*, 13425.
- (426) Umezawa, N.; Tanaka, K.; Urano, Y.; Kikuchi, K.; Higuchi, T.; Nagano, T. *Angew. Chem., Int. Ed.* **1999**, *38*, 2899.
- (427) Tanaka, K.; Miura, T.; Umezawa, N.; Urano, Y.; Kikuchi, K.; Higuchi, T.; Nagano, T. *J. Am. Chem. Soc.* **2001**, *123*, 2530.
- (428) Zhang, G. X.; Li, X. H.; Ma, H. M.; Zhang, D. Q.; Li, J.; Zhu, D. B. *Chem. Commun.* **2004**, *40*, 2072.
- (429) Li, X. H.; Zhang, G. X.; Ma, H. M.; Zhang, D. Q.; Li, J.; Zhu, D. B. *J. Am. Chem. Soc.* **2004**, *126*, 11543.
- (430) Zheng, X. P.; Sun, S. N.; Zhang, D. Q.; Ma, H. M.; Zhu, D. B. *Anal. Chim. Acta* **2006**, *575*, 62.
- (431) Song, B.; Wang, G. L.; Tan, M. Q.; Yuan, J. L. *J. Am. Chem. Soc.* **2006**, *128*, 13442.
- (432) Song, B.; Wang, G. L.; Yuan, J. L. *Chem. Commun.* **2005**, *41*, 3553.
- (433) Tan, M. Q.; Song, B.; Wang, G. L.; Yuan, J. L. *Free Radical Biol. Med.* **2006**, *40*, 1644.
- (434) Liu, Y. J.; Wang, K. Z. *Eur. J. Inorg. Chem.* **2008**, *2008*, 5214.
- (435) Xu, K. H.; Wang, L. L.; Qiang, M. M.; Wang, L. Y.; Li, P.; Tang, B. *Chem. Commun.* **2011**, *47*, 7386.
- (436) Chaudhury, S.; Sarkar, P. K. *Biochim. Biophys. Acta* **1983**, *763*, 93.
- (437) Kozumbo, W. J.; Trush, M. A.; Kensler, T. W. *Chem.-Biol. Interact.* **1985**, *54*, 199.
- (438) Zhao, H. T.; Kalivendi, S.; Zhang, H.; Joseph, J.; Nithipatikom, K.; Vásquez Vivar, J.; Kalyanaraman, B. *Free Radical Biol. Med.* **2003**, *34*, 1359.
- (439) Zhao, H. T.; Joseph, J.; Fales, H. M.; Sokoloski, E. A.; Levine, R. L.; Vasquez Vivar, J.; Kalyanaraman, B. *Proc. Natl. Acad. Sci. U.S.A.* **2005**, *102*, 5727.
- (440) Robinson, K. M.; Janes, M. S.; Pehar, M.; Monette, J. S.; Ross, M. F.; Hagen, T. M.; Murphy, M. P.; Beckman, J. S. *Proc. Natl. Acad. Sci. U.S.A.* **2006**, *103*, 15038.
- (441) Tang, B.; Zhang, L.; Hu, J. X.; Li, P.; Zhang, H.; Zhao, Y. X. *Anal. Chim. Acta* **2004**, *502*, 125.
- (442) Tang, B.; Zhang, L.; Zhang, L. L. *Anal. Biochem.* **2004**, *326*, 176.
- (443) Gao, J. J.; Xu, K. H.; Tang, B.; Yin, L. L.; Yang, G. W.; An, L. G. *FEBS J.* **2007**, *274*, 1725.
- (444) Kundu, K.; Knight, S. F.; Willett, N.; Lee, S.; Taylor, W. R.; Murthy, N. *Angew. Chem., Int. Ed.* **2009**, *48*, 299.
- (445) Medvedeva, N.; Martin, V. V.; Weis, A. L.; Likhtenshten, G. I. *J. Photochem. Photobiol. A* **2004**, *163*, 45.
- (446) Maeda, H.; Yamamoto, K.; Nomura, Y.; Kohno, I.; Hafsi, L.; Ueda, N.; Yoshida, S.; Fukuda, M.; Fukuyasu, Y.; Yamauchi, Y.; Itoh, N. *J. Am. Chem. Soc.* **2005**, *127*, 68.
- (447) Maeda, H.; Yamamoto, K.; Kohno, I.; Hafsi, L.; Itoh, N.; Nakagawa, S.; Kanagawa, N.; Suzuki, K.; Uno, T. *Chem.—Eur. J.* **2007**, *13*, 1946.
- (448) Xu, K. H.; Liu, X.; Tang, B.; Yang, G. W.; Yang, Y.; An, L. G. *Chem.—Eur. J.* **2007**, *13*, 1411.
- (449) Xu, K. H.; Liu, X.; Tang, B. *ChemBioChem* **2007**, *8*, 453.
- (450) Yang, X. F.; Guo, X. Q. *Anal. Chim. Acta* **2001**, *434*, 169.
- (451) Yang, X. F.; Guo, X. Q. *Analyst* **2001**, *126*, 1800.
- (452) Maki, T.; Soh, N.; Fukaminato, T.; Nakajima, H.; Nakano, K.; Imato, T. *Anal. Chim. Acta* **2009**, *639*, 78.
- (453) Li, P.; Xie, T.; Duan, X.; Yu, F. B.; Wang, X.; Tang, B. *Chem.—Eur. J.* **2010**, *16*, 1834.
- (454) Yapici, N. B.; Jockusch, S.; Moscatelli, A.; Mandalapu, S. R.; Itagaki, Y.; Bates, D. K.; Wiseman, S.; Gibson, K. M.; Turro, N. J.; Bi, L. *Org. Lett.* **2012**, *14*, 50.

- (455) Soh, N.; Makihara, K.; Sakoda, E.; Imato, T. *Chem. Commun.* **2004**, *40*, 496.
- (456) Tang, B.; Zhang, N.; Chen, Z.; Xu, K.; Zhuo, L.; An, L.; Yang, G. *Chem.—Eur. J.* **2008**, *14*, 522.
- (457) Soh, N.; Makihara, K.; Ariyoshi, T.; Seto, D.; Maki, T.; Nakajima, H.; Nakano, K.; Imato, T. *Anal. Sci.* **2008**, *24*, 293.
- (458) Perry, C. C.; Tang, V. J.; Konigsfeld, K. M.; Aguilera, J. A.; Milligan, J. R. *J. Phys. Chem. B* **2011**, *115*, 9889.
- (459) Page, S. E.; Wilke, K. T.; Pierre, V. C. *Chem. Commun.* **2010**, *46*, 2423.
- (460) Babior, B. M.; Takeuchi, C.; Ruedi, J.; Gutierrez, A.; Wentworth, P. *Proc. Natl. Acad. Sci. U.S.A.* **2003**, *100*, 3031.
- (461) Garner, A. L.; Croix, C. M.; St; Pitt, B. R.; Leikauf, G. D.; Ando, S.; Koide, K. *Nat. Chem.* **2009**, *1*, 316.
- (462) Schafer, F. Q.; Buettner, G. R. *Free Radical Biol. Med.* **2001**, *30*, 1191.
- (463) Liu, Y.; Zhu, M. J.; Xu, J. J.; Zhang, H.; Tian, M. *Analyst* **2011**, *136*, 4316.
- (464) Shinohara, E. T.; Maity, A. *Curr. Mol. Med.* **2009**, *9*, 1034.
- (465) Williams, K. J.; Albertella, M. R.; Fitzpatrick, B.; Loadman, P. M.; Shnyder, S. D.; Chinje, E. C.; Telfer, B. A.; Dunk, C. R.; Harris, P. A.; Stratford, I. *J. Mol. Cancer Ther.* **2009**, *8*, 3266.
- (466) Zhu, W. P.; Dai, M.; Xu, Y. F.; Qian, X. H. *Bioorg. Med. Chem.* **2008**, *16*, 3255.
- (467) Dai, M.; Zhu, W. P.; Xu, Y. F.; Qian, X. H.; Liu, Y.; Xiao, Y.; You, Y. *J. Fluoresc.* **2008**, *18*, 591.
- (468) Cui, L.; Zhong, Y.; Zhu, W. P.; Xu, Y. F.; Du, Q. S.; Wang, X.; Qian, X. H.; Xiao, Y. *Org. Lett.* **2011**, *13*, 928.
- (469) Kiyose, K.; Hanaoka, K.; Oushiki, D.; Nakamura, T.; Kajimura, M.; Suematsu, M.; Nishimatsu, H.; Yamane, T.; Terai, T.; Hirata, Y.; Nagano, T. *J. Am. Chem. Soc.* **2010**, *132*, 15846.
- (470) Bove, P. F.; van der Vliet, A. *Free Radical Bio. Med.* **2006**, *41*, 515.
- (471) Furchtgott, R. F. *Angew. Chem., Int. Ed.* **1999**, *38*, 1870.
- (472) Ignarro, L. J. *Angew. Chem., Int. Ed.* **1999**, *38*, 1882.
- (473) Murad, F. *Angew. Chem., Int. Ed.* **1999**, *38*, 1857.
- (474) Moncada, S.; Palmer, R. M.; Higgs, E. A. *Pharmacol. Rev.* **1991**, *43*, 109.
- (475) Conner, E. M.; Grisham, M. B. *Methods* **1995**, *7*, 3.
- (476) Nagano, T.; Yoshimura, T. *Chem. Rev.* **2002**, *102*, 1235.
- (477) Miller, E. W.; Chang, C. J. *Curr. Opin. Chem. Biol.* **2007**, *11*, 620.
- (478) McQuade, L. E.; Lippard, S. J. *Curr. Opin. Chem. Biol.* **2010**, *14*, 43.
- (479) Suzuki, N.; Kojima, H.; Urano, Y.; Kikuchi, K.; Hirata, Y.; Nagano, T. *J. Biol. Chem.* **2002**, *277*, 47.
- (480) Kojima, H.; Nakatsubo, N.; Kikuchi, K.; Kawahara, S.; Kirino, Y.; Nagoshi, H.; Hirata, Y.; Nagano, T. *Anal. Chem.* **1998**, *70*, 2446.
- (481) Itoh, Y.; Ma, F. H.; Hoshi, H.; Oka, M.; Noda, K.; Ukai, Y.; Kojima, H.; Nagano, T.; Toda, N. *Anal. Biochem.* **2000**, *287*, 203.
- (482) Kojima, H.; Hirotani, M.; Nakatsubo, N.; Kikuchi, K.; Urano, Y.; Higuchi, T.; Hirata, Y.; Nagano, T. *Anal. Chem.* **2001**, *73*, 1967.
- (483) Gabe, Y.; Urano, Y.; Kikuchi, K.; Kojima, H.; Nagano, T. *J. Am. Chem. Soc.* **2004**, *126*, 3357.
- (484) Gabe, Y.; Ueno, T.; Urano, Y.; Kojima, H.; Nagano, T. *Anal. Bioanal. Chem.* **2006**, *386*, 621.
- (485) Hu, J. X.; Yin, L. L.; Xu, K. H.; Gao, J. J.; Tong, L. L.; Tang, B. *Anal. Chim. Acta* **2008**, *606*, 57.
- (486) Heiduschka, P.; Thanos, S. *Neuroreport* **1998**, *9*, 4051.
- (487) Galindo, F.; Kabir, N.; Gavrilovic, J.; Russell, D. A. *Photochem. Photobio. Sci.* **2008**, *7*, 126.
- (488) Sasaki, E.; Kojima, H.; Nishimatsu, H.; Urano, Y.; Kikuchi, K.; Hirata, Y.; Nagano, T. *J. Am. Chem. Soc.* **2005**, *127*, 3684.
- (489) Zhang, R.; Ye, Z. Q.; Wang, G. L.; Zhang, W. Z.; Yuan, J. L. *Chem.—Eur. J.* **2010**, *16*, 6884.
- (490) Yang, Y. J.; Seidlits, S. K.; Adams, M. M.; Lynch, V. M.; Schmidt, C. E.; Anslyn, E. V.; Shear, J. B. *J. Am. Chem. Soc.* **2010**, *132*, 13114.
- (491) Zheng, H.; Shang, G. Q.; Yang, S. Y.; Gao, X.; Xu, J. G. *Org. Lett.* **2008**, *10*, 2357.
- (492) Sun, C. D.; Shi, W.; Song, Y. C.; Chen, W.; Ma, H. M. *Chem. Commun.* **2011**, *47*, 8638.
- (493) Hilderbrand, S. A.; Lippard, S. J. *Inorg. Chem.* **2004**, *43*, 4674.
- (494) Franz, K. J.; Singh, N.; Spangler, B.; Lippard, S. J. *Inorg. Chem.* **2000**, *39*, 4081.
- (495) Hilderbrand, S. A.; Lim, M. H.; Lippard, S. J. *J. Am. Chem. Soc.* **2004**, *126*, 4972.
- (496) Lim, M. H.; Lippard, S. J. *Inorg. Chem.* **2004**, *43*, 6366.
- (497) Tsuge, K.; DeRosa, F.; Lim, M. D.; Ford, P. C. *J. Am. Chem. Soc.* **2004**, *126*, 6564.
- (498) Lim, M. H.; Lippard, S. J. *J. Am. Chem. Soc.* **2005**, *127*, 12170.
- (499) Lim, M. H.; Xu, D.; Lippard, S. J. *Nat. Chem. Biol.* **2006**, *2*, 375.
- (500) Lim, M. H.; Wong, B. A.; Pitcock, W. H.; Mokshagundam, D.; Baik, M. H.; Lippard, S. J. *J. Am. Chem. Soc.* **2006**, *128*, 14364.
- (501) McQuade, L. E.; Lippard, S. J. *Inorg. Chem.* **2010**, *49*, 7464.
- (502) McQuade, L. E.; Ma, J.; Lowe, G.; Ghatpande, A.; Gelperin, A.; Lippard, S. J. *Proc. Natl. Acad. Sci. U.S.A.* **2010**, *107*, 8525.
- (503) Pluth, M. D.; Chan, M. R.; McQuade, L. E.; Lippard, S. J. *Inorg. Chem.* **2011**, *50*, 9385.
- (504) Pluth, M. D.; McQuade, L. E.; Lippard, S. J. *Org. Lett.* **2010**, *12*, 2318.
- (505) Hu, X. Y.; Wang, J.; Zhu, X.; Dong, D. P.; Zhang, X. L.; Wu, S. O.; Duan, C. Y. *Chem. Commun.* **2011**, *47*, 11507.
- (506) Tennyson, A. G.; Do, L.; Smith, R. C.; Lippard, S. J. *Polyhedron* **2007**, *26*, 4625.
- (507) Rosenthal, J.; Lippard, S. J. *J. Am. Chem. Soc.* **2010**, *132*, 5536.
- (508) Pacher, P.; Beckman, J. S.; Liaudet, L. *Physiol. Rev.* **2007**, *87*, 315.
- (509) Yang, D.; Tang, Y. C.; Chen, J.; Wang, X. C.; Bartberger, M. D.; Houk, K. N.; Olson, L. *J. Am. Chem. Soc.* **1999**, *121*, 11976.
- (510) Yang, D.; Wang, H. L.; Sun, Z. N.; Chung, N. W.; Shen, J. G. *J. Am. Chem. Soc.* **2006**, *128*, 6004.
- (511) Sun, Z. N.; Wang, H. L.; Liu, F. Q.; Chen, Y.; Tam, P. K. H.; Yang, D. *Org. Lett.* **2009**, *11*, 1887.
- (512) Peng, T.; Yang, D. *Org. Lett.* **2010**, *12*, 4932.
- (513) Yu, F. B.; Li, P.; Li, G. Y.; Zhao, G. J.; Chu, T. S.; Han, K. L. *J. Am. Chem. Soc.* **2011**, *133*, 11030.
- (514) Xu, K.; Chen, H.; Tian, J.; Ding, B.; Xie, Y.; Qiang, M.; Tang, B. *Chem. Commun.* **2011**, *47*, 9468.
- (515) Tian, J. W.; Chen, H. C.; Zhuo, L. H.; Xie, Y. X.; Li, N.; Tang, B. *Chem.—Eur. J.* **2011**, *17*, 6626.
- (516) Ueno, T.; Urano, Y.; Kojima, H.; Nagano, T. *J. Am. Chem. Soc.* **2006**, *128*, 10640.
- (517) Philips, S.; Laanbroek, H. J.; Verstraete, W. *Origins Rev. Environ. Sci. Biotechnol.* **2002**, *1*, 115.
- (518) Ghosh, A.; Das, P.; Saha, S.; Banerjee, T.; Bhatt, H. B.; Das, A. *Inorg. Chim. Acta* **2011**, *372*, 115.
- (519) Dey, R.; Chatterjee, T.; Ranu, B. C. *Tetrahedron Lett.* **2011**, *52*, 461.
- (520) Seth, D.; Stamler, J. S. *Curr. Opin. Chem. Biol.* **2011**, *15*, 129.
- (521) Li, L.; Rose, P.; Moore, P. K. *Annu. Rev. Pharmacol. Toxicol.* **2011**, *51*, 169.
- (522) Rahman, I.; MacNee, W. *Free Radical Biol. Med.* **2000**, *28*, 1405.
- (523) Ros-Lis, J. V.; García, B.; Jiménez, D.; Martínez-Máñez, R.; Sancenón, F.; Soto, J.; Gonzalvo, F.; Valldecabres, M. C. *J. Am. Chem. Soc.* **2004**, *126*, 4064.
- (524) Sreejith, S.; Divya, K. P.; Ajayaghosh, A. *Angew. Chem., Int. Ed.* **2008**, *47*, 7883.
- (525) Clark, J. H. *Chem. Rev.* **1980**, *80*, 429.
- (526) Lin, W. Y.; Yuan, L.; Cao, Z. C.; Feng, Y. M.; Long, L. L. *Chem.—Eur. J.* **2009**, *15*, 5096.
- (527) Kim, G. J.; Lee, K.; Kwon, H.; Kim, H. J. *Org. Lett.* **2011**, *13*, 2799.
- (528) Ha, H. J.; Yoon, D. H.; Park, S.; Kim, H. J. *Tetrahedron* **2011**, *67*, 7759.
- (529) Lim, S. Y.; Lee, S.; Park, S. B.; Kim, H. J. *Tetrahedron Lett.* **2011**, *S2*, 3902.

- (530) Du, J.; Yang, Z.; Qi, H. P.; Yang, X. F. *Luminescence* **2011**, *26*, 486.
- (531) Yi, L.; Li, H. Y.; Sun, L.; Liu, L. L.; Zhang, C. H.; Xi, Z. *Angew. Chem., Int. Ed.* **2009**, *48*, 4034.
- (532) Matsumoto, T.; Urano, Y.; Shoda, T.; Kojima, H.; Nagano, T. *Org. Lett.* **2007**, *9*, 3375.
- (533) Weh, J.; Duerkop, A.; Wolfbeis, O. S. *ChemBioChem* **2007**, *8*, 122.
- (534) Lo, K. K. W.; Hui, W. K.; Ng, D. C. M.; Cheung, K. K. *Inorg. Chem.* **2002**, *41*, 40.
- (535) Chen, X. Q.; Ko, S. K.; Kim, M. J.; Shin, I.; Yoon, J. Y. *Chem. Commun.* **2010**, *46*, 2751.
- (536) Lo, K. K. W.; Ng, D. C. M.; Chung, C. K. *Organometallics* **2001**, *20*, 4999.
- (537) Wang, S. P.; Deng, W. J.; Sun, D.; Yan, M.; Zheng, H.; Xu, J. G. *Org. Biomol. Chem.* **2009**, *7*, 4017.
- (538) Li, X.; Qian, S. J.; He, Q. J.; Yang, B.; Li, J.; Hu, Y. Z. *Org. Biomol. Chem.* **2010**, *8*, 3627.
- (539) Zhao, C. C.; Zhou, Y.; Lin, Q. N.; Zhu, L. Y.; Feng, P.; Zhang, Y. L.; Cao, J. *J. Phys. Chem. B* **2011**, *115*, 642.
- (540) Lan, M. H.; Wu, J. S.; Liu, W. M.; Zhang, H. Y.; Zhang, W. J.; Zhuang, X. Q.; Wang, P. F. *Sens. Actuators, B* **2011**, *156*, 332.
- (541) Jiang, W.; Fu, Q. Q.; Fan, H. Y.; Ho, J.; Wang, W. *Angew. Chem., Int. Ed.* **2007**, *46*, 8445.
- (542) Bouffard, J.; Kim, Y.; Swager, T. M.; Weissleder, R.; Hilderbrand, S. A. *Org. Lett.* **2008**, *10*, 37.
- (543) Ji, S. M.; Guo, H. M.; Yuan, X. L.; Li, X. H.; Ding, H. D.; Gao, P.; Zhao, C. X.; Wu, W. T.; Wu, W. H.; Zhao, J. Z. *Org. Lett.* **2010**, *12*, 2876.
- (544) Lin, W. Y.; Long, L. L.; Tan, W. *Chem. Commun.* **2010**, *46*, 1503.
- (545) Yang, X. F.; Su, Z.; Liu, C. H.; Qi, H. P.; Zhao, M. L. *Anal. Bioanal. Chem.* **2010**, *396*, 2667.
- (546) Zhu, B. C.; Zhang, X. L.; Li, Y. M.; Wang, P. F.; Zhang, H. Y.; Zhuang, X. Q. *Chem. Commun.* **2010**, *46*, 5710.
- (547) Lim, C. S.; Masanta, G.; Kim, H. J.; Han, J. H.; Kim, H. M.; Cho, B. R. *J. Am. Chem. Soc.* **2011**, *133*, 11132.
- (548) Lee, J. H.; Lim, C. S.; Tian, Y. S.; Han, J. H.; Cho, B. R. *J. Am. Chem. Soc.* **2010**, *132*, 1216.
- (549) Lee, M. H.; Han, J. H.; Kwon, P. S.; Bhuniya, S.; Kim, J. Y.; Sessler, J. L.; Kang, C.; Kim, J. S. *J. Am. Chem. Soc.* **2012**, *134*, 1316.
- (550) Tang, B.; Xing, Y. L.; Li, P.; Zhang, N.; Yu, F. B.; Yang, G. W. *J. Am. Chem. Soc.* **2007**, *129*, 11666.
- (551) Tang, B.; Yin, L. L.; Wang, X.; Chen, Z. Z.; Tong, L. L.; Xu, K. H. *Chem. Commun.* **2009**, *45*, 5293.
- (552) Dawson, P. E.; Muir, T. W.; Clarklewis, I.; Kent, S. B. H. *Science* **1994**, *266*, 776.
- (553) Long, L. L.; Lin, W. Y.; Chen, B. B.; Gao, W. S.; Yuan, L. *Chem. Commun.* **2011**, *47*, 893.
- (554) Cao, X. W.; Lin, W. Y.; Yu, Q. X. *J. Org. Chem.* **2011**, *76*, 7423.
- (555) Jung, H. S.; Han, J. H.; Habata, Y.; Kang, C.; Kim, J. S. *Chem. Commun.* **2011**, *47*, 5142.
- (556) Dang, D. T.; Chen, F.; Kohli, M.; Rago, C.; Cummins, J. M.; Dang, L. H. *Cancer Res.* **2005**, *65*, 9485.
- (557) Fujikawa, Y.; Urano, Y.; Komatsu, T.; Hanaoka, K.; Kojima, H.; Terai, T.; Inoue, H.; Nagano, T. *J. Am. Chem. Soc.* **2008**, *130*, 14533.
- (558) Shahrokhian, S. *Anal. Chem.* **2001**, *73*, 5972.
- (559) Refsum, H.; Ueland, P. M.; Nygard, O.; Vollset, S. E. *Annu. Rev. Med.* **1998**, *49*, 31.
- (560) van Meurs, J. B. J.; Dhonukshe-Rutten, R. A. M.; Pluijm, S. M. F.; van der Klift, M.; de Jonge, R.; Lindemans, J.; de Groot, L. C. P. G. M.; Hofman, A.; Witteman, J. C. M.; van Leeuwen, J. P. T. M.; Breteler, M. M. B.; Lips, P.; Pols, H. A. P.; Uitterlinden, A. G. N. *Engl. J. Med.* **2004**, *350*, 2033.
- (561) Tanaka, F.; Mase, N.; Barbas, C. F., III *Chem. Commun.* **2004**, *40*, 1762.
- (562) Lee, K. S.; Kim, T. K.; Lee, J. H.; Kim, H. J.; Hong, J. I. *Chem. Commun.* **2008**, *44*, 6173.
- (563) Zhang, X. J.; Ren, X. S.; Xu, Q. H.; Loh, K. P.; Chen, Z. K. *Org. Lett.* **2009**, *11*, 1257.
- (564) Hu, M. M.; Fan, J. L.; Li, H. L.; Song, K. D.; Wang, S.; Cheng, G. H.; Peng, X. *Org. Biomol. Chem.* **2011**, *9*, 980.
- (565) Yuan, L.; Lin, W. Y.; Yang, Y. T. *Chem. Commun.* **2011**, *47*, 6275.
- (566) Zhang, M.; Li, M. Y.; Zhao, Q.; Li, F. Y.; Zhang, D. Q.; Zhang, J. P.; Yi, T.; Huang, C. H. *Tetrahedron Lett.* **2007**, *48*, 2329.
- (567) Zhang, M. Doctoral thesis, Fudan University, 2007.
- (568) Xiong, L. Q.; Zhao, Q.; Chen, H. L.; Wu, Y. B.; Dong, Z. S.; Zhou, Z. G.; Li, F. Y. *Inorg. Chem.* **2010**, *49*, 6402.
- (569) Ma, Y.; Liu, S. J.; Yang, H. R.; Wu, Y. Q.; Yang, C. J.; Liu, X. M.; Zhao, Q.; Wu, H. Z.; Liang, J. C.; Li, F. Y.; Huang, W. *J. Mater. Chem.* **2011**, *21*, 18974.
- (570) Huang, K. W.; Yang, H.; Zhou, Z. G.; Chen, H. L.; Li, F. Y.; Yi, T.; Huang, C. H. *Inorg. Chim. Acta* **2009**, *362*, 2577.
- (571) Li, M. J.; Zhan, C. Q.; Nie, M. J.; Chen, G. N.; Chen, X. J. *Inorg. Biochem.* **2011**, *105*, 420.
- (572) Chen, H. L.; Zhao, Q.; Wu, Y. B.; Li, F. Y.; Yang, H.; Yi, T.; Huang, C. H. *Inorg. Chem.* **2007**, *46*, 11075.
- (573) Zhang, M.; Yu, M. X.; Li, F. Y.; Zhu, M. W.; Li, M. Y.; Gao, Y. H.; Li, L.; Liu, Z. Q.; Zhang, J. P.; Zhang, D. Q.; Yi, T.; Huang, C. H. *J. Am. Chem. Soc.* **2007**, *129*, 10322.
- (574) Jung, H. S.; Ko, K. C.; Kim, G. H.; Lee, A. R.; Na, Y. C.; Kang, C.; Lee, J. Y.; Kim, J. S. *Org. Lett.* **2011**, *13*, 1498.
- (575) Sun, Y. Q.; Chen, M. L.; Liu, J.; Lv, X.; Li, J. F.; Guo, W. *Chem. Commun.* **2011**, *47*, 11029.
- (576) Yang, X. F.; Guo, Y. X.; Strongin, R. M. *Angew. Chem., Int. Ed.* **2011**, *50*, 10690.
- (577) Papapetropoulos, A.; Pyriochou, A.; Altaany, Z.; Yang, G.; Marazioti, A.; Zhou, Z.; Jeschke, M. G.; Branski, L. K.; Herndon, D. N.; Wang, R.; Szabó, C. *Proc. Natl. Acad. Sci. U.S.A.* **2009**, *106*, 21972.
- (578) Yang, G.; Wu, L.; Jiang, B.; Yang, B.; Qi, J.; Cao, K.; Meng, Q.; Mustafa, A. K.; Mu, W.; Zhang, S.; Snyder, S. H.; Wang, R. *Science* **2008**, *322*, 587.
- (579) Yang, W.; Yang, G. D.; Jia, X. M.; Wu, L. Y.; Wang, R. *J. Physiol.* **2005**, *569*, 519.
- (580) Kamoun, P.; Belardinelli, M. C.; Chabli, A.; Lallouchi, K.; Chadefaux-Velkemans, B. *Am. J. Med. Genet.* **2003**, *116A*, 310.
- (581) Warenciuc, M. W.; Goodwin, L. R.; Benishin, C. G.; Reiffenstein, R. J.; Francom, D. M.; Taylor, J. D.; Dieken, F. R. *Biochem. Pharmacol.* **1989**, *38*, 973.
- (582) Lippert, A. R.; New, E. J.; Chang, C. *J. Am. Chem. Soc.* **2011**, *133*, 10078.
- (583) Peng, H. J.; Cheng, Y. F.; Dai, C. F.; King, A. L.; Predmore, B. L.; Lefer, D. J.; Wang, B. H. *Angew. Chem., Int. Ed.* **2011**, *50*, 9672.
- (584) Liu, C. R.; Pan, J.; Li, S.; Zhao, Y.; Wu, L. Y.; Berkman, C. E.; Whorton, A. R.; Xian, M. *Angew. Chem., Int. Ed.* **2011**, *50*, 10327.
- (585) Choi, M. G.; Cha, S.; Lee, H.; Jeon, H. L.; Chang, S. K. *Chem. Commun.* **2009**, *47*, 7390.
- (586) Zhang, R.; Yu, X. J.; Yin, Y. J.; Ye, Z. Q.; Wang, G. L.; Yuan, J. L. *Anal. Chim. Acta* **2011**, *691*, 83.
- (587) Sasakura, K.; Hanaoka, K.; Shibuya, N.; Mikami, Y.; Kimura, Y.; Komatsu, T.; Ueno, T.; Terai, T.; Kimura, H.; Naganot, T. *J. Am. Chem. Soc.* **2011**, *133*, 18003.
- (588) Yang, X. F.; Wang, L. P.; Xu, H. M.; Zhao, M. L. *Anal. Chim. Acta* **2009**, *631*, 91.
- (589) Qian, Y.; Karpus, J.; Kabil, O.; Zhang, S. Y.; Zhu, H. L.; Banerjee, R.; Zhao, J.; He, C. *Nat. Commun.* **2011**, *2*, 495.
- (590) Taylor, S. L.; Higley, N. A.; Bush, R. K. *Adv. Food Res.* **1986**, *30*, 1.
- (591) Vally, H.; Misso, N. L. A.; Madan, V. *Clin. Exp. Allergy* **2009**, *39*, 1643.
- (592) Choi, M. G.; Hwang, J.; Eor, S.; Chang, S. K. *Org. Lett.* **2010**, *12*, 5624.
- (593) Gu, X. F.; Liu, C. H.; Zhu, Y. C.; Zhu, Y. Z. *J. Agric. Food Chem.* **2011**, *59*, 11935.
- (594) McFeters, R. F. *J. Food. Prot.* **1998**, *61*, 885.

- (595) Yang, X. F.; Zhao, M. L.; Wang, G. *Sens. Actuators, B* **2011**, 152, 8.
- (596) Chen, K. Y.; Guo, Y.; Lu, Z. H.; Yang, B. Q.; Shi, Z. *Chin. J. Chem.* **2010**, 28, 55.
- (597) Hill, A. A.; Lipert, R. J.; Porter, M. D. *Talanta* **2010**, 80, 1606.
- (598) Mohammadpoor-Baltork, I.; Sadeghi, M. M.; Esmayilpour, K. *Synth. Commun.* **2003**, 33, 953.
- (599) Eor, S.; Hwang, J.; Choi, M. G.; Chang, S. K. *Org. Lett.* **2011**, 13, 370.
- (600) Ikeda, A.; Shinkai, S. *Chem. Rev.* **1997**, 97, 1713.
- (601) Danil de Namor, A. F. D.; Cleverly, R. M.; Zapata Ormachea, M. L. *Chem. Rev.* **1998**, 98, 2495.
- (602) Zhang, S. W.; Swager, T. M. *J. Am. Chem. Soc.* **2003**, 125, 3420.
- (603) Dale, T. J.; Rebek, J. *J. Am. Chem. Soc.* **2006**, 128, 4500.
- (604) Weerasinghe, A. J.; Schrniesing, C.; Sinn, E. *Tetrahedron* **2011**, 67, 2833.
- (605) Kang, S.; Kim, S.; Yang, Y. K.; Bae, S.; Tae, J. *Tetrahedron Lett.* **2009**, 50, 2010.
- (606) Wu, X. J.; Wu, Z. S.; Han, S. F. *Chem. Commun.* **2011**, 47, 11468.
- (607) Bencic-Nagale, S.; Sternfeld, T.; Walt, D. R. *J. Am. Chem. Soc.* **2006**, 128, 5041.
- (608) Lo, K. K. W.; Chung, C. K.; Zhu, N. Y. *Chem.—Eur. J.* **2003**, 9, 475.
- (609) Saito, H.; Goodnough, L. T.; Boyle, J. M.; Heimburger, N. *Am. J. Med.* **1982**, 73, 179.
- (610) Jones, A. L.; Hulett, M. D.; Parish, C. R. *Immunol. Cell Biol.* **2005**, 83, 106.
- (611) Sullivan, D. J.; Gluzman, I. Y.; Goldberg, D. E. *Science* **1996**, 271, 219.
- (612) Ma, D. L.; Wong, W. L.; Chung, W. H.; Chan, F. Y.; So, P. K.; Lai, T. S.; Zhou, Z. Y.; Leung, Y. C.; Wong, K. Y. *Angew. Chem., Int. Ed.* **2008**, 47, 3735.
- (613) Li, C. Y.; Yu, M. X.; Sun, Y.; Wu, Y. Q.; Huang, C. H.; Li, F. Y. *J. Am. Chem. Soc.* **2011**, 133, 11231.
- (614) Kapuscinski, J. *Biotech. Histochem.* **1995**, 70, 220.
- (615) Latt, S. A.; Stetten, G.; Juergens, L. A.; Willard, H. F.; Scher, C. *D. J. Histochem. Cytochem.* **1975**, 23, 493.
- (616) LiC. Y. Doctoral Thesis. Fudan University. 2012
- (617) Van Houten, K. A.; Heath, D. C.; Pilato, R. S. *J. Am. Chem. Soc.* **1998**, 120, 12359.

NOTE ADDED AFTER ASAP PUBLICATION

This paper was published on the Web on June 18, 2012. The corrected version was reposted on November 1, 2012. The authors provide this addition to correct the omission of a key reference in the original review. The authors are grateful to Dr. Kelly A. Van Houten, Johns Hopkins University Applied Physics Laboratory, for bringing this to our attention.

10.1. DCP-Induced Intramolecular Cyclization Process. The first luminescent chemodosimeter based on an intramolecular cyclization process should be compound **1** reported by Pilato et al.⁶¹⁷ Upon exposure to selected phosphate esters, this platinum complex with an appended alcohol could be converted to a room-temperature lumiphore.

